Optical image sensors for analytical chemiluminescence biosensors

Reza Abbasi

Biological and Biomedical Engineering Graduate Program

McGill University, Montreal

December 2024

A thesis submitted to McGill University in partial fulfillment of the requirements of the degree of Doctor of Philosophy in Biological and Biomedical Engineering

Table of Contents

Abstract

This PhD thesis explores the development and application of advanced biosensors aimed at creating efficient, portable, and cost-effective diagnostic tools for point-of-need applications. The research highlights significant advancements in the integration of optical, microfluidic, and chemiluminescence technologies, addressing critical needs in various fields such as medical diagnostics, environmental monitoring, and food safety.

The thesis begins with a comprehensive review of optical biosensors, known for their high sensitivity and specificity in detecting various biomolecules. By integrating these biosensors into lab-on-a-chip (LOC) platforms, which leverage optical phenomena such as chemiluminescence and electrochemiluminescence, real-time detection and quantification of analytes are achieved. The incorporation of pixelated CMOS image sensors further enhances these platforms by providing high-resolution imaging, spatially resolved measurements, and the capability to detect multiple analytes simultaneously. This integration results in portable and efficient diagnostic devices suitable for point-of-care settings.

Building on this foundation, the research introduces a novel CMOS image sensor-based biosensor for ATP-mediated chemiluminescence detection, designed to assess microbial contamination on various surfaces. This biosensor demonstrates high photon collection efficiency and a strong correlation with commercial luminometers, offering a rapid and portable alternative to traditional microbial detection methods. The ability to detect microbial pathogens efficiently and accurately on surfaces such as personal electronic devices, and office and laboratory equipment has significant implications for improving sanitation and safety in various environments.

Further advancements are presented through the integration of microfluidic and electrochemiluminescence (ECL) systems on a CMOS chip, specifically for detecting uric acid (UA), a biomarker of gout disease. The single-electrode ECL platform exhibits high selectivity, reusability, and significant improvements in photon collection efficiency, proving its potential for point-of-need medical diagnostics. The device's performance was evaluated in simulated saliva and urine samples, demonstrating its potential utility in real-world medical diagnosis and monitoring of diseases at the point of care.

The thesis concludes with the development of a single-electrode ECL (SE-ECL) configuration for multiplexed detection of multiple analytes. This innovative method allows for the

simultaneous emission and detection of different colors by selectively exciting ECL luminophores. Optimization of SE-ECL intensity and the use of alternating current (AC) voltage to enhance light intensity are demonstrated, along with the successful implementation of multiplexed multicolor SE-ECL on a CMOS image sensor, enabling simultaneous measurement of multiple analytes. This capability is particularly valuable for applications requiring comprehensive and rapid analysis, such as complex diagnostic procedures and high-throughput screening.

Overall, this research advances the field of optical biosensors by integrating optical, microfluidic, and chemiluminescence technologies with CMOS image sensors, resulting in sophisticated, efficient, and accessible diagnostic tools. The developed platforms hold significant potential for applications in medical diagnostics, environmental monitoring, and food safety, paving the way for more advanced point-of-need analysis solutions. The findings of this thesis contribute to the broader understanding and development of next-generation biosensors, offering promising avenues for future research and technological innovation.

Résumé

Cette thèse de doctorat se concentre sur le développement et l'application de biosenseurs avancés visant à créer des outils de diagnostic efficaces, portables et rentables pour les applications au point d'utilisation. La recherche a révélé des avancées significatives dans l'intégration des technologies optiques, microfluidiques et de chimiluminescence, répondant à des besoins critiques dans divers domaines tels que les diagnostics médicaux, la surveillance environnementale et la sécurité alimentaire.

La thèse débute par une revue approfondie des biosenseurs optiques, reconnus pour leur haute sensibilité et spécificité dans la détection de diverses biomolécules. En intégrant ces biosenseurs dans des plateformes « lab-on-a-chip » (LOC) qui exploitent des phénomènes optiques tels que la chimiluminescence et l'électrochimiluminescence, la détection et la quantification en temps réel des analytes sont réalisées. L'incorporation de capteurs d'image CMOS pixelisés apporte une valeur ajoutée à ces plateformes en fournissant des imageries haute résolution, des mesures spatialement résolues et la capacité de détecter simultanément plusieurs analytes. Cette intégration aboutit à des dispositifs de diagnostic portables et efficaces adaptés aux paramètres de soins au point de service.

En s'appuyant sur ce solide fondement, la recherche propose une innovation majeure : un biosenseur basé sur un capteur d'image CMOS, conçu pour la détection par chimiluminescence médiée par l'ATP, permettant d'évaluer la contamination microbienne sur une variété de surfaces. Ce dispositif présente une efficacité élevée de collecte de photons et montre une forte corrélation avec les luminomètres commerciaux, offrant ainsi une alternative rapide et portables aux méthodes traditionnelles de détection microbienne. La capacité de détecter de manière efficiente et précise les agents pathogènes microbiens sur des surfaces telles que les dispositifs électroniques individuels, et les équipements de bureau et de laboratoire, a un impact significatif dans l'amélioration de l'hygiène et de la sécurité dans divers environnements.

D'autre progrès avancés sont réalisés grâce à l'intégration de systèmes microfluidiques et d'électrochimiluminescence (ECL) sur une puce CMOS, spécifiquement pour la détection de l'acide urique (UA), un biomarqueur de la goutte. La plateforme ECL à électrode unique présente une haute sélectivité, une réutilisabilité et des améliorations significatives de l'efficacité de collecte de photons, démontrant ainsi son potentiel pour les diagnostics médicaux au point d'utilisation. Les performances de l'appareil ont été évaluées dans des échantillons de

salive et d'urine simulés, mettant en évidence son utilité potentielle dans le diagnostic médical et la surveillance des maladies au point de soin.

La conclusion de cette thèse représente une avancée significative avec le développement d'une configuration d'électrochimiluminescence à électrode unique (SE-ECL) pour la détection multiplexée de plusieurs analytes. Cette approche novatrice permet l'émission et la détection simultanées de différentes couleurs en excitant sélectivement les luminophores ECL. La recherche démontre une optimisation de l'intensité SE-ECL ainsi que l'utilisation efficace d'une tension alternative (AC) pour amplifier l'intensité lumineuse. De plus, elle souligne la réussite de l'implémentation de la SE-ECL multiplexée multicolore sur un capteur d'image CMOS, permettant ainsi la mesure simultanée de plusieurs analytes. Cette capacité s'avère particulièrement précieuse pour les applications nécessitant une analyse complète et rapide, telles que les procédures diagnostiques complexes et le dépistage à haut débit.

En conclusion, cette recherche représente une avancée majeure dans le domaine des biosenseurs optiques en intégrant de marinière innovante les technologies optiques, microfluidiques et de chimiluminescence avec des capteurs d'image CMOS. Cette intégration complexe donne naissance à des outils de diagnostic sophistiqués, efficaces et accessibles. Les plateformes développées ouvrent des nouvelles perspectives d'application dans les domaines cruciaux tels que les diagnostics médicaux, la surveillance environnementale et la sécurité alimentaire, ouvrant ainsi la voie à des solutions d'analyse de pointe. Les découvertes réalisées au cours de cette recherche enrichissent notre compréhension globale et encouragent le progrès continu des biosenseurs de prochaine génération, offrant ainsi des perspectives prometteuses pour la recherche future et l'innovation technologique.

Acknowledgment

First and foremost, I would like to express my deepest gratitude to my esteemed supervisor, **Prof. Sebastian Wachsmann-Hogiu**, for granting me the opportunity to study at McGill University and for his unwavering support, invaluable advice, and endless patience throughout my PhD journey. His extensive knowledge and experience have been a constant source of inspiration, guiding me through the complexities of my academic research and personal growth.

I would also like to extend my heartfelt thanks to **Dr. Meruyert Imanbekova, Dr. Sorina Suarasan**, **Dr. Juanjuan Liu**, and **Ms. Xinyue Hu** for their insightful comments, suggestions, and significant contributions to my work. Their expertise and collaboration have been instrumental in the success of this research. I am deeply grateful to the members of my PhD committee, **Dr. Amine Kamen**, **Dr. Adam Hendricks**, and **Dr. Christopher Moraes**, whose guidance and support have been crucial in shaping the direction of my research.

I am also deeply appreciative of the entire lab and office team for the cherished moments and the supportive environment we created together. In particular, I would like to thank my good friend **Mr. Pouria Tirgar Bahnamiri**, whose assistance, encouragement, and friendship have been invaluable during my PhD.

Finally, **I dedicate this thesis to my beloved family**, whose unwavering support and endless love have been my foundation. To my parents, my brother, my sister-in-law, and my darling niece — who bring immense love and joy to my life each and every day —thank you for your constant encouragement and belief in me. A special acknowledgment goes to my sister, **Dr. Samaneh Abbasi**, whose guidance and support have been a pillar of strength throughout all these years of my academic pursuit. This accomplishment would not have been possible without all of you.

Contribution to original knowledge

During my PhD, I focused on the development and application of advanced biosensor technologies aimed at creating efficient, portable, and cost-effective diagnostic tools for point-of-need applications. My research made significant contributions by integrating optical, microfluidic, and chemiluminescence technologies with CMOS image sensors to address critical challenges in medical diagnostics, environmental monitoring, and food safety. I developed a novel CMOS image sensor-based biosensor for ATP-mediated chemiluminescence detection, demonstrating its efficacy as a portable alternative to commercial luminometers for microbial contamination assessment. Additionally, I advanced the field by designing a single-electrode electrochemiluminescence (ECL) platform on a CMOS chip for the detection of uric acid, showcasing its high selectivity, reusability, and potential for real-world medical diagnostics. My work also introduced a pioneering single-electrode ECL configuration for multiplexed detection of multiple analytes, enabling simultaneous multicolor detection through selective excitation of ECL luminophores. These innovations have resulted in sophisticated diagnostic platforms that are not only portable and efficient but also hold significant promise for diverse applications, contributing to the advancement of next-generation biosensor technologies. The details of my contribution to this study will be described in the following section.

The details of each work in my first-author publications are presented below.

The first article [1]*,* provides a comprehensive review of the integration of optical biosensors with microfluidic technology to develop compact, portable devices for rapid and precise analysis. It highlights the creation of lab-on-a-chip platforms utilizing optical phenomena like chemiluminescence and electrochemiluminescence for real-time detection of analytes. The review emphasizes the shift from traditional single-point optical detectors to advanced pixelated sensors, particularly CMOS image sensors, which offer enhanced resolution, sensitivity, and integration capabilities. These advancements show significant potential for point-of-care diagnostics and other applications requiring rapid, on-site analysis.

In the second publication [2], a novel biosensor utilizing a CMOS image sensor for detecting ATP via bioluminescence is introduced as the first demonstration of the platform. Samples were collected from various surface types, including personal devices and laboratory equipment using UltraSnap swabs and directly applied to the sensor. The close proximity between the

sample and the sensor optimized light capture, enabling accurate quantification of microbial contamination through bioluminescence intensity analysis. The biosensor demonstrated a wide linear range and high sensitivity for ATP detection. A comparative analysis with a commercial luminometer revealed a strong correlation and comparable performance, while the CMOS-based biosensor offered a significant cost reduction.

In the third publication [3], an ECL platform integrated with a CMOS image sensor is developed for point-of-care detection of uric acid, a biomarker for gout disease. The biosensor uses a single-electrode electrochemical system with an indium tin oxide (ITO) electrode to drive the ECL reaction, with signals detected by the CMOS sensor. A microfluidic device with two parallel channels is employed to precisely control a small sample volume, yielding a linear detection range of 25-300 μM for hydrogen peroxide and uric acid. The proximity of the ECL reaction to the sensor surface enhances sensitivity, surpassing cellphone and microscope-based methods. The device showed good reproducibility and reusability and successfully measured uric acid in saliva and urine, demonstrating its potential for point-of-care applications.

In the fourth publication [4], an optimized, miniaturized, and multicolor single-electrode electrochemiluminescence (SE-ECL) system capable of detecting four different analytes is introduced. To simplify the detection process and enable simultaneous analysis of multiple analytes, the optimized SE-ECL approach was implemented. By carefully controlling the applied voltage, distinct ECL emissions were generated, allowing for the differentiation of various analytes. The influence of electrode dimensions on light emission intensity was investigated, with longer and wider electrodes demonstrating enhanced signal output. Additionally, the application of alternating current (AC) voltage was explored, resulting in significantly increased light intensity compared to direct current. A proof-of-concept demonstration showcased the potential of this method for multiplexed detection by simultaneously distinguishing four distinct colors on a CMOS image sensor within a compact device format.

Contribution of authors

- **Chapter II**

This chapter presents a comprehensive review focused on developing and integrating chemiluminescence-based biosensors with lensless imaging technology for point-of-care applications. Particular emphasis was placed on understanding the fundamental principles of chemiluminescence signal generation and its subsequent capture through image-based detection systems.

The contributions of the authors are as follows:

RA and SWH conceived the idea and defined the structure and content of the manuscript; RA wrote the manuscript with a partial contribution of XH, AZ, and ID. SWH supervised the project. All authors reviewed and approved the manuscript in its current form.

- **Chapter III**

This chapter presents the fabrication, characterization, and application of a chemiluminescence device integrated with a CMOS image sensor. The device configuration involved removing the optical lens and IR filter from the CMOS sensor, allowing direct exposure of the sensor surface to the bioluminescence reaction of luciferin and ATP in the presence of luciferase. This setup enabled the sensor to capture nearly half of the chemiluminescence signals. The biosensor's ability to detect surface contamination via ATP concentration, collected using commercial Ultrasnap swabs, was evaluated. The device's performance was compared with a commercial luminometer, the industry standard for assessing surface cleanliness. The CMOS-based biosensor demonstrated similar performance to the luminometer but at a significantly lower cost, making it a viable option for use in food-related industries such as kitchens, restaurants, and warehouses.

The contributions of each author are as below:

RA and SWH conceived the study concept. RA and MI designed the experiments. RA and MI conducted the experiments, and RA analyzed the results. RA and MI wrote the main text of the manuscript. RA drafted and revised the article. SWH supervised the project. All authors reviewed and approved the manuscript in its current form and confirmed that this manuscript is only being used in the current thesis.

- **Chapter IV**

This chapter presents the development of a miniaturized ECL sensor integrated into a CMOS chip. The platform combines microfluidics with a luminol-based ECL system for on-chip sample handling and data acquisition, utilizing a single-electrode ECL (SE-ECL) configuration to achieve a compact design. The sensor was evaluated under various conditions, demonstrating accurate and selective detection of uric acid at physiologically relevant levels. Advantages of this CMOS-based SE-ECL platform include enhanced light collection efficiency, low cost, portability, and spatial control over the ECL reaction.

The contributions of each author are as follows:

RA and SWH conceived the idea. RA and SS designed the experiments. RA performed the experiments with assistance from JL and SS. RA analyzed the data and wrote the manuscript with input from all co-authors. SWH supervised the project. All authors reviewed and approved the manuscript in its current form.

- **Chapter V**

This chapter introduces an optimized, miniaturized, and multicolor SE-ECL system capable of detecting four different analytes. The approach simplifies the detection process and enables simultaneous analysis of multiple analytes by generating distinct ECL emissions through controlled voltage. The study also explored the influence of electrode dimensions and the application of alternating current (AC) voltage, which significantly increased light intensity. A proof-of-concept demonstrated the method's potential for multiplexed detection by simultaneously distinguishing four distinct colors on a CMOS image sensor within a compact device format.

The contributions of the authors are as follows:

RA and SWH conceived the idea. RA designed and performed the experiments, analyzed the data, and wrote the main body of the manuscript. SWH supervised the project. RA and SWH reviewed and approved the manuscript in its current form.

List of Publications

First-author publications

1. **Abbasi, R**.; Liu, J.; Suarasan, S.; Wachsmann-Hogiu, S. SE-ECL on CMOS: A Miniaturized Electrochemiluminescence Biosensor. *Lab on a Chip* **2022**, 22 (5), 994-1005. (**IF:6.1**)
2. **Abbasi, R**.; Imanbekova, M.; Wachsmann-Hogiu, S. On-chip Bioluminescence Biosensor for the Detection of Microbial Surface Contamination. *Biosensors and Bioelectronics* **2024**, 254, 116200. (**IF: 10.7**)
3. **Abbasi, R**.; Wachsmann-Hogiu, S. Optimization and Miniaturization of SE-ECL for Potential-Resolved, Multi-Color, Multi-Analyte Detection. *Biosensors and Bioelectronics* **2024**, 257, 116322. (**IF:10.7**)
4. **Abbasi, R**.; Hu, X.; Zhang, A. P.; Dummer, I.; Wachsmann-Hogiu, S. Optical Image Sensors for Smart Analytical Chemiluminescence Biosensors. *Bioengineering* **2024**. 11, 912. (**IF:3.8**)

Co-author publications (contributions to other projects)

1. Hu, X.; **Abbasi, R**.; Wachsmann-Hogiu, S. Microfluidics on Lensless, Semiconductor Optical Image Sensors: Challenges and Opportunities for Democratization of Biosensing at the Micro- and Nano-Scale. *Nanophotonics* **2024**, 12 (21), 3977-4008. (**IF: 6.5**)
2. Imanbekova, M.; **Abbasi, R**.; Hu, X.; Sharma, M.; Vandewynckele-Bossut, M.; Haldavnekar, R.; Wachsmann-Hogiu, S. Physical Modifications of Kombucha-Derived Bacterial Nanocellulose: Toward a Functional Bionanocomposite Platform. *Macromolecular Materials and Engineering* **2024**, 2400041. (**IF: 4.2**)

Conferences

1. **R. Abbasi**, J. Liu, S. Suarason, S. Wachsmann-Hogiu: “ECL-on-CMOS; a miniaturized electrochemiluminescence biosensor for point of care applications”; **Oral presentation** (Presented by SWH due to inability to travel). *SPIE Photonics West*, 22 - 27 January 2022, San Francisco, California, United States.

2. **R. Abbasi**, J. Liu, S. Suarason, S. Wachsmann-Hogiu: “Electrochemiluminescence detection of uric acid at point-of-need by using a lab-on-a-CMOS platform”; **Oral presentation**. *SPIE Photonics West*, 28 January – 2 February 2023, San Francisco, California, United States
3. **R. Abbasi**; S. Wachsmann-Hogiu, “Potential-Resolved Multicolor, Multianalyte Electrochemiluminescence Detection on CMOS Semiconductor Image Sensor: Optimized and Miniaturized SE-ECL.” **Oral presentation**. *Photonics North 2024*, Vancouver, Canada, May 28–30, 2024.
4. **R. Abbasi**; S. Wachsmann-Hogiu: “Fully Integrated Multicolor, Multiplex Optical Biosensor for Detecting Multiple Analytes for Health Monitoring at Point of Need.” *MicroTAS 2024*, Montréal, Canada, October 13–17, 2024.

Patent

- **R. Abbasi**, M.Imanbekova, J.Liu, S.Wachsmann-Hogiu “ Biosensor and method of use thereof”; Provisional US patent (filed USPTO) , 9110118198: US 63/307,492; Y/R: D2022-0096; O/R: 05001770-948USPR

List of figures and tables

(non-manuscript sections)

List of Abbreviations

AC	Alternating Current
APD	Avalanche Photodiodes
APS	Active Pixel Sensor
ATP	Adenosine Triphosphate
BL	Bioluminescence
BPE	BiPolar Electrode
BSI	back-side illuminated
CCD	Charge-Coupled Device
CL	Chemiluminescence
CMOS	Complementary Metal Oxide Semiconductor
CNN	convolutional neural networks
CNT	Carbon Nanotube
DBAE	Dibutylamine
DC	Direct Current
DNA	Deoxyribonucleic Acid
ECL	Electrochemiluminescence
ELISA	Enzyme-Linked Immunosorbent Assay
FBD	foodborne diseases
FL	fluorescence
FOV	Field Of View
FSI	front-side illuminated
HIgG	Human Immunoglobulin G
ITO	Indium Tin Oxide
LCL	Luminol Chemiluminescence
LFA	Lateral Flow Assay
LiDAR	Light Detection And Ranging
LIG	laser-induced graphene
LOC	Lab On a Chip
LOD	limit of detection
MDF	Multiclass Decision Forest

MEC	Metal-Enhanced Chemiluminescence
microTAS	micro total analysis systems
MIgG	Mouse Immunoglobulin G
ML	machine learning
MNP	Metallic Nano Particle
MOS	Metal-Oxide-Semiconductor
MOSFET	Metal-Oxide-Semiconductor Field-Effect Transistor
MP	Mega Pixel
NNRMs	neural network regression models
NP	Nano Particles
PDMS	Polydimethylsiloxane
PET	Poly Ethylene Terephthalate
PMT	Photomultiplier Tubes
POC	Point Of Care
PON	Point Of Need
PPD	Pinned Photodiode
RGB	Red Green Blue
RIgG	Rabbit Immunoglobulin G
RLU	Relative Light Units
RSD	relative standard deviation
SE-ECL	Single Electrode Electrochemiluminescence
SEES	Single Electrode Electrochemical System
SNR	Signal to Noise Ratio
SPADs	Single-Photon Avalanche Photodiodes
TEA	Triethylamine
TPrA	Tripropylamine
UA	Uric Acid
ULT	urate-lowering therapy
WE	Working Electrode

Chapter I. Introduction

A biosensor is an analytical device in which biological or chemical reactions are monitored by converting the reaction information to detectable signals proportional to the concentration of an analyte. Biosensors show great potential in many areas such as drug discovery, medical diagnostics, disease monitoring, and detection of disease-causing micro-organisms and markers that are indicators of disease in body fluids (blood, urine, saliva, sweat). Current biosensors often face challenges related to sensitivity, specificity, cost-effectiveness, and portability. For instance, most devices fail to provide accurate readings in resource-limited settings due to reliance on bulky instrumentation or complex protocols.

A typical biosensor consists of three main components: a sensitive biological element, a transducer, and associated electronics or signal processors that are mainly responsible for the display of the results in a user-friendly way. There are various types of transducers based on the recorded biorecognition such as mechanical, electric and magnetic, temperature, electrochemical, and optical. Many of the transducers generate optical or electrical signals proportional to the amount of interactions between analytes and biorecognition elements. One of the optical phenomena in this regard is Chemiluminescence [5].

Chemiluminescence (CL), the emission of light resulted from a chemical reaction, has gained an increasing attraction in different biological applications due to its high signal-to-noise ratio (SNR) and its sensitivity which is even higher than enzyme-linked immunosorbent assay (ELISA) [19]

Luminol chemiluminescence (LCL) is a favorable method of detection in many cases because of its selectivity, simplicity, high sensitivity and low cost. LCL methods can be used as biosensors in environmental monitoring [6], for pharmaceutical cellular localization [7] and as biological tracers, in reporter gene-based assays and several other immunoassays [8, 9].

Electrochemiluminescence (or electrogenerated chemiluminescence, ECL) is an electrochemical process which involves high-energy electron transfer reactions in molecules at electrode surfaces to generate excited states for light emission [10, 11]. ECL is a powerful tool with an extensive application range in different assays due to the advantages like rapidity, simplicity, and high sensitivity [12]. ECL is intrinsically considered as a combination of electrochemistry and spectroscopy. Therefore, the development and miniaturization of ECL systems extremely depend on the electrochemical methods [13]. As it is shown in **Figure 1**, in

ECL, an electrolytic cell is used which consists of 2 solid electrodes (cathode and anode). These electrodes are immersed in a conducting liquid, usually an aqueous solution or a molten salt. Also, an electrical supply is connected to the electrodes and provides the energy to drive a reaction. Recently ECL has been done by a new method and using a single electrode instead of two, which will be described later in the approach section.

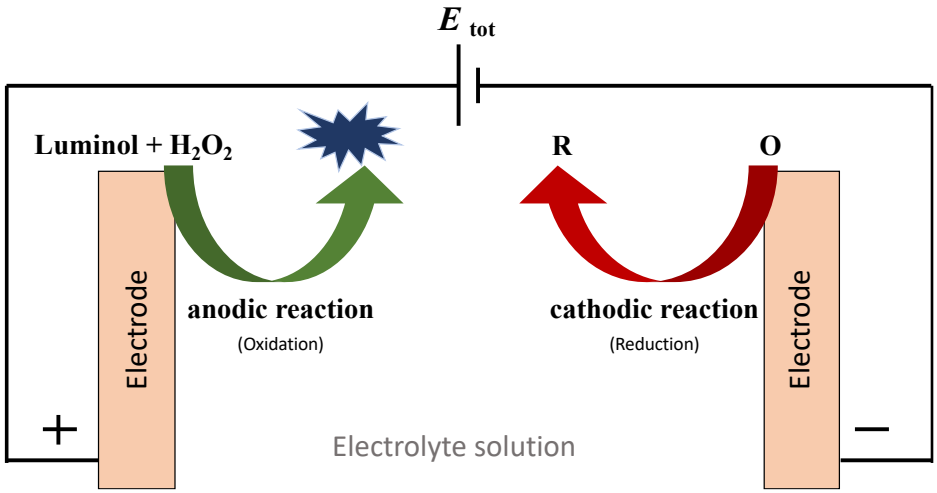

Figure 1: Schematic of electrolytic cell for ECL

The process of light emission from the CL reaction is relatively complicated, but briefly, the oxidation of a CL agent, such as luminol, paired with other chemicals, like hydrogen peroxide (H_2O_2), exhibits CL light. The whole reaction occurs in the presence of a catalyst, for example, iron (present in hemoglobin) or gold (or gold nanoparticles (AuNPs)). Although the reaction can slowly continue, even without a catalyst, the emitted signal will be quite weak to visualize [14, 15].

The development of easy-to-use, cost-effective, and portable analysis tools that provide accurate and rapid results is crucially important for early detection and appropriate treatment [16]. ECL is a powerful tool with a great application range in different assays because of advantages like rapidity, simplicity, and high sensitivity as well as good specificity [12]. However, in ECL devices, reaching the optimal space of high performance and low complexity, cost, and size is still challenging. In this project, the goal is to build an electrochemiluminescence-based point-of-care platform and to apply the system in addressing healthcare-related problems.

Due to the increasing demand for accurate diagnosis and precise prognosis during the past decade, ECL has gained significant attention to simultaneously detect multiple biomarkers in a single sample [17]. ECL is a very promising candidate for multiplexing because of its low cost outstanding analytical performance and also ability to apply multiple detection strategies [18-20]. In multiplexing, simultaneous detection of multiple targets is enabled in a single run/volume employing multiplex bioassays. In comparison to single plex detection, multiplexing or using multiplex bioassays features different benefits. It lowers the cost, reduces the size of the sample volume, increases analytical throughput, and generates more information [21-23]. More significantly, detecting several disease biomarkers simultaneously might improve the accuracy of diagnosis by lowering the false positive rate [24, 25]. One approach to ECL multiplexing is to use separated electrodes (electrode arrays) using a single detector for each working electrode (WE) [17]. For example, Fu et al. introduced an immunosensor array coupled with a non-array detector for the detection of human immunoglobulin G (HIgG), rabbit immunoglobulin G (RIgG) and mouse immunoglobulin G (MIgG) using 6 individual electrodes (4 working electrodes -WE) [26]. Later on, they also introduced a paper-based ECL sensor with three working electrodes using the same principals of their previous work [27]. To lower the array functional area, Walt et al. developed a bead-based ECL microarray platform for the simultaneous detection of multiple antigens via immunoassay by binding the receptors to the beads [28]. Similarly, Xu et al. reported an on-chip microarray-based platform for multiplex analysis of cancer-cell-surface biomarkers by ECL resonance energy transfer using 16 PDMS-decorated ITO strips which were coated with 64 antigen-decorated CdS nanorod spots (four spots per strip), enabling multiple detection of antigens [29]. To improve the sensitivity and the ECL signal, Yu et al. introduced a flow-injection combined ECL strategy for the sensitive detection of tumor markers [30]. Furthermore, to improve the stability and the cost-efficiency of the ECL devices, Rusling et al. developed a 3D printed and automated immunoassay and used a precise microfluidic device for multiplex detection of protein biomarkers [31].

During the past few years, paper-based ECL devices have been introduced to improve the feasibility. For instance, Chen et al. described a rotational paper-based electrochemiluminescence immunodevices for sensitive and multiplexed detection of cancer biomarkers by the employment of rotational valves [32]. Also, in this category, Zhang et al. developed a paper fluidic closed bipolar electrode, an electrical conductor that promotes unbalanced oxidation reductions at two ends [33], ECL sensing platform for hydrogen peroxide

and glucose [34]. However, using a bipolar electrode can cause the background signal from the working electrode. To overcome this problem, Wang et al. combined a microfluidic chip and ECL and introduced the microfluidic-based closed bipolar system to increase the electrical current and remove the background signal [35]. Later on, they improved their work to 3 3-channel bipolar electrode system for the detection of multiple targets [36] such as tripropylamine, dopamine, H_2O_2, CEA, and AFP [37].

Moreover, in order to work on the portability of the ECL devices and to make them suitable for POC diagnosis, Xu et al. improved an ECL system with wireless power to avoid complicated electrical connections [38]. However, the use of alternating current may cause some problems such as weak ECL signal which can be solved by converting the AC to DC current by mini-diode [39]

Despite all the great aforementioned advantages of spatially resolved ECL devices, they need a complicated electrode array which has a negative effect on reproducibility. One way to overcome this problem is to use a potentially resolved approach or in other words using different ECL probe pairs [17]. Several ECL probes such as quantum dots (QD) [40-42], luminol [43, 44], $Ru(bpy)_3^{2+}$ derivatives [45-49] , and metal nanoclusters [50, 51] were used at the same time in this approach. However, since they have broad emission spectrum ranges, it might be difficult to separately detect them. In this case, using ECL probe pairs with various emission spectra can facilitate the detection [52-55].

On the other hand, there are diseases that are interconnected meaning that if you have one you are most likely to get the other one. For example, it has been found that gout, diabetes, and heart diseases are interrelated [56-61] and therefore, it is crucial to simultaneously detect uric acid [62], glucose [63] , and cholesterol[64, 65] , which their concentrations play a direct role in those diseases respectively. Gout is a type of inflammatory arthritis causing painful inflammation [66]. Some scientists believe that inflammation can also affect diabetes [67]. Besides, it has been found that the level of uric acid will be often high in the blood of people with type 2 diabetes and that can be caused by the extra fat. The body of overweight people creates more insulin and that creates difficulties for their kidneys to eliminate uric acid, which may in turn lead to gout [68]. Researchers in one study evaluated the health records of participants in the Framingham Heart Study which is a research project on heart disease. It's been found that the participants were more likely to get type 2 diabetes if they had higher uric acid levels in their blood. More precisely, for every 1 milligram per deciliter (mg/dL) increase

in uric acid level, the chance of diabetes was elevated by 20% [68]. In this regard, EC and ECL biosensors have attracted considerable attentions to detect glucose, uric acid, and cholesterol because of advantages like high sensitivity, simplicity, and low cost [69-73].

Following the aforementioned introduction, it was deemed necessary to develop and integrate optical, microfluidic, and imaging technologies to create a stand-alone device. Typically, the first modality employed is fluorescence. Fluorescence is a photophysical phenomenon where a substance absorbs light at a specific wavelength and subsequently emits light at a longer wavelength. This property is widely exploited in the field of biological research, particularly through fluorescence microscopy. Fluorescence microscopy enables the visualization of specific cellular components, proteins, and other biomolecules by tagging them with fluorescent markers. These markers, when excited by a light source, emit light that can be detected and imaged, providing high-resolution, real-time visualization of dynamic biological processes. The sensitivity and specificity of fluorescence microscopy have revolutionized cell biology, allowing for detailed study of cellular structures and functions at the molecular level.

In comparison, chemiluminescence involves the emission of light as a result of a chemical reaction without the need for external light excitation. This intrinsic generation of light offers significant advantages over fluorescence, particularly in terms of background noise reduction and sensitivity. In fluorescence microscopy, the requirement for an external light source can lead to photobleaching and phototoxicity, potentially damaging the biological sample and limiting observation time. Chemiluminescence, however, eliminates these issues, as it does not require light excitation, resulting in minimal background interference and allowing for longer observation periods. Additionally, the high sensitivity of chemiluminescent assays makes them particularly advantageous for detecting low-abundance targets, thereby enhancing the accuracy and reliability of biological measurements. Furthermore, chemiluminescence does not require the use of filter sets and dichroic mirrors, which are essential in fluorescence microscopy to separate excitation light from emission light. This simplification not only reduces equipment complexity and cost but also improves the ease of use and maintenance. These attributes make chemiluminescence a superior choice for certain applications in biological research and diagnostics.

It is hypothesized that electrochemiluminescence (ECL) and microfluidics can be combined and integrated on a semiconductor image sensor for the rapid, sensitive, and simultaneous detection of biomarkers. The goal of this project is to develop an integrated optical,

microfluidic, and electrochemiluminescence system via a complementary metal-oxide-semiconductor (CMOS) chip. The successful fulfillment of the project objectives will be accomplished by organizing the research into three aims. Specifically:

Aim 1: Conduct a comprehensive literature review with the goal of integrating different modalities onto the chip to create a point-of-care (POC) ECL biosensor. This review will modify and customize the CMOS chip by integrating optical, microfluidic, and electrochemiluminescence modalities and altering the setup to capture images in these modes.

Aim 2: Evaluate the performance and capabilities of the system using an analyte. The first platform will utilize chemiluminescence on an imaging sensor to detect ATP for food safety applications. This platform will then be further developed for electrochemiluminescence by employing a single-electrode electrochemical system to detect uric acid.

Aim 3: Increase the degree of parallelization, application of the improved system, and optimization. The proposed platform will be tested for the visualization and detection of different biomolecules, such as uric acid and glucose, via ECL on the CMOS chip.

Although the unique advantages of chemiluminescence (CL) and electrochemiluminescence (ECL) biosensors, along with their high analytical performances, have been widely explained in the literature, several challenges remain in this field. CL and ECL-based multiplex systems require complex protocols and bulky, costly instruments that are not always readily available. Furthermore, ECL is a relatively new detection technique, and only a few ECL point-of-care (POC) devices have been developed to date. In many studies, the assay system has been adapted for on-chip or on-paper testing, where the challenge of the short lifetime of CL emission was mitigated by microfluidic sample handling. Comparatively, reviewing the optical design to detect the emitted light has received little attention. Therefore, achieving the optimal balance of high performance, low complexity, cost, and size in ECL devices remains challenging. Developing a cost-effective CL device that also promotes portability, as well as accurate and rapid results, is crucial for early detection and appropriate treatment. Additionally, there is a need to build a POC diagnostic device capable of simultaneously detecting interconnected diseases such as gout and diabetes through the multiplexed detection of uric acid and glucose. Miniaturizing ECL systems requires balancing sensitivity, durability, and signal stability. Key challenges include managing thermal dissipation, ensuring consistent reagent distribution, and maintaining system robustness under varied conditions. These challenges motivate the

development of POC diagnostic and prognostic tools with new modalities, such as electrochemiluminescence, for healthcare applications.

Transition to Chapter II

As has been highlighted in Chapter I, while chemiluminescence (CL) and electrochemiluminescence (ECL) biosensors offer exceptional analytical capabilities, their practical application is hindered by several challenges. Multiplex CL and ECL assays often require complex procedures and expensive, bulky instrumentation, limiting their accessibility. ECL, in particular, is a relatively new technology with limited point-of-care implementations. Although microfluidic systems have addressed some issues related to CL's short emission lifetime, the optimization of optical detection systems for both CL and ECL remains an understudied area. Consequently, developing ECL devices that balance high performance with affordability, simplicity, and compact size continues to be a significant challenge.

The aims of Chapter II are 1) systematically review state-of-the-art literature on optical and especially CL biosensors and the optical detectors in these systems for Health monitoring and food safety applications with evidence from basic research and review articles, and to 2) determine a niche for further technological developments.

The review includes published studies up to July 2024 that are relevant to the topic of the thesis. This chapter explores the integration of optical biosensors with microfluidic technology to create compact, portable devices capable of rapid and precise analysis. By combining these technologies, researchers have developed lab-on-a-chip platforms that employ optical phenomena like chemiluminescence and electrochemiluminescence for real-time detection and quantification of various analytes. The review highlights the transition from traditional single-point optical detectors to advanced pixelated sensors, particularly CMOS image sensors, which offer superior performance in terms of resolution, sensitivity, and integration capabilities. These advancements hold significant promise for point-of-care diagnostics and other applications requiring rapid, on-site analysis. Future research will focus on harnessing machine learning to further enhance the capabilities of these integrated platforms.

This chapter is based on my recently submitted first-author article. The contributions of the authors are as follows:

RA and SWH conceived the idea and defined the structure and content of the manuscript; RA wrote the manuscript with a partial contribution of XH, AZ, and ID. SWH supervised the project. All authors reviewed and approved the manuscript in its current form.

Chapter II. Comprehensive literature review

Optical image sensors for smart analytical chemiluminescence biosensors

Reza Abbasi [a], Xinyue Hu [a], Alain P. Zhang [a], Isabelle Dummer [a], Sebastian Wachsmann-Hogiu[a]

[a] Department of Bioengineering, McGill University, Montreal, QC, H3A 0E9, Canada

Email: sebastian.wachsmannhogiu@mcgill.ca

2.1 Abstract

Optical biosensors have emerged as a powerful tool in analytical biochemistry, offering high sensitivity and specificity in the detection of various biomolecules. This article explores the advancements in the integration of optical biosensors with microfluidic technologies, creating lab-on-a-chip (LOC) platforms that enable rapid, efficient, and miniaturized analysis at the point of need. These LOC platforms leverage optical phenomena such as chemiluminescence and electrochemiluminescence to achieve real-time detection and quantification of analytes, making them ideal for applications in medical diagnostics, environmental monitoring, and food safety.

Various optical detectors used for detecting chemiluminescence are reviewed, including single-point detectors such as photomultiplier tubes (PMT) and avalanche photodiodes (APD), and pixelated detectors such as charge-coupled devices (CCD) and complementary metal-oxide-semiconductor (CMOS) sensors. A significant advancement discussed in this review is the integration of optical biosensors with pixelated image sensors, particularly CMOS image sensors. These sensors provide numerous advantages over traditional single-point detectors, including high-resolution imaging, spatially resolved measurements, and the ability to simultaneously detect multiple analytes. Their compact size, low power consumption, and cost-effectiveness further enhance their suitability for portable and point-of-care diagnostic devices.

In the future, the integration of machine learning algorithms with these technologies promises to enhance data analysis and interpretation, driving the development of more sophisticated, efficient, and accessible diagnostic tools for diverse applications.

2.2 Introduction

Biosensors are analytical devices that use biological components to detect, convert, quantify, and report biological information such as metabolite concentration. They are essential tools for diagnosing and monitoring health conditions such as infectious diseases [1-4] and glucose level [5-7], as well as environmental sensing for chemical pollution [8-10] and microbial contamination [11-14]. Biosensors with point of care (POC) and point of need (PON) capability address spatial and temporal constraints of sample handling by offering portability and rapid results, making these devices suitable for use in field settings including at home, at bedside, and during clinical appointments [15]. Given their use case scenarios, key criteria for POC and PON biosensors include sensitivity, specificity, portability, and fast result turnover.

Transducers in biosensors convert the binding events between the target analyte and the biorecognition element into various types of signals, including electrochemical, optical, mechanical, temperature, electric, or magnetic signals [16, 17]. Biosensors can be categorized based on the type of signals the transducer produce, with electrochemical and optical biosensors being the most commonly available biosensors translated from laboratory to market due to their high sensitivity and ease of integration with miniaturized, on-chip systems. Various articles have reviewed the topic of biosensors, offering comprehensive overviews that describe their components, mechanisms, historical development, current trends towards miniaturization and wearability, and applications across various fields including medical diagnosis and environmental monitoring [17-19]. In this paper, we will focus on optical biosensors due to their superior signal-to-noise ratio and visual readout capability.

Biosensors that utilize an optical transducing mechanism, commonly known as optical biosensors, are the most prevalent type of biosensor. The optical transducer converts binding events between target analyte and biorecognition element into optical signals such as light emission or spectral change. Optical biosensors offer several advantages across a broad range of applications, particularly due to their high sensitivity, high specificity, reliability, versatility, and real-time detection capabilities [16-19]. As highly sensitive and easy-to-use devices, optical biosensors have been extensively applied in research, particularly as lab-on-chip devices in drug discovery and in characterization of biomolecular interactions [20, 21]. They are also prominent in POC and PON applications, including pathogen detection for clinical diagnostics, on-site pollution detection for environmental monitoring, and contaminant detection in food [22-24].

Optical biosensors can be categorized into three main types: colorimetric, luminescent, and refractive index-based, each with distinct signal generation mechanisms. Colorimetric biosensors detect changes resulting from reflection, absorption, or scattering of light, often involving coupling with chromogenic indicators or nanoparticle agglutination that produce visible color changes in the presence of a target analyte [25, 26]. Luminescent biosensors measure light emitted from analyte-specific biochemical reactions that cause excited molecules to emit light as they return to ground state. Refractive index-based biosensors detect changes in the refractive index of sample using plasmonic, resonance, or interference methods [27].

Luminescence-based biosensors offer significant advantages due to their higher signal-to-noise ratio, which enhances the sensitivity of biosensors. Therefore, luminescence-based biosensors are particularly useful in applications requiring high sensitivity and low background interference. Their ability to detect analytes at low concentrations makes luminescence-based biosensors highly valuable in clinical diagnostics and environmental monitoring. Luminescence can be generated through fluorescence, chemiluminescence (CL), bioluminescence (BL), and electrochemiluminescence (ECL). Fluorescence-based biosensors rely on the emission of light from fluorophores when excited by a specific wavelength of light [28]. In chemiluminescence-based biosensors, detection involves the light generated from chemical reactions that induce an excited state in a species [29]. Bioluminescence is a special type of chemiluminescence that occurs within biological systems, such as those involving luciferin and luciferase. Electrochemiluminescence, on the other hand, is chemiluminescence induced by an electrical potential. Among luminescence-based biosensors, chemiluminescence, bioluminescence and electrochemiluminescence are particularly advantageous as they bypass the need for external illumination, resulting in simpler systems with even higher signal-to-noise ratios. ECL further stands out from bioluminescence and chemiluminescence as the timing and intensity of its reactions can be controlled by the applied electrical potential, enabling temporal and quantitative control of the reaction.

To measure the optical signal produced during analyte-specific reactions, optical detectors are an integral part of an optical biosensor. Optical detectors in luminescence-based biosensors function by converting light to electrical signals. These detectors can be point detectors such as photomultiplier tubes (PMTs), which use photosensitive tubes with dynodes to transfer and exponentially amplify electronic signals through cascading secondary emissions. Multiple PMTs can be arranged in multiplex configurations to create a plate reader with higher throughput. Although PMTs are sensitive and low-noise, they are not ideal for POC

applications due to their delicate materials, high voltage requirements, and high cost. Alternatively, avalanche photodiodes (APDs) use doped semiconductive materials to convert photons into electrons, which are then amplified through impact ionization. Arrays of APDs can be used to build image sensors, such as complementary metal-oxide-semiconductor (CMOS) image sensors, which offer multiplexity and spatial resolution. While APDs generally have higher noise levels than PMTs, they are sensitive, high-speed, inexpensive, and compact. Therefore, image sensors are ideal for POC and PON optical detection.

While image sensors are traditionally coupled with lenses to adjust their focal distance, field of view (FOV), and spatial resolution, the lenses introduce a trade-off between FOV and spatial resolution. On the other hand, using image sensors without lenses eliminates this trade-off, as the FOV will be determined by the number and size of the pixels in the sensor and the spatial resolution will be determined by the size of the pixels. With the absence of lenses, the distance between the sample and the image sensor must be minimized to obtain a clear, sharp image and avoid diffraction patterns. This configuration, known as lensless contact imaging, maximizes photon collection efficiency due to the close proximity between sample and sensor and is ideal for luminescence-based biosensors [30]. Fluorescence imaging requires an emission filter to be positioned between the sample and the sensor to eliminate excitation wavelengths, complicating its implementation in a lensless contact setup. Therefore, luminescence-based biosensors in lensless contact configurations commonly utilize CL, ECL, and BL as signal generation methods. To facilitate more precise as well as spatially and temporally controlled sample handling, lensless contact imaging is often integrated with microfluidic components. Additionally, microfluidic components enable multiplexity by introducing multiple channels. These advantages favor the development of microfluidic-integrated lensless image sensing configurations in optical biosensors, which will be discussed in this paper. As the spatial resolution of lensless image sensor in contact mode is determined by the pixel size, which is typically a few micrometers but can be sub-micrometer, lensless contact imaging has been used as a compact and inexpensive microscope in POC or PON settings for cell imaging. Moreover, microfluidic-integrated lensless image sensor with luminescence-based analyte detection technique is also used in various biosensing applications beyond its traditional imaging roles.

In this paper, we focus on chemiluminescence-based biosensors integrated with lensless contact-mode image sensors for POC and PON applications, highlighting the integration of such system with microfluidic components and artificial intelligence. We begin by discussing the fundamental principles of signal generation in chemiluminescence-based biosensors and

optical detection technologies used in these biosensors. We then explore the integration of image sensors with luminescence-based biosensing technologies, microfluidic sample handling methodologies, and artificial intelligence. Finally, we discuss the applications of image-based biosensors at the POC and PON, providing an outlook for the field of optical biosensing.

While several reviews have discussed the recent advancements in optical biosensors, covering the fabrication, application, historical overview, and strengths and weaknesses of various types of optical sensor, as well as the integration of optical biosensors with microfluidic channels for point-of-care testing [20, 21, 35, 36]. These articles mainly present fundamental principles and applications, lacking a focused perspective. Our paper offers an outlook and road map for the development of smart optical biosensors by specifically exploring chemiluminescence-based optical biosensors, not only detailing the mechanisms of signal generation and detection but also examining the integration of optical biosensors with microfluidic systems for sample handling, image sensors for readout, and machine learning for signal processing and interpretation.

2.3 Mechanisms of signal generation for chemiluminescence biosensors

Luminescence-based optical biosensors offer several significant advantages, including contactless detection, high sensitivity, and the ability to detect a wide range of analytes through labeling [31]. These biosensors are suitable for a diverse array of applications (Fig. 1a), such as medical diagnostics, environmental monitoring, food safety, drug discovery, and biomedical research. Chemiluminescence and electrochemiluminescence (Fig. 1b), which simplify signal transduction, provide means of producing luminescence without need for excitation light. Both methods rely on chemical reactions to generate light, with their differences leading to notable variations in sensor design, performance, and application. Each method has distinct advantages and drawbacks, contributing to their respective suitability for specific applications.

2.3.1 Chemiluminescence

The mechanisms underlying chemiluminescence are varied and sometimes debated, though it is generally accepted that electron transfer plays a critical role prior to the emission of light [32]. In this context, chemiluminescence can be seen as the inverse of the electron transfer process triggered by photoexcitation, where light is the end product rather than the initiator. When the energy level of the electron transfer state exceeds that of the excited state, photo-induced electron transfer is not feasible. However, if radical cations and anions ($A^{\bullet+} + B^{\bullet-}$) are

generated through chemical reactions, the recombination of these charges can lead to the formation of an excited state (C^*). If this excited state (C*) is emissive, it results in the emission of light, defined as chemiluminescence, represented by the reaction (1):

$$A^{\bullet+} + B^{\bullet-} \rightarrow C^* + D \rightarrow C + D + hn \qquad (1)$$

This process converts chemical energy into light energy, analogous to the reverse of photochemical electron transfer. [33]

The chemiluminescence process involves three key steps: (1)formation of high-energy intermediates such as 1,2-dioxetane, 1,2-dioxetanone, and 1,2-dioxetanedione[34], which release sufficient energy to produce visible light (ranging from 40–70 kcal/mol); (2)decomposition of these high-energy intermediates and chemiexcitation to an excited state; (3)emission of light from the excited state. [33]

The quantum yield of chemiluminescence is an essential parameter for assessing the efficiency

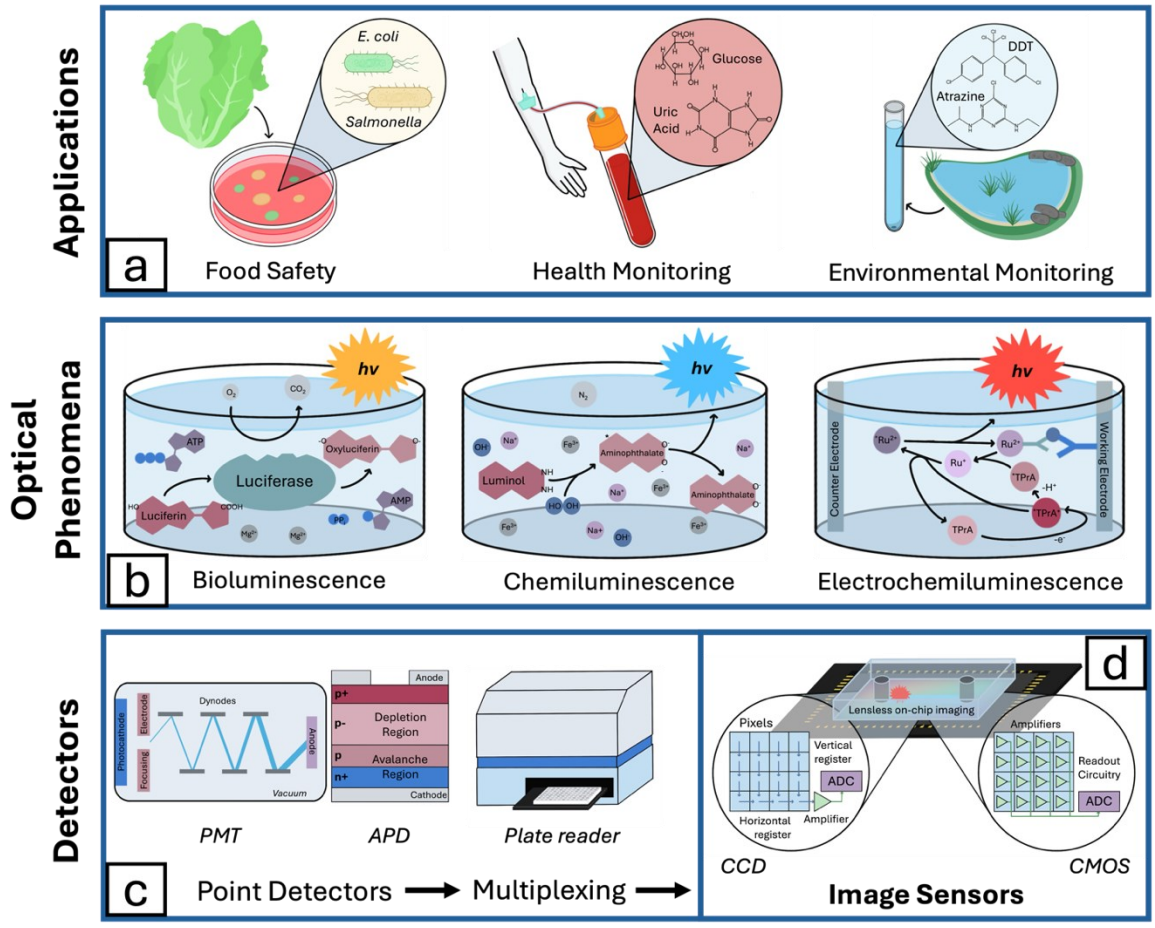

Fig.1 Overview of the analytical chemiluminescence sensors: a) Application of analytical

chemiluminescence in food safety, health monitoring, and environmental monitoring. b) Optical phenomena including Bioluminescence, Chemiluminescence, and Electrochemiluminescence. c) Optical detectors from point detectors (left) including photomultiplier tub, and avalanche photodiode, to multiplexing (plate reader) d) Optical image sensors including CCD and CMOS image sensors.

of different chemiluminescent systems. It is defined as the ratio of moles of photons emitted to moles of the limiting reagent, with the unit being einsteins per mole. For example, the chemiluminescence quantum yield of the luminol system is 1.29×10^{-2} einsteins/mol, indicating that 1 mol of luminol produces 1.29×10^{-2} mol of photons. The theoretical maximum quantum yield is 1 einstein/mol, meaning that 1 mol of substrate can produce a maximum of 1 mol of photons. It is crucial to distinguish between chemiluminescence intensity and the number of photons (in counts), as intensity is influenced not only by the number of photons but also by their frequency.[35, 36]

Unlike photoluminescence, chemiluminescence does not require an excitation light source and accompanying excitation/emission filters. Thus, chemiluminescent optical biosensors produce a signal which can be measured directly using a photodetector resulting in a simpler compact device. The lack of an excitation source also improves signal-to-noise ratio with reduced background noise [31]. CL biosensors also demonstrate a wide dynamic range allowing for simultaneous detection of strong and weak luminescence [37].

To enhance the light emission of CL optical biosensors, advances in CL amplification have been essential, particularly the introduction of nanomaterials. A class of material that has garnered significant attention for amplification purposes are metallic nanoparticles (MNPs). Amplification has been achieved through a variety of MNP properties, notably MNP catalytic activity for higher reaction yields and surface plasmon resonance resulting in metal-enhanced chemiluminescence (MEC) [38, 39] improving the overall quantum yield. Likewise, the CL biosensor presented by Xu at al. exploited the catalytic capacity of copper nanoclusters as a nano-mimic enzyme for peroxidase [38].

A promising avenue for chemiluminescence optical biosensing is utilizing bioluminescence (Fig. 1b) in which high energy intermediates are synthesized via metabolic processes. Bioluminescence optical biosensors are particularly attractive due to the high efficiency of bioluminescence with metabolism of luciferin specifically exhibiting very high quantum yield [40]. Luciferin-based bioluminescence biosensors have been demonstrated to effectively detect

the concentration of ATP with a linear relationship between analyte concentration and bioluminescence intensity [41, 42].

2.3.2 Electrochemiluminescence (ECL)

Electrochemiluminescence (ECL) is a process that combines electrochemical reactions with chemiluminescence to produce light. In ECL, reactive species are generated at the surface of an electrode through electrochemical reactions, involving the oxidation or reduction of a luminescent molecule (luminophore) and, in some cases, a co-reactant. The mechanisms underlying ECL can be categorized into three main pathways: the annihilation pathway, the co-reactant pathway, and the cathodic pathway. [43, 44]

The annihilation pathway involves the generation of both oxidized and reduced forms of the luminophore at the electrodes. These forms then interact (annihilate) to produce an excited state that emits light. This mechanism typically involves alternating the potential at the electrode to sequentially generate the radical cation and radical anion of the luminophore. For example, the luminophore $[Ru(bpy)_3]^{2+}$ is oxidized to $[Ru(bpy)_3]^{3+}$ and reduced to $[Ru(bpy)_3]^{+}$. When these species annihilate, they form the excited state $[Ru(bpy)_3]^{2+*}$, which then emits light as it returns to the ground state. [37, 43, 44]

The co-reactant pathway utilizes an additional molecule (co-reactant) that participates in the electrochemical reactions to produce the excited state. The co-reactant is typically oxidized or reduced to form a reactive intermediate, which then reacts with the oxidized or reduced luminophore to generate the excited state. For instance, in the $[Ru(bpy)_3]^{2+}$/TPrA system, $[Ru(bpy)_3]^{2+}$ is oxidized to $[Ru(bpy)_3]^{3+}$, and TPrA is oxidized and then converts to TPrA$^{\bullet}$. The interaction between $[Ru(bpy)_3]^{3+}$ and TPrA$^{\bullet}$ forms the excited state $[Ru(bpy)_3]^{2+*}$, which emits light upon returning to the ground state [43]. Due to the direct relationship between the intensity of the emitted light and the concentration of the emitter or co-reactant, this form of ECL has been extensively utilized in analytical applications, especially in highly sensitive bioanalysis [45].

The cathodic pathway involves reduction reactions occurring at the cathode to generate the excited state [46]. In this pathway, the luminophore and/or co-reactant are reduced at the cathode to form reactive intermediates that produce the excited state. Although less common than the oxidative (annihilation and co-reactant) pathways, the cathodic path can be significant in certain systems. For example, $[Ru(bpy)_3]^{2+}$ can be reduced to $[Ru(bpy)_3]^{+}$, which then reacts

with a reduced co-reactant to form the excited state $[Ru(bpy)_3]^{2+*}$ that emits light as it returns to the ground state [43, 47].

Box 1 | Electrochemiluminescence Mechanisms and application of common co-reactants:

Electrochemiluminescence (ECL) involves the generation of reactive species at the electrode surface through electrochemical reactions, including the oxidation or reduction of a luminophore and sometimes a co-reactant. ECL mechanisms can be categorized into three pathways: annihilation, co-reactant, and cathodic. The **annihilation pathway** involves generating both oxidized and reduced forms of the luminophore, which then interact to form an excited state that emits light. The **cathodic pathway** involves reduction reactions at the cathode, generating reactive intermediates that produce an excited state. The **co-reactant pathway**, which is particularly significant for its sensitivity in analytical bioanalysis, utilizes an additional molecule (co-reactant) that participates in the electrochemical reactions. In the $[Ru(bpy)_3]^{2+}$/TPrA system, $[Ru(bpy)_3]^{2+}$ is oxidized to $[Ru(bpy)_3]^{3+}$, and TPrA is oxidized to TPrA$^{\bullet}$. The interaction between $[Ru(bpy)_3]^{3+}$ and TPrA$^{\bullet}$ forms the excited state $[Ru(bpy)_3]^{2+*}$, which emits light as it returns to the ground state. This mechanism's direct correlation between light emission intensity and the concentration of the emitter or co-reactant makes it widely used in sensitive bioanalytical applications.

The most common ECL co-reactant systems include:

1. ***$[Ru(bpy)_3]^{2+}$ / TPrA:***
   - **Luminophore:** Tris(2,2'-bipyridyl)ruthenium(II) ($[Ru(bpy)_3]^{2+}$)
   - **Co-reactant:** Tripropylamine (TPrA)

This is one of the most extensively used systems due to its high efficiency and sensitivity in bioanalytical applications. The application of this co-reactant system that results in an emission of red ECL is as follows:

Immunoassays: The $[Ru(bpy)_3]^{2+}$/TPrA system is extensively used in immunoassays, where ECL tags help detect and quantify antigens or antibodies in samples [48-56]. This is crucial for disease diagnosis and monitoring. As an alternative labeling strategy, co-reactants employed in ECL reactions can be utilized for tagging biomolecules [57, 58].

DNA Analysis: $[Ru(bpy)_3]^{2+}$-based DNA detection methods are instrumental in diverse areas such as clinical diagnostics, pathogen identification for infectious diseases, forensic analysis, and the diagnosis of genetically linked human diseases [49, 59-71].

Aptamer-based Biosensing: The unique properties of aptamers, which are functional nucleic acids capable of specific target recognition, have been combined with ECL detection for the development of a multitude of aptasensors [72-88].

2. ***Luminol / H_2O_2:***
   - **Luminophore:** Luminol (3-aminophthalhydrazide)
   - **Co-reactant:** Hydrogen Peroxide (H_2O_2)

Luminol is oxidized by hydrogen peroxide in the presence of a catalyst (often a metal ion like Fe^{2+} or a peroxidase enzyme) to form an excited state intermediate (3-aminophthalate). This intermediate then emits light as it returns to the ground state. The Luminol/H_2O_2 system is renowned for its applications in chemiluminescence (CL) and electrochemiluminescence (ECL) due to its strong blue light-emitting capabilities and reagent availabilities [89]. It is widely utilized in:

Biological substrates: Since H_2O_2 is the co-reactant of luminol, any substrate that produces H_2O_2 through enzymatic oxidation can be detected using this ECL system. Examples of these analytes include glucose[90-97], uric acid[98-100], cholesterol[101-104], l-lactate and creatinine.

Genetic detection: Including DNA detection for clinical research[105, 106] and miRNA sensing for cancer diagnosis [107-109].
Immunosensing: In immunoassays and other diagnostic tests where high sensitivity is required [110-118].

3. Other pairs:

There are also other ECL luminophore-co-reactant pairs. For $[Ru(bpy)_3]^{2+}$ and $[Ru(phen)_3]^{2+}$ luminophores, apart from TPrA some other co-reactants including Dibutylamine (DBAE) and Triethylamine (TEA), have been explored. Green ECL can be achieved using various luminophore and co-reactant pairs including $Ir(ppy)_3$ (tris(2-phenylpyridine)iridium(III)) and TPrA [99, 119, 120].

The general ECL process thus includes the electrochemical generation of reactive intermediates, the formation of excited states through interactions between these intermediates, and the emission of light as these excited states relax to the ground state. This ability to control the generation of excited states electrochemically makes ECL a powerful technique for various applications, including bioassays, sensing, and imaging.

Beyond the mechanistic aspects of ECL reactions, it is crucial to examine the spectroscopic and electrochemical characteristics of the reaction partners. These properties influence the thermodynamics and the resulting kinetics of the reactions that produce the excited state, thereby determining the efficiency of the ECL process.

The efficiency of electrochemiluminescence (Φ_{ECL}) is defined by the ratio of photons emitted to the total number of electron transfer events during ECL reactions [45]. Φ_{ECL} comprises two components: Φ_{ex}, which indicates the yield of excited states, and Φ_{PL}, which represents the probability of photon emission from these excited states (analogous to the photoluminescence quantum yield).

$$\Phi_{ECL} = \Phi_{PL} \times \Phi_{ex} \qquad (2)$$

Φ_{ex} is influenced by the kinetics and thermodynamics of the reaction pathways and various experimental factors, such as the stability of precursors and their likelihood of undergoing side reactions. Conversely, Φ_{PL} is an intrinsic photophysical property affected by the solvent and the susceptibility of the excited state to quenching interactions.

Energetically, for an excited state to form from a bimolecular reaction, the energy available from the reactants must exceed the energy of the excited state product. Electrochemical experiments can often assess the free energy of these reactions using the redox potentials of the reactants. For instance, in ruthenium-based ECL, the energy of the excited state product (E_{em}) can be estimated from the maximum emission wavelength (λ_{max} = 620 nm) using the equation

$E = hc/\lambda_{max}$ [45]. Here, h is Planck's constant (4.13×10^{-15} eVs), and c is the speed of light (3.00×10^{8} m/s), yielding an E_{em} value of 2.05 eV. Given that the free energy of ECL pathways is 2.61 eV for annihilation and 2.98 eV for co-reactant pathways, these reactions sufficiently energize the 2.05 eV excited state of the ruthenium complex.

A central question in radiative and reactive intermediate electron transfer reactions concerns the population of excited states rather than the thermodynamically favored ground state. Marcus' theory offers a compelling explanation [121, 122]. It posits that electron transfer occurs on a significantly faster timescale compared to nuclear rearrangements, solvent reorganization, and bond vibrations. Consequently, when these reactions release substantial energy on an ultrafast timescale (shorter than a typical vibrational period), the system does not efficiently dissipate this energy through vibrational relaxation. This, in turn, makes the pathway leading to an electronically excited product more favorable.

In conclusion, understanding ECL efficiency and mechanisms is essential for optimizing its analytical applications. By examining factors influencing Φ_{ECL}, such as kinetics, thermodynamics, and experimental conditions, researchers can improve ECL system performance. Future studies should focus on these areas to enhance ECL's utility in various fields.

2.3.2.1 Electrode configurations in ECL

In an ECL device, the electrode setup is a critical component that influences the efficiency, sensitivity, and overall performance of the ECL system. Various configurations, such as the three-electrode setup, bipolar electrode ECL, and single-electrode ECL, each offer unique advantages and applications. The three-electrode setup, comprising a working electrode, reference electrode, and counter electrode, is the most commonly used configuration, providing precise control over the electrochemical environment and facilitating accurate measurements. Bipolar electrode ECL, on the other hand, simplifies the experimental setup by eliminating the need for multiple connections, making it suitable for miniaturized and portable devices. Single-electrode ECL further reduces complexity and can be advantageous in specific applications where space and simplicity are paramount. Understanding the distinctions of these different electrode setups is essential for optimizing ECL systems for diverse analytical and diagnostic applications.

Conventional/Three-Electrode ECL. The three-electrode cell is the classic configuration for electrochemiluminescence (ECL). It consists of three electrodes: the working electrode, the counter electrode, and the reference electrode [123]. This configuration was developed to address the limitations of earlier two-electrode systems, which often struggled to maintain a stable potential necessary for accurately measuring resistance at the interface of the working electrode and the solution [124]. In the three-electrode system, the reference electrode serves as a stable reference point for measuring and regulating the working electrode's potential without allowing any current flow [124]. Consequently, this setup enables precise determination of potential changes at the working electrode, unaffected by fluctuations at the counter electrode [124]. The potential sweeps in this setup are typically characterized by a gradual rise in current followed by a subsequent decline, representing a two-step process involving the mass transfer of electroactive materials toward the working electrode's surface and subsequent electron transfer reactions [124].

Recent advancements in three-electrode ECL systems have been notable. For example, a method was developed to use emissions on the counter electrode to enhance multicolor and potential-resolved ECL systems [132]. The multicolor ECL from mixed luminophores, $Ir(ppy)_3$ and $[Ru(bpy)]_3^{2+}$, at glassy carbon working and counter electrodes was investigated, analyzing the simultaneous ECL processes [132]. Under these conditions, spatially resolved emissions at different electrodes were observed, suggesting the potential for more multiplexed detection systems [132].

Additionally, new materials have been incorporated into ECL to enhance detection sensitivity. For instance, a folding microfluidic paper-based analytical device (μ-PAD) was developed using carbonate/carboxymethyl chitosan ($CaCO_3$/CMC) hybrid microspheres for signal amplification [133]. These microspheres, coated in silver nanoparticles and immobilized with single-stranded DNA (ssDNA) strands, significantly augmented sensitivity.

Bipolar ECL. Bipolar electroluminescence (BP-ECL) significantly differs from the conventional three-electrode setup, as the working electrode is replaced by the control of the solution potential [134]. A bipolar electrode (BPE) is a floating conductor that does not require a direct electrical connection to a power source or external circuit (Fig.2a). Instead, polarization is achieved by an electric field generated by two driving electrodes placed at opposite ends of an electrochemical cell. When a sufficiently high voltage is applied to the solution, simultaneous oxidation and reduction reactions occur at either end of the bipolar electrode

[135]. This phenomenon occurs because the same number of electrons released by an oxidation reaction also participate in the co-occurring reduction reaction. This setup provides key advantages over the classic three-electrode system. As the BPE system is wireless and does not require an external power supply or a multichannel potentiostat, it is capable of conducting many simultaneous reactions with a single pair of driving electrodes and a power supply, making it useful for multiplexing and parallel sensing (Fig.2f) [134].

The difference between a closed and open bipolar system lies in the presence of a wall between the anodic and cathodic solutions. In a closed BP-ECL system, the cathode and anode solutions are physically separated so that the only path between the half cells is through the BPE (Fig.2i) [138].

The driving voltage E can be described by the following equation using Kirchhoff's second law:

$$E = \Delta\varphi(D2) - \Delta\varphi(C) + \Delta\varphi(A) - \Delta\varphi(D1) \qquad (3)$$

where Δφ(D1), Δφ(C), Δφ(A) and Δφ(D2) are the potentials of driving electrode 1, the cathodic pole, the anodic pole, and driving electrode 2 with respect to the solution [141]. The driving voltage of an open bipolar electrode cannot be defined in this way, as it lacks the wall separating the two solutions [141].

To find the potential of the BPE, two parameters are considered: the overpotential along the electrode interface and the kinetic characteristics of the redox couple [139]. The potential difference between the solution and the two poles of the BPE, ΔE_{elec}, represents the driving force available to couple the two reactions occurring simultaneously at either end of the BPE (Fig.2e). For the electrode to maintain its electroneutrality, these co-occurring reactions must have equal electron consumption and production [145]. ΔE_{elec} can be approximated by the following equation (4) [139]:

$$\Delta E_{elec} = \frac{E_{tot}}{l_{channel}} l_{elec} \qquad (4)$$

where E_{tot} is the voltage applied to the driving electrodes, l_{elec} is the length of the electrode, and $l_{channel}$ is the distance between the driving electrodes.

Having gained an understanding of the principles and significance of bipolar electrochemiluminescence, a comprehensive review of the key research papers that have

explored its diverse applications will now be conducted. Compared to the traditional three-electrode system ECL, BP-ECL has a much greater capacity for high-throughput detection (Fig.2d). To exploit this high-throughput capability of BP-ECL, a microfluidic array chip was developed to allow for multiplexed detection of prostate cancer biomarkers (Fig.2b) [137]. Immunosensing requires multiple steps, such as the loading of reagents and washing of the detection region, which limit its multiplexing capabilities [137]. To overcome this limitation, the design of the chip allows for the careful control of liquid flow through the channels, keeping the samples uniformly separated. These samples are then directed towards the BPE array, where they are captured by their corresponding antibodies. Glucose oxidase labeling allows for the production of hydrogen peroxide, which generates the ECL reaction [137].

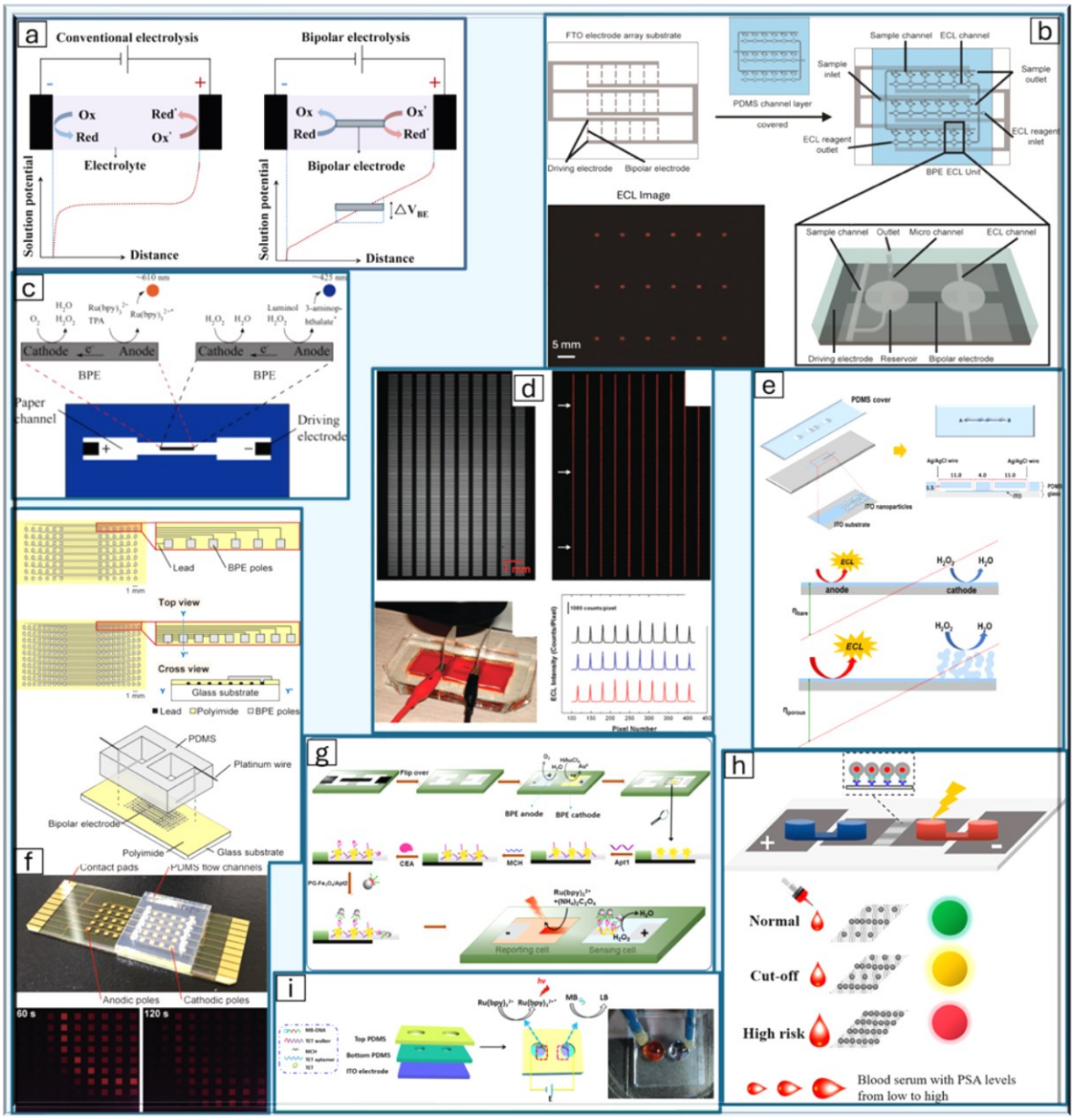

Fig.2 Electrochemiluminescence with Bipolar configuration: a) Electrode configuration in conventional ECL with a three-electrode setup (left), and in Bipolar ECL (BPE) where a conductor is placed between the electrochemical cell, and the potential difference across the conductor drives the ECL reaction (right) [142]. b) Bipolar electrode array for multiplexed detection of prostate cancer biomarkers [143]. Liquid flow is directed by using a specialized channel structure that leverages differential flow resistance c) Paper-based BPE ECL for imaging and sensing [144]. Microfluidic channels are fabricated on filter paper using wax screen printing, while carbon ink-based BPE and driving electrodes are also screen-printed onto the paper. d) ECL using 1000 BPE arrays. Optical image (top left), ECL image (top right), electrochemical cell setup (bottom left), and ECL intensity profile (bottom right) of these arrays [145]. The simplified device uses a single pair of driving electrodes to activate a 500 µm x 50 µm electrode array, and the BPEs are placed in a shallow electrolyte pool between parallel plates to ensure

uniform electric field e) Porous BPE using ITO nanoparticles. Top view and cross-section (top), H_2O_2 sensing (bottom) [146]. PDMS cover with 90 μm microchannels seals the BPE channel, separating detection and reporting channels. A nanoporous ITO layer detects H_2O_2, while a bare ITO layer reports ECL. The PDMS cover and ITO-coated glass form the complete BPE microchip. f) BPE arrays for ECL imaging and multiplex sensing. Schematic of the device (Top), real device and ECL images (bottom) [147]. The device features integrated cathodic and anodic poles and leads, insulated by a polyimide layer. Platinum and gold BPEs were fabricated using arrays of these poles. g) Fabrication process of paper-based PBE aptasensor for detection of carcinoembryonic antigen [148]. Janus-like gold-coated Fe3O4 nanospheres are synthesized in this device and showed catalytic activity for H_2O_2 reduction. h) Multicolor ECL using BPE configuration to detect prostate-specific antigen [149]. Selective ECL excitation is enabled by tuning the interfacial potential of the BPE poles in this device. i) BPE ECL sensor using gold and glassy carbon beads for detection of tetracycline [150]. Au particles were selectively deposited on one side of a GCB electrode, controlling coverage from 0 to 45.3% using bipolar electroplating. This modified GCB allows for varying biomolecule conjugation. Modified with permission from [142-150].

Single Electrode ECL. While bipolar electrode arrays have shown promise in areas of multiplexing, a significant drawback remains in the requirement for electrode arrays for these multiplex experiments. These electrode arrays are expensive and time-consuming to manufacture, which underscores the relevance of single-electrode ECL [134]. The basic premise behind the design of the single-electrode electrochemical system (SEES) is the reduction of the electrochemical cell to a single electrode. This is achieved by creating a potential difference along the surface of the electrode [100]. The initial SEES electrode was developed by applying an external voltage to both ends of the electrode, creating a potential gradient due to the varying resistance of the electrode [100]. The electrical potential produced by this process is directly proportional to the length of the cell and the applied voltage [98]. This method can then be utilized for ECL by generating excited states of luminol along the electrode, producing the ECL signal.

The potential difference between the ends of the cell (ΔE_c) primarily depends on the ratio between the electrochemical cell's length L_c and the length of the plastic film [100]. When ΔE_c is sufficiently large, reduction and oxidation will occur simultaneously at either end of the microelectrochemical cell, resulting in the following formula (Fig.3a) [98, 100]:

$$\Delta E_c = \frac{E_{tot}}{L_c} \times L_c \qquad (5)$$

The very first single-electrode ECL system was developed using an indium tin oxide (ITO) electrode and a self-adhesive label with holes poked into it [100]. This system was designed for multiplexed experiments targeted towards high-throughput analysis, as each hole serves as an independent microelectrochemical cell. Initially, this system demonstrated its use in detecting luminol, hydrogen peroxide, uric acid, and glucose (Fig.3b) [100]. Later, the single-electrode system was adapted to be wireless by incorporating wireless energy transfer modules and a rectifying diode [149]. The resulting system exhibited a linear range from 1 to 150 μM and a detection limit of 0.26 μM. Additionally, visual detection was carried out using a smartphone, indicating promising potential for point-of-care applications.

In 2021, a graphene-based single electrode on a polyimide substrate was developed for the detection of multiple analytes using a luminol-based chemical reaction (Fig.3h) [155]. The electrodes were fabricated with a CO_2 infrared laser, forming laser-induced graphene on the surface of the polyimide substrate. This differs from the original single electrode developed on an ITO substrate, allowing for a miniaturized form with applications in numerous industries. The system was later adapted for the detection of vitamin B_{12} [156].

In 2022, several single-electrode systems using paper as the substrate were developed. One such system involved a disposable paper-based single electrode fabricated with carbon paint and commercial glow stick dye [150]. When an electric field is applied to the device, anodic and cathodic reactions occur at either end, separated by the dumbbell shape of the paper. The materials used were deliberately chosen to be common to maximize accessibility. Another paper-based single electrode was fabricated by embedding reduced graphene oxide through blue laser ablation, demonstrating effectiveness in the detection of glucose and lactate (Fig.3f) [153].

Building on the advancements in single-electrode ECL systems, the strong π-π stacking interaction of carbon nanotube (CNT)/graphene was exploited to immobilize $[Ru(phen)]_3^{2+}$ to create a modified single electrode (Fig.3g) [154]. The resistance of the $[Ru(phen)]_3^{2+}$ modified CNT/graphene film then induces SEES when a voltage is applied, allowing for the visual detection of ECL. This system has been applied for dopamine detection since dopamine quenches this ECL.

The potential applications for SEES in high-throughput systems have also been expanded by several researchers. A single-electrode ECL for a high-throughput immunoassay was developed

by using a carbon ink screen electrode, with cardiac troponin I (cTnI) antibodies immobilized along its surface [157]. When these antibodies bind to cTnI, electron transfer along the electrode is inhibited, resulting in a decrease in ECL intensity. Additionally, a gradient potential distribution typically used in bipolar electrochemistry was adapted for use on a single electrode by modifying a classic ITO single-electrode setup through the electrodeposition of a gradient polypyrrole (PPy) conductive film, resulting in a high-throughput electroanalysis system (Fig.3e) [152].

Most recently, efforts to increase the sensitivity of single-electrode electrochemical biosensor systems have been made by modifying the surface of the electrode with MXene structures and Co-Pt nanoparticles (Fig.3d) [151]. MXene structures have garnered interest due to their properties such as high electron conductivity and ion adsorption, which enable their use in sensitive ECL systems. Co-Pt nanoparticles were incorporated due to their effectiveness in enhancing the ECL of luminol in the presence of H_2O_2. Finally, by incorporating a Raspberry Pi computer and an Artificial Neural Network, a system was created that significantly enhances the sensitivity of detection [134].

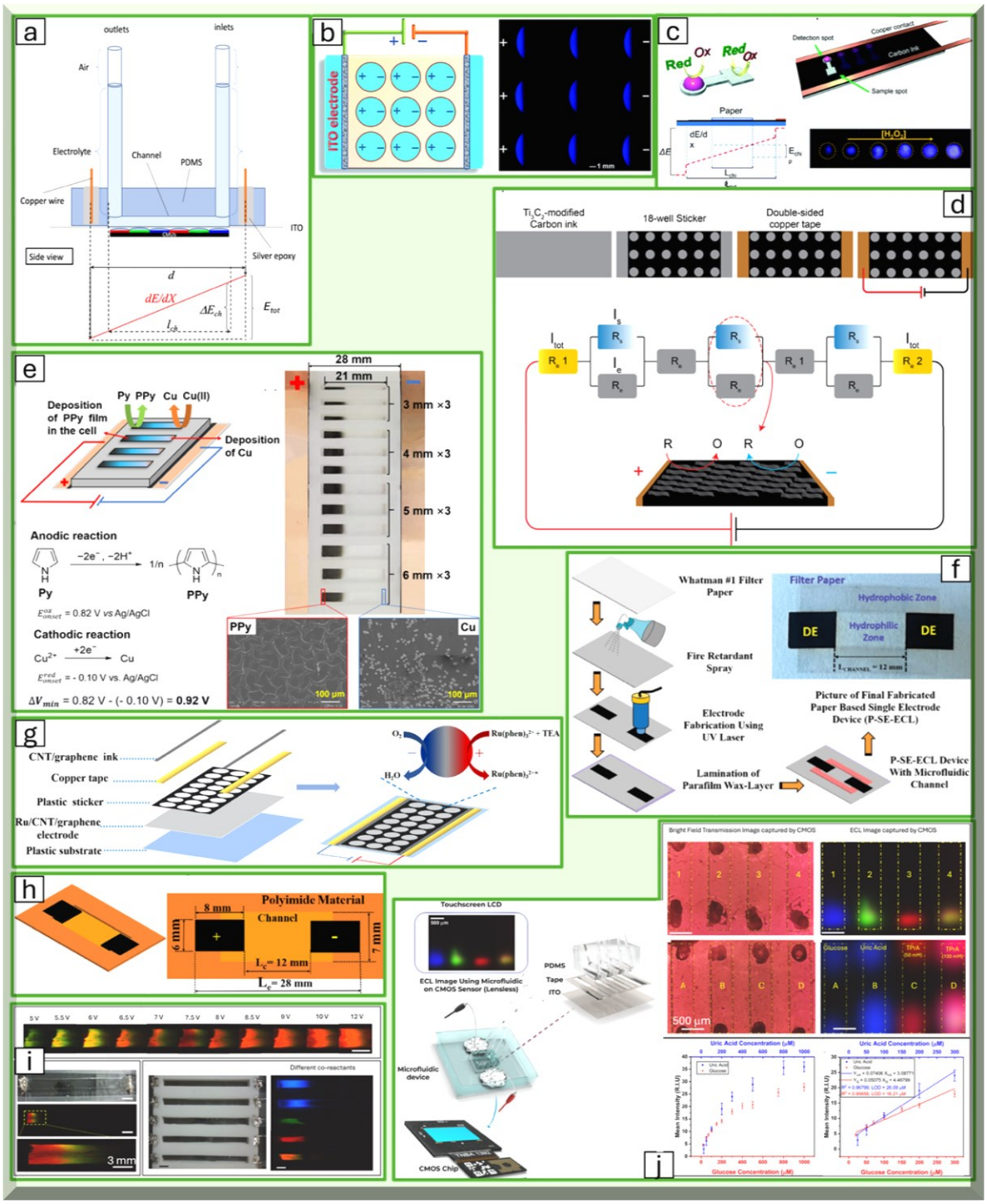

Fig.3 Electrochemiluminescence with single electrode (SE) configuration: a) schematic of SE ECL on CMOS image sensor (top), structure of SE configuration and distribution of potential along the single electrode (bottom) [104]. b) First demonstration of SE-ECL, multiplex ECL using SE configuration [106]. SE-ECL for single and multiplex experiments are created by attaching labels with varying hole patterns onto ITO electrodes. c) Paper-based SE-ECL on carbon ink [156]. A paper-based biosensor used glow sticks as a luminophore, detected by a smartphone. A two-compartment paper device enabled separate optimization of sensing and detection reactions. d) Fabrication of multiple-well SE-ECL on

carbon ink (top), and equivalent circuit (bottom) for immunoassays application [157]. This paper-based SE-ECL, featuring a perforated sticker on a carbon ink electrode, utilized antibody immobilization and Co–Pt nanoparticles for sensitive SARS-CoV-2 detection. e) SE-ECL with multiple channels fabricated by punching polypyrrole film and attaching it to the carbon ink layer (top), and ECL reactions on the cathodic and anodic side of each well (bottom) [158]. f) Paper-based SE-ECL fabricated by reducing graphene oxide via laser and wax printing to form a microfluidic channels for glucose and lactate sensing [159]. g) Multiplex SE-ECL fabricated using $Ru(phen)_3^{2+}$ modified carbon nanotube/graphene film and a plastic sticker with 24 holes for dopamine detection [160]. h) SE-ECL device fabricated using laser-induced graphene and polyimide film [161]. i) First multicolor SE-ECL device fabricated by 3D-printed channels. Multicolor ECL using different potential in different channels (top), multicolor ECL using potential gradient along the SE (bottom left), photo of the 3D-printed SE-ECL (bottom center), and multicolor SE-ECL on different channels (bottom right) [105]. j) Miniaturized and microfluidic-integrated SE-ECL on CMOS image sensor: schematic of the device (left), detection of multiple analyte including glucose and uric acid with this device (right) [105]. Modified with permission from [104-106, 156-161].

2.4 From point detectors to optical image sensors

In emission-based optical biosensing, a photodetector is essential for detecting light and converting it into an electrical signal. Photodetectors operate based on the photoelectric effect, a phenomenon where incident photons with sufficient energy are absorbed by a material, causing the ejection of electrons known as photoelectrons. The photoelectric effect was first documented by Heinrich Hertz, with further experiments by Philipp Lenard and Robert Millikan demonstrating the dependence of the number of emitted photoelectrons on the intensity and wavelength of the incident light, respectively [158-160]. These findings were later explained by Albert Einstein [161]. According to Einstein's explanation, the energy of incoming radiation is quantified as hn, where n is the frequency of light. Therefore, the energy imparted to a photoelectron is related to the wavelength of the absorbed light. Assuming that each photon with sufficient energy excites only one electron, the light intensity, or rate of photons, must correspond to the number of photoelectrons emitted.

Several important qualities are used to evaluate the performance of a photodetector, including sensitivity, noise, spectral response, response time, and quantum efficiency [162-164]. Sensitivity describes a photodetector's ability to detect low levels of light. This is particularly crucial for chemiluminescence optical biosensors due to the weak emission typically produced by chemiluminescence. However, achieving high sensitivity can also introduce unwanted

noise. Therefore, it is important to optimize the photodetector's gain to achieve sufficient sensitivity while minimizing noise. The spectral response of a photodetector refers to the range of light frequencies it can detect. A broader spectral response allows for a wider range of applications. For real-time monitoring, the response time of a photodetector is critical, with shorter response times enabling more accurate temporal measurements. Lastly, quantum efficiency, defined as the ratio of photogenerated charge carriers to incident photons, indicates how efficiently a light signal is converted into an electrical signal. High quantum efficiency is essential for low-light and high-accuracy applications.

While photodetectors may follow the same fundamental photoelectric principle for light-to-electric signal conversion, the way this conversion is achieved can greatly affect the detector's performance. In the following sections, two-point detectors (Fig. 1c), photomultiplier tubes (PMTs) and avalanche photodiodes (APDs), will be introduced and compared to imaging-based detectors (Fig. 1d), including charge-coupled devices (CCDs) and complementary metal-oxide semiconductor (CMOS) sensors.

2.4.1 Photomultiplier tubes (PMTs)

The initial development of PMTs dates back to the early twentieth century, coinciding with the development of vacuum tubes and advancements in the understanding of photoelectric phenomena. In the late 1800s, the discovery of the photoelectric effect by Heinrich Hertz and its further explanation by Albert Einstein demonstrated the ejection of electrons from a material when exposed to light [158, 161]. However, the first applications of this phenomenon were not realized until the invention of the phototube in the 1920s. Phototubes comprised a photosensitive material that ejected electrons upon exposure to light, producing a small and often too weak electric current, thus necessitating the need for amplification methods.

The innovation of the PMT soon followed, with Leonid Kubetsky's work on secondary emission for electron amplification eventually leading to the development of the first commercially available PMTs by the 1930s [165]. After World War II, PMT technology saw rapid improvements driven by the demands of research and industry. Advancements in vacuum technology, photosensitive materials, and amplification techniques greatly enhanced PMT performance and reliability. The modern PMT is a highly sensitive instrument capable of single-photon detection with high efficiency and low noise across a wide spectral response. Recent innovations in the manufacturing processes of PMTs have resulted in more robust and

versatile devices, making them suitable for a variety of applications, including medical diagnostics and astronomy [166, 167].

PMTs offer several key advantages, including high sensitivity, fast response time, high gain with low noise, and a wide spectral response. With the development of high quantum efficiency photocathodes, dynodes, and optimized electronics, PMTs are capable of sensing single-photon emissions by applying high amounts of gain [168]. Due to the controlled manner of amplification, with each dynode adding predictable amounts of gain, PMTs can achieve high gain with low over-multiplication noise while exhibiting a linear response over a wide range of incident light intensities [169]. Additionally, since amplification does not occur at the photocathode, PMTs benefit from a large variety of available materials for photocathodes, enabling a wide spectral response.

While PMTs are an excellent choice for high-sensitivity, low-noise applications, they also have several drawbacks. Since PMTs are made from glass vacuum tubes, they are generally quite delicate. Additionally, PMTs are sensitive to magnetic fields, which can interfere with the trajectory of emitted electrons passing through the vacuum tube, reducing efficiency, causing gain variations, and adding signal noise [168, 170, 171]. This problem can be addressed using magnetic shielding or active compensation coils [168, 171]. For point-of-care (POC) applications, PMTs may not be suitable because they require a high voltage power supply for amplification [168]. Furthermore, the combination of specialized photocathode and dynode materials, complex design, magnetic interference countermeasures, and power supply requirements result in high costs, making PMTs less ideal for POC applications.

PMTs have been utilized in numerous experimental designs across various applications. For example, the chemiluminescence biosensor for detecting cholesterol by Xu *et al.* employed a PMT. Multiple fiber-optic based biosensors for detecting sorbitol have also been demonstrated using PMT detectors [172, 173]. In particular, Gessei *et al.* devised and evaluated the performance of a biosensor using both a spectrometer and a PMT. The study found that using a PMT for detection improved the signal-to-noise ratio by approximately 2.6 times. This high sensitivity of the PMT was crucial for detecting low concentrations of sorbitol that were undetectable by the spectrometer.

2.4.2 Avalanche Photodiodes (APDs)

An avalanche photodiode is a semiconductor device used for converting light into an electrical current. The initial concept for the APD originated from the seminal work of Jun-ichi Nishizawa in the 1950s, who proposed the avalanche multiplication effect in semiconductors. In the following decade, research in semiconductor materials, particularly silicon and germanium, led to the development of more efficient photodiodes and early versions of APDs [170]. By the late 1980s and early 1990s, APDs had become commercially available, thanks to significant advancements in semiconductor fabrication [170]. Since then, APDs have continued to undergo further development to improve sensitivity, speed, reduce noise, and increase bandwidth [174-176]. These properties have made APDs suitable for use in several industries and technologies, including telecommunications, light detection and ranging (LiDAR), and medical imaging [174-176].

Similar to PMTs, APDs offer high sensitivity and gain [175]. Additionally, APDs generally have high quantum efficiency due to their intrinsic design and material properties. Since APDs internally amplify current through impact ionization, charge carriers are contained and can efficiently interact with other atoms in the depletion region. This mechanism also results in fast response times, making APDs suitable for high-speed detection applications [175]. Furthermore, optimization of the depletion region and electric field reduces the probability of electron-hole recombination, leading to greater charge accumulation [177]. For optimal photoemission, semiconductor materials can be tailored for specific wavelengths of light with high absorption to promote charge carrier generation [175].

The internal gain mechanism of APDs, while providing many benefits, is also responsible for the amplification noise associated with APDs [175]. Unlike the predictable gain offered by PMTs, impact ionization in APDs is stochastic. Thus, while impact ionization amplifies the signal current, it also generates statistical noise known as Poisson noise. APDs are also limited in maximum gain. Since a high reverse-bias voltage must be applied to the p-n junction for impact ionization, APDs are limited by the breakdown voltage of the diode. This issue has been addressed to some degree in Geiger-mode Single-Photon APDs (SPADs). However, while APDs operate as linear amplifiers, SPADs operate using a very strong electric field to trigger self-sustaining impact ionization that is quenched to stop the avalanche process and given time to recover [178]. Thus, SPADs must operate at a lower count rate to produce single-photon detection events as signal pulses.

A whole-cell bioluminescent sensor for detecting E. coli presented by Daniel *et al.* used an SPAD for signal detection [179]. While PMTs were considered for this application, it was determined that PMTs were too large and unsuited for mobile biosensing applications, and relatively expensive compared to SPADs. As a silicon-based photon counting element, SPADs could also be integrated with the signal processing unit, allowing for compact sensor integration. A similar bioluminescent sensor also used an SPAD for the detection of E. coli [180]. This study also considered PMTs as well as charge-coupled devices (CCDs) as alternative detectors but ultimately selected SPADs due to their high quantum efficiency, relatively low cost, and low operating voltage. The sensor was integrated into a small lightproof container to create a compact bioluminescent biosensor. Performance testing of the sensor demonstrated a proportional increase in SPAD readout with the concentration of generated oxyluciferin, indicating an increase in E. coli activity.

2.4.3 Plate Readers

For measuring individual samples, PMTs and APDs provide a sensitive, high-gain, fast, and low-noise tool for light measurement. However, as point detectors, scaling to larger sample sizes proves to be challenging, with low throughput and a labor-intensive and time-consuming process. To resolve this, the multiplexed integration of PMTs into plate readers can significantly improve the viability of PMTs in higher-throughput applications.

The first plate readers appeared in the 1970s as simple devices designed primarily to measure absorbance for colorimetric assays [181, 182]. Future innovations soon incorporated additional detection modes, including fluorescence and luminescence assays [183, 184]. Fast-forwarding to the modern era, current plate reading devices feature several improvements, including automation, user-friendly software integration, and multi-unit detectors, to meet the demands of drug discovery, clinical diagnostics, and life science use cases [184, 185].

Plate readers are widely used in laboratories for their efficiency and versatility in high-throughput screening, enzyme-linked immunosorbent assays (ELISAs), and other biochemical assays. One of the primary advantages of plate readers is their ability to rapidly process multiple samples simultaneously, significantly increasing productivity and data throughput [186]. They offer high sensitivity and accuracy in detecting absorbance, fluorescence, and luminescence, which are essential for quantitative analyses [187]. Additionally, their automation capabilities reduce human error and variability, enhancing the reproducibility and reliability of results

[188]. However, plate readers also have drawbacks. The initial cost of purchasing a plate reader can be substantial, and the maintenance and calibration required to ensure accurate readings can be time-consuming and expensive [189]. Furthermore, most of old plate readers may not be suitable for all types of assays, particularly those requiring real-time kinetic measurements, where more specialized equipment might be needed [185]. Thus, plate readers are generally ill-suited for POC and PON applications.

2.4.4 Optical image sensors

Image sensors consist of an array of point photodetectors that form pixels, the smallest spatially resolvable units with submicron size in state-of-the-art technologies, enabling spatial resolution. The structure of image sensors involves an array of microlens at the top, followed by a color filter, photodiodes, and electronic components for converting the collected photons into electrical currents [190, 191]. The layer of microlenses at top of the pixel array focuses incoming light onto the photodiodes, enhancing the fill factor determined by the ratio of a pixel's photosensitive area to its total area. The mosaic color filter array commonly adopts a Bayer filter arrangement with 1:2:1 ratio of red (R), green (G) and blue (B) to separate the incoming light into RGB color channels, enabling color resolution. Since its invention in 1980, the pinned photodiode (PPD) has been widely adopted in most image sensors [192]. In a PPD, a thin p-type layer located on top of the n-type region of the photodiode stabilizes the surface potential of the photodiode, resulting in lower noise, higher quantum efficiency, and lower dark current [192]. Electronic components transform incoming photons into voltage signals, with amplifiers to increase signal-to-noise ratio and enhance dynamic range, while analog-to-digital converters (ADCs) transform the voltage signals into digital values, and digital I/O and column decoder store and output the digitized results [193].

The two main types of image sensors are charge-coupled devices (CCDs) and complementary metal-oxide-semiconductor (CMOS) image sensors. CCDs and CMOS image sensors differ fundamentally in their architecture and signal readout mechanisms, with CCDs built on p-doped metal-oxide-semiconductor (MOS) capacitors and CMOS image sensors using p and n-doped MOS field-effect transistor (MOSFET).

2.4.4.1 Charge Coupled Devices (CCDs)

The CCD image sensor was the first solid-state image sensor developed. After CCDs were invented in 1969 at Bell Labs by Boyle and Smith [194], the first CCD image sensor was

reported in 1970 [195]. A CCD consists of an array of connected capacitors that transfers electric charge to neighboring capacitors. The electric charge is generated when photons hit the photoactive area of the capacitor array and subsequently transferred across the series of capacitors [196]. A common readout point with a charge amplifier is located after the last capacitor to convert the charge into a readable voltage [196]. The use of a common readout point outside of the pixels and reduced circuitry in each pixel of CCD contributes to a high fill factor, leading to better photon collection efficiency that creates higher image quality with lower noise. However, CCDs suffer from slower readout speed and consume more power due to the continuous sequential charge transfer process. Since CCDs generally provide superior image quality and better performance in low-light conditions, they are ideal for applications such as astronomy, professional photography, and medical imaging [197].

2.4.4.2 Complementary Metal-Oxide Semiconductors (CMOS) sensors

CCDs require high charge transfer performance, leading to several challenges, including manufacturing difficulties and issues with operating at low temperatures and high frame rates [198]. An active pixel sensor (APS), where each pixel is equipped with a transistor, can overcome these inherent problems with CCDs [198]. The first CMOS image sensor using APS was invented in the mid-1990s by Fossum *et al.* at NASA Jet Propulsion Laboratory [199]. PMOS and NMOS transistors exhibit low electrical resistance between their source and drain when a low and high voltage is applied, respectively. Therefore, connecting the sources and drains of PMOS and NMOS transistors in CMOS transistors results in reduced electrical resistance across broader applied voltage range, leading to lower power consumption and less heat generation which contribute to reduced noise [200].

CMOS image sensors were initially front-side illuminated (FSI), where the photodiodes are located below the electronic interconnects. Newer generations of CMOS image sensors have adopted back-side illumination (BSI) by placing the photodiodes above the interconnects to enhance the photon collection efficiency [201]. The state-of-the-art technology in the new generation of CMOS image sensors includes notable advancements such as PureCel®Plus Technology. This technology advances CMOS image sensors through several key innovations, including the implementation of a buried color filter array (BCFA) and deep trench isolation (DTI)[202]. The BCFA significantly enhances the ability to capture light from various incident angles. Meanwhile, DTI minimizes crosstalk by creating isolation walls between pixels within the silicon, thereby improving chief ray angle (CRA) tolerance. The second generation of

PureCel®Plus further refines DTI for superior pixel isolation and enhanced low-light performance. Additionally, composite metal grid (CMG) technology boosts pixel sensitivity by forming walls above the silicon surface, which further reduces pixel color crosstalk. These advancements collectively contribute to superior image quality, making PureCel®Plus Technology a leading innovation in CMOS image sensor technology.

Unlike CCDs, CMOS image sensors have individual readout circuits on each pixel, enabling faster, parallel readout of image data with lower power consumption as well as random access to pixel information [201]. Although the pixel-level readout circuitry in CMOS image sensors reduces the area available for photon capture compared to CCDs, resulting in historically lower signal-to-noise ratio, advancements such as BSI have significantly improved their performance, offering comparable image quality. Since CMOS image sensors are more power-efficient, they are suitable for portable devices that are battery-powered such as smartphones [203] and cameras. CMOS image sensors also offer faster readout speeds and greater flexibility in data handling, making them ideal for high-speed imaging and applications requiring rapid real-time processing. These characteristics make CMOS image sensors ideal optical readers for POC biosensors where portability and fast readout are essential.

2.5 Parameters that affect the analytical performance of a biosensor.

Biosensors are analytical devices that exploit biological or chemical reactions to generate measurable signals proportional to the concentration of a target analyte within a sample. The analytical performance of biosensors is influenced by various parameters, which can be categorized into two main groups: experimental parameters and component parameters [204]. Experimental parameters include factors such as applied potential, scan rate, frequency range, pH, temperature, incubation time, analyte concentration, and mixing speed. Each of these parameters plays a crucial role in determining the sensitivity, selectivity, and overall efficiency of the biosensor [204]. For instance, the applied potential can affect the electron transfer processes, while the scan rate influences the kinetics of the electrochemical reactions. The frequency range is pertinent in impedance-based biosensors, as it determines the response characteristics. Additionally, the pH and temperature conditions are critical, as they can alter the biochemical activity and stability of the biological recognition elements. Incubation time impacts the interaction between the analyte and the bioreceptor, and analyte concentration is directly related to the biosensor's detection limit and dynamic range. Lastly, the mixing speed

ensures homogeneity in the sample solution, thereby affecting the reproducibility and accuracy of the measurements.

The analytical performance of a biosensor is also intricately linked to several key component parameters. A typical biosensor system comprises three key components: biorecognition elements, transducers, and output systems. The selection of the transducer, which converts a physicochemical change into a measurable signal, is crucial. Common choices include electrochemical, optical, piezoelectric, and thermal devices, each offering specific signal conversion advantages [205]. Equally important is the selection of the biorecognition element, the biomolecule responsible for target recognition. Enzymes, antibodies, nucleic acids, and others can be employed depending on the specific analyte. The interaction between the target and the biorecognition element triggers a physicochemical change that the transducer can detect [206].

To ensure efficient target-biorecognition element interaction, a suitable immobilization technique must be chosen. Techniques such as adsorption, entrapment, encapsulation, covalent attachment, and cross-linking significantly influence the efficiency of immobilization and, consequently, the overall performance of the biosensor [207]. Furthermore, the selection of an appropriate support material is essential. Ideal support materials should possess excellent chemical and mechanical stability, offer reactive functional groups for biomolecule attachment, provide a high surface area, and exhibit inert, biocompatible, and cost-effective characteristics [208]. These materials can be broadly categorized as organic (e.g., alginate, chitosan) or inorganic (e.g., mesoporous silica, nanoparticles) [209]. Finally, additional constructional parameters include the selection and ratio of other biosensing components like crosslinkers, surfactants, and signal enhancers. The chosen coating method on the electrode surface (e.g., electrodeposition, drop-casting) also significantly affects the biosensor's performance [210, 211]. By carefully considering these constructional parameters, researchers can optimize biosensor design for superior analytical performance.

A biosensor's effectiveness hinges on its ability to accurately detect and quantify an analyte within a specific concentration range. This performance is governed by a complex interplay of factors affecting the linear range, sensitivity (represented by the slope of the linear range), and limit of detection (LOD).

Linear Range. The linear range, where the response correlates directly with analyte concentration, is influenced by bioreceptor properties [212]. High-affinity bioreceptors can lead to a narrower range due to rapid saturation at low concentrations. Conversely, lower affinity interactions might extend the range but compromise sensitivity [213-215]. The transducer's characteristics, particularly its sensitivity and dynamic range, also play a role. Highly sensitive transducers might exhibit a limited linear range. Surface coverage of bioreceptors can further impact this range, with higher densities causing faster saturation. Mass transport limitations, affecting analyte arrival at the sensor surface, can cause deviations from linearity at higher concentrations. Fortunately, strategies exist to manipulate the linear range. Signal amplification mechanisms can extend it by enhancing the sensor response at low concentrations. Additionally, sensor design considerations, such as geometry and size of the sensing element, can improve mass transport, leading to a wider linear range. Environmental factors like temperature, pH, ionic strength, and sample matrix interferences can also affect linearity. Optimizing these parameters is crucial for reliable measurements.

Sensitivity (slope of the Linear Range). The slope of the linear range, representing the sensitivity of the biosensor, is influenced by several factors. The affinity of the bioreceptor for the analyte directly impacts sensitivity, with high-affinity interactions producing a steeper slope. The efficiency of the transducer in converting biorecognition events into measurable signals is crucial; more efficient transducers generate larger signal changes per unit concentration of analyte, resulting in a steeper slope [216, 217]. Bioreceptor density on the sensor surface affects sensitivity, as higher densities enhance the likelihood of analyte binding. Signal amplification strategies, such as enzymatic reactions or nanoparticle use, increase sensor response, steepening the slope. The surface chemistry and immobilization methods employed can preserve bioreceptor functionality, optimizing sensitivity. Mass transport effects, ensuring efficient analyte delivery to the sensor surface, and minimizing diffusion limitations, also contribute to a steeper slope. Optimal environmental conditions and reduced interference from non-specific binding maintain a high sensitivity, while sensor design factors such as electrode material and surface area further influence the slope.

*Limit of Detection***.** The limit of detection (LOD) of a biosensor, indicating the lowest detectable analyte concentration, is determined by various factors. The signal-to-noise ratio (SNR) is critical, as a higher SNR allows better distinction of the analyte signal from background noise, lowering the LOD. Bioreceptor affinity and specificity enhance the detection of low analyte concentrations, improving the LOD. The transducer's intrinsic sensitivity also affects the LOD,

with more sensitive transducers detecting smaller signal changes. [218, 219]**.** Effective surface chemistry and immobilization techniques that maintain bioreceptor activity enhance the LOD. Signal amplification methods increase the generated signal per analyte molecule, lowering the LOD. Sample volume and pre-concentration techniques can improve the LOD by increasing the analyte molecules available for detection. Efficient mass transport to the sensor surface ensures that low analyte concentrations reach the bioreceptor sites, enhancing detection capabilities. Minimizing background interference and optimizing environmental conditions such as pH and temperature improve the bioreceptor-analyte interaction, lowering the LOD. Advanced data processing and analysis techniques further distinguish the signal from noise and compensate for background interference, improving the LOD.

The performance of optical biosensors, in particular, directly depends on the performance of the optical detector. As shown in Table 1, different types of optical detectors, such as PMT, APD, CCD, and CMOS sensors, exhibit distinct characteristics that affect their performance in biosensing applications. PMTs and APDs are highly sensitive with substantial gain, making them suitable for detecting low-intensity signals. CCDs and CMOS sensors, while less sensitive in comparison, offer sufficient sensitivity for most biosensing applications, with CMOS sensors improving rapidly in this aspect [220].

PMTs generally have low noise but can be affected by dark current and afterpulsing. APDs exhibit higher noise levels, particularly at high-gain settings. CCDs are known for their low noise, particularly when cooled, whereas CMOS sensors have historically had higher noise but are continually improving with technological advancements [222]. CCDs excel in providing a high dynamic range and full well capacity, allowing for the detection of both low and high signal intensities without saturation. CMOS sensors are catching up, offering a competitive dynamic range and full well capacity in modern designs. PMTs and APDs, while highly sensitive, can have limited dynamic ranges in comparison.

Table 1. Optical detectors and their characteristics

CHARACTERISTICS	**PMT**	**APD**	**Plate reader* (*PMT*)**	**CCD**	**CMOS**
Photosensitivity (A/W)	0.02-0.09	0.2-0.9	*0.02-0.09*	0.3-0.4	0.3-0.5
Gain	10^5-10^7	10-100	10^5-10^7	-----	-----
Dynamic Range (dB)	-----	-----	-----	60-90	50-70
Quantum Efficiency (%)	20-35	70-85	*20-25*	75-90	70-90
Dark Current** (nA)	0.5-5	0.1-100	*0.5-5*	10^{-10}-10^{-8}	10^{-8}-10^{-7}

Cost	Expensive	Moderate	Expensive	Moderate	Low
Power Consumption	High	Moderate	High	High	Low
Size/Portability	Bulky	Compact	Bulky	Compact	Compact
Multiplexing	No	No	Yes	Yes	Yes
POC	No	Yes	No	Yes	Yes

*Italicized specifications for plate reader are identical to PMT
**CCD and CMOS dark current per pixel calculated from e^-/p/s CMOS dark current calculated from DN/s to e^-/p/s with conversion factor. Specifications for PMT, APD, CCD, and CMOS were sourced from Hamamatsu datasheets. Website: https://www.hamamatsu.com/us/en.html [221]

By carefully optimizing these factors, the performance of biosensors can be significantly improved, allowing for more accurate and sensitive detection of target analytes across a range of applications.

2.6 Integration of chemiluminescence, optical image sensors, and microfluidic components

Any biosensing/bioimaging device requires a detector. For the system to be fully independent and stand-alone, this detector must be integrated with other components of the system.

Despite the excellent sensitivity of single-point detectors, achieved through electron multiplication or avalanche effects, their application at the point of care remains limited. Efforts have been made to integrate these detectors with optical fibers to extend their use beyond the laboratory [223], but challenges persist due to their high voltage requirements, size, and cost. As an alternative, integrating optical detectors with analytical sensors using cellphone cameras has been explored. As smartphones become increasingly powerful and abundant, the feasibility of adapting their features into point-of-care sensing applications grows, making smartphone-integrated CL biosensors an exciting opportunity for accessible, affordable, and effective health monitoring tools. Numerous studies have employed cellphone cameras as biosensor detectors [224-252]. However, the variability in camera quality, sensor types, and focal planes across different cellphone models necessitates additional calibration steps, hindering the widespread application of this approach. Additionally, in resource-poor areas, access to cellphones with high-quality cameras is often limited.

Traditional bioimaging relies on magnification via lenses to achieve high spatial resolution. Advancements in digital sensor technology have led to the development of lens-based digital imaging. This technique combines magnifying lenses with high-resolution digital sensors,

enabling rapid image acquisition and facilitating storage and processing. Notably, the convergence of CMOS image sensors, commonly found in mobile phones, with external magnifying lenses paves the way for portable and user-friendly microscopic imaging [203, 253, 254]. Lens-based imaging presents inherent trade-offs. Firstly, achieving high spatial resolution often comes at the expense of a reduced field of view (FOV) [255]. FOV denotes the total observable area captured by the sensor [203]. Secondly, lenses can introduce optical aberrations, manifesting as defocus and image distortion [253]. Finally, lens-based systems typically generate images with only intensity contrast, limiting the extraction of three-dimensional (3D) information. In contrast, lensless imaging overcomes limitations inherent to lens-based systems. It achieves aberration-free high-resolution images while preserving a large FOV. In lensless imaging, spatial resolution is defined by the image sensor's pixel size and signal-to-noise ratio (SNR). The FOV, on the other hand, is directly proportional to the active area of the image sensor, reaching up to 30 mm^2 for CMOS and 20 mm^2 for CCD sensors, with pixel sizes as small as 0.7 μm [200, 256]. For comparison, a conventional bench-top optical microscope equipped with a 10× objective lens (numerical aperture of 0.2) offers a limited field of view (FOV) of less than 4 mm^2 and a theoretical spatial resolution of 1.5 μm, significantly restricting the sample area captured in a single image [257]. Additionally, lensless digital holographic imaging provides the distinct advantage of acquiring depth-resolved 3D information. Moreover, the absence of lenses translates to enhanced portability and cost-efficiency for these systems.

Integrated lensless optical systems can be categorized into two main types based on the signal they detect from the sample: shadow-based systems and luminescence-based systems. Shadow-based systems record a signal representative of the sample's physical shape [190], while luminescence-based systems detect photons emitted by the sample. For enhanced ease and flexibility in sample handling, these two optical platforms were additionally integrated with optofluidic techniques. Within optofluidics, microfluidic devices enable precise manipulation of samples directly above the sensor arrays.

2.6.1 Integrated CL-based optical systems

Lensless luminescence imaging offers distinct advantages. This technique captures the luminescence emitted by the sample, leading to enhanced optical contrast. Additionally, it yields quantified results in the form of light intensity, enabling the calculation of analyte concentration [200].

CL-based lensless imaging offers a versatile approach for biomolecule quantification [130]. This technique relies on placing the sample directly on the image sensor surface and capturing light emitted during chemiluminescent reactions [258, 259]. CL imaging allows for the detection of various biomolecules, ranging from toxins [258] to disease markers [259], making it valuable for applications in food safety [42], diagnostics, and health monitoring. BL-based lensless imaging utilizes genetically engineered yeast or bacteria cells [260]. These cells express recognition elements that activate luciferase enzymes upon analyte interaction, leading to bioluminescence emission. The bioluminescent cells are then immobilized on or transferred to the image sensor's active area, enabling the capture of light emissions. Since the BL signal directly correlates with cell viability [261], lensless imaging systems capable of measuring BL can be powerful tools for drug research (toxicity detection) and environmental monitoring [262]. ECL-based lensless imaging involves capturing light emitted from an electrochemical process [98]. This process is driven by an electric field that creates excited states through energetic electron transfer reactions in molecules at electrode surfaces [263]. Unlike CL, which often requires catalysts for significant light emission, ECL reactions utilize the electric potential difference for a more controlled excited state formation. This controlled nature makes ECL advantageous over CL for applications in lensless contact imaging.

2.6.2 Integration of microfluidic components with optical systems

Microfluidic devices offer precise handling of small volumes of samples, making their application ubiquitous across various areas of biological sciences [264]. A microfluidic device mainly consists of inlets for introducing fluids, outlets for removing fluids, microchannels for guiding, separating, and mixing fluids, and chambers for retaining samples or facilitating reactions [265]. Fluid movement within a microfluidic device can be driven passively through capillary forces within the microchannels or actively using externally applied forces such as pressure from syringe pumps [266]. Additional elements such as valves and flow resistors can be incorporated to regulate the flow within the device.

Lensless image sensors can be integrated with microfluidic devices to facilitate sample manipulation through spatial and temporal control, while enabling capabilities such as multiplexing. In this configuration, the microfluidic device is bonded to the lensless image sensor, allowing the region of interest in the microfluidic device directly contact the active area of the image sensor. Samples and reagents are introduced into the microfluidic device through inlets, with the target analytes within the sample often remaining in chambers that are patterned

to physically capture them or functionalized with biorecognition elements to bind them. By surface functionalizing the chamber or adding reaction reagents, analyte-specific reactions can occur in the chamber, enabling analyte quantification by capturing and analyzing the resulting optical signals with the integrated image sensor. This integrated approach originated in 2005 by Lange *et al.*, who placed a microfluidic chamber containing Caenorhabditis elegans on a lensless CMOS image sensor to study the impact of spaceflight on its behavior [267]. Since then, the combination of microfluidic devices and lensless imaging has been adopted in various platforms, enabling the identification, quantification, and monitoring of cells and organisms as well as the detection of biological elements including metabolites, viruses, and proteins [42, 98, 99, 200].

Integrating microfluidics with image sensors combines the capabilities and advantages of both technologies. The microfluidic component allows for multiplexing through separate channels for different reactions, precise fluid handling with spatial and temporal control, low sample and reagent consumption due to small volume intake into the device, and a compact size. Meanwhile, image sensors enable quantification of target analytes by measuring the optical changes from the analyte-specific reactions happening in the microfluidic device. The combination results in lensless microfluidic imaging systems that are compact, provide high spatial resolution without compromising the FOV, and produce sensitive results due to the close sample to sensor proximity and high photon collection efficiency.

In lensless contact imaging, the proximity between the sample and the image sensor is critical for optimal performance. This technique can be implemented using either shadow-based or luminescence-based methods. Shadow-based imaging benefits from minimal diffraction artifacts and does not require complex image reconstruction, while luminescence-based imaging—including CL, ECL, and BL—provides enhanced optical contrast and quantitative analyte detection. In both cases, maintaining a minimal distance between the sample and the image sensor is essential for achieving high image clarity and maximizing light collection efficiency. To ensure close contact, the design of the microfluidic device must accommodate the topography of the image sensor. This can be challenging due to the size difference between sensor elements and microfluidic channels, but it can be managed by confining the microfluidic device within the sensor's active area or by embedding the sensor in a planarizing material to match the fluidic channel dimensions.

2.7 Applications of optical image-based sensors at point-of-care/need

2.7.1 Applications of integrated CL biosensors at point-of-care/need

Integrated optical biosensing technology offers several advantages over traditional microscopy, such as increased compactness, improved photon collection efficiency, and the elimination of complex image reconstruction steps. This technique is versatile, enabling applications like cell detection, classification, counting, and continuous monitoring [269-273]. Blood cell counting is particularly well-suited due to the portability and automation benefits compared to traditional methods like microscopy and flow cytometry [270-272, 274]. For instance, the ePetri platform exemplifies this versatility, allowing continuous monitoring of cells and microorganisms, including pathogen identification like waterborne parasites and malaria [273, 275-277].

Biomicrofluidics and optoelectronics further enhance biosensing capabilities by utilizing CL or ECL for the detection and quantification of metabolites, antibodies, proteins, viruses in bodily fluids, and antibiotic residues in food [98, 278-280]. These platforms hold significant implications for POC diagnostics and disease monitoring, such as uric acid measurement in saliva for gout diagnosis and choline concentration monitoring in blood for cancer and cardiovascular disease. The microfluidic channels in many platforms facilitated both the detection of flowing samples and subpixel spatial resolution by leveraging the sample's sub-pixel movements as it passed through the channel [275, 281-283].

Despite significant advances, optical transducers in fluorescence imaging-based biosensors remain limited by their dependence on specific light sources and the need for dedicated optical filters [284]. However, researchers have developed innovative solutions to address these challenges, such as shifting from fluorescence to chemiluminescence-based biosensors. One notable development is a CCD-based CL biosensor that simultaneously quantifies three targets: alkaline phosphatase, parvovirus B19 DNA, and horseradish peroxidase [259]. This was achieved by placing a transparent microfluidic reaction chip made of PDMS or glass slide in close proximity to a thermoelectrically cooled CCD sensor. A fiber optic taper facilitated the efficient transmission of light between the microfluidic chip and the image sensor [259, 285]. Additionally a photodiode array, consisting of 32 individual photodiodes arranged in a 4 x 8 grid configuration, was explored for its potential application in integrated CL microarray readout [286]. Since LFAs were the first option for point-of-care testing due to their portability and inexpensive components, there have been increased efforts to integrate them with image

sensors to create independent yet efficient analytical devices. In this context, aflatoxin B1 and type B-fumonisins have been detected in maize samples using a multiplex CL biosensor that integrates a multiplex indirect competitive LFA, enzymatic CL reaction, and lensless CCD image sensor [258]. Furthermore, the LFA-CL system was integrated with a CCD image sensor to detect ovalbumin and collagen. This LFA-CL system exhibited detection limits two orders of magnitude lower than those of a similar colorimetric system [287]. Building upon these advancements, a 3D-printed biosensor employing an LFA with CL detection was designed for the on-site analysis of salivary cortisol in astronauts [288]. This sensor incorporates a sealed microfluidic cartridge activated by buttons and capillary forces. Cortisol detection is achieved using a highly sensitive, cooled CCD camera-based CL reader. Despite these research developments, the commercialization of LFA-CL immunoassays faces challenges due to two key limitations: (1) limited bioreagent stability over time and (2) the need for manual reagent addition during the analytical process. These limitations hinder their ability to meet the demands of end-users [289].

Shifting focus from CL-based optical sensors, another study presented a novel bioluminescence ATP detection device utilizing a pixelated CMOS image sensor. This platform effectively assessed ATP levels following environmental swabs from various surfaces, including fast-food restaurant tables, kitchen counters, and personal cell phones. These findings highlight the potential of CMOS devices in the food safety industry, particularly for establishing standardized surface cleanliness protocols.[42]

In addition to CL and bioluminescence sensors, ECL based biosensors have also shown significant promise. One early example described a microfluidic microsystem that combined CMOS technology for high-resolution, direct-contact optical imaging of biochemical analyte reactions [290]. This microsystem utilized a two-layered, soft polymer microfluidic network integrated with a CMOS image sensor featuring a 64 × 128 pixel array to detect both CL and ECL of luminol/H_2O_2 reaction [290]. Similarly, a different study described a microfluidic platform integrating luminol/hydrogen peroxide ECL detection with a 5-megapixel CMOS image sensor on a single chip[98]. This design allows both sample manipulation and data acquisition on the same platform. Using a single electrode as the electrochemical transducer and a CMOS chip as the integrated detector, the applicability of this platform for detecting uric acid, a relevant biomarker for gout disease, was demonstrated [98].

Recent research describes advancements in single-electrode ECL (SE-ECL) configurations designed to enhance sensitivity, specificity, and compactness for integration with CMOS image sensors in analyte detection. By manipulating the electrical potentials applied to single electrodes within the electrochemical cell, researchers can selectively excite ECL luminophores to produce distinct emission colors (Fig.3i,j) [99]. This strategy employs a single-electrode design for color-coded ECL reactions, integrates microfluidic techniques for efficient sample handling, and utilizes a cost-effective CMOS image sensor to capture emitted light. These improvements show significant promise for developing miniaturized and highly accurate biosensors suitable for POC diagnostics in biomedical, food safety, and environmental monitoring applications.

Overall, integrated optical biosensing platforms offer powerful tools for live specimen imaging, POC diagnostics, and disease monitoring, with significant potential to impact biomedical research, healthcare, and beyond.

2.7.2 Limitations of integrated CL biosensors for point-of-care applications

Integrated optical biosensing platforms offer significant advantages for point-of-care diagnostics, such as portability, cost-effectiveness, and rapid imaging. However, their widespread adoption faces several challenges.

While integrated optical biosensing platforms can achieve reasonable resolution, they typically fall short of traditional lens-based microscopy for resolving fine details. High-resolution imaging requires sophisticated reconstruction algorithms, which can limit practical utility due to their computational intensity. The reliance on advanced algorithms can slow down data processing and necessitate significant computing power. Additionally, these platforms struggle to distinguish objects at different depths due to their relatively shallow depth of field. This limitation makes imaging thick samples or obtaining accurate 3D reconstructions challenging. Sample preparation is also critical, as the technique is sensitive to dust, debris, and bubbles. This meticulous preparation requirement may render integrated optical biosensing platforms unsuitable for certain sample types. Moreover, the field of view is limited due to the nature of the setup, and adjusting magnification is not as straightforward as in traditional microscopy. Despite these challenges, advancements in computational imaging, machine learning, and sample preparation techniques offer promising solutions to overcome these limitations. By addressing these challenges, integrated optical biosensing platforms can significantly enhance

their utility for point-of-care applications. [30, 291-293] The reusability of lensless sensors, such as those utilizing CMOS or CCD imaging chips, is dependent on the specific application and sensor design. Generally, these sensors are designed for multiple uses, though their longevity can be influenced by factors like sensor surface stability, sample nature, and required sensitivity. For example, in the case of chemiluminescence biosensors, it was observed that a CMOS sensor exhibited good reusability, with a low Relative Standard Deviation (RSD) in measurements after five uses, and maintained acceptable performance after ten uses [104]. Additionally, the affordability of CMOS chips, due to advancements in manufacturing, has made them suitable for use as disposable components in single-use biosensors, especially in point-of-care diagnostics. While CCD chips offer higher sensitivity and image quality, they are typically more expensive, and their use as disposable elements is more application-specific, depending on the required sensitivity and cost considerations.

Box 2 | Chemiluminescence-Based Biosensors: Types, Configurations, and Integration

Chemiluminescence (CL) is a phenomenon where light is emitted as a result of a chemical reaction. CL-based biosensors leverage this property to detect and quantify various analytes with high sensitivity and specificity. These biosensors are particularly valued for their ability to produce measurable optical signals without the need for external light sources.

Chemiluminescence (CL) biosensors include various phenomena, including chemiluminescence, bioluminescence, and electrochemiluminescence (ECL). **Chemiluminescence** biosensors utilize direct chemical reactions to emit light, while **Bioluminescence** biosensors employ biological molecules to produce light through biochemical reactions, often utilizing ATP assays for detecting cellular activity. **Electrochemiluminescence** biosensors combine electrochemical and chemiluminescent techniques to trigger light emission. Each type offers unique advantages: chemiluminescence biosensors are simple and highly sensitive, bioluminescence biosensors provide high specificity for detecting biological substances, particularly through ATP assays, and ECL biosensors offer precise control and high sensitivity for a wide range of applications.

ECL systems can be configured in various ways to optimize performance and application:

- *Three Electrode System*: Consists of a working electrode, a reference electrode, and a counter electrode. This configuration allows precise control over the electrochemical environment, enhancing the accuracy of measurements.
- *Bipolar Electrode System*: Utilizes a floating conductor, serving as both the anode and cathode, with the potential of the solution playing a crucial role in driving the redox reactions. This setup is advantageous for miniaturized and portable applications.
- *Single Electrode System*: Relies on a gradient potential over the surface of a single, partially conductive electrode, such as ITO. This configuration simplifies the design while still facilitating effective ECL reactions.

Optical signal detection in CL biosensors is achieved using *point detectors* and *pixelated detectors*.

- ***Point detectors***, such as Photomultiplier Tubes (PMT) and Avalanche Photodiodes (APD), convert light into electrical signals through the photoelectric effect and avalanche multiplication process, respectively, offering high sensitivity for weak light signals.

- ***Pixelated detectors***, including Charge-Coupled Devices (CCD) and Complementary Metal-Oxide-Semiconductor (CMOS) sensors, use arrays of photodiodes to capture light and produce high-resolution images. CCDs provide excellent sensitivity and image quality, while CMOS sensors are favored for their low power consumption, faster readout speeds, and cost-effectiveness, enhancing their suitability for portable and point-of-care devices.

The integration of CL biosensors with microfluidic technologies and CMOS sensors has led to significant advancements. **Microfluidic** systems, often referred to as lab-on-a-chip (LOC) platforms, enable the miniaturization and automation of assays, reducing sample and reagent volumes and enhancing reaction efficiency. **CMOS image sensors** provide high-resolution imaging, enabling spatially resolved measurements and the simultaneous detection of multiple analytes. The combined system offers compactness, portability, and the potential for point-of-care diagnostic applications.

2.8 Landscape and outlook of optical image sensors and machine learning in analytical chemiluminescence biosensors

The development of biosensors has seen remarkable progress, marked by distinct generations, each introducing significant advancements. The first generation of biosensors utilized natural receptors such as enzymes, antibodies, and cells as biorecognition elements. These elements interacted with target analytes to generate a signal, which was then converted by a transducer into a measurable and identifiable form. [294]

In the second generation, the focus shifted towards enhancing the transducer itself. By incorporating nanomaterials to modify the transducer surface, there was a marked improvement in sensitivity and signal amplification. This era also saw the miniaturization of biosensors, making them suitable for point-of-care and portable applications. [294, 295]

The third generation introduced the capability of simultaneous detection of multiple analytes, achieved through direct signal transfer between transducers and analytes. This advancement significantly improved the specificity and sensitivity of biosensors. The fourth generation further integrated nanotechnology, the Internet of Things (IoT), and bioinspired biomimetic materials [296] with microfluidic platforms. This integration enabled real-time monitoring of biological processes, resulting in instantaneous measurements. Wearable and implantable devices became more prevalent, with Lab-on-Chip platforms exemplifying this generation. [294, 295, 297]

Looking to the future, the fifth generation of biosensors, illustrated by the concept of a hospital-on-chip, is expected to refine existing technologies even further. The sixth generation will

likely incorporate 6G networks and holographic technology into microfluidic systems, potentially leading to innovations such as surgery-on-chip. The Internet of Medical Things (IoMT) will also expand applications in telemedicine.[294, 295, 297]

A rapidly growing field within optical biosensing is quantum sensing, which leverages quantum phenomena like quantum interference, entanglement, and coherence to detect physical properties such as temperature, electromagnetic fields, and strain. Quantum materials can significantly enhance the precision of conventional analytical observations. Numerous quantum biosensors have already been developed for disease diagnosis, and integrating quantum biosensing with fifth and sixth-generation technologies promises novel and exciting possibilities. [295, 298]

The future of quantum biosensing holds transformative potential. Anticipated advancements include unprecedented sensitivity, enabling the detection of minute biomarker concentrations, which could revolutionize early disease detection and monitoring, significantly improving patient outcomes. Integrating quantum biosensing with nanotechnology is expected to lead to the miniaturization of devices, enhancing portability and making them suitable for wearable applications. These developments promise a shift towards user-friendly, cost-effective, and rapid POC applications, marking a paradigm shift in disease diagnosis and monitoring. [295, 298]

Despite these advancements, traditional laboratory assays still outperform POC testing in terms of reliability and accuracy. The integration of machine learning (ML) methods into POCT offers an opportunity to bridge this gap. ML can improve sensor reliability and accuracy in real sample measurements. Smartphone applications integrated with ML algorithms could provide direct readouts of POCT biosensors, potentially pushing these technologies towards home-testing and self-testing scenarios. [299]

Single-molecule detection presents significant challenges due to poor signal-to-noise ratios, signal overlap, and dispersive signals. In single-molecule sequencing biosensors, large datasets must be analyzed, and traditional hypothesis-driven data exploration may miss unexpected signals. ML methods can reduce noise and extract multidimensional signal features, improving pattern recognition resolution and sensitivity in single-molecule biosensors. [299, 300]

The combination of wearable biosensors and ML presents a significant opportunity for health monitoring. Wearable biosensors can noninvasively monitor human physiology through

various biological fluids, such as sweat, tears, and saliva. The vision is to integrate a series of sensor networks on flexible patches that continuously monitor biomarkers. ML can parse time-series data from multiplexed sensors to identify health states. However, ML in these applications must be explainable rather than a black-box system. Medical professionals and decision-makers must understand machine decisions, and incorporating human knowledge and reasoning into deep learning systems can enforce and regulate the learning process, reducing the sample size needed for training. [299, 301, 302]

Like other optical biosensors, the development of chemiluminescence biosensors, particularly ECL microscopy, has also shown significant promise. ECL microscopy combines the high sensitivity of electrochemical methods with the spatial resolution of microscopy, making it a powerful tool for visualizing biochemical and cellular processes at a molecular level. This technique has been employed in two experimental configurations: positive ECL (PECL) and shadow ECL (SECL) [303]. In PECL, the imaged object generates ECL directly or is labeled with an ECL-active luminophore, resulting in a bright image against a dark background. SECL, a label-free method, produces a dark image of the object against a bright background by blocking the diffusional flow of the luminophore and co-reactant towards the electrode surface. Both configurations mitigate issues of photobleaching and phototoxicity associated with classical microscopy techniques, contributing to the detailed and precise investigation of various biological systems and reactions. Integrating the advancements in ECL microscopy with the innovative technologies in optical biosensing could further enhance the capabilities and applications of biosensors in biomedical research and clinical diagnostics.

The landscape of optical biosensors is rapidly evolving, with each generation bringing significant advancements in technology and functionality. Quantum sensing and machine learning integration are poised to revolutionize biosensing further, enhancing sensitivity, specificity, and usability. These developments herald a future where disease diagnosis and monitoring are more precise, portable, and accessible, paving the way for groundbreaking advancements in healthcare.

Despite these advancements, traditional laboratory assays still outperform POC testing in terms of reliability and accuracy. The integration of machine learning (ML) methods into POCT offers an opportunity to bridge this gap. ML can improve sensor reliability and accuracy in real sample measurements. Smartphone applications integrated with ML algorithms could provide

direct readouts of POCT biosensors, potentially pushing these technologies towards home-testing and self-testing scenarios. [305]

Single-molecule detection presents significant challenges due to poor signal-to-noise ratios, signal overlap, and dispersive signals. In single-molecule sequencing biosensors, large datasets must be analyzed, and traditional hypothesis-driven data exploration may miss unexpected signals. ML methods can reduce noise and extract multidimensional signal features, improving pattern recognition resolution and sensitivity in single-molecule biosensors. [305, 309]

Building on these advancements, the application of ML in enhancing CL and ECL biosensors has garnered significant attention. In the following sections, recent progress in integrating ML techniques with ECL and CL biosensors will be reviewed, highlighting how these approaches can improve sensor performance, data analysis, and ultimately, the practical implementation of these technologies in various testing scenarios.

2.8.1 Machine Learning-Assisted ECL Sensing

Electrochemiluminescence (ECL) sensing offers a powerful technique for detection due to its high signal-to-noise ratio [304]. Traditionally, researchers relied on analyzing ECL data directly. However, recent advancements leverage the power of machine learning (ML) to extract valuable insights from images captured by smartphone cameras. The intensity of light in these images correlates directly with the target analyte's concentration [305, 306].

The field of healthcare diagnostics is a prime beneficiary of this integration. ECL assays are highly sensitive and specific, making them ideal for biomarker detection in body fluids. Early and accurate diagnosis is crucial for effective patient management, and ML-assisted ECL holds significant promise in achieving this goal. Studies have shown that ML techniques can improve detection accuracy in ECL-based assays for various analytes, including glucose, lactate, and choline [307].

Researchers have also explored ML-assisted ECL for environmental and food safety applications. For instance, one study employed a portable molecularly imprinted polymer ECL system with smartphone camera capture and artificial neural networks (ANNs) to detect nitrofurazone, a banned carcinogen [246]. Similarly, another study utilized convolutional neural networks (CNNs) to analyze images from an ECL system designed to detect the harmful

pesticide 2,4-Dichlorophenoxyacetic acid (2,4-D) [238]. These examples showcase the versatility of the approach for diverse analytes.

Recent advancements have even extended ML-assisted ECL to the realm of infectious diseases. In response to the COVID-19 pandemic, researchers developed an ML-assisted ECL immunosensor for SARS-CoV-2 detection [308]. This sensor was designed to provide user-friendly readouts comparable to RT-PCR CT values, a familiar metric for healthcare professionals.

Overall, the synergy between ML and ECL sensing is demonstrably powerful. By leveraging image analysis capabilities, this approach offers enhanced accuracy, user-friendliness, and broader applicability across various detection fields, particularly in healthcare diagnostics.

2.8.2 Machine Learning-Assisted Chemiluminescence and Bioluminescence Sensing

Light-emitting luminescence techniques offer valuable tools for analytical detection. Chemiluminescence (CL), where a chemical reaction excites molecules leading to light emission, avoids limitations of fluorescence (FL) like scattering and background noise [309, 310]. However, CL suffers from high blank signals and interference from other oxidants and quenchers [311, 312].

One study explored CL's potential for profiling phenolic compounds in wine using a machine learning-assisted assay. Capitalizing on CL's established role in evaluating food antioxidants, researchers employed neural network regression models (NNRMs) to detect phenolic compounds within a wide concentration range (5 μmol dm^{-3} to 2 mol dm^{-3}) [313].

Bioluminescence (BL), a subclass of CL, involves light emission by organisms like fireflies. It offers advantages such as minimal background signal, low required analyte concentration, and high sensitivity due to enzymatic turnover. However, its limitations include dependence on advanced molecular biology techniques for large-scale production of recombinant enzymes [48, 314].

While ML-aided BL detection is still less explored compared to other strategies, recent research demonstrates promising applications. A study employed a whole-cell sensing array with genetically modified E. coli strains, each expressing a bioluminescence reporter system. This system allowed detection and classification of various antibiotics based on unique bioluminescence patterns [315]. The patterns were processed into different indices and used to

train a Multiclass Decision Forest (MDF) model. This approach achieved over 70% accuracy in classifying eight antibiotics and could even categorize unknown antibiotics based on known samples.

Another study utilized a bioluminescent bacterial system to detect water contaminants. Here, a multilayer perceptron model was trained on light emission kinetics in response to different contaminants, showcasing promising results for rapid detection [316].

Despite the limited number of published studies on ML-assisted CL and BL detection, these examples highlight the exciting potential of this approach for enhancing sensing and biosensing capabilities.

2.9 Conclusions

The integration of optical biosensors into lab-on-a-chip (LOC) platforms represents a significant advancement in the field of analytical biochemistry, enabling precise, real-time detection of various analytes at the point of need. These integrated systems leverage optical phenomena such as fluorescence, chemiluminescence, and electrochemiluminescence to provide high sensitivity and specificity in biomolecular detection. By combining these optical biosensors with microfluidic technologies, it is possible to achieve rapid and efficient sample handling, reducing the overall assay time and minimizing sample volumes.

A crucial development in this field is the coupling of optical biosensors with pixelated image sensors, such as CMOS image sensors, which offer significant advantages over traditional single-point detectors. CMOS image sensors provide high-resolution imaging capabilities, allowing for the simultaneous detection of multiple analytes across a wide field of view. Their pixelated nature enables spatially resolved measurements, which is particularly beneficial for applications requiring detailed mapping and analysis of complex biological samples. Additionally, CMOS sensors are known for their low power consumption, compact size, and cost-effectiveness, making them ideal for integration into portable and point-of-need diagnostic devices.

The development of fully integrated optical biosensors has shown promising results in various applications, including medical diagnostics, environmental monitoring, and food safety. These systems are not only efficient and effective but also pave the way for more widespread and accessible diagnostic solutions.

Looking forward, several exciting developments are anticipated to shape the future of integrated optical biosensors. One of the key areas of growth is the incorporation of machine learning algorithms to enhance the data analysis and interpretation capabilities of these biosensors. Machine learning can facilitate the processing of complex datasets, identify patterns, and provide predictive analytics, thereby improving the accuracy and reliability of biosensor outputs.

Advancements in microfluidic technology are expected to further refine the integration process, allowing for more complex and multifunctional LOC platforms. Innovations in material science and nanotechnology will likely contribute to the development of more sensitive and selective biosensors, expanding their range of detectable analytes and improving their performance in diverse environments.

Additionally, the continued miniaturization and integration of optical components, coupled with advancements in portable power sources and wireless communication technologies, will enable the development of truly portable and user-friendly point-of-need diagnostic devices. These devices will be particularly valuable in resource-limited settings, providing essential diagnostic capabilities without the need for extensive laboratory infrastructure.

In summary, the future of fully integrated optical biosensors holds immense potential, driven by advancements in microfluidics, material science, and machine learning. These innovations will pave the way for more sophisticated, efficient, and accessible diagnostic tools, revolutionizing point-of-need applications across various fields.

2.10 Acknowledgment

This work was financially supported by the National Sciences and Engineering Research Council of Canada (NSERC), Discovery Grant RGPIN-2018-05675, and Louis-Ho Scholarship in Technological Innovation from the Faculty of Engineering, McGill University. RA acknowledges funding from the McGill Engineering Doctoral Award (MEDA) and Fonds de Recherche du Quebec - Nature et Technologies (FRQNT) for doctoral studies. McGill University Faculty of Engineering provided financial support to APZ (SURE internship). Gratitude is extended to Pouria Tirgarbahnamiri for his invaluable assistance in reviewing the manuscript and enhancing the language.

2.11 Conflict of Interest

RA, XH and SWH are co-founders of a 2023 McGill spinoff company, Phoela Health Inc.

2.12 References

[1] W. R. de Araujo, H. Lukas, M. D. T. Torres, W. Gao, and C. de la Fuente-Nunez, "Low-Cost Biosensor Technologies for Rapid Detection of COVID-19 and Future Pandemics," *ACS Nano,* vol. 18, no. 3, pp. 1757-1777, 2024/01/23 2024, doi: 10.1021/acsnano.3c01629.

[2] M. G. Jiménez-Rodríguez, F. Silva-Lance, L. Parra-Arroyo, D. A. Medina-Salazar, M. Martínez-Ruiz, E. M. Melchor-Martínez, M. A. Martínez-Prado, H. M. N. Iqbal, R. Parra-Saldívar, D. Barceló, and J. E. Sosa-Hernández, "Biosensors for the detection of disease outbreaks through wastewater-based epidemiology," (in eng), *Trends Analyt Chem,* vol. 155, p. 116585, Oct 2022, doi: 10.1016/j.trac.2022.116585.

[3] J. Cheon, J. Qin, L. P. Lee, and H. Lee, "Advances in Biosensor Technologies for Infection Diagnostics," *Accounts of Chemical Research,* vol. 55, no. 2, pp. 121-122, 2022/01/18 2022, doi: 10.1021/acs.accounts.1c00647.

[4] F. S. Rodrigues Ribeiro Teles, L. A. Pires de Távora Tavira, and L. J. Pina da Fonseca, "Biosensors as rapid diagnostic tests for tropical diseases," *Critical Reviews in Clinical Laboratory Sciences,* vol. 47, no. 3, pp. 139-169, 2010/06/01 2010, doi: 10.3109/10408363.2010.518405.

[5] P.-H. Lin, S.-C. Sheu, C.-W. Chen, S.-C. Huang, and B.-R. Li, "Wearable hydrogel patch with noninvasive, electrochemical glucose sensor for natural sweat detection," *Talanta,* vol. 241, p. 123187, 2022/05/01/ 2022, doi: https://doi.org/10.1016/j.talanta.2021.123187.

[6] H. Zafar, A. Channa, V. Jeoti, and G. M. Stojanović, "Comprehensive Review on Wearable Sweat-Glucose Sensors for Continuous Glucose Monitoring," (in eng), *Sensors (Basel),* vol. 22, no. 2, Jan 14 2022, doi: 10.3390/s22020638.

[7] R. B. Rakhi, P. Nayak, C. Xia, and H. N. Alshareef, "Novel amperometric glucose biosensor based on MXene nanocomposite," *Scientific Reports,* vol. 6, no. 1, p. 36422, 2016/11/10 2016, doi: 10.1038/srep36422.

[8] N. Verma and A. Bhardwaj, "Biosensor Technology for Pesticides—A review," *Applied Biochemistry and Biotechnology,* vol. 175, no. 6, pp. 3093-3119, 2015/03/01 2015, doi: 10.1007/s12010-015-1489-2.

[9] T. O. Hara and B. Singh, "Electrochemical Biosensors for Detection of Pesticides and Heavy Metal Toxicants in Water: Recent Trends and Progress," *ACS ES&T Water,* vol. 1, no. 3, pp. 462-478, 2021/03/12 2021, doi: 10.1021/acsestwater.0c00125.

[10] S. Gavrilaș, C. Ursachi, S. Perța-Crișan, and F. D. Munteanu, "Recent Trends in Biosensors for Environmental Quality Monitoring," (in eng), *Sensors (Basel),* vol. 22, no. 4, Feb 15 2022, doi: 10.3390/s22041513.

[11] M. Marin, M. V. Nikolic, and J. Vidic, "Rapid point-of-need detection of bacteria and their toxins in food using gold nanoparticles," *Comprehensive Reviews in Food Science and Food Safety,* vol. 20, no. 6, pp. 5880-5900, 2021, doi: https://doi.org/10.1111/1541-4337.12839.

[12] A. A. Ali, A. B. Altemimi, N. Alhelfi, and S. A. Ibrahim, "Application of Biosensors for Detection of Pathogenic Food Bacteria: A Review," (in eng), *Biosensors (Basel),* vol. 10, no. 6, May 30 2020, doi: 10.3390/bios10060058.

[13] R. Abbasi, M. Imanbekova, and S. Wachsmann-Hogiu, "On-chip bioluminescence biosensor for the detection of microbial surface contamination," (in eng), *Biosens Bioelectron,* vol. 254, p. 116200, Jun 15 2024, doi: 10.1016/j.bios.2024.116200.

[14] S. V. Hamidi, A. K. Jahromi, I. I. Hosseini, R. S. Moakhar, C. Collazos, Q. Pan, C. Liang, and S. Mahshid, "Surface-Based Multimeric Aptamer Generation and Bio-Functionalization for Electrochemical Biosensing Applications," *Angewandte Chemie International Edition,* vol. n/a, no. n/a, p. e202402808, doi: https://doi.org/10.1002/anie.202402808.

[15] A. A. Akhlaghi, H. Kaur, B. R. Adhikari, and L. Soleymani, "Editors' Choice—Challenges and Opportunities for Developing Electrochemical Biosensors with Commercialization Potential in the Point-of-Care Diagnostics Market," *ECS Sensors Plus,* vol. 3, no. 1, p. 011601, 2024/03/14 2024, doi: 10.1149/2754-2726/ad304a.

[16] P. Damborský, J. Švitel, and J. Katrlík, "Optical biosensors," (in eng), *Essays Biochem,* vol. 60, no. 1, pp. 91-100, Jun 30 2016, doi: 10.1042/ebc20150010.

[17] C. Chen and J. Wang, "Optical biosensors: an exhaustive and comprehensive review," *Analyst,* 10.1039/C9AN01998G vol. 145, no. 5, pp. 1605-1628, 2020, doi: 10.1039/C9AN01998G.

[18] S. Geschwindner, J. F. Carlsson, and W. Knecht, "Application of Optical Biosensors in Small-Molecule Screening Activities," *Sensors,* vol. 12, no. 4, pp. 4311-4323, 2012. [Online]. Available: https://www.mdpi.com/1424-8220/12/4/4311.

[19] V. M. N. Passaro, F. Dell'Olio, B. Casamassima, and F. De Leonardis, "Guided-Wave Optical Biosensors," *Sensors,* vol. 7, no. 4, pp. 508-536, 2007. [Online]. Available: https://www.mdpi.com/1424-8220/7/4/508.

[20] G. Conant, B. F. L. Lai, R. X. Z. Lu, A. Korolj, E. Y. Wang, and M. Radisic, "High-Content Assessment of Cardiac Function Using Heart-on-a-Chip Devices as Drug Screening Model," *Stem Cell Reviews and Reports,* Article vol. 13, no. 3, pp. 335-346, 2017, doi: 10.1007/s12015-017-9736-2.

[21] D. Yang, A. Singh, H. Wu, and R. Kroe-Barrett, "Comparison of biosensor platforms in the evaluation of high affinity antibody-antigen binding kinetics," *Analytical Biochemistry,* vol. 508, pp. 78-96, 2016/09/01/ 2016, doi: https://doi.org/10.1016/j.ab.2016.06.024.

[22] D. Bhatta, E. Stadden, E. Hashem, I. J. G. Sparrow, and G. D. Emmerson, "Multi-purpose optical biosensors for real-time detection of bacteria, viruses and toxins," *Sensors and Actuators B: Chemical,* vol. 149, no. 1, pp. 233-238, 2010/08/06/ 2010, doi: https://doi.org/10.1016/j.snb.2010.05.040.

[23] L. A. Terry, S. F. White, and L. J. Tigwell, "The Application of Biosensors to Fresh Produce and the Wider Food Industry," *Journal of Agricultural and Food Chemistry,* vol. 53, no. 5, pp. 1309-1316, 2005/03/01 2005, doi: 10.1021/jf040319t.

[24] Q. Huang, F. Luo, C. Lin, J. Wang, B. Qiu, and Z. Lin, "Electrochemiluminescence biosensor for thrombin detection based on metal organic framework with electrochemiluminescence indicator embedded in the framework," *Biosensors and Bioelectronics,* vol. 189, p. 113374, 2021/10/01/ 2021, doi: https://doi.org/10.1016/j.bios.2021.113374.

[25] G. G. Morbioli, T. Mazzu-Nascimento, A. M. Stockton, and E. Carrilho, "Technical aspects and challenges of colorimetric detection with microfluidic paper-based analytical devices (μPADs) - A review," *Analytica Chimica Acta,* vol. 970, pp. 1-22, 2017/06/01/ 2017, doi: https://doi.org/10.1016/j.aca.2017.03.037.

[26] T. AbdElFatah, M. Jalali, S. G. Yedire, I. I. Hosseini, C. del Real Mata, H. Khan, S. V. Hamidi, O. Jeanne, R. Siavash Moakhar, M. McLean, D. Patel, Z. Wang, G. McKay, M. Yousefi, D. Nguyen, S. M. Vidal, C. Liang, and S. Mahshid, "Nanoplasmonic amplification in microfluidics enables accelerated colorimetric quantification of nucleic acid biomarkers from pathogens," *Nature Nanotechnology,* vol. 18, no. 8, pp. 922-932, 2023/08/01 2023, doi: 10.1038/s41565-023-01384-5.

[27] R. A. Mahmud, R. H. Sagor, and M. Z. M. Khan, "Surface plasmon refractive index biosensors: A review of optical fiber, multilayer 2D material and gratings, and MIM

configurations," *Optics & Laser Technology,* vol. 159, p. 108939, 2023/04/01/ 2023, doi: https://doi.org/10.1016/j.optlastec.2022.108939.

[28] A. Sharma, M. Majdinasab, R. Khan, Z. Li, A. Hayat, and J. L. Marty, "Nanomaterials in fluorescence-based biosensors: Defining key roles," *Nano-Structures & Nano-Objects,* vol. 27, p. 100774, 2021/07/01/ 2021, doi: https://doi.org/10.1016/j.nanoso.2021.100774.

[29] M. A. Tzani, D. K. Gioftsidou, M. G. Kallitsakis, N. V. Pliatsios, N. P. Kalogiouri, P. A. Angaridis, I. N. Lykakis, and M. A. Terzidis, "Direct and Indirect Chemiluminescence: Reactions, Mechanisms and Challenges," (in eng), *Molecules,* vol. 26, no. 24, Dec 17 2021, doi: 10.3390/molecules26247664.

[30] A. Ozcan and E. McLeod, "Lensless Imaging and Sensing," *Annual Review of Biomedical Engineering,* vol. 18, no. Volume 18, 2016, pp. 77-102, 2016, doi: https://doi.org/10.1146/annurev-bioeng-092515-010849.

[31] K. Deshpande, R. K. Mishra, and S. Bhand, "A high sensitivity micro format chemiluminescence enzyme inhibition assay for determination of Hg(II)," *Sensors,* Article vol. 10, no. 7, pp. 6377-6394, 2010, doi: 10.3390/s100706377.

[32] H. Isobe, S. Yamanaka, S. Kuramitsu, and K. Yamaguchi, "Regulation Mechanism of Spin−Orbit Coupling in Charge-Transfer-Induced Luminescence of Imidazopyrazinone Derivatives," *Journal of the American Chemical Society,* vol. 130, no. 1, pp. 132-149, 2008/01/01 2008, doi: 10.1021/ja073834r.

[33] Z. Wang, J. Huang, J. Huang, B. Yu, K. Pu, and F.-J. Xu, "Chemiluminescence: From mechanism to applications in biological imaging and therapy," *Aggregate,* vol. 2, no. 6, p. e140, 2021, doi: https://doi.org/10.1002/agt2.140.

[34] M. Vacher, I. Fdez. Galván, B.-W. Ding, S. Schramm, R. Berraud-Pache, P. Naumov, N. Ferré, Y.-J. Liu, I. Navizet, D. Roca-Sanjuán, W. J. Baader, and R. Lindh, "Chemi- and Bioluminescence of Cyclic Peroxides," *Chemical Reviews,* vol. 118, no. 15, pp. 6927-6974, 2018/08/08 2018, doi: 10.1021/acs.chemrev.7b00649.

[35] F. A. Augusto, G. A. de Souza, S. P. de Souza Júnior, M. Khalid, and W. J. Baader, "Efficiency of Electron Transfer Initiated Chemiluminescence," *Photochemistry and Photobiology,* vol. 89, no. 6, pp. 1299-1317, 2013, doi: https://doi.org/10.1111/php.12102.

[36] J. Yang, W. Yin, R. Van, K. Yin, P. Wang, C. Zheng, B. Zhu, K. Ran, C. Zhang, M. Kumar, Y. Shao, and C. Ran, "Turn-on chemiluminescence probes and dual-amplification of signal for detection of amyloid beta species in vivo," *Nature Communications,* vol. 11, no. 1, p. 4052, 2020/08/13 2020, doi: 10.1038/s41467-020-17783-4.

[37] A. Roda and M. Guardigli, "Analytical chemiluminescence and bioluminescence: latest achievements and new horizons," *Analytical and Bioanalytical Chemistry,* vol. 402, no. 1, pp. 69-76, 2012/01/01 2012, doi: 10.1007/s00216-011-5455-8.

[38] Y. Ma, Y. Zhao, X. Xu, S. Ding, and Y. Li, "Magnetic covalent organic framework immobilized gold nanoparticles with high-efficiency catalytic performance for chemiluminescent detection of pesticide triazophos," *Talanta,* Article vol. 235, 2021, Art no. 122798, doi: 10.1016/j.talanta.2021.122798.

[39] C. Zong, D. Zhang, F. Jiang, H. Yang, S. Liu, and P. Li, "Metal-enhanced chemiluminescence detection of C-reaction protein based on silver nanoparticle hybrid probes," *Talanta,* Article vol. 199, pp. 164-169, 2019, doi: 10.1016/j.talanta.2019.02.060.

[40] Y. Ando, K. Niwa, N. Yamada, T. Enomoto, T. Irie, H. Kubota, Y. Ohmiya, and H. Akiyama, "Firefly bioluminescence quantum yield and colour change by pH-sensitive green emission," *Nature Photonics,* vol. 2, no. 1, pp. 44-47, 2008/01/01 2008, doi: 10.1038/nphoton.2007.251.

[41] E. Karimi, M. Nikkhah, and S. Hosseinkhani, "Label-Free and Bioluminescence-Based Nano-Biosensor for ATP Detection," *Biosensors,* Article vol. 12, no. 11, 2022, Art no. 918, doi: 10.3390/bios12110918.

[42] R. Abbasi, M. Imanbekova, and S. Wachsmann-Hogiu, "On-chip bioluminescence biosensor for the detection of microbial surface contamination," *Biosensors and Bioelectronics,* vol. 254, p. 116200, 2024/06/15/ 2024, doi: https://doi.org/10.1016/j.bios.2024.116200.

[43] M. M. Richter, "Electrochemiluminescence (ECL)," *Chemical Reviews,* vol. 104, no. 6, pp. 3003-3036, 2004/06/01 2004, doi: 10.1021/cr020373d.

[44] W. Miao, "Electrogenerated chemiluminescence and its biorelated applications," (in eng), *Chem Rev,* vol. 108, no. 7, pp. 2506-53, Jul 2008, doi: 10.1021/cr068083a.

[45] S. Carrara, P. S. Francis, and C. F. Hogan, "Electrochemiluminescence," in *Springer Handbook of Inorganic Photochemistry*, D. Bahnemann and A. O. T. Patrocinio Eds. Cham: Springer International Publishing, 2022, pp. 1777-1809.

[46] H. Qi and C. Zhang, "Electrogenerated Chemiluminescence Biosensing," *Analytical Chemistry,* vol. 92, no. 1, pp. 524-534, 2020/01/07 2020, doi: 10.1021/acs.analchem.9b03425.

[47] A. W. Knight, "A review of recent trends in analytical applications of electrogenerated chemiluminescence," *TrAC Trends in Analytical Chemistry,* vol. 18, no. 1, pp. 47-62, 1999/01/01/ 1999, doi: https://doi.org/10.1016/S0165-9936(98)00086-7.

[48] A. Roda, M. Guardigli, E. Michelini, and M. Mirasoli, "Bioluminescence in analytical chemistry and in vivo imaging," *TrAC Trends in Analytical Chemistry,* vol. 28, no. 3, pp. 307-322, 2009/03/01/ 2009, doi: https://doi.org/10.1016/j.trac.2008.11.015.

[49] X. Yang, R. Yuan, Y. Chai, Y. Zhuo, L. Mao, and S. Yuan, "Ru(bpy)32+-doped silica nanoparticles labeling for a sandwich-type electrochemiluminescence immunosensor," *Biosensors and Bioelectronics,* vol. 25, no. 7, pp. 1851-1855, 2010/03/15/ 2010, doi: https://doi.org/10.1016/j.bios.2009.12.027.

[50] M. Zhou, J. Roovers, G. P. Robertson, and C. P. Grover, "Multilabeling Biomolecules at a Single Site. 1. Synthesis and Characterization of a Dendritic Label for Electrochemiluminescence Assays," *Analytical Chemistry,* vol. 75, no. 23, pp. 6708-6717, 2003/12/01 2003, doi: 10.1021/ac034664d.

[51] W. Zhan and A. J. Bard, "Electrogenerated Chemiluminescence. 83. Immunoassay of Human C-Reactive Protein by Using Ru(bpy)32+-Encapsulated Liposomes as Labels," *Analytical Chemistry,* vol. 79, no. 2, pp. 459-463, 2007/01/01 2007, doi: 10.1021/ac061336f.

[52] H. Wei, J. Liu, L. Zhou, J. Li, X. Jiang, J. Kang, X. Yang, S. Dong, and E. Wang, "[Ru(bpy)3]2+-Doped Silica Nanoparticles within Layer-by-Layer Biomolecular Coatings and Their Application as a Biocompatible Electrochemiluminescent Tag Material," *Chemistry – A European Journal,* vol. 14, no. 12, pp. 3687-3693, 2008, doi: https://doi.org/10.1002/chem.200701518.

[53] H. Wei, L. Zhou, J. Li, J. Liu, and E. Wang, "Electrochemical and electrochemiluminescence study of Ru(bpy)2+3-doped silica nanoparticles with covalently grafted biomacromolecules," *Journal of Colloid and Interface Science,* vol. 321, no. 2, pp. 310-314, 2008/05/15/ 2008, doi: https://doi.org/10.1016/j.jcis.2008.02.012.

[54] N. Sardesai, S. Pan, and J. Rusling, "Electrochemiluminescent immunosensor for detection of protein cancer biomarkers using carbon nanotube forests and [Ru-(bpy)3]2+-doped silica nanoparticles," *Chemical Communications,* 10.1039/B909220J no. 33, pp. 4968-4970, 2009, doi: 10.1039/B909220J.

[55] R. Kurita, K. Arai, K. Nakamoto, D. Kato, and O. Niwa, "Development of Electrogenerated Chemiluminescence-Based Enzyme Linked Immunosorbent Assay for Sub-pM Detection," *Analytical Chemistry,* vol. 82, no. 5, pp. 1692-1697, 2010/03/01 2010, doi: 10.1021/ac902045y.

[56] J. Qian, Z. Zhou, X. Cao, and S. Liu, "Electrochemiluminescence immunosensor for ultrasensitive detection of biomarker using Ru(bpy)32+-encapsulated silica nanosphere

labels," *Analytica Chimica Acta,* vol. 665, no. 1, pp. 32-38, 2010/04/14/ 2010, doi: https://doi.org/10.1016/j.aca.2010.03.013.

[57] X.-B. Yin, B. Qi, X. Sun, X. Yang, and E. Wang, "4-(Dimethylamino)butyric Acid Labeling for Electrochemiluminescence Detection of Biological Substances by Increasing Sensitivity with Gold Nanoparticle Amplification," *Analytical Chemistry,* vol. 77, no. 11, pp. 3525-3530, 2005/06/01 2005, doi: 10.1021/ac0503198.

[58] X.-B. Yin, Y. Du, X. Yang, and E. Wang, "Microfluidic chip with electrochemiluminescence detection using 2-(2-aminoethyl)-1-methylpyrrolidine labeling," *Journal of Chromatography A,* vol. 1091, no. 1, pp. 158-162, 2005/10/14/ 2005, doi: https://doi.org/10.1016/j.chroma.2005.07.046.

[59] L. Dennany, R. J. Forster, and J. F. Rusling, "Simultaneous Direct Electrochemiluminescence and Catalytic Voltammetry Detection of DNA in Ultrathin Films," *Journal of the American Chemical Society,* vol. 125, no. 17, pp. 5213-5218, 2003/04/01 2003, doi: 10.1021/ja0296529.

[60] W. Miao and A. J. Bard, "Electrogenerated Chemiluminescence. 77. DNA Hybridization Detection at High Amplification with [Ru(bpy)3]2+-Containing Microspheres," *Analytical Chemistry,* vol. 76, no. 18, pp. 5379-5386, 2004/09/01 2004, doi: 10.1021/ac0495236.

[61] H. Wei, Y. Du, J. Kang, and E. Wang, "Label free electrochemiluminescence protocol for sensitive DNA detection with a tris(2,2′-bipyridyl)ruthenium(II) modified electrode based on nucleic acid oxidation," *Electrochemistry Communications,* vol. 9, no. 7, pp. 1474-1479, 2007/07/01/ 2007, doi: https://doi.org/10.1016/j.elecom.2007.01.053.

[62] H. Wei and E. Wang, "Electrochemiluminescence-based DNA Detection Using Guanine Oxidation at Electrostatic Self-assembly of Ru(bpy)32+-doped Silica Nanoparticles on Indium Tin Oxide Electrode," *Chemistry Letters,* vol. 36, no. 2, pp. 210-211, 2006, doi: 10.1246/cl.2007.210.

[63] J.-G. Lee, K. Yun, G.-S. Lim, S. E. Lee, S. Kim, and J.-K. Park, "DNA biosensor based on the electrochemiluminescence of Ru(bpy)32+ with DNA-binding intercalators," *Bioelectrochemistry,* vol. 70, no. 2, pp. 228-234, 2007/05/01/ 2007, doi: https://doi.org/10.1016/j.bioelechem.2006.09.003.

[64] J. WEI and L. ZHANG, "DETECTION OF XANTHOMONAS ORYZAE PV. ORYZICOLA BY ELECTROCHEMILUMINESCENCE POLYMERASE CHAIN REACTION METHOD," in *Bioluminescence and Chemiluminescence*, 2008, pp. 297-300.

[65] D. Zhu, Y. Tang, D. Xing, and W. R. Chen, "PCR-Free Quantitative Detection of Genetically Modified Organism from Raw Materials. An Electrochemiluminescence-Based Bio Bar Code Method," *Analytical Chemistry,* vol. 80, no. 10, pp. 3566-3571, 2008/05/01 2008, doi: 10.1021/ac0713306.

[66] D. Zhu, D. Xing, Y. Tang, and L. Zhang, "A novel mutant allele specific amplification and electrochemiluminescence method for the detection of point mutation in clinical samples," *Biosensors and Bioelectronics,* vol. 24, no. 11, pp. 3306-3310, 2009/07/15/ 2009, doi: https://doi.org/10.1016/j.bios.2009.04.027.

[67] R. Duan, X. Zhou, and D. Xing, "Electrochemiluminescence Biobarcode Method Based on Cysteamine−Gold Nanoparticle Conjugates," *Analytical Chemistry,* vol. 82, no. 8, pp. 3099-3103, 2010/04/15 2010, doi: 10.1021/ac100018z.

[68] Q. Su, D. Xing, and X. Zhou, "Magnetic beads based rolling circle amplification–electrochemiluminescence assay for highly sensitive detection of point mutation," *Biosensors and Bioelectronics,* vol. 25, no. 7, pp. 1615-1621, 2010/03/15/ 2010, doi: https://doi.org/10.1016/j.bios.2009.11.025.

[69] S. W. Bae, J.-W. Oh, I.-S. Shin, M. S. Cho, Y.-R. Kim, H. Kim, and J.-I. Hong, "Highly sensitive detection of DNA by electrogenerated chemiluminescence amplification using dendritic Ru(bpy)32+-doped silica nanoparticles," *Analyst,* 10.1039/B920998K vol. 135, no. 3, pp. 603-607, 2010, doi: 10.1039/B920998K.

[70] W. Cao, J. P. Ferrance, J. Demas, and J. P. Landers, "Quenching of the Electrochemiluminescence of Tris(2,2‘-bipyridine)ruthenium(II) by Ferrocene and Its Potential Application to Quantitative DNA Detection," *Journal of the American Chemical Society,* vol. 128, no. 23, pp. 7572-7578, 2006/06/01 2006, doi: 10.1021/ja060162g.

[71] X. Wang, W. Yun, P. Dong, J. Zhou, P. He, and Y. Fang, "A Controllable Solid-State Ru(bpy)32+ Electrochemiluminescence Film Based on Conformation Change of Ferrocene-Labeled DNA Molecular Beacon," *Langmuir,* vol. 24, no. 5, pp. 2200-2205, 2008/03/01 2008, doi: 10.1021/la702345p.

[72] L. Hu and G. Xu, "Applications and trends in electrochemiluminescence," *Chemical Society Reviews,* 10.1039/B923679C vol. 39, no. 8, pp. 3275-3304, 2010, doi: 10.1039/B923679C.

[73] B. Sun, H. Qi, F. Ma, Q. Gao, C. Zhang, and W. Miao, "Double Covalent Coupling Method for the Fabrication of Highly Sensitive and Reusable Electrogenerated Chemiluminescence Sensors," *Analytical Chemistry,* vol. 82, no. 12, pp. 5046-5052, 2010/06/15 2010, doi: 10.1021/ac9029289.

[74] J. G. Bruno and J. L. Kiel, "In vitro selection of DNA aptamers to anthrax spores with electrochemiluminescence detection," *Biosensors and Bioelectronics,* vol. 14, no. 5, pp. 457-464, 1999/05/31/ 1999, doi: https://doi.org/10.1016/S0956-5663(99)00028-7.

[75] J. G. Bruno and J. L. Kiel, "Use of magnetic beads in selection and detection of biotoxin aptamers by electrochemiluminescence and enzymatic methods," (in eng), *Biotechniques,* vol. 32, no. 1, pp. 178-80, 182-3, Jan 2002, doi: 10.2144/02321dd04.

[76] Y. Li, H. Qi, Y. Peng, J. Yang, and C. Zhang, "Electrogenerated chemiluminescence aptamer-based biosensor for the determination of cocaine," *Electrochemistry Communications,* vol. 9, no. 10, pp. 2571-2575, 2007/10/01/ 2007, doi: https://doi.org/10.1016/j.elecom.2007.07.038.

[77] X. Wang, J. Zhou, W. Yun, S. Xiao, Z. Chang, P. He, and Y. Fang, "Detection of thrombin using electrogenerated chemiluminescence based on Ru(bpy)32+-doped silica nanoparticle aptasensor via target protein-induced strand displacement," *Analytica Chimica Acta,* vol. 598, no. 2, pp. 242-248, 2007/08/29/ 2007, doi: https://doi.org/10.1016/j.aca.2007.07.050.

[78] J. Bai, H. Wei, B. Li, L. Song, L. Fang, Z. Lv, W. Zhou, and E. Wang, "[Ru(bpy)2(dcbpy)NHS] Labeling/Aptamer-Based Biosensor for the Detection of Lysozyme by Increasing Sensitivity with Gold Nanoparticle Amplification," *Chemistry – An Asian Journal,* vol. 3, no. 11, pp. 1935-1941, 2008, doi: https://doi.org/10.1002/asia.200800104.

[79] L. Fang, Z. Lü, H. Wei, and E. Wang, "A electrochemiluminescence aptasensor for detection of thrombin incorporating the capture aptamer labeled with gold nanoparticles immobilized onto the thio-silanized ITO electrode," *Analytica Chimica Acta,* vol. 628, no. 1, pp. 80-86, 2008/10/17/ 2008, doi: https://doi.org/10.1016/j.aca.2008.08.041.

[80] W. Guo, J. Yuan, B. Li, Y. Du, E. Ying, and E. Wang, "Nanoscale-enhanced Ru(bpy)32+ electrochemiluminescence labels and related aptamer-based biosensing system," *Analyst,* 10.1039/B806301J vol. 133, no. 9, pp. 1209-1213, 2008, doi: 10.1039/B806301J.

[81] T. Li, Y. Du, and E. Wang, "Polyethyleneimine-Functionalized Platinum Nanoparticles with High Electrochemiluminescence Activity and Their Applications to Amplified Analysis of Biomolecules," *Chemistry – An Asian Journal,* vol. 3, no. 11, pp. 1942-1948, 2008, doi: https://doi.org/10.1002/asia.200800152.

[82] Y. Li, H. Qi, Y. Peng, Q. Gao, and C. Zhang, "Electrogenerated chemiluminescence aptamer-based method for the determination of thrombin incorporating quenching of tris(2,2′-bipyridine)ruthenium by ferrocene," *Electrochemistry Communications,* vol. 10, no. 9, pp. 1322-1325, 2008/09/01/ 2008, doi: https://doi.org/10.1016/j.elecom.2008.06.027.

[83] X.-Y. WANG, W. YUN, J.-M. ZHOU, P. DONG, P.-G. HE, and Y.-Z. FANG, "Ru(bpy)32+-doped Silica Nanoparticle Aptasensor for Detection of Thrombin Based on Electrogenerated Chemiluminescence," *Chinese Journal of Chemistry,* vol. 26, no. 2, pp. 315-320, 2008, doi: https://doi.org/10.1002/cjoc.200890061.

[84] L. Hu, Z. Bian, H. Li, S. Han, Y. Yuan, L. Gao, and G. Xu, "[Ru(bpy)2dppz]2+ Electrochemiluminescence Switch and Its Applications for DNA Interaction Study and Label-free ATP Aptasensor," *Analytical Chemistry,* vol. 81, no. 23, pp. 9807-9811, 2009/12/01 2009, doi: 10.1021/ac901925x.

[85] X. Wang, P. Dong, W. Yun, Y. Xu, P. He, and Y. Fang, "A solid-state electrochemiluminescence biosensing switch for detection of thrombin based on ferrocene-labeled molecular beacon aptamer," *Biosensors and Bioelectronics,* vol. 24, no. 11, pp. 3288-3292, 2009/07/15/ 2009, doi: https://doi.org/10.1016/j.bios.2009.04.019.

[86] W. Yao, L. Wang, H. Wang, X. Zhang, and L. Li, "An aptamer-based electrochemiluminescent biosensor for ATP detection," *Biosensors and Bioelectronics,* vol. 24, no. 11, pp. 3269-3274, 2009/07/15/ 2009, doi: https://doi.org/10.1016/j.bios.2009.04.016.

[87] X.-B. Yin, Y.-Y. Xin, and Y. Zhao, "Label-Free Electrochemiluminescent Aptasensor with Attomolar Mass Detection Limits Based on a Ru(phen)32+-Double-Strand DNA Composite Film Electrode," *Analytical Chemistry,* vol. 81, no. 22, pp. 9299-9305, 2009/11/15 2009, doi: 10.1021/ac901609g.

[88] X. Wang, P. Dong, P. He, and Y. Fang, "A solid-state electrochemiluminescence sensing platform for detection of adenosine based on ferrocene-labeled structure-switching signaling aptamer," *Analytica Chimica Acta,* vol. 658, no. 2, pp. 128-132, 2010/01/25/ 2010, doi: https://doi.org/10.1016/j.aca.2009.11.007.

[89] C. Fang, H. Li, J. Yan, H. Guo, and T. Yifeng, "Progress of the Electrochemiluminescence Biosensing Strategy for Clinical Diagnosis with Luminol as the Sensing Probe," *ChemElectroChem,* vol. 4, no. 7, pp. 1587-1593, 2017, doi: https://doi.org/10.1002/celc.201700465.

[90] L. Qingwen, L. Guoan, W. Yiming, and Z. Xingrong, "Immobilization of glucose oxidase in sol–gel matrix and its application to fabricate chemiluminescent glucose sensor," *Materials Science and Engineering: C,* vol. 11, no. 1, pp. 67-70, 2000/06/30/ 2000, doi: https://doi.org/10.1016/S0928-4931(00)00130-2.

[91] B. Qiu, Z. Lin, J. Wang, Z. Chen, J. Chen, and G. Chen, "An electrochemiluminescent biosensor for glucose based on the electrochemiluminescence of luminol on the nafion/glucose oxidase/poly(nickel(II)tetrasulfophthalocyanine)/multi-walled carbon nanotubes modified

electrode," *Talanta,* vol. 78, no. 1, pp. 76-80, 2009/04/15/ 2009, doi: https://doi.org/10.1016/j.talanta.2008.10.067.

[92] B. Haghighi, A. Tavakoli, and S. Bozorgzadeh, "Improved electrogenerated chemiluminescence of luminol by cobalt nanoparticles decorated multi-walled carbon nanotubes," *Journal of Electroanalytical Chemistry,* vol. 762, pp. 80-86, 2016/02/01/ 2016, doi: https://doi.org/10.1016/j.jelechem.2015.12.035.

[93] X. Tian, S. Lian, L. Zhao, X. Chen, Z. Huang, and X. Chen, "A novel electrochemiluminescence glucose biosensor based on platinum nanoflowers/graphene oxide/glucose oxidase modified glassy carbon electrode," *Journal of Solid State Electrochemistry,* vol. 18, no. 9, pp. 2375-2382, 2014/09/01 2014, doi: 10.1007/s10008-014-2485-0.

[94] F.-F. Jia, H. Zhong, W.-G. Zhang, X.-R. Li, G.-Y. Wang, J. Song, Z.-P. Cheng, J.-Z. Yin, and L.-P. Guo, "A novel nonenzymatic ECL glucose sensor based on perovskite LaTiO3-Ag0.1 nanomaterials," *Sensors and Actuators B: Chemical,* vol. 212, pp. 174-182, 2015/06/01/ 2015, doi: https://doi.org/10.1016/j.snb.2015.02.011.

[95] L. Yu, X. Wei, C. Fang, and Y. Tu, "A disposable biosensor for noninvasive diabetic diagnosis rest on the Au/TiO2 nano-composite intensified electrochemiluminescence," *Electrochimica Acta,* vol. 211, pp. 27-35, 2016/09/01/ 2016, doi: https://doi.org/10.1016/j.electacta.2016.06.034.

[96] X.-m. Chen, Z.-m. Cai, Z.-j. Lin, T.-t. Jia, H.-z. Liu, Y.-q. Jiang, and X. Chen, "A novel non-enzymatic ECL sensor for glucose using palladium nanoparticles supported on functional carbon nanotubes," *Biosensors and Bioelectronics,* vol. 24, no. 12, pp. 3475-3480, 2009/08/15/ 2009, doi: https://doi.org/10.1016/j.bios.2009.04.046.

[97] S. Park, H. Boo, and T. D. Chung, "Electrochemical non-enzymatic glucose sensors," *Analytica Chimica Acta,* vol. 556, no. 1, pp. 46-57, 2006/01/18/ 2006, doi: https://doi.org/10.1016/j.aca.2005.05.080.

[98] R. Abbasi, J. Liu, S. Suarasan, and S. Wachsmann-Hogiu, "SE-ECL on CMOS: a miniaturized electrochemiluminescence biosensor," *Lab on a Chip,* 10.1039/D1LC00905B vol. 22, no. 5, pp. 994-1005, 2022, doi: 10.1039/D1LC00905B.

[99] R. Abbasi and S. Wachsmann-Hogiu, "Optimization and miniaturization of SE-ECL for potential-resolved, multi-color, multi-analyte detection," *Biosensors and Bioelectronics,* vol. 257, p. 116322, 2024/08/01/ 2024, doi: https://doi.org/10.1016/j.bios.2024.116322.

[100] W. Gao, K. Muzyka, X. Ma, B. Lou, and G. Xu, "A single-electrode electrochemical system for multiplex electrochemiluminescence analysis based on a resistance induced

potential difference," *Chemical Science,* 10.1039/C8SC00410B vol. 9, no. 16, pp. 3911-3916, 2018, doi: 10.1039/C8SC00410B.

[101] F. Jameison, R. I. Sanchez, L. Dong, J. K. Leland, D. Yost, and M. T. Martin, "Electrochemiluminescence-Based Quantitation of Classical Clinical Chemistry Analytes," *Analytical Chemistry,* vol. 68, no. 8, pp. 1298-1302, 1996/01/01 1996, doi: 10.1021/ac950990k.

[102] M. Zhang, R. Yuan, Y. Chai, S. Chen, X. Zhong, H. Zhong, and C. Wang, "A cathodic electrogenerated chemiluminescence biosensor based on luminol and hemin-graphene nanosheets for cholesterol detection," *RSC Advances,* 10.1039/C2RA20374J vol. 2, no. 11, pp. 4639-4641, 2012, doi: 10.1039/C2RA20374J.

[103] X. Ou, X. Tan, X. Liu, H. Chen, Y. Fan, S. Chen, and S. Wei, "A cathodic luminol-based electrochemiluminescence biosensor for detecting cholesterol using 3D-MoS2–PANI nanoflowers and Ag nanocubes for signal enhancement," *RSC Advances,* 10.1039/C5RA09638C vol. 5, no. 81, pp. 66409-66415, 2015, doi: 10.1039/C5RA09638C.

[104] S. Tang, Q. Zhao, and Y. Tu, "A sensitive electrochemiluminescent cholesterol biosensor based on Au/hollowed-TiO2 nano-composite pre-functionalized electrode," *Sensors and Actuators B: Chemical,* vol. 237, pp. 416-422, 2016/12/01/ 2016, doi: https://doi.org/10.1016/j.snb.2016.06.110.

[105] X. Wang, L. Ge, Y. Yu, S. Dong, and F. Li, "Highly sensitive electrogenerated chemiluminescence biosensor based on hybridization chain reaction and amplification of gold nanoparticles for DNA detection," *Sensors and Actuators B: Chemical,* vol. 220, pp. 942-948, 2015/12/01/ 2015, doi: https://doi.org/10.1016/j.snb.2015.06.032.

[106] H.-F. Zhao, R.-P. Liang, J.-W. Wang, and J.-D. Qiu, "One-pot synthesis of GO/AgNPs/luminol composites with electrochemiluminescence activity for sensitive detection of DNA methyltransferase activity," *Biosensors and Bioelectronics,* vol. 63, pp. 458-464, 2015/01/15/ 2015, doi: https://doi.org/10.1016/j.bios.2014.07.079.

[107] P. Zhang, X. Wu, R. Yuan, and Y. Chai, "An “Off–On” Electrochemiluminescent Biosensor Based on DNAzyme-Assisted Target Recycling and Rolling Circle Amplifications for Ultrasensitive Detection of microRNA," *Analytical Chemistry,* vol. 87, no. 6, pp. 3202-3207, 2015/03/17 2015, doi: 10.1021/ac504455z.

[108] P. Zhang, X. Wu, Y. Chai, and R. Yuan, "An electrochemiluminescent microRNA biosensor based on hybridization chain reaction coupled with hemin as the signal enhancer," *Analyst,* 10.1039/C4AN00284A vol. 139, no. 11, pp. 2748-2753, 2014, doi: 10.1039/C4AN00284A.

[109] N. Hao, X.-L. Li, H.-R. Zhang, J.-J. Xu, and H.-Y. Chen, "A highly sensitive ratiometric electrochemiluminescent biosensor for microRNA detection based on cyclic enzyme amplification and resonance energy transfer," *Chemical Communications,* 10.1039/C4CC06801G vol. 50, no. 94, pp. 14828-14830, 2014, doi: 10.1039/C4CC06801G.

[110] W. Wen, X. Yan, C. Zhu, D. Du, and Y. Lin, "Recent Advances in Electrochemical Immunosensors," *Analytical Chemistry,* vol. 89, no. 1, pp. 138-156, 2017/01/03 2017, doi: 10.1021/acs.analchem.6b04281.

[111] E. M. Gross, S. S. Maddipati, and S. M. Snyder, "A Review of Electrogenerated Chemiluminescent Biosensors for Assays in Biological Matrices," *Bioanalysis,* vol. 8, no. 19, pp. 2071-2089, 2016/10/01 2016, doi: 10.4155/bio-2016-0178.

[112] Y. Huang, J. Lei, Y. Cheng, and H. Ju, "Ratiometric electrochemiluminescent strategy regulated by electrocatalysis of palladium nanocluster for immunosensing," *Biosensors and Bioelectronics,* vol. 77, pp. 733-739, 2016/03/15/ 2016, doi: https://doi.org/10.1016/j.bios.2015.10.038.

[113] J. Shu, W. Shen, and H. Cui, "Ultrasensitive label-free electrochemiluminescence immunosensor based on N-(4-aminobutyl)-N-ethylisoluminol-functionalized graphene composite," *Science China Chemistry,* vol. 58, no. 3, pp. 425-432, 2015/03/01 2015, doi: 10.1007/s11426-015-5320-2.

[114] W. Kong, H. Zhou, H. Ouyang, Z. Li, and Z. Fu, "A disposable label-free electrochemiluminescent immunosensor for transferrin detection based on a luminol-reduced gold nanoparticle-modified screen-printed carbon electrode," *Analytical Methods,* 10.1039/C3AY42272K vol. 6, no. 9, pp. 2959-2964, 2014, doi: 10.1039/C3AY42272K.

[115] W. Zhu, Q. Wang, H. Ma, X. Lv, D. Wu, X. Sun, B. Du, and Q. Wei, "Single-step cycle pulse operation of the label-free electrochemiluminescence immunosensor based on branched polypyrrole for carcinoembryonic antigen detection," *Scientific Reports,* vol. 6, no. 1, p. 24599, 2016/04/19 2016, doi: 10.1038/srep24599.

[116] J.-X. Wang, Y. Zhuo, Y. Zhou, H.-J. Wang, R. Yuan, and Y.-Q. Chai, "Ceria Doped Zinc Oxide Nanoflowers Enhanced Luminol-Based Electrochemiluminescence Immunosensor for Amyloid-β Detection," *ACS Applied Materials & Interfaces,* vol. 8, no. 20, pp. 12968-12975, 2016/05/25 2016, doi: 10.1021/acsami.6b00021.

[117] Y. Cheng, R. Yuan, Y. Chai, H. Niu, Y. Cao, H. Liu, L. Bai, and Y. Yuan, "Highly sensitive luminol electrochemiluminescence immunosensor based on ZnO nanoparticles and glucose oxidase decorated graphene for cancer biomarker detection," *Analytica Chimica Acta,* vol. 745, pp. 137-142, 2012/10/01/ 2012, doi: https://doi.org/10.1016/j.aca.2012.08.010.

[118] X. Jiang, Y. Chai, R. Yuan, Y. Cao, Y. Chen, H. Wang, and X. Gan, "An ultrasensitive luminol cathodic electrochemiluminescence immunosensor based on glucose oxidase and nanocomposites: Graphene–carbon nanotubes and gold-platinum alloy," *Analytica Chimica Acta,* vol. 783, pp. 49-55, 2013/06/14/ 2013, doi: https://doi.org/10.1016/j.aca.2013.04.028.

[119] D. Bruce and M. M. Richter, "Green Electrochemiluminescence from Ortho-Metalated Tris(2-phenylpyridine)iridium(III)," *Analytical Chemistry,* vol. 74, no. 6, pp. 1340-1342, 2002/03/01 2002, doi: 10.1021/ac0111513.

[120] T. Zhai, Q. Zhang, F. Yang, H. Zhou, L. Bai, T. Hao, Z. Guo, and Z. Chen, "A green EC/ECL dual-mode biosensing platform for detection of Vibrio parahaemolyticus," *Sensors and Actuators B: Chemical,* vol. 415, p. 136010, 2024/09/15/ 2024, doi: https://doi.org/10.1016/j.snb.2024.136010.

[121] R. A. Marcus, "On the Theory of Chemiluminescent Electron-Transfer Reactions," *The Journal of Chemical Physics,* vol. 43, no. 8, pp. 2654-2657, 1965, doi: 10.1063/1.1697190.

[122] R. A. Marcus, "Exchange reactions and electron transfer reactions including isotopic exchange. Theory of oxidation-reduction reactions involving electron transfer. Part 4.—A statistical-mechanical basis for treating contributions from solvent, ligands, and inert salt," *Discussions of the Faraday Society,* 10.1039/DF9602900021 vol. 29, no. 0, pp. 21-31, 1960, doi: 10.1039/DF9602900021.

[123] F. Zhang, J. Liu, I. Ivanov, M. C. Hatzell, W. Yang, Y. Ahn, and B. E. Logan, "Reference and counter electrode positions affect electrochemical characterization of bioanodes in different bioelectrochemical systems," *Biotechnology and Bioengineering,* vol. 111, no. 10, pp. 1931-1939, 2014/10/01 2014, doi: https://doi.org/10.1002/bit.25253.

[124] V. Periasamy, P. N. N. Elumalai, S. Talebi, R. T. Subramaniam, R. Kasi, M. Iwamoto, and G. Gnana Kumar, "Novel same-metal three electrode system for cyclic voltammetry studies," (in eng), *RSC Adv,* vol. 13, no. 9, pp. 5744-5752, Feb 14 2023, doi: 10.1039/d3ra00457k.

[125] N. Harvey, "Luminescence during Electrolysis," *The Journal of Physical Chemistry,* vol. 33, no. 10, pp. 1456-1459, 1929/10/01 1929, doi: 10.1021/j150304a002.

[126] T. Kuwana, B. Epstein, and E. T. Seo, "ELECTROCHEMICAL GENERATION OF SOLUTION LUMINESCENCE," *The Journal of Physical Chemistry,* vol. 67, no. 10, pp. 2243-2244, 1963/10/01 1963, doi: 10.1021/j100804a516.

[127] J. G. Gall and M. L. Pardue, "Formation and detection of RNA-DNA hybrid molecules in cytological preparations," (in eng), *Proc Natl Acad Sci U S A,* vol. 63, no. 2, pp. 378-83, Jun 1969, doi: 10.1073/pnas.63.2.378.

[128] H. Zhou, J. Liu, J.-J. Xu, S. Zhang, and H.-Y. Chen, "Chapter Two - Advances in DNA/RNA detection using nanotechnology," in *Advances in Clinical Chemistry*, vol. 91, G. S. Makowski Ed.: Elsevier, 2019, pp. 31-98.

[129] S. Mahadevarao Premnath and M. Zubair, "Electrochemiluminescence Method," in *StatPearls*. Treasure Island (FL) relationships with ineligible companies. Disclosure: Muhammad Zubair declares no relevant financial relationships with ineligible companies.: StatPearls Publishing

[130] J. Wu and H. X. Ju, "3.07 - Clinical Immunoassays and Immunosensing," in *Comprehensive Sampling and Sample Preparation*, J. Pawliszyn Ed. Oxford: Academic Press, 2012, pp. 143-167.

[131] Y. Ikariyama, H. Kunoh, and M. Aizawa, "Electrochemical luminescence-based homogeneous immunoassay," *Biochemical and Biophysical Research Communications,* vol. 128, no. 2, pp. 987-992, 1985/04/30/ 1985, doi: https://doi.org/10.1016/0006-291X(85)90144-5.

[132] L. C. Soulsby, D. J. Hayne, E. H. Doeven, L. Chen, C. F. Hogan, E. Kerr, J. L. Adcock, and P. S. Francis, "Electrochemically, Spectrally, and Spatially Resolved Annihilation-Electrogenerated Chemiluminescence of Mixed-Metal Complexes at Working and Counter Electrodes," *ChemElectroChem,* vol. 5, no. 12, pp. 1543-1547, 2018/06/12 2018, doi: https://doi.org/10.1002/celc.201800312.

[133] M. Li, Y. Wang, Y. Zhang, J. Yu, S. Ge, and M. Yan, "Graphene functionalized porous Au-paper based electrochemiluminescence device for detection of DNA using luminescent silver nanoparticles coated calcium carbonate/carboxymethyl chitosan hybrid microspheres as labels," *Biosensors and Bioelectronics,* vol. 59, pp. 307-313, 2014/09/15/ 2014, doi: https://doi.org/10.1016/j.bios.2014.03.072.

[134] L. Bouffier, D. Manojlovic, A. Kuhn, and N. Sojic, "Advances in bipolar electrochemiluminescence for the detection of biorelevant molecular targets," *Current Opinion in Electrochemistry,* vol. 16, pp. 28-34, 2019/08/01/ 2019, doi: https://doi.org/10.1016/j.coelec.2019.04.004.

[135] M. Wu, N. Xu, J. Qiao, J. Chen, and L. Jin, "Bipolar electrode-electrochemiluminescence (ECL) biosensor based on a hybridization chain reaction," *Analyst,* 10.1039/C9AN01022J vol. 144, no. 15, pp. 4633-4638, 2019, doi: 10.1039/C9AN01022J.

[136] Y.-L. Wang, J.-T. Cao, and Y.-M. Liu, "Bipolar Electrochemistry – A Powerful Tool for Micro/Nano-Electrochemistry," *ChemistryOpen,* vol. 11, no. 12, p. e202200163, 2022, doi: https://doi.org/10.1002/open.202200163.

[137] Y. Liu, N. Zhang, J.-B. Pan, J. Song, W. Zhao, H.-Y. Chen, and J.-J. Xu, "Bipolar Electrode Array for Multiplexed Detection of Prostate Cancer Biomarkers," *Analytical Chemistry,* vol. 94, no. 6, pp. 3005-3012, 2022/02/15 2022, doi: 10.1021/acs.analchem.1c05383.

[138] R. Liu, C. Zhang, and M. Liu, "Open bipolar electrode-electrochemiluminescence imaging sensing using paper-based microfluidics," *Sensors and Actuators B: Chemical,* vol. 216, pp. 255-262, 2015/09/01/ 2015, doi: https://doi.org/10.1016/j.snb.2015.04.014.

[139] F. Mavré, R. K. Anand, D. R. Laws, K.-F. Chow, B.-Y. Chang, J. A. Crooks, and R. M. Crooks, "Bipolar Electrodes: A Useful Tool for Concentration, Separation, and Detection of Analytes in Microelectrochemical Systems," *Analytical Chemistry,* vol. 82, no. 21, pp. 8766-8774, 2010/11/01 2010, doi: 10.1021/ac101262v.

[140] M. Seo, S. Y. Yeon, J. Yun, and T. D. Chung, "Nanoporous ITO implemented bipolar electrode sensor for enhanced electrochemiluminescence," *Electrochimica Acta,* vol. 314, pp. 89-95, 2019/08/10/ 2019, doi: https://doi.org/10.1016/j.electacta.2019.05.052.

[141] A. J. Hsueh, N. A. A. Mutalib, Y. Shirato, and H. Suzuki, "Bipolar Electrode Arrays for Chemical Imaging and Multiplexed Sensing," (in eng), *ACS Omega,* vol. 7, no. 23, pp. 20298-20305, Jun 14 2022, doi: 10.1021/acsomega.2c02298.

[142] X. Zhang, N. Bao, X. Luo, and S.-N. Ding, "Patchy gold coated Fe3O4 nanospheres with enhanced catalytic activity applied for paper-based bipolar electrode-electrochemiluminescence aptasensors," *Biosensors and Bioelectronics,* vol. 114, pp. 44-51, 2018/08/30/ 2018, doi: https://doi.org/10.1016/j.bios.2018.05.016.

[143] Y.-Z. Wang, C.-H. Xu, W. Zhao, Q.-Y. Guan, H.-Y. Chen, and J.-J. Xu, "Bipolar Electrode Based Multicolor Electrochemiluminescence Biosensor," *Analytical Chemistry,* vol. 89, no. 15, pp. 8050-8056, 2017/08/01 2017, doi: 10.1021/acs.analchem.7b01494.

[144] L. Jin, J. Qiao, J. Chen, N. Xu, and M. Wu, "Combination of area controllable sensing surface and bipolar electrode-electrochemiluminescence approach for the detection of tetracycline," *Talanta,* vol. 208, p. 120404, 2020/02/01/ 2020, doi: https://doi.org/10.1016/j.talanta.2019.120404.

[145] C. Mwanza and S.-N. Ding, "Newly Developed Electrochemiluminescence Based on Bipolar Electrochemistry for Multiplex Biosensing Applications: A Consolidated Review," *Biosensors*, vol. 13, no. 6, doi: 10.3390/bios13060666.

[146] K. L. Rahn and R. K. Anand, "Recent Advancements in Bipolar Electrochemical Methods of Analysis," *Analytical Chemistry,* vol. 93, no. 1, pp. 103-123, 2021/01/12 2021, doi: 10.1021/acs.analchem.0c04524.

[147] C. Liu, D. Wang, and C. Zhang, "A novel paperfluidic closed bipolar electrode-electrochemiluminescence sensing platform: Potential for multiplex detection at crossing-channel closed bipolar electrodes," *Sensors and Actuators B: Chemical,* vol. 270, pp. 341-352, 2018/10/01/ 2018, doi: https://doi.org/10.1016/j.snb.2018.04.180.

[148] H. Li, L. Bouffier, S. Arbault, A. Kuhn, C. F. Hogan, and N. Sojic, "Spatially-resolved multicolor bipolar electrochemiluminescence," *Electrochemistry Communications,* vol. 77, pp. 10-13, 2017/04/01/ 2017, doi: https://doi.org/10.1016/j.elecom.2017.02.006.

[149] X. Ma, L. Qi, W. Gao, F. Yuan, Y. Xia, B. Lou, and G. Xu, "A portable wireless single-electrode system for electrochemiluminescent analysis," *Electrochimica Acta,* vol. 308, pp. 20-24, 2019/06/10/ 2019, doi: https://doi.org/10.1016/j.electacta.2019.04.015.

[150] E. Vidal, C. E. Domini, D. C. Whitehead, and C. D. Garcia, "From glow-sticks to sensors: single-electrode electrochemical detection for paper-based devices," *Sensors & Diagnostics,* 10.1039/D2SD00041E vol. 1, no. 3, pp. 496-503, 2022, doi: 10.1039/D2SD00041E.

[151] A. Firoozbakhtian, M. Hosseini, Y. Guan, and G. Xu, "Boosting Electrochemiluminescence Immunoassay Sensitivity via Co–Pt Nanoparticles within a Ti3C2 MXene-Modified Single Electrode Electrochemical System on Raspberry Pi," *Analytical Chemistry,* vol. 95, no. 40, pp. 15110-15117, 2023/10/10 2023, doi: 10.1021/acs.analchem.3c03285.

[152] Y. Shi, E. Villani, Y. Chen, Y. Zhou, Z. Chen, A. Hussain, G. Xu, and S. Inagi, "High-Throughput Electrosynthesis of Gradient Polypyrrole Film Using a Single-Electrode Electrochemical System," *Analytical Chemistry,* vol. 95, no. 2, pp. 1532-1540, 2023/01/17 2023, doi: 10.1021/acs.analchem.2c04570.

[153] M. L. Bhaiyya, S. Gangrade, P. K. Pattnaik, and S. Goel, "Laser Ablated Reduced Graphene Oxide on Paper to Realize Single Electrode Electrochemiluminescence Standalone Miniplatform Integrated With a Smartphone," *IEEE Transactions on Instrumentation and Measurement,* vol. 71, pp. 1-8, 2022, doi: 10.1109/TIM.2022.3179008.

[154] F. Du, Z. Dong, F. Liu, S. Anjum, M. Hosseini, and G. Xu, "Single-electrode electrochemical system based on tris(1,10-phenanthroline)ruthenium modified carbon nanotube/graphene film electrode for visual electrochemiluminescence analysis,"

Electrochimica Acta, vol. 420, p. 140431, 2022/07/10/ 2022, doi: https://doi.org/10.1016/j.electacta.2022.140431.

[155] M. L. Bhaiyya, P. K. Pattnaik, and S. Goel, "Miniaturized Electrochemiluminescence Platform With Laser-Induced Graphene-Based Single Electrode for Interference-Free Sensing of Dopamine, Xanthine, and Glucose," *IEEE Transactions on Instrumentation and Measurement,* vol. 70, pp. 1-8, 2021, doi: 10.1109/TIM.2021.3071215.

[156] M. Bhaiyya, P. K. Pattnaik, and S. Goel, "Electrochemiluminescence sensing of vitamin B12 using laser-induced graphene based bipolar and single electrodes in a 3D-printed portable system," *Microfluidics and Nanofluidics,* vol. 25, no. 5, p. 41, 2021/04/07 2021, doi: 10.1007/s10404-021-02442-x.

[157] F. Du, Z. Dong, Y. Guan, A. M. Zeid, D. Ma, J. Feng, D. Yang, and G. Xu, "Single-Electrode Electrochemical System for the Visual and High-Throughput Electrochemiluminescence Immunoassay," *Analytical Chemistry,* vol. 94, no. 4, pp. 2189-2194, 2022/02/01 2022, doi: 10.1021/acs.analchem.1c04709.

[158] H. Hertz, "Ueber einen Einfluss des ultravioletten Lichtes auf die electrische Entladung," *Annalen der Physik,* vol. 267, no. 8, pp. 983-1000, 1887, doi: https://doi.org/10.1002/andp.18872670827.

[159] R. A. Millikan, "A Direct Photoelectric Determination of Planck's "h"," *Physical Review,* vol. 7, no. 3, pp. 355-388, 03/01/ 1916, doi: 10.1103/PhysRev.7.355.

[160] P. Lenard, "Ueber die lichtelektrische Wirkung," *Annalen der Physik,* vol. 313, no. 5, pp. 149-198, 1902, doi: https://doi.org/10.1002/andp.19023130510.

[161] A. Einstein, "Über einen die Erzeugung und Verwandlung des Lichtes betreffenden heuristischen Gesichtspunkt," *Annalen der Physik,* Article vol. 322, no. 6, pp. 132-148, 1905, doi: 10.1002/andp.19053220607.

[162] G. Konstantatos, M. Badioli, L. Gaudreau, J. Osmond, M. Bernechea, F. P. G. De Arquer, F. Gatti, and F. H. L. Koppens, "Hybrid graphene–quantum dot phototransistors with ultrahigh gain," *Nature Nanotechnology,* Article vol. 7, no. 6, pp. 363-368, 2012, doi: 10.1038/nnano.2012.60.

[163] F. Xia, T. Mueller, Y. M. Lin, A. Valdes-Garcia, and P. Avouris, "Ultrafast graphene photodetector," *Nature Nanotechnology,* Article vol. 4, no. 12, pp. 839-843, 2009, doi: 10.1038/nnano.2009.292.

[164] R. A. Yotter and D. M. Wilson, "A review of photodetectors for sensing light-emitting reporters in biological systems," *IEEE Sensors Journal,* Review vol. 3, no. 3, pp. 288-303, 2003, doi: 10.1109/JSEN.2003.814651.

[165] S. V. Polyakov, "Chapter 3 - Photomultiplier Tubes," in *Experimental Methods in the Physical Sciences*, vol. 45, A. Migdall, S. V. Polyakov, J. Fan, and J. C. Bienfang Eds.: Academic Press, 2013, pp. 69-82.

[166] Y. Haemisch, T. Frach, C. Degenhardt, and A. Thon, "Fully Digital Arrays of Silicon Photomultipliers (dSiPM) – a Scalable Alternative to Vacuum Photomultiplier Tubes (PMT)," *Physics Procedia,* vol. 37, pp. 1546-1560, 2012/01/01/ 2012, doi: https://doi.org/10.1016/j.phpro.2012.03.749.

[167] G. Barbarino, F. C. T. Barbato, L. Campajola, R. de Asmundis, G. De Rosa, C. M. Mollo, and D. Vivolo, "Vacuum silicon photomultipliers: Recent developments," *Nuclear Instruments and Methods in Physics Research Section A: Accelerators, Spectrometers, Detectors and Associated Equipment,* vol. 718, pp. 582-583, 2013/08/01/ 2013, doi: https://doi.org/10.1016/j.nima.2012.11.175.

[168] D. Renker, "New trends on photodetectors," *Nuclear Instruments and Methods in Physics Research Section A: Accelerators, Spectrometers, Detectors and Associated Equipment,* vol. 571, no. 1, pp. 1-6, 2007/02/01/ 2007, doi: https://doi.org/10.1016/j.nima.2006.10.016.

[169] J. Kang, Q. Li, and Y. Wan, "Experimental observation of the linear gain of back-illuminated ultraviolet avalanche photodiodes using a GaN/AlN periodically stacked structure," *Journal of Physics D: Applied Physics,* vol. 54, no. 28, p. 285107, 2021/05/10 2021, doi: 10.1088/1361-6463/abf957.

[170] D. Renker and E. Lorenz, "Advances in solid state photon detectors," *Journal of Instrumentation,* vol. 4, no. 04, p. P04004, 2009/04/07 2009, doi: 10.1088/1748-0221/4/04/P04004.

[171] T. Gogami, A. Asaturyan, J. Bono, P. Baturin, C. Chen, A. Chiba, N. Chiga, Y. Fujii, D. Kawama, T. Maruta, V. Maxwell, A. Mkrtchyan, S. Nagao, S. N. Nakamura, J. Reinhold, A. Shichijo, L. Tang, N. Taniya, S. A. Wood, and Z. Ye, "Bucking coil implementation on PMT for active canceling of magnetic field," *Nuclear Instruments and Methods in Physics Research, Section A: Accelerators, Spectrometers, Detectors and Associated Equipment,* Article vol. 729, pp. 816-824, 2013, doi: 10.1016/j.nima.2013.08.047.

[172] S. M. Gautier, L. J. Blum, and P. R. Coulet, "Fibre-optic biosensor based on luminescence and immobilized enzymes: Microdetermination of sorbitol, ethanol and oxaloacetate," *Journal of Bioluminescence and Chemiluminescence,* vol. 5, no. 1, pp. 57-63, 1990, doi: https://doi.org/10.1002/bio.1170050112.

[173] T. Gessei, T. Arakawa, H. Kudo, and K. Mitsubayashi, "A fiber-optic sorbitol biosensor based on NADH fluorescence detection toward rapid diagnosis of diabetic complications," *Analyst,* 10.1039/C4AN01593B vol. 140, no. 18, pp. 6335-6342, 2015, doi: 10.1039/C4AN01593B.

[174] X. Yi, S. Xie, B. Liang, L. W. Lim, J. S. Cheong, M. C. Debnath, D. L. Huffaker, C. H. Tan, and J. P. R. David, "Extremely low excess noise and high sensitivity AlAs0.56Sb0.44 avalanche photodiodes," *Nature Photonics,* vol. 13, no. 10, pp. 683-686, 2019/10/01 2019, doi: 10.1038/s41566-019-0477-4.

[175] J. C. Campbell, "Recent advances in avalanche photodiodes," in *2006 Digest of the LEOS Summer Topical Meetings*, 17-19 July 2006 2006, pp. 5-6, doi: 10.1109/LEOSST.2006.1694040.

[176] M. Nada, T. Yoshimatsu, Y. Muramoto, H. Yokoyama, and H. Matsuzaki, "Design and Performance of High-Speed Avalanche Photodiodes for 100-Gb/s Systems and Beyond," *Journal of Lightwave Technology,* vol. 33, no. 5, pp. 984-990, 2015, doi: 10.1109/JLT.2014.2377034.

[177] D. Li, K. Jiang, X. Sun, and C. Guo, "AlGaN photonics: Recent advances in materials and ultraviolet devices," *Advances in Optics and Photonics,* Review vol. 10, no. 1, pp. 43-110, 2018, doi: 10.1364/AOP.10.000043.

[178] C. Bruschini, H. Homulle, I. M. Antolovic, S. Burri, and E. Charbon, "Single-photon avalanche diode imagers in biophotonics: review and outlook," *Light: Science & Applications,* vol. 8, no. 1, p. 87, 2019/09/18 2019, doi: 10.1038/s41377-019-0191-5.

[179] R. Daniel, R. Almog, A. Ron, S. Belkin, and Y. S. Diamand, "Modeling and measurement of a whole-cell bioluminescent biosensor based on a single photon avalanche diode," *Biosensors and Bioelectronics,* vol. 24, no. 4, pp. 882-887, 2008/12/01/ 2008, doi: https://doi.org/10.1016/j.bios.2008.07.026.

[180] F. Lin, M. M. Sweeney, M. M. Sheehan, and A. Mathewson, "A protein biosensor using Geiger mode avalanche photodiodes," *Journal of Physics: Conference Series,* vol. 10, no. 1, p. 333, 2005/01/01 2005, doi: 10.1088/1742-6596/10/1/082.

[181] J. An and W. W. Carmichael, "Use of a colorimetric protein phosphatase inhibition assay and enzyme linked immunosorbent assay for the study of microcystins and nodularins," *Toxicon,* Article vol. 32, no. 12, pp. 1495-1507, 1994, doi: 10.1016/0041-0101(94)90308-5.

[182] M. B. A. Ashour, S. J. Gee, and B. D. Hammock, "Use of a 96-well microplate reader for measuring routine enzyme activities," *Analytical Biochemistry,* Article vol. 166, no. 2, pp. 353-360, 1987, doi: 10.1016/0003-2697(87)90585-9.

[183] P. Hodder, R. Mull, J. Cassaday, K. Berry, and B. Strulovici, "Miniaturization of intracellular calcium functional assays to 1536-well plate format using a fluorometric imaging plate reader," (in eng), *J Biomol Screen,* vol. 9, no. 5, pp. 417-26, Aug 2004, doi: 10.1177/1087057104264038.

[184] A. J. Kolb, "The role of microplate selection and assay design in the application of automation and robotics," *Chemometrics and Intelligent Laboratory Systems,* vol. 26, no. 2, pp. 107-113, 1994/11/01/ 1994, doi: https://doi.org/10.1016/0169-7439(94)90052-3.

[185] H. J. Heusinkveld and R. H. S. Westerink, "Caveats and limitations of plate reader-based high-throughput kinetic measurements of intracellular calcium levels," *Toxicology and Applied Pharmacology,* vol. 255, no. 1, pp. 1-8, 2011/08/15/ 2011, doi: https://doi.org/10.1016/j.taap.2011.05.020.

[186] L. F. Montaño-Gutierrez, N. M. Moreno, I. L. Farquhar, Y. Huo, L. Bandiera, and P. S. Swain, "Analysing and meta-analysing time-series data of microbial growth and gene expression from plate readers," *PLOS Computational Biology,* vol. 18, no. 5, p. e1010138, 2022, doi: 10.1371/journal.pcbi.1010138.

[187] S. Botasini, L. Luzuriaga, M. F. Cerdá, E. Méndez, G. Ferrer-Sueta, and A. Denicola, "Multiple Experiments and a Single Measurement: Introducing Microplate Readers in the Laboratory," *Journal of Chemical Education,* vol. 87, no. 10, pp. 1011-1014, 2010/10/01 2010, doi: 10.1021/ed100789j.

[188] K. Szymula, M. S. Magaraci, M. Patterson, A. Clark, S. G. Mannickarottu, and B. Y. Chow, "An Open-Source Plate Reader," *bioRxiv,* p. 413781, 2018, doi: 10.1101/413781.

[189] V. Sendilraj, M. Gulati, J. Standeven, and S. Bhamla, "Plate-Q: A Frugal Microplate-Reader for Bacterial Signal Quantification," *bioRxiv,* p. 2022.06.11.495768, 2022, doi: 10.1101/2022.06.11.495768.

[190] M. Imanbekova, A. S. Perumal, S. Kheireddine, D. V. Nicolau, and S. Wachsmann-Hogiu, "Lensless, reflection-based dark-field microscopy (RDFM) on a CMOS chip," *Biomed. Opt. Express,* vol. 11, no. 9, pp. 4942-4959, 2020/09/01 2020, doi: 10.1364/BOE.394615.

[191] M. Imanbekova, A. M. Saridag, M. Kahraman, J. Liu, H. Caglayan, and S. Wachsmann-Hogiu, "Complementary Metal-Oxide-Semiconductor-Based Sensing Platform for Trapping, Imaging, and Chemical Characterization of Biological Samples," *ACS Applied Optical Materials,* vol. 1, no. 1, pp. 329-339, 2023/01/27 2023, doi: 10.1021/acsaom.2c00066.

[192] E. R. Fossum and D. B. Hondongwa, "A Review of the Pinned Photodiode for CCD and CMOS Image Sensors," *IEEE Journal of the Electron Devices Society,* vol. 2, no. 3, pp. 33-43, 2014, doi: 10.1109/JEDS.2014.2306412.

[193] A. E. Gamal and H. Eltoukhy, "CMOS image sensors," *IEEE Circuits and Devices Magazine,* vol. 21, no. 3, pp. 6-20, 2005, doi: 10.1109/MCD.2005.1438751.

[194] W. S. Boyle and G. E. Smith, "Charge coupled semiconductor devices," *The Bell System Technical Journal,* vol. 49, no. 4, pp. 587-593, 1970, doi: 10.1002/j.1538-7305.1970.tb01790.x.

[195] M. F. Tompsett, G. F. Amelio, and G. E. Smith, "CHARGE COUPLED 8-BIT SHIFT REGISTER," *Applied Physics Letters,* vol. 17, no. 3, pp. 111-115, 1970, doi: 10.1063/1.1653327.

[196] M. Bigas, E. Cabruja, J. Forest, and J. Salvi, "Review of CMOS image sensors," *Microelectronics Journal,* vol. 37, no. 5, pp. 433-451, 2006/05/01/ 2006, doi: https://doi.org/10.1016/j.mejo.2005.07.002.

[197] N. Waltham, "CCD and CMOS sensors," in *Observing Photons in Space: A Guide to Experimental Space Astronomy*, M. C. E. Huber, A. Pauluhn, J. L. Culhane, J. G. Timothy, K. Wilhelm, and A. Zehnder Eds. New York, NY: Springer New York, 2013, pp. 423-442.

[198] R. F. Eric, "Active pixel sensors: are CCDs dinosaurs?," in *Proc.SPIE*, 1993, vol. 1900, pp. 2-14, doi: 10.1117/12.148585. [Online]. Available: https://doi.org/10.1117/12.148585

[199] S. Mendis, S. E. Kemeny, and E. R. Fossum, "CMOS active pixel image sensor," *IEEE Transactions on Electron Devices,* vol. 41, no. 3, pp. 452-453, 1994, doi: 10.1109/16.275235.

[200] X. Hu, R. Abbasi, and S. Wachsmann-Hogiu, "Microfluidics on lensless, semiconductor optical image sensors: challenges and opportunities for democratization of biosensing at the micro-and nano-scale," *Nanophotonics,* vol. 12, no. 21, pp. 3977-4008, 2023, doi: doi:10.1515/nanoph-2023-0301.

[201] N. Callens and G. G. E. Gielen, "Analysis and Comparison of Readout Architectures and Analog-to-Digital Converters for 3D-Stacked CMOS Image Sensors," *IEEE Transactions on Circuits and Systems I: Regular Papers,* vol. 68, no. 8, pp. 3117-3130, 2021, doi: 10.1109/TCSI.2021.3085027.

[202] S. Choi, S. Lee, T. Lee, H. Ji, H. Park, D. Im, D. Lee, J. Kim, S. You, and J. Choi, "World smallest 200Mp CMOS image sensor with 0.56 μm pixel equipped with novel deep trench isolation structure for better sensitivity and higher CG," in *Proceedings of the Int'l Image Sensor Workshop (IISW), Crieff, UK*, 2023, pp. 22-25.

[203] S. Kheireddine, Z. J. Smith, D. V. Nicolau, and S. Wachsmann-Hogiu, "Simple adaptive mobile phone screen illumination for dual phone differential phase contrast (DPDPC) microscopy," *Biomed. Opt. Express,* vol. 10, no. 9, pp. 4369-4380, 2019/09/01 2019, doi: 10.1364/BOE.10.004369.

[204] İ. Polatoğlu, L. Aydın, B. Ç. Nevruz, and S. Özer, "A Novel Approach for the Optimal Design of a Biosensor," *Analytical Letters,* vol. 53, no. 9, pp. 1428-1445, 2020/06/12 2020, doi: 10.1080/00032719.2019.1709075.

[205] V. Gaudin, "Advances in biosensor development for the screening of antibiotic residues in food products of animal origin – A comprehensive review," *Biosensors and Bioelectronics,* vol. 90, pp. 363-377, 2017/04/15/ 2017, doi: https://doi.org/10.1016/j.bios.2016.12.005.

[206] S. GS, A. CV, and B. B. Mathew, "Biosensors: A Modern Day Achievement," *Journal of Instrumentation Technology,* vol. 2, no. 1, pp. 26-39, 2014. [Online]. Available: http://pubs.sciepub.com/jit/2/1/5.

[207] J. Castillo, S. Gáspár, S. Leth, M. Niculescu, A. Mortari, I. Bontidean, V. Soukharev, S. A. Dorneanu, A. D. Ryabov, and E. Csöregi, "Biosensors for life quality: Design, development and applications," *Sensors and Actuators B: Chemical,* vol. 102, no. 2, pp. 179-194, 2004/09/13/ 2004, doi: https://doi.org/10.1016/j.snb.2004.04.084.

[208] N. R. Mohamad, N. H. C. Marzuki, N. A. Buang, F. Huyop, and R. A. Wahab, "An overview of technologies for immobilization of enzymes and surface analysis techniques for immobilized enzymes," *Biotechnology & Biotechnological Equipment,* vol. 29, no. 2, pp. 205-220, 2015/03/04 2015, doi: 10.1080/13102818.2015.1008192.

[209] M. Asal, Ö. Özen, M. Şahinler, H. T. Baysal, and İ. Polatoğlu, "An overview of biomolecules, immobilization methods and support materials of biosensors," *Sensor Review,* vol. 39, no. 3, pp. 377-386, 2019, doi: 10.1108/SR-04-2018-0084.

[210] J. Narang and C. S. Pundir, *Biosensors: an introductory textbook*. CRC Press, 2017.

[211] T. Rinken, "Biosensors," ed. Rijeka: IntechOpen, 2015.

[212] N. Bhalla, P. Jolly, N. Formisano, and P. Estrela, "Introduction to biosensors," (in eng), *Essays Biochem,* vol. 60, no. 1, pp. 1-8, Jun 30 2016, doi: 10.1042/ebc20150001.

[213] S. Vigneshvar, C. C. Sudhakumari, B. Senthilkumaran, and H. Prakash, "Recent Advances in Biosensor Technology for Potential Applications – An Overview," (in English), *Frontiers in Bioengineering and Biotechnology,* Review vol. 4, 2016-February-16 2016, doi: 10.3389/fbioe.2016.00011.

[214] M. A. Cooper, "Optical biosensors in drug discovery," *Nature Reviews Drug Discovery,* vol. 1, no. 7, pp. 515-528, 2002/07/01 2002, doi: 10.1038/nrd838.

[215] J. Homola, "Surface Plasmon Resonance Sensors for Detection of Chemical and Biological Species," *Chemical Reviews,* vol. 108, no. 2, pp. 462-493, 2008/02/01 2008, doi: 10.1021/cr068107d.

[216] J. F. Humbert, "Advances in the detection of phycotoxins and cyanotoxins," *Analytical and Bioanalytical Chemistry,* vol. 397, no. 5, pp. 1653-1654, 2010/07/01 2010, doi: 10.1007/s00216-010-3779-4.

[217] A. Sassolas, B. D. Leca-Bouvier, and L. J. Blum, "DNA Biosensors and Microarrays," *Chemical Reviews,* vol. 108, no. 1, pp. 109-139, 2008/01/01 2008, doi: 10.1021/cr0684467.

[218] D. M. Rissin and D. R. Walt, "Digital concentration readout of single enzyme molecules using femtoliter arrays and Poisson statistics," (in eng), *Nano Lett,* vol. 6, no. 3, pp. 520-3, Mar 2006, doi: 10.1021/nl060227d.

[219] X. Fan, I. M. White, S. I. Shopova, H. Zhu, J. D. Suter, and Y. Sun, "Sensitive optical biosensors for unlabeled targets: A review," *Analytica Chimica Acta,* vol. 620, no. 1, pp. 8-26, 2008/07/14/ 2008, doi: https://doi.org/10.1016/j.aca.2008.05.022.

[220] A. J. P. Theuwissen, "CMOS image sensors: State-of-the-art," *Solid-State Electronics,* vol. 52, no. 9, pp. 1401-1406, 2008/09/01/ 2008, doi: https://doi.org/10.1016/j.sse.2008.04.012.

[221] Hamamatsu Photonics K.K. https://www.hamamatsu.com/us/en.html (accessed.

[222] R. H. Hadfield, "Single-photon detectors for optical quantum information applications," *Nature Photonics,* vol. 3, no. 12, pp. 696-705, 2009/12/01 2009, doi: 10.1038/nphoton.2009.230.

[223] Y. Yu, W. Nie, K. Chu, X. Wei, and Z. J. Smith, "Highly Sensitive, Portable Detection System for Multiplex Chemiluminescence Analysis," *Analytical Chemistry,* vol. 95, no. 39, pp. 14762-14769, 2023/10/03 2023, doi: 10.1021/acs.analchem.3c02920.

[224] A. Roda, E. Michelini, L. Cevenini, D. Calabria, M. M. Calabretta, and P. Simoni, "Integrating biochemiluminescence detection on smartphones: mobile chemistry platform for point-of-need analysis," (in eng), *Anal Chem,* vol. 86, no. 15, pp. 7299-304, Aug 5 2014, doi: 10.1021/ac502137s.

[225] D. Calabria, M. Zangheri, I. Trozzi, E. Lazzarini, A. Pace, M. Mirasoli, and M. Guardigli, "Smartphone-Based Chemiluminescent Origami μPAD for the Rapid Assessment of Glucose Blood Levels," *Biosensors,* vol. 11, no. 10, p. 381, 2021. [Online]. Available: https://www.mdpi.com/2079-6374/11/10/381.

[226] G. Liu, Y. Wu, Y. Wang, W. Ye, M. Wu, and Q. Liu, "Smartphone-Based Portable Sensing Systems for Point-of-Care Detections," in *Portable and Wearable Sensing Systems*, 2024, pp. 89-110.

[227] J. Ma, Y. Guan, F. Xing, Y. Wang, X. Li, Q. Yu, and X. Yu, "Smartphone-based chemiluminescence detection of aflatoxin B1 via labelled and label-free dual sensing systems,"

Food Chemistry, vol. 413, p. 135654, 2023/07/01/ 2023, doi: https://doi.org/10.1016/j.foodchem.2023.135654.

[228] Y. Cai, H. Zhou, W. Li, C. Yao, J. Wang, and Y. Zhao, "A chemiluminescence method induced by microplasma jet for nitrites detection and the miniature detection system using smartphone," *Analytica Chimica Acta,* vol. 1267, p. 341339, 2023/08/01/ 2023, doi: https://doi.org/10.1016/j.aca.2023.341339.

[229] D. Calabria, A. Pace, E. Lazzarini, I. Trozzi, M. Zangheri, M. Guardigli, S. Pieraccini, S. Masiero, and M. Mirasoli, "Smartphone-Based Chemiluminescence Glucose Biosensor Employing a Peroxidase-Mimicking, Guanosine-Based Self-Assembled Hydrogel," *Biosensors,* vol. 13, no. 6, p. 650, 2023. [Online]. Available: https://www.mdpi.com/2079-6374/13/6/650.

[230] H. Chen, Y. Feng, F. Liu, C. Tan, N. Xu, Y. Jiang, and Y. Tan, "Universal smartphone-assisted label-free CRISPR/Cas12a-DNAzyme chemiluminescence biosensing platform for on-site detection of nucleic acid and non-nucleic acid targets," *Biosensors and Bioelectronics,* vol. 247, p. 115929, 2024/03/01/ 2024, doi: https://doi.org/10.1016/j.bios.2023.115929.

[231] P. Singh, N. Kumari, R. P. Ojha, N. R. Nirala, and R. Prakash, "Smartphone-Based Noninvasive Glucose Monitoring in Diabetic Patients Utilizing Enhanced Chemiluminescence Imaging Technique," *physica status solidi (a),* vol. 220, no. 24, p. 2300077, 2023, doi: https://doi.org/10.1002/pssa.202300077.

[232] S. Rink, A. Duerkop, and A. J. Baeumner, "Enhanced Chemiluminescence of a Superior Luminol Derivative Provides Sensitive Smartphone-Based Point-of-Care Testing with Enzymatic μPAD," *Analysis & Sensing,* vol. 3, no. 4, p. e202200111, 2023, doi: https://doi.org/10.1002/anse.202200111.

[233] J. Wen, D. He, S. Luo, S. Zhou, and Y. Yuan, "Cloud-based smartphone-assisted chemiluminescent assay for rapid screening of electroactive bacteria," *Science China Technological Sciences,* vol. 66, no. 3, pp. 743-750, 2023/03/01 2023, doi: 10.1007/s11431-022-2296-6.

[234] R. S. Rafee, H. R. Pouretedal, and S. Damiri, "Quantitative analysis of CL-20 explosive by smartphone-based chemiluminescence method," *Luminescence,* vol. 39, no. 5, p. e4775, 2024, doi: https://doi.org/10.1002/bio.4775.

[235] S. Wang, F. Qu, R. Zhang, T. Jin, T. Zheng, J. Shu, and H. Cui, "Emission Onset Time-Adjustable Chemiluminescent Gold Nanoparticles with Ultrastrong Emission for Smartphone-Based Immunoassay of Severe Acute Respiratory Syndrome Coronavirus 2 Antigen,"

Analytical Chemistry, vol. 95, no. 33, pp. 12497-12504, 2023/08/22 2023, doi: 10.1021/acs.analchem.3c02240.

[236] Y. Wu, D. Qin, Z. Luo, S. Hu, L. Xu, and B. Deng, "Construction of a smartphone-based electrochemiluminescence imaging device to guide the improvement of sensing performance via surface regulation," *Sensors and Actuators B: Chemical,* vol. 389, p. 133885, 2023/08/15/ 2023, doi: https://doi.org/10.1016/j.snb.2023.133885.

[237] A. Kumar, D. Jain, J. Bahuguna, M. Bhaiyya, S. K. Dubey, A. Javed, and S. Goel, "Machine learning assisted and smartphone integrated homogeneous electrochemiluminescence biosensor platform for sample to answer detection of various human metabolites," *Biosensors and Bioelectronics,* vol. 238, p. 115582, 2023/10/15/ 2023, doi: https://doi.org/10.1016/j.bios.2023.115582.

[238] Z. Lu, S. Dai, T. Liu, J. Yang, M. Sun, C. Wu, G. Su, X. Wang, H. Rao, H. Yin, X. Zhou, J. Ye, and Y. Wang, "Machine learning-assisted Te–CdS@Mn3O4 nano-enzyme induced self-enhanced molecularly imprinted ratiometric electrochemiluminescence sensor with smartphone for portable and visual monitoring of 2,4-D," *Biosensors and Bioelectronics,* vol. 222, p. 114996, 2023/02/15/ 2023, doi: https://doi.org/10.1016/j.bios.2022.114996.

[239] W. Nie, R. Zhang, C. Hu, T. Jin, X. Wei, and H. Cui, "A self-enhanced electrochemiluminescence array chip for portable label-free detection of SARS-CoV-2 nucleocapsid protein with smartphone," *Biosensors and Bioelectronics,* vol. 240, p. 115662, 2023/11/15/ 2023, doi: https://doi.org/10.1016/j.bios.2023.115662.

[240] M.-M. Chen, M.-L. Zhang, X. Song, J. Jiang, X. Tang, Q. Zhang, X. Zhang, and P. Li, "Smartphone-assisted electrochemiluminescence imaging test strips towards dual-signal visualized and sensitive monitoring of aflatoxin B1 in corn samples," *Chinese Chemical Letters,* p. 109785, 2024/03/18/ 2024, doi: https://doi.org/10.1016/j.cclet.2024.109785.

[241] E. Tamiya, S. Osaki, and H. Nagai, "Wireless electrochemiluminescent biosensors: Powering innovation with smartphone technology," *Biosensors and Bioelectronics,* vol. 252, p. 116083, 2024/05/15/ 2024, doi: https://doi.org/10.1016/j.bios.2024.116083.

[242] K. Zheng, J. Pan, Z. Yu, C. Yi, and M.-J. Li, "A smartphone-assisted electrochemiluminescent detection of miRNA-21 in situ using Ru(bpy)32+@MOF," *Talanta,* vol. 268, p. 125310, 2024/02/01/ 2024, doi: https://doi.org/10.1016/j.talanta.2023.125310.

[243] Y. Yao, H. Li, D. Wang, C. Liu, and C. Zhang, "An electrochemiluminescence cloth-based biosensor with smartphone-based imaging for detection of lactate in saliva," *Analyst,* 10.1039/C7AN01008G vol. 142, no. 19, pp. 3715-3724, 2017, doi: 10.1039/C7AN01008G.

[244] L. Chen, C. Zhang, and D. Xing, "Paper-based bipolar electrode-electrochemiluminescence (BPE-ECL) device with battery energy supply and smartphone read-out: A handheld ECL system for biochemical analysis at the point-of-care level," *Sensors and Actuators B: Chemical,* vol. 237, pp. 308-317, 2016/12/01/ 2016, doi: https://doi.org/10.1016/j.snb.2016.06.105.

[245] E. Kerr, R. Farr, E. H. Doeven, Y. H. Nai, R. Alexander, R. M. Guijt, B. Prieto-Simon, P. S. Francis, M. Dearnley, D. J. Hayne, L. C. Henderson, and N. H. Voelcker, "Amplification-free electrochemiluminescence molecular beacon-based microRNA sensing using a mobile phone for detection," *Sensors and Actuators B: Chemical,* vol. 330, p. 129261, 2021/03/01/ 2021, doi: https://doi.org/10.1016/j.snb.2020.129261.

[246] T. Liu, J. He, Z. Lu, M. Sun, M. Wu, X. Wang, Y. Jiang, P. Zou, H. Rao, and Y. Wang, "A visual electrochemiluminescence molecularly imprinted sensor with Ag+@UiO-66-NH2 decorated CsPbBr3 perovskite based on smartphone for point-of-care detection of nitrofurazone," *Chemical Engineering Journal,* vol. 429, p. 132462, 2022/02/01/ 2022, doi: https://doi.org/10.1016/j.cej.2021.132462.

[247] S. Li, D. Zhang, J. Liu, C. Cheng, L. Zhu, C. Li, Y. Lu, S. S. Low, B. Su, and Q. Liu, "Electrochemiluminescence on smartphone with silica nanopores membrane modified electrodes for nitroaromatic explosives detection," *Biosensors and Bioelectronics,* vol. 129, pp. 284-291, 2019/03/15/ 2019, doi: https://doi.org/10.1016/j.bios.2018.09.055.

[248] S. Zhang, Z. Lu, S. Li, T. Wang, J. Li, M. Chen, S. Chen, M. Sun, Y. Wang, H. Rao, and T. Liu, "Portable smartphone device-based multi-signal sensing system for on-site and visual determination of alkaline phosphatase in human serum," *Microchimica Acta,* vol. 188, no. 5, p. 157, 2021/04/06 2021, doi: 10.1007/s00604-021-04803-3.

[249] L. Zhu, S. Li, W. Liu, J. Chen, Q. Yu, Z. Zhang, Y. Li, J. Liu, and X. Chen, "Real time detection of 3-nitrotyrosine using smartphone-based electrochemiluminescence," *Biosensors and Bioelectronics,* vol. 187, p. 113284, 2021/09/01/ 2021, doi: https://doi.org/10.1016/j.bios.2021.113284.

[250] K. L. Rahn, T. D. Rhoades, and R. K. Anand, "Alternating Current Voltammetry at a Bipolar Electrode with Smartphone Luminescence Imaging for Point-of-Need Sensing," *ChemElectroChem,* vol. 7, no. 5, pp. 1172-1181, 2020, doi: https://doi.org/10.1002/celc.202000079.

[251] S. Li, Y. Lu, L. Liu, S. S. Low, B. Su, J. Wu, L. Zhu, C. Li, and Q. Liu, "Fingerprints mapping and biochemical sensing on smartphone by electrochemiluminescence," *Sensors and*

Actuators B: Chemical, vol. 285, pp. 34-41, 2019/04/15/ 2019, doi: https://doi.org/10.1016/j.snb.2019.01.035.

[252] L. Zhu, W. Fu, J. Chen, S. Li, X. Xie, Z. Zhang, J. Liu, L. Zhou, B. Su, and X. Chen, "A fully integrated and handheld electrochemiluminescence device for detection of dopamine in bio-samples," *Sensors and Actuators B: Chemical,* vol. 366, p. 131972, 2022/09/01/ 2022, doi: https://doi.org/10.1016/j.snb.2022.131972.

[253] Z. J. Smith, K. Chu, A. R. Espenson, M. Rahimzadeh, A. Gryshuk, M. Molinaro, D. M. Dwyre, S. Lane, D. Matthews, and S. Wachsmann-Hogiu, "Cell-Phone-Based Platform for Biomedical Device Development and Education Applications," *PLOS ONE,* vol. 6, no. 3, p. e17150, 2011, doi: 10.1371/journal.pone.0017150.

[254] S. Kheireddine, A. Sudalaiyadum Perumal, Z. J. Smith, D. V. Nicolau, and S. Wachsmann-Hogiu, "Dual-phone illumination-imaging system for high resolution and large field of view multi-modal microscopy," *Lab on a Chip,* 10.1039/C8LC00995C vol. 19, no. 5, pp. 825-836, 2019, doi: 10.1039/C8LC00995C.

[255] F. C. M. J. M. van Delft, G. Ipolitti, D. V. Nicolau, A. Sudalaiyadum Perumal, O. Kašpar, S. Kheireddine, S. Wachsmann-Hogiu, and D. V. Nicolau, "Something has to give: scaling combinatorial computing by biological agents exploring physical networks encoding NP-complete problems," *Interface Focus,* vol. 8, no. 6, p. 20180034, 2018, doi: doi:10.1098/rsfs.2018.0034.

[256] Y. Wu and A. Ozcan, "Lensless digital holographic microscopy and its applications in biomedicine and environmental monitoring," *Methods,* vol. 136, pp. 4-16, 2018/03/01/ 2018, doi: https://doi.org/10.1016/j.ymeth.2017.08.013.

[257] I. Pushkarsky, Y. Liu, W. Weaver, T.-W. Su, O. Mudanyali, A. Ozcan, and D. Di Carlo, "Automated single-cell motility analysis on a chip using lensfree microscopy," *Scientific Reports,* vol. 4, no. 1, p. 4717, 2014/04/17 2014, doi: 10.1038/srep04717.

[258] M. Zangheri, F. Di Nardo, L. Anfossi, C. Giovannoli, C. Baggiani, A. Roda, and M. Mirasoli, "A multiplex chemiluminescent biosensor for type B-fumonisins and aflatoxin B1 quantitative detection in maize flour," *Analyst,* 10.1039/C4AN01613K vol. 140, no. 1, pp. 358-365, 2015, doi: 10.1039/C4AN01613K.

[259] A. Roda, M. Mirasoli, L. S. Dolci, A. Buragina, F. Bonvicini, P. Simoni, and M. Guardigli, "Portable Device Based on Chemiluminescence Lensless Imaging for Personalized Diagnostics through Multiplex Bioanalysis," *Analytical Chemistry,* vol. 83, no. 8, pp. 3178-3185, 2011/04/15 2011, doi: 10.1021/ac200360k.

[260] E. K. Bolton, G. S. Sayler, D. E. Nivens, J. M. Rochelle, S. Ripp, and M. L. Simpson, "Integrated CMOS photodetectors and signal processing for very low-level chemical sensing with the bioluminescent bioreporter integrated circuit," *Sensors and Actuators B: Chemical,* vol. 85, no. 1, pp. 179-185, 2002/06/20/ 2002, doi: https://doi.org/10.1016/S0925-4005(02)00106-5.

[261] A. Roda, L. Cevenini, S. Borg, E. Michelini, M. M. Calabretta, and D. Schüler, "Bioengineered bioluminescent magnetotactic bacteria as a powerful tool for chip-based whole-cell biosensors," *Lab on a Chip,* 10.1039/C3LC50868D vol. 13, no. 24, pp. 4881-4889, 2013, doi: 10.1039/C3LC50868D.

[262] J. Ma, B. Veltman, Z. Tietel, L. Tsror, Y. Liu, and E. Eltzov, "Monitoring of infection volatile markers using CMOS-based luminescent bioreporters," *Talanta,* vol. 219, p. 121333, 2020/11/01/ 2020, doi: https://doi.org/10.1016/j.talanta.2020.121333.

[263] X. Chen, W. Wang, and B. Li, "Chapter 6 - Novel Nanomaterials for the Fabrication of Electrochemiluminescent Sensors," in *Novel Nanomaterials for Biomedical, Environmental and Energy Applications*, X. Wang and X. Chen Eds.: Elsevier, 2019, pp. 189-214.

[264] P. Tirgar, F. Sarmadi, M. Najafi, P. Kazemi, S. AzizMohseni, S. Fayazi, G. Zandi, N. Ziaie, A. Shoushtari Zadeh Naseri, A. Ehrlicher, and M. Dashtizad, "Toward embryo cryopreservation-on-a-chip: A standalone microfluidic platform for gradual loading of cryoprotectants to minimize cryoinjuries," *Biomicrofluidics,* vol. 15, no. 3, 2021, doi: 10.1063/5.0047185.

[265] M. M. Mardanpour, A. Sudalaiyadum Perumal, Z. Mahmoodi, K. Baassiri, G. Montiel-Rubies, K. M. LeDez, and D. V. Nicolau, "Investigation of air bubble behaviour after gas embolism events induced in a microfluidic network mimicking microvasculature," *Lab on a Chip,* 10.1039/D4LC00087K vol. 24, no. 9, pp. 2518-2536, 2024, doi: 10.1039/D4LC00087K.

[266] Y. Liu, H. Shen, X. Yang, S. Kang, L. Cai, T. Tian, R. Su, C. Yang, and Z. Zhu, "Recent progress in microfluidic biosensors with different driving forces," *TrAC Trends in Analytical Chemistry,* vol. 158, p. 116894, 2023/01/01/ 2023, doi: https://doi.org/10.1016/j.trac.2022.116894.

[267] D. Lange, C. W. Storment, C. A. Conley, and G. T. A. Kovacs, "A microfluidic shadow imaging system for the study of the nematode Caenorhabditis elegans in space," *Sensors and Actuators B: Chemical,* vol. 107, no. 2, pp. 904-914, 2005/06/29/ 2005, doi: https://doi.org/10.1016/j.snb.2004.12.039.

[268] S. M. Scott and Z. Ali, "Fabrication Methods for Microfluidic Devices: An Overview," (in eng), *Micromachines (Basel),* vol. 12, no. 3, Mar 18 2021, doi: 10.3390/mi12030319.

[269] X. Huang, U. Farooq, J. Chen, Y. Ge, H. Gao, J. Su, X. Wang, S. Dong, and J. K. Luo, "A Surface Acoustic Wave Pumped Lensless Microfluidic Imaging System for Flowing Cell Detection and Counting," *IEEE Transactions on Biomedical Circuits and Systems,* vol. 11, no. 6, pp. 1478-1487, 2017, doi: 10.1109/TBCAS.2017.2732828.

[270] X. Liu, X. Huang, Y. Jiang, H. Xu, J. Guo, H. W. Hou, M. Yan, and H. Yu, "A Microfluidic Cytometer for Complete Blood Count With a 3.2-Megapixel, 1.1- μm-Pitch Super-Resolution Image Sensor in 65-nm BSI CMOS," *IEEE Transactions on Biomedical Circuits and Systems,* vol. 11, no. 4, pp. 794-803, 2017, doi: 10.1109/TBCAS.2017.2697451.

[271] X. Huang, J. Guo, X. Wang, M. Yan, Y. Kang, and H. Yu, "A contact-imaging based microfluidic cytometer with machine-learning for single-frame super-resolution processing," (in eng), *PLoS One,* vol. 9, no. 8, p. e104539, 2014, doi: 10.1371/journal.pone.0104539.

[272] X. Huang, Y. Jiang, X. Liu, H. Xu, Z. Han, H. Rong, H. Yang, M. Yan, and H. Yu, "Machine Learning Based Single-Frame Super-Resolution Processing for Lensless Blood Cell Counting," *Sensors,* vol. 16, no. 11, p. 1836, 2016. [Online]. Available: https://www.mdpi.com/1424-8220/16/11/1836.

[273] G. Zheng, S. A. Lee, Y. Antebi, M. B. Elowitz, and C. Yang, "The ePetri dish, an on-chip cell imaging platform based on subpixel perspective sweeping microscopy (SPSM)," (in eng), *Proc Natl Acad Sci U S A,* vol. 108, no. 41, pp. 16889-94, Oct 11 2011, doi: 10.1073/pnas.1110681108.

[274] Y. Liao, N. Yu, D. Tian, S. Li, and Z. Li, "A Quantized CNN-Based Microfluidic Lensless-Sensing Mobile Blood-Acquisition and Analysis System," *Sensors,* vol. 19, no. 23, p. 5103, 2019. [Online]. Available: https://www.mdpi.com/1424-8220/19/23/5103.

[275] S. A. Lee, G. Zheng, N. Mukherjee, and C. Yang, "On-chip continuous monitoring of motile microorganisms on an ePetri platform," *Lab on a Chip,* 10.1039/C2LC40090A vol. 12, no. 13, pp. 2385-2390, 2012, doi: 10.1039/C2LC40090A.

[276] J. H. Jung and J. E. Lee, "Real-time bacterial microcolony counting using on-chip microscopy," *Scientific Reports,* vol. 6, no. 1, p. 21473, 2016/02/23 2016, doi: 10.1038/srep21473.

[277] S. A. Lee, J. Erath, G. Zheng, X. Ou, P. Willems, D. Eichinger, A. Rodriguez, and C. Yang, "Imaging and Identification of Waterborne Parasites Using a Chip-Scale Microscope," *PLOS ONE,* vol. 9, no. 2, p. e89712, 2014, doi: 10.1371/journal.pone.0089712.

[278] V. F. Annese, C. Giagkoulovits, C. Hu, M. A. Al-Rawhani, J. Grant, S. B. Patil, and D. R. S. Cumming, "Micromolar Metabolite Measurement in an Electronically Multiplexed

Format," (in eng), *IEEE Trans Biomed Eng,* vol. 69, no. 9, pp. 2715-2722, Sep 2022, doi: 10.1109/tbme.2022.3147855.

[279] B. Van Dorst, M. Brivio, E. Van Der Sar, M. Blom, S. Reuvekamp, S. Tanzi, R. Groenhuis, A. Adojutelegan, E. J. Lous, F. Frederix, and L. J. Stuyver, "Integration of an optical CMOS sensor with a microfluidic channel allows a sensitive readout for biological assays in point-of-care tests," (in eng), *Biosens Bioelectron,* vol. 78, pp. 126-131, Apr 15 2016, doi: 10.1016/j.bios.2015.11.027.

[280] W.-C. Kao, S. Belkin, and J.-Y. Cheng, "Microbial biosensing of ciprofloxacin residues in food by a portable lens-free CCD-based analyzer," *Analytical and Bioanalytical Chemistry,* vol. 410, no. 4, pp. 1257-1263, 2018/02/01 2018, doi: 10.1007/s00216-017-0792-x.

[281] S. A. Lee, R. Leitao, G. Zheng, S. Yang, A. Rodriguez, and C. Yang, "Color Capable Sub-Pixel Resolving Optofluidic Microscope and Its Application to Blood Cell Imaging for Malaria Diagnosis," *PLOS ONE,* vol. 6, no. 10, p. e26127, 2011, doi: 10.1371/journal.pone.0026127.

[282] G. Zheng, S. A. Lee, S. Yang, and C. Yang, "Sub-pixel resolving optofluidic microscope for on-chip cell imaging," *Lab on a Chip,* 10.1039/C0LC00213E vol. 10, no. 22, pp. 3125-3129, 2010, doi: 10.1039/C0LC00213E.

[283] S. Pang, X. Cui, J. DeModena, Y. M. Wang, P. Sternberg, and C. Yang, "Implementation of a color-capable optofluidic microscope on a RGB CMOS color sensor chip substrate," *Lab on a Chip,* 10.1039/B919004J vol. 10, no. 4, pp. 411-414, 2010, doi: 10.1039/B919004J.

[284] Y. D. Han, H. J. Chun, and H. C. Yoon, "Low-cost Point-of-Care Biosensors Using Common Electronic Components as Transducers," *BioChip Journal,* vol. 14, no. 1, pp. 32-47, 2020/03/01 2020, doi: 10.1007/s13206-020-4104-8.

[285] M. Mirasoli, F. Bonvicini, L. S. Dolci, M. Zangheri, G. Gallinella, and A. Roda, "Portable chemiluminescence multiplex biosensor for quantitative detection of three B19 DNA genotypes," *Analytical and Bioanalytical Chemistry,* vol. 405, no. 2, pp. 1139-1143, 2013/01/01 2013, doi: 10.1007/s00216-012-6573-7.

[286] J. Baader, H. Klapproth, S. Bednar, T. Brandstetter, J. Rühe, M. Lehmann, and I. Freund, "Polysaccharide microarrays with a CMOS based signal detection unit," *Biosensors and Bioelectronics,* vol. 26, no. 5, pp. 1839-1846, 2011/01/15/ 2011, doi: https://doi.org/10.1016/j.bios.2010.01.021.

[287] G. Sciutto, M. Zangheri, L. Anfossi, M. Guardigli, S. Prati, M. Mirasoli, F. Di Nardo, C. Baggiani, R. Mazzeo, and A. Roda, "Miniaturized Biosensors to Preserve and Monitor Cultural Heritage: from Medical to Conservation Diagnosis," *Angewandte Chemie*

International Edition, vol. 57, no. 25, pp. 7385-7389, 2018, doi: https://doi.org/10.1002/anie.201713298.

[288] M. Zangheri, M. Mirasoli, M. Guardigli, F. Di Nardo, L. Anfossi, C. Baggiani, P. Simoni, M. Benassai, and A. Roda, "Chemiluminescence-based biosensor for monitoring astronauts' health status during space missions: Results from the International Space Station," *Biosensors and Bioelectronics,* vol. 129, pp. 260-268, 2019/03/15/ 2019, doi: https://doi.org/10.1016/j.bios.2018.09.059.

[289] M. M. Calabretta, M. Zangheri, D. Calabria, A. Lopreside, L. Montali, E. Marchegiani, I. Trozzi, M. Guardigli, M. Mirasoli, and E. Michelini, "Paper-Based Immunosensors with Bio-Chemiluminescence Detection," *Sensors,* vol. 21, no. 13, p. 4309, 2021. [Online]. Available: https://www.mdpi.com/1424-8220/21/13/4309.

[290] R. R. Singh, L. Leng, A. Guenther, and R. Genov, "A CMOS-Microfluidic Chemiluminescence Contact Imaging Microsystem," *IEEE Journal of Solid-State Circuits,* vol. 47, no. 11, pp. 2822-2833, 2012, doi: 10.1109/JSSC.2012.2214182.

[291] A. Greenbaum, Y. Zhang, A. Feizi, P.-L. Chung, W. Luo, S. R. Kandukuri, and A. Ozcan, "Wide-field computational imaging of pathology slides using lens-free on-chip microscopy," *Science Translational Medicine,* vol. 6, no. 267, pp. 267ra175-267ra175, 2014, doi: doi:10.1126/scitranslmed.3009850.

[292] Z. Göröcs and A. Ozcan, "On-Chip Biomedical Imaging," *IEEE Reviews in Biomedical Engineering,* vol. 6, pp. 29-46, 2013, doi: 10.1109/RBME.2012.2215847.

[293] S. Moon, H. O. Keles, Y. G. Kim, D. Kuritzkes, and U. Demirci, "Lensless imaging for point-of-care testing," in *2009 Annual International Conference of the IEEE Engineering in Medicine and Biology Society*, 3-6 Sept. 2009 2009, pp. 6376-6379, doi: 10.1109/IEMBS.2009.5333765.

[294] V. Chaudhary, A. Kaushik, H. Furukawa, and A. Khosla, "Review—Towards 5th Generation AI and IoT Driven Sustainable Intelligent Sensors Based on 2D MXenes and Borophene," *ECS Sensors Plus,* vol. 1, no. 1, p. 013601, 2022/04/07 2022, doi: 10.1149/2754-2726/ac5ac6.

[295] N. Sagar Shrikrishna, R. Sharma, J. Sahoo, A. Kaushik, and S. Gandhi, "Navigating the landscape of optical biosensors," *Chemical Engineering Journal,* vol. 490, p. 151661, 2024/06/15/ 2024, doi: https://doi.org/10.1016/j.cej.2024.151661.

[296] A. Amini, A. Khavari, F. Barthelat, and A. J. Ehrlicher, "Centrifugation and index matching yield a strong and transparent bioinspired nacreous composite," *Science,* vol. 373, no. 6560, pp. 1229-1234, 2021, doi: doi:10.1126/science.abf0277.

[297] S. Jain, M. Nehra, R. Kumar, N. Dilbaghi, T. Hu, S. Kumar, A. Kaushik, and C.-z. Li, "Internet of medical things (IoMT)-integrated biosensors for point-of-care testing of infectious diseases," *Biosensors and Bioelectronics,* vol. 179, p. 113074, 2021/05/01/ 2021, doi: https://doi.org/10.1016/j.bios.2021.113074.

[298] V. Chugh, A. Basu, N. K. Kaushik, A. Kaushik, Y. K. Mishra, and A. K. Basu, "Smart nanomaterials to support quantum-sensing electronics," *Materials Today Electronics,* vol. 6, p. 100067, 2023/12/01/ 2023, doi: https://doi.org/10.1016/j.mtelec.2023.100067.

[299] F. Cui, Y. Yue, Y. Zhang, Z. Zhang, and H. S. Zhou, "Advancing Biosensors with Machine Learning," *ACS Sensors,* vol. 5, no. 11, pp. 3346-3364, 2020/11/25 2020, doi: 10.1021/acssensors.0c01424.

[300] M. Taniguchi, "Combination of Single-Molecule Electrical Measurements and Machine Learning for the Identification of Single Biomolecules," *ACS Omega,* vol. 5, no. 2, pp. 959-964, 2020/01/21 2020, doi: 10.1021/acsomega.9b03660.

[301] H. Jeong, J. A. Rogers, and S. Xu, "Continuous on-body sensing for the COVID-19 pandemic: Gaps and opportunities," *Science Advances,* vol. 6, no. 36, p. eabd4794, 2020, doi: doi:10.1126/sciadv.abd4794.

[302] S. Sundaram, P. Kellnhofer, Y. Li, J.-Y. Zhu, A. Torralba, and W. Matusik, "Learning the signatures of the human grasp using a scalable tactile glove," *Nature,* vol. 569, no. 7758, pp. 698-702, 2019/05/01 2019, doi: 10.1038/s41586-019-1234-z.

[303] S. Knežević, E. Kerr, B. Goudeau, G. Valenti, F. Paolucci, P. S. Francis, F. Kanoufi, and N. Sojic, "Bimodal Electrochemiluminescence Microscopy of Single Cells," *Analytical Chemistry,* vol. 95, no. 18, pp. 7372-7378, 2023/05/09 2023, doi: 10.1021/acs.analchem.3c00869.

[304] A. Firoozbakhtian, N. Sojic, G. Xu, and M. Hosseini, "Electrochemiluminescence Sensors in Bioanalysis," in *Encyclopedia of Sensors and Biosensors (First Edition)*, R. Narayan Ed. Oxford: Elsevier, 2023, pp. 317-340.

[305] M. Bhaiyya, P. K. Pattnaik, and S. Goel, "A brief review on miniaturized electrochemiluminescence devices: From fabrication to applications," *Current Opinion in Electrochemistry,* vol. 30, p. 100800, 2021/12/01/ 2021, doi: https://doi.org/10.1016/j.coelec.2021.100800.

[306] M. Mousavizadegan, A. Firoozbakhtian, M. Hosseini, and H. Ju, "Machine learning in analytical chemistry: From synthesis of nanostructures to their applications in luminescence sensing," *TrAC Trends in Analytical Chemistry,* vol. 167, p. 117216, 2023/10/01/ 2023, doi: https://doi.org/10.1016/j.trac.2023.117216.

[307] S. K. Srivastava, M. Bhaiyya, S. Dudala, C. Hota, and S. Goel, "A machine learning approach for electrochemiluminescence based point of care testing device to detect multiple biomarkers," *Sensors and Actuators A: Physical,* vol. 350, p. 114135, 2023/02/01/ 2023, doi: https://doi.org/10.1016/j.sna.2022.114135.

[308] A. Firoozbakhtian, M. Hosseini, M. N. Sheikholeslami, F. Salehnia, G. Xu, H. Rabbani, and E. Sobhanie, "Detection of COVID-19: A Smartphone-Based Machine-Learning-Assisted ECL Immunoassay Approach with the Ability of RT-PCR CT Value Prediction," *Analytical Chemistry,* vol. 94, no. 47, pp. 16361-16368, 2022/11/29 2022, doi: 10.1021/acs.analchem.2c03502.

[309] C. Dodeigne, L. Thunus, and R. Lejeune, "Chemiluminescence as diagnostic tool. A review," *Talanta,* vol. 51, no. 3, pp. 415-439, 2000/03/06/ 2000, doi: https://doi.org/10.1016/S0039-9140(99)00294-5.

[310] L. J. Kricka, "Clinical applications of chemiluminescence," *Analytica Chimica Acta,* vol. 500, no. 1, pp. 279-286, 2003/12/19/ 2003, doi: https://doi.org/10.1016/S0003-2670(03)00809-2.

[311] N. Barnett and P. Francis, "Chemiluminescence: liquid-phase," 2005. [Online]. Available: https://dro.deakin.edu.au/articles/journal_contribution/Chemiluminescence_liquid-phase/20569734.

[312] A. Firoozbakhtian and M. Hosseini, "Chemiluminescence Sensors in Bioanalysis," in *Encyclopedia of Sensors and Biosensors (First Edition)*, R. Narayan Ed. Oxford: Elsevier, 2023, pp. 341-356.

[313] A. Kazak, Y. Plugatar, J. Johnson, Y. Grishin, P. Chetyrbok, V. Korzin, P. Kaur, and T. Kokodey, "The Use of Machine Learning for Comparative Analysis of Amperometric and Chemiluminescent Methods for Determining Antioxidant Activity and Determining the Phenolic Profile of Wines," *Applied System Innovation,* vol. 5, no. 5, p. 104, 2022. [Online]. Available: https://www.mdpi.com/2571-5577/5/5/104.

[314] A. J. Syed and J. C. Anderson, "Applications of bioluminescence in biotechnology and beyond," *Chemical Society Reviews,* 10.1039/D0CS01492C vol. 50, no. 9, pp. 5668-5705, 2021, doi: 10.1039/D0CS01492C.

[315] W.-C. Huang, C.-D. Wei, S. Belkin, T.-H. Hsieh, and J.-Y. Cheng, "Machine-learning assisted antibiotic detection and categorization using a bacterial sensor array," *Sensors and Actuators B: Chemical,* vol. 355, p. 131257, 2022/03/15/ 2022, doi: https://doi.org/10.1016/j.snb.2021.131257.

[316] I. A. Denisov, "Luciferase-based bioassay for rapid pollutants detection and classification by means of multilayer artificial neural networks," *Sensors and Actuators B: Chemical,* vol. 242, pp. 653-657, 2017/04/01/ 2017, doi: https://doi.org/10.1016/j.snb.2016.11.071.

Transition to Chapter III

The previous chapter provided a review of the combination of chemiluminescence-based biosensors with lensless image sensors for point-of-care and point-of-need applications. We reviewed optical modalities that can be used in an optical biosensor, and we explored the integration of these systems with microfluidics and artificial intelligence. The fundamental principles of chemiluminescence signal generation and optical detection methods were discussed. Subsequently, we delved into the integration of image sensors with luminescent biosensors, microfluidic sample handling, and artificial intelligence.

Among all optical modalities, chemiluminescence demonstrates significant potential for the purpose of this thesis, which aims to develop a fully integrated analytical device. Chemiluminescence offers distinct advantages over other optical methods, such as the absence of the need for a light source or filter sets. Among various optical detectors, CMOS sensors emerge as the optimal choice due to their superior performance and ability to integrate seamlessly with other components of the biosensor. Developing a cost-effective chemiluminescent (CL) device that also promotes portability, accuracy, and rapid results is crucial for early detection and appropriate treatment. Additionally, there is a critical need to construct a point-of-care (POC) diagnostic device suitable for food safety applications. These challenges underscore the motivation to develop POC diagnostic and prognostic tools with new modalities, such as CL, specifically for food safety applications.

In this chapter and as the first demonstration of the platform, we introduce a novel biosensor utilizing a CMOS image sensor for detecting ATP via bioluminescence. Samples were collected from various surfaces using UltraSnap swabs and directly applied to the sensor. The close proximity between the sample and the sensor optimized light capture, enabling accurate quantification of microbial contamination through bioluminescence intensity analysis. The biosensor demonstrated a wide linear range and high sensitivity for ATP detection. Comparative analysis with a commercial luminometer revealed strong correlation and comparable performance, while the CMOS-based biosensor offered a significant cost reduction.

This chapter is based on my co-first-author publication. The contributions of each author are as below:

RA and SWH conceived the study concept. RA and MI designed the experiments. RA and MI conducted the experiments, and RA analyzed the results. RA and MI wrote the main text of the manuscript. RA drafted and revised the article. SWH supervised the project. All authors reviewed and approved the manuscript in its current form and confirmed that this manuscript is only being used in the current thesis.

Chapter III. On-chip bioluminescence biosensor for the detection of microbial surface contamination

Reza Abbasi [a,b], Meruyert Imanbekova [a,b], Sebastian Wachsmann-Hogiu [a*]

[a] Department of Bioengineering, McGill University, Montreal, QC, H3A 0E9, Canada

[b] Equal contributions

Email: sebastian.wachsmannhogiu@mcgill.ca

3.1 Abstract

Detection of microbial pathogens is important for food safety reasons, and for monitoring sanitation in laboratory environments and health care settings. Traditional detection methods such as culture-based and nucleic acid-based methods are time-consuming, laborious, and require expensive laboratory equipment. Recently, ATP-based bioluminescence methods were developed to assess surface contamination, with commercial products available. In this study, we introduce a biosensor based on a CMOS image sensor for ATP-mediated chemiluminescence detection. The original lens and IR filter were removed from the CMOS sensor revealing a 12 MP periodic microlens/pixel array on an area of 6.5 mm × 3.6 mm. UltraSnap swabs are used to collect samples from solid surfaces including personal electronic devices, and office and laboratory equipment. Samples mixed with chemiluminescence reagents were placed directly on the surface of the imaging sensor. Close proximity of the sample to the photodiode array leads to high photon collection efficiency. The population of microorganisms can be assessed and quantified by analyzing the intensity of measured chemiluminescence. We report a linear range and limit of detection for measuring ATP in UltraSnap buffer of 10-1000 nM and 225 fmol, respectively. The performance of the CMOS-based device was compared to a commercial luminometer, and a high correlation with a Pearson's correlation coefficient of 0.98589 was obtained. The Bland-Altman plot showed no significant bias between the results of the two methods. Finally, microbial contamination of different surfaces was analyzed with both methods, and the CMOS biosensor exhibited the same trend as the commercial luminometer.

Keywords: bioluminescence; CMOS image sensor; ATP; microbial contamination; food safety

3.2 Introduction

According to the World Health Organization, foodborne diseases (FBD) are mainly caused by microbial contamination[1]. Pathogenic microorganisms including *Salmonella spp., Listeria spp., Clostridium spp.,* and *E. coli spp.* are main common causes of FBD outbreaks with high hospitalizations and death rates in Canada and worldwide[2, 3]. Environmental swabbing techniques are traditionally used to quantify the level of bacterial contamination of surfaces[4, 5]. One of the established methods for quantification is microbiological evaluation of surfaces, which involves a substantial number of samples and long periods of incubation. This process is followed by the isolation of bacterial colonies and subsequent biochemical and serological analysis, making this technique highly time-consuming (5-14 days), labor-intensive, and potentially posing the risk of bacterial contamination[6]. Therefore, more efficient and accessible methods for surface cleanliness assessment have been developed, including immunoassays[7], nucleic acids analysis[8], and adenosine- -5′-triphosphate (ATP)-based ChemiLuminescence (CL) assays[9, 10]. Among these, the latter has gained popularity due to its convenience and the rapid, almost real-time results it provides. This method has become an important tool for ensuring food safety, offering impressive sensitivity and accuracy in detecting contaminants. This advancement is mainly attributed to the application of chemiluminescence for detecting adenosine triphosphate (ATP).

ATP is an energy-providing molecule that has been found in all living organisms[9, 11, 12]. It acts as an energy unit in the anabolic processes and therefore presence of ATP reflects the existence of metabolic cells. This phenomenon is used to assess microbial load in the analyzed samples including food[13]. The quantification of the ATP amount gives insight into the level of environmental contamination[14] and measures microbial biomass[15]. ATP measurements indicate the presence of various types of living organic materials including microbial contamination and organic contamination such as food residues, skin fragments, and body fluids. The analysis of various surfaces, particularly floors, has revealed significantly elevated concentrations of extracellular ATP. In certain instances, these levels are two to three orders of magnitude higher than the corresponding intracellular values. This high ATP concentration is likely attributed to cells that have undergone lysis or are no longer viable[15]. However, these cells lack the ability to produce ATP, and any ATP synthesized in them is rapidly degraded within a few minutes post-lysis. Therefore, measuring intracellular ATP serves as an appropriate indicator for determining the quantity of viable cells[16].

ATP-based CL is a process in which ATP reacts with luciferin resulting in light emission based on the following equation[12]:

$$Luciferin + ATP + O_2 \xrightarrow{Luciferase,\, Mg^{2+}} Oxyluciferin + AMP + Pyrophosphate + CO_2 + h\nu \quad (1)$$

The reaction is catalyzed by luciferase, an enzyme that has high substrate specificity and reacts only with luciferin, in the presence of oxygen (O_2) and magnesium cations (Mg^2)[17]. During the reaction, adenosine triphosphate is converted to adenosine monophosphate (AMP) with the emission of light, which can be detected using an optical detector. One of the most common devices for measuring emitted light during the reaction is a luminometer. The key element of a luminometer is a light detector that can be a photomultiplier tube or photodiode. The light detector converts a photon flux emitted during a chemiluminescence reaction into an electrical current. In addition to the light detector, another important part of a luminometer is a dark chamber that provides absolute protection from external light. The intensity of the optical signal is expressed in Relative Light Units (RLU) and correlates with the total ATP molecules. The ATP results are available within seconds which enables immediate feedback. Low RLU values are indicative of a safe environment that is free of microbiological contaminants. High RLU values on the other hand show points of contamination. There is a wide range of commercially available luminometers including microplate readers and portable luminometers. The detection limit of currently commercial luminometers is 0.1 pg of ATP per sample[16]. The samples measured could be in solid as well as in liquid form. Portable luminometers have particularly gained popularity due to ease of operation, and fast reading time. These luminometers have been applied for the assessment of microbial contamination of surfaces contaminated with food residues[18] and beverages in various locations[19, 20].

Following sample collection, the extraction of ATP is the next important step. While ATP-bioluminescence assays offer rapid detection of ATP these technologies lack specificity of detection and fail to discriminate the type or species of the contaminant[15, 21, 22]. In addition, commercially available luminometers and bioluminescence kits are expensive compared to traditional culture-based techniques[23].

To date, improvements in ATP bioluminescence detection include the incorporation of nanoparticles to enhance the intensity of the CL under resonance excitation[24-27], the development of immunoassays[28] and electrochemical methods[29-31]. While these

techniques provide accurate ATP measurements with good repeatability, they have several drawbacks that limit their universal and commercial use. Recently reported portable detection platforms aimed at achieving low-cost detection of ATP have shown promising results in simplification of the sensing part by introducing ATP-sensing paper technology[32, 33]. Yet, the detection of the CL using a smartphone results in a signal loss and subsequently affects the sensitivity of the platform.

To address the shortcomings of the existing bioluminescence detection methodologies and ultimately to promote food safety and human well-being, we aimed to develop accurate, rapid, and cost-effective technology that allows the detection of environmental contamination and enables the assessment of the quality of cleaning and maintenance. To achieve this goal, we turned our attention to the field of contact mode, on-chip, lensless microscopy. The use of lensless CMOS image sensors in contact-mode imaging has been previously explored to integrate optoelectronic and microfluidic components[34]. As an example, our group has demonstrated the integration of microfluidic systems and electrochemiluminescence (ECL) systems onto a CMOS sensor. This integration resulted in the creation of a compact ECL biosensor, facilitating both sample handling and data collection on a unified platform[35]. The system's superiority over other detection systems results from its proximity of the sample to the detector, resulting in a substantial solid angle for the collection of photons. In this study, we introduce a new, directly on-chip CL detection strategy for the measurement of intracellular ATP collected from various surfaces. This was achieved by using an inexpensive CMOS imaging sensor and placing the sample directly on the sensor’s surface, thus enabling high photon collection efficiency and subsequent high sensitivity while maintaining low cost and portability of the biosensing device. The performance of the device is compared with a commercial luminometer.

3.3 Materials and methods

3.3.1 Chemicals and reagents

PDMS (polydimethylsiloxane) (SYLGARD™ 184 silicone elastomer kit) was purchased from DOW Corning Corporation. Raspberry Pi 4 2GB Model B-128 GB was purchased from CanaKit. Raspberry Pi Camera Module 3 was obtained from PiShop (Ontario, Canada). ATP determination kit was purchased from Invitrogen (A22066) and includes the following

reagents: D-luciferin, 5mg/ml solution of firefly luciferase, dithiothreitol (DTT), 5 mM solution of adenosine-5'-triphosphate in TE buffer, and 20X reaction buffer containing 25 mM Tricine buffer, pH 7.8, 5 mM $MgSO_4$, 100 µM EDTA, and 100 µM sodium azide. UltraSnap ATP-sampling tests were purchased from Hygiena and measured using the Hygiena Ensure luminometer. ATP-sampling tests contain pre-moistened swab buds and bulbs with luciferin/luciferase reagent. Milli Q water was used to prepare solutions and wash the CMOS sensor imaging sensor between experiments.

3.3.2 Design and fabrication of the biosensor

To fabricate the sample well, PDMS was prepared in a 10:1 (monomer: crosslinker) ratio, mixed with white resin dye, and cured at 70 °C for 4 hours. Next, using a leather puncher, a cavity with a diameter of 3 mm was punched in the white PDMS, establishing the PDMS well for sample handling. To fabricate the biosensor, we removed the original lens and IR filter from the CMOS sensor (IMX708, SONY) revealing a microlens array of 6.5 mm × 3.6 mm. By removing the IR filter and the lens, we can use the CMOS image sensor in contact mode. This proved to improve the photon collection efficiency by a factor of 10 compared with a lens-based CMOS (such as a cell phone) and a factor of 8 compared with a microscope that uses a 4x magnification, 0.1 NA (that provides a comparable field of view with the CMOS image sensor)[35]. The field of view (FOV) of the device is 7.07 mm^2, representing the area of the well on the CMOS sensor, and the spatial resolution of the system is constrained to 1.4 µm, determined by the pixel size. The PDMS well prepared before was then precisely aligned and mounted onto the active area of the CMOS imaging sensor using the adhesive microfluidic tape (ARcare®-90445Q, Adhesive Research Inc). The CL emission was observed and recorded using a Raspberry Pi 4 computer with an ISO of 800 and exposure time of 15 seconds, which is comparable to the reading time of the luminometer.

3.3.3 Measurement of ATP

The measurements of ATP were performed using both an EnSURE luminometer (Hygiena) and CMOS imaging sensor, therefore results were reported in RLU and pixel intensity. ATP and standard reaction solution were prepared following the kit protocol (Invitrogen). Briefly, 1 mL of 1X reaction buffer was prepared by 50 µL of 20X reaction buffer to 950 µL of deionized water. Then 1 mL of a 10mM d-luciferin stock solution was prepared by mixing 1 mL of 1X reaction buffer with one vial of d-luciferin and stored protected from the light in the freezer. A

100 mM DTT stock solution was prepared by adding 1.62 mL of deionized water to the veil containing 25mg of DTT. The standard reaction solution was prepared by combining components of the reaction including 8.9 mL of deionized water, 0.5 mL of 20X reaction buffer, 0.1 mL of 0.1 M DDT, 0.5 mL of 10 mM d-luciferin, 2.5 µL of firefly luciferase 5 mg/mL stock solution. The solution then gently mixed in the fridge (+4˚C) protected from light. The series of ATP concentrations (1 nM, 10 nM, 50 nM, 100 nM, 300 nM, 700 nM, 800 nM, and 1 µM) were prepared for the generation of the calibration curve. To create a calibration curve using the EnSURE UltraSnap luminometer, 30 µL of various ATP concentrations were added to the swab tube where the swab bud was removed, and the 270 µL of reagents were released from the swab bulb prior addition of the ATP. CL measurements of samples were performed within 30 seconds after activation. The swab tube then was gently shaken for 5-10 seconds to allow reagent mixing. Additionally, we performed ATP measurements using the same amount (270 µL) of Invitrogen standard reaction solution added to the luminometer sample tube instead of UltraSnap swab kit reagents. For building calibration curves for each type of reagents solution using the CMOS image sensor, 9 µL of Invitrogen and UltraSnap Swab reagents solutions were added to the PDMS well. Then, 1 µL of ATP samples of various concentrations were added to the reagent solution mix followed by gentle pipetting. The CL measurements were performed immediately after adding the samples. The reading time was 15 sec. All measurements using the CMOS image sensor were performed in a complete darkroom. To compare and validate the CMOS measurement with another instrument, we measured ATP luminescence with a Multimode Microplate reader (BioTek, USA) with a white opaque 96-well plate. Each well was loaded with 45 µL of UltraSnap buffer. Subsequently, 5 µL of varying ATP concentrations were added to each well, and luminescence readings were immediately taken after the addition of ATP for 15 seconds of exposure time. The corresponding luminescence values for ATP concentrations ranging from 0 to 10^6 nM were obtained, and a linear fit was plotted for the range of 1-1000 nM.

3.3.4 Surface swabbing procedure

ATP samples were collected from flat surfaces. In order to minimize sampling variability, surface swabbing was conducted by one researcher. Tested surfaces include the common kitchen counter, food court table, tables in fast-food chain restaurants, personal cell phone, five-dollar Canadian bills, microwave buttons, and elevator buttons. The analyzed surfaces were mechanically wiped before sample collection to eliminate food residue and dust. An area of 100 cm^2 was thoroughly swabbed with an UltraSnap swab in three directions horizontally,

vertically, and diagonally as recommended by the manufacturer's guidelines for conducting sample collection. The swab tip was rotated during sample collection and sufficient pressure was applied to ensure sufficient sample collection. Once the swab was placed into a swab tube the reaction solution was added by breaking the SnapValve bulb located on top of the sample tube. Then, the swab bud was bathed in the reaction solution for 10 seconds. The activated sample was read immediately by placing the UltraSnap sample tube into a Hygiena luminometer positioned upright with an exposure time of 15 seconds. The ATP concentrations were then measured using both an EnSURE luminometer and the CMOS image sensor. In CMOS-based measurements, only 10 µl of the sample was used while in EnSURE luminometer the sample size is 300 µl.

3.3.5 Data analysis and statistics

All images were analyzed using Fiji ImageJ and visualized using OriginPro (OriginLab, Northampton, MA). Calibration graphs were constructed by correlating RLU values obtained from the luminometer with mean intensity values derived from CL images across varying concentrations of ATP. Best-fit lines were applied to each plot, and the coefficient of determination was subsequently reported. For the comparative analysis, we initially prepared spiked samples with varying ATP concentrations (1 nM, 10 nM, 50 nM, 100 nM, 300 nM, 700 nM, 800 nM, and 1 µM). Subsequently, we measured these samples using both Hygina EnSURE the luminometer and CMOS image sensor, recording the respective signals. Employing the calibration equation and the recorded signals, we calculated the recovered ATP concentrations and plotted them for both the Luminometer and CMOS devices to facilitate comparison. The recovered ATP concentrations were then utilized to generate a Bland-Altman plot. In this plot, the differences between the measurements of the two devices were plotted against the average of the two methods. The mean value of the difference and the limit of agreement were calculated based on the mean ± 1.96 times the standard deviation (SD).

3.4 Results and discussion

3.4.1 Design and fabrication of the biosensor

Fig. 1 illustrates the fabrication and use of the device. To construct this platform, we utilized a backside-illuminated 12-megapixel imaging CMOS sensor camera module (IMX708, SONY), controlled by a Raspberry Pi 4 computer. The original lens and IR filter were removed to minimize the distance between the sample and the sensor surface, maximizing photon

collection efficiency. We decided to use this inexpensive, user-friendly, and portable CMOS image sensor as the detector. We demonstrated previously that by enabling contact-mode imaging capability, CMOS can collect 8 times more signal compared to using a microscope and cellphone as detectors for the CL or ECL biosensor [35].

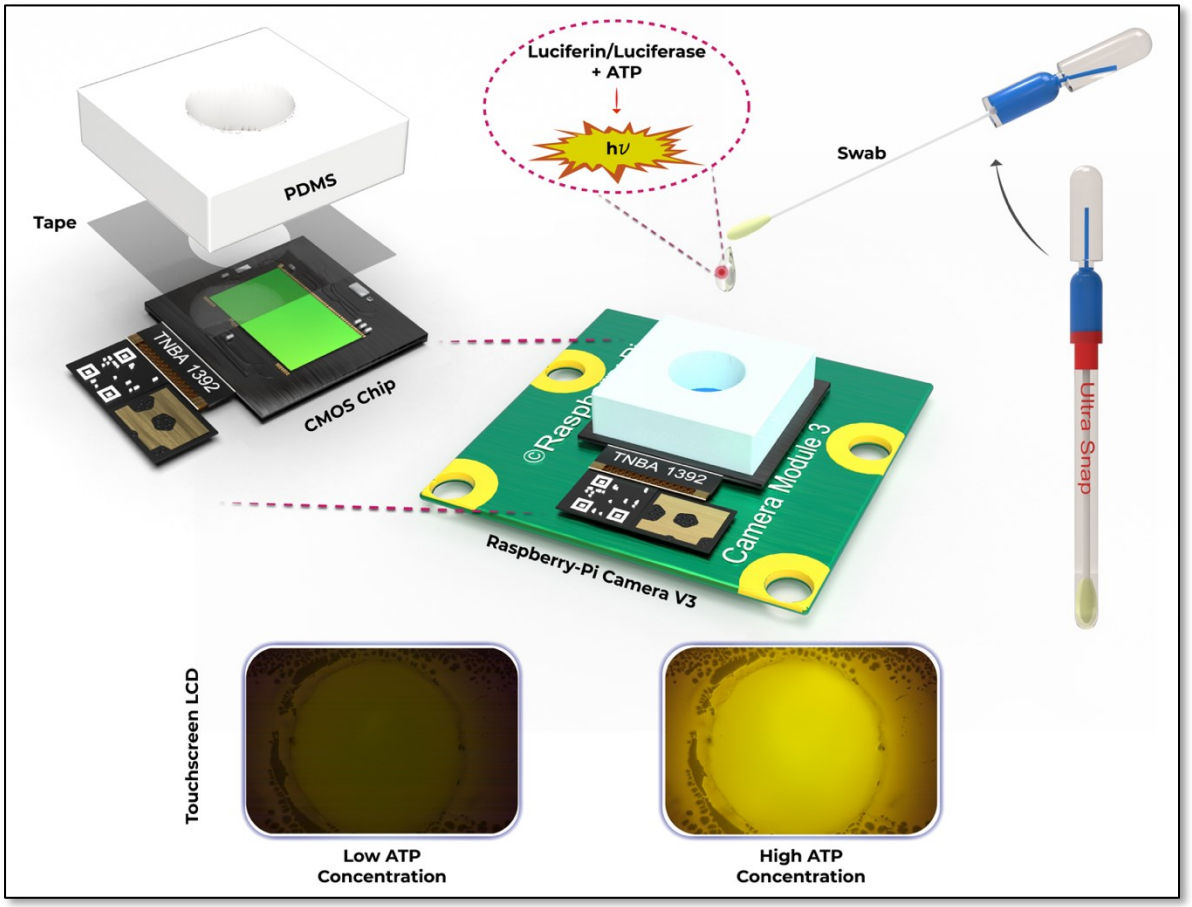

Fig. 1. Schematic of CMOS device: On-chip CL biosensor for the detection of surface contamination. In this platform, a backside-illuminated 12-megapixel imaging CMOS sensor (Raspberry Pi Camera Module 3) controlled by a Raspberry Pi 4 computer was utilized. The original lens and IR filter were removed to enable contact-mode imaging capability. For the sample holder, PDMS prepared in a 10:1 (monomer: crosslinker) ratio was mixed with white resin dye, cured, and then punched with a 3mm diameter hole. Attaching the sample holder to the CMOS sensor was achieved by cutting pressure-sensitive double-faced tape to match the dimensions of the microfluidic channels and precisely aligning it with the CMOS sensor. To operate the device, the selected surface was swabbed using Hygiena UltraSnap swabs. The swab was subsequently combined with the UltraSnap buffer, and 10 µl of the resulting solution containing liquid-stable reagents and ATP extracted from the surface were transferred to the CMOS device. The CL emission was promptly measured in a dark room, with the signal recorded for 15 seconds (exposure time). The results were then illustrated on a Raspberry Pi touchscreen LCD.

A higher ATP concentration indicates more surface contamination and results in a more intense CL emission.

For the sample holder, PDMS prepared in a 10:1 (monomer: crosslinker) ratio was mixed with white resin dye and cured at 70 °C for 4 hours. After curing, this device was punched with a 3mm diameter using a leather puncher. The attachment of this opaque-white PDMS device to the CMOS sensor was achieved by cutting pressure-sensitive double-faced tape to match the dimensions of the microfluidic channels and precisely aligning it with the CMOS sensor using a mask aligner (OAI Model 200). The field of view (FOV) of the device is 7.07 mm^2, representing the area of the hole on the CMOS sensor, and the spatial resolution of the system is 1.4 µm, constrained by the pixel size. The opaque-white PDMS prevents the reflection of CL signals and enhances the signal-to-background ratio.

To operate the CMOS device, the selected surface was swabbed using a pre-moistened swab bud, following the standard Hygiena UltraSnap swabbing protocol. The swab was subsequently combined with the UltraSnap buffer. Next, 10 µl of the resulting solution containing liquid-stable reagents and ATP extracted from the surface, was transferred to the CMOS image sensor, and the CL emission was promptly measured in a dark room to address the issue of the rapid emission kinetics characteristic of ATP CL that is associated with the elevated concentration of luciferase in the assay[36]. The signal was recorded for 15 seconds (exposure time) to ensure a fair comparison with the EnSURE Luminometer, which also utilizes the same amount of time to read the signal. The results were then projected on the touchscreen LCD that was connected to the Raspberry 4 computer and processed with Fiji ImageJ. A higher ATP concentration indicates more surface contamination and results in a more intense CL emission.

3.4.2 Characterization of the surface of the CMOS sensor

Fig. 2 shows data collected for the characterization of the CMOS image sensor. The CMOS sensor with the IR filter and lens is shown in Fig. 2a, while by removing the lens and IR filter, the bare CMOS image sensor is exposed (Fig. 2.b). The PDMS well capable of holding the sample is shown in Fig. 2c. As previously reported for another, 5MP CMOS image sensor, the surface of the sensor exhibits a pitch of the size of the pixels (1.4 µm), as evidenced by optical and AFM images in Fig. 2d,e [37, 38]. This square unit cell pattern has a 3D morphology as shown in Fig. 2e-g, which is typical for the microlens array deposited by the manufacturer to ensure a high fill factor of individual pixels.

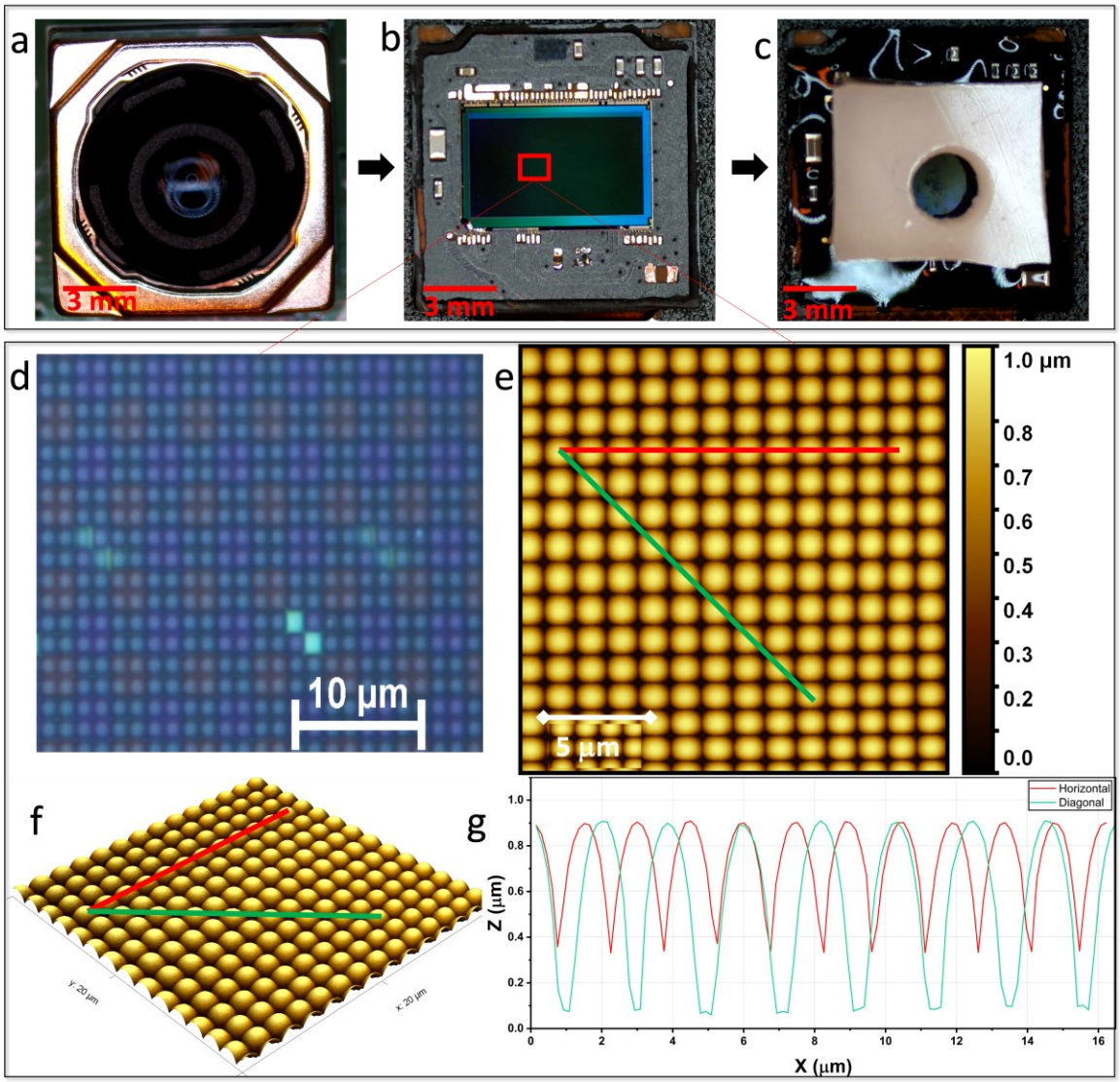

Fig. 2: Characterization of the CMOS image sensor. Top: Photographs of the CMOS image sensor with the lens (a), without the lens and IR filter (b), and with the PDMS well on top of the bare CMOS image sensor (c). Middle: Optical image at 100x magnification (d) and AFM image (e) of the bare CMOS image sensor. Bottom: AFM 3D representation of the surface of the CMOS sensor (f) with the profile line plots indicating the size of the domes and wells (g).

3.4.3 Analytical performance of the biosensor

To assess and compare the performance of the device, we measured the sensitivity and Limit of Detection (LOD) of the CMOS device and EnSURE Luminometer for ATP detection. The CL intensity corresponding to ATP at varying concentrations in two distinct buffers (Invitrogen Buffer and UltraSnap Buffer) was recorded. A minimum of three experiments were conducted for each concentration. Based on the average intensity at each concentration, a calibration plot illustrating the relationship between ATP concentration and CL intensity was generated. Fig.

3a exhibits the calibration plot for ATP detection in the Invitrogen buffer using the luminometer, while Fig. 3b portrays the calibration plot for ATP detection in the same buffer using the CMOS device. Correspondingly, calibration plots for ATP detection in the UltraSnap buffer using the Luminometer and CMOS device are displayed in Fig. 3c and Fig. 3d, respectively.

For ATP detection in the Invitrogen buffer using the Luminometer, a linear detection range from 0 to 20,000 nM was established, yielding a coefficient of determination (R^2) of 0.88. The linear detection range for ATP detection in the Invitrogen buffer using the CMOS sensor extended from 1,000 to 200,000 nM with an R^2 of 0.83. In the case of ATP detection in the UltraSnap buffer, both the Luminometer and CMOS sensor exhibited linear detection ranges of 1 to 1,000 nM. The linear range of the ATP detection with different buffer solutions (Invitrogen and UltraSnap) depends largely on the chemical composition of the solutions (proprietary to the manufacturer). These solutions were optimized by the manufacturer for specific applications to work in desired concentration regimes. The Invitrogen buffer was optimized for research applications such that it worked on a wider linear range of ATP concentrations.

The Limit of Detection (LOD) for ATP was calculated to be 0.38 nM and 22.5 nM for the Hygiena EnSURE Luminometer and CMOS, respectively. The LOD was determined using the formula LOD = 3SD/S, where SD represents the standard deviation of blank measurements in the absence of analyte, and S is the slope of the linear equation derived from the calibration plot. It is worth mentioning that the sample volume used in the CMOS-based platform was 10 µL, whereas the luminometer utilized 300 µL of samples. This implies that for each concentration, the CMOS device measured a quantity of ATP moles in the sample that was 30 times lower, and the limit of detection (LOD) for CMOS device is 225 fmol, which is relatively close to the LOD of the Luminometer (115 fmol). The proportional reduction of the sample volume leads to the lower number of ATP molecules contributing to light emission. In addition, reaction rates might be affected by different (larger) diffusion rates in the lower volume. Yet, when converted to moles, the limit of detection of the CMOS image sensor has been measured at 225 fmol, which is close to the limit of detection of Hygiena EnSURE Luminometer (115 fmol). This further indicates that the reduction in the reaction volume used in the CMOS sensor does not have a significant impact on the sensitivity of the CMOS sensor.

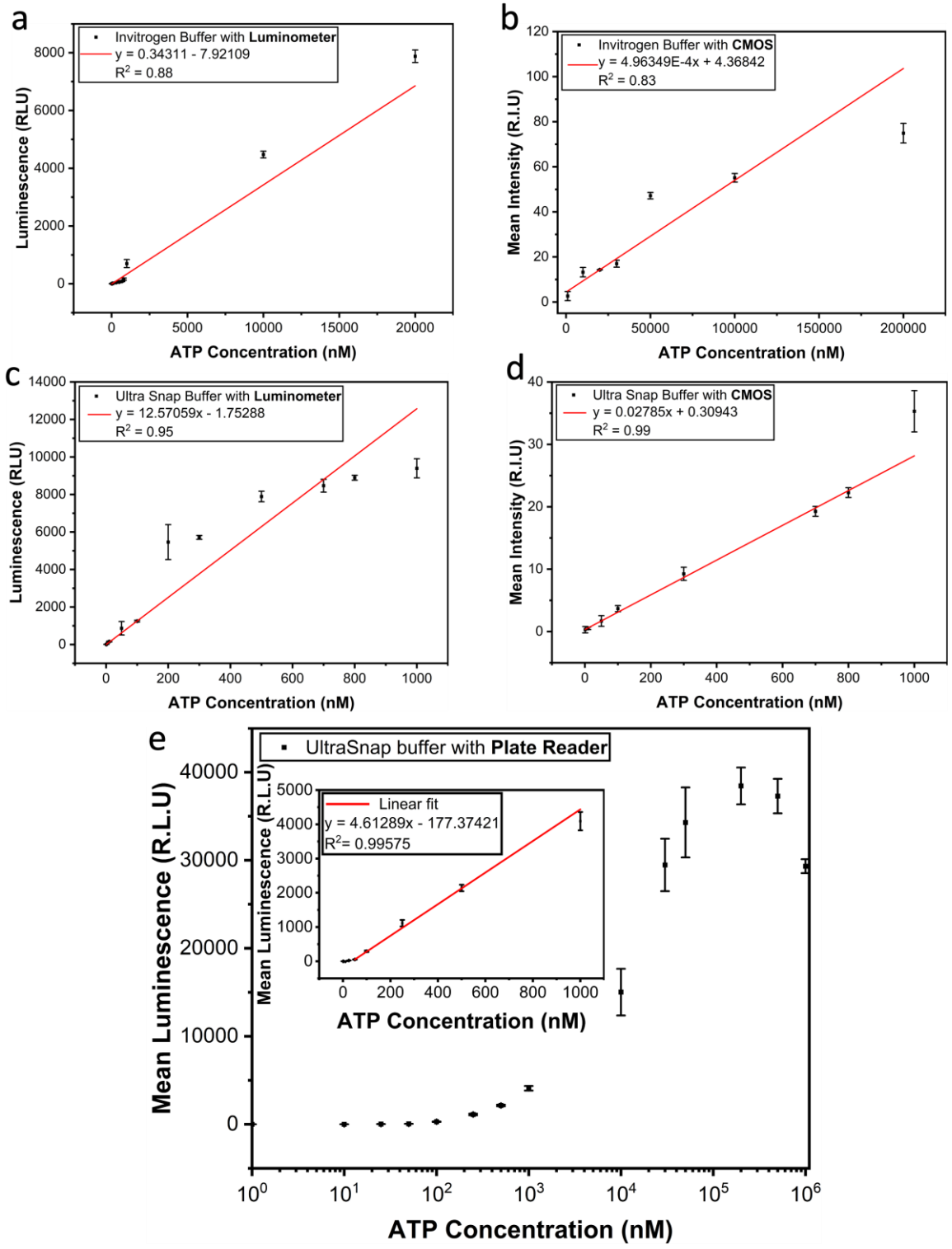

Fig. 3. Analytical performance of the CMOS device, Luminometer, and Plate Reader for detection of ATP in different buffers and comparison. CL image-based intensity of the Luciferin-Luciferase system in the presence of different concentrations of ATP: a) Detection of ATP in Invitrogen buffer using Hygiena EnSURE Luminometer as the detector; b) Detection of ATP in Invitrogen buffer using CMOS as the detector; c) Detection of ATP in UltraSnap buffer using Hygiena EnSURE Luminometer as the detector; d) Detection of ATP in UltraSnap buffer using CMOS as the detector; e) Detection of ATP

luminescence in UltraSnap buffer with the plate reader . ATP concentration is shown in logarithmic scale to cover the entire concentration range. A linear range that is similar to the other two devices is shown in the inset. Invitrogen standard reaction solution contains 0.5 mM D-luciferin, 1.25 µg/mL firefly luciferase, 25 mM Tricine buffer, pH 7.8, 5 mM $MgSO_4$, 100 µM EDTA, 1 mM DTT, and 100 µM sodium azide.

As the linear ranges of both devices fall within the same range for the UltraSnap buffer, all subsequent experiments were conducted using this buffer. It also offers superior sensitivity for ATP detection and enhances the signal.

To compare the performance of the Luminometer and CMOS image sensor with a third instrument, we performed additional quantitative measurements of ATP luminescence in UltraSnap buffer with a plate reader. The data is presented in Fig. 3e and indicates a wider concentration range than both other portable devices. For the concentration range typical for the other devices (1-1000 nM) a linear range was determined with an R^2 of 0.99, and the calculated LOD is 0.3 nM. Since the volume of sample used with the plate reader was 50 µL, the corresponding mass-adjusted limit of detection is 15 fmol. While this LOD is lower than that obtained with both portable devices, it is important to note that the plate reader is a research-grade instrument and therefore better results are expected.

3.4.4 Reproducibility and reusability of the biosensor

Essential parameters for demonstrating the viability of a biosensor for practical applications are its capacity for consistent performance across diverse devices (reproducibility) and its potential for reuse in various experiments (repeatability). Consequently, these parameters were measured, and the results are illustrated in Fig. 4a and Fig. 4b.

In order to study the reproducibility of the manufacturing process, ten distinct devices were inspected for their ability to detect 1 µM of ATP individually in the UltraSnap buffer. The collected CL intensities were then analyzed, revealing a relative standard deviation (RSD) of 9.20% for the intensity across these ten experiments. This percentage signifies favorable reproducibility within the linear detection range for ATP. The CMOS device has the capability for cleaning and subsequent reuse. To assess the practicality of this approach, the reusability or repeatability of the device for multiple experiments was investigated, focusing

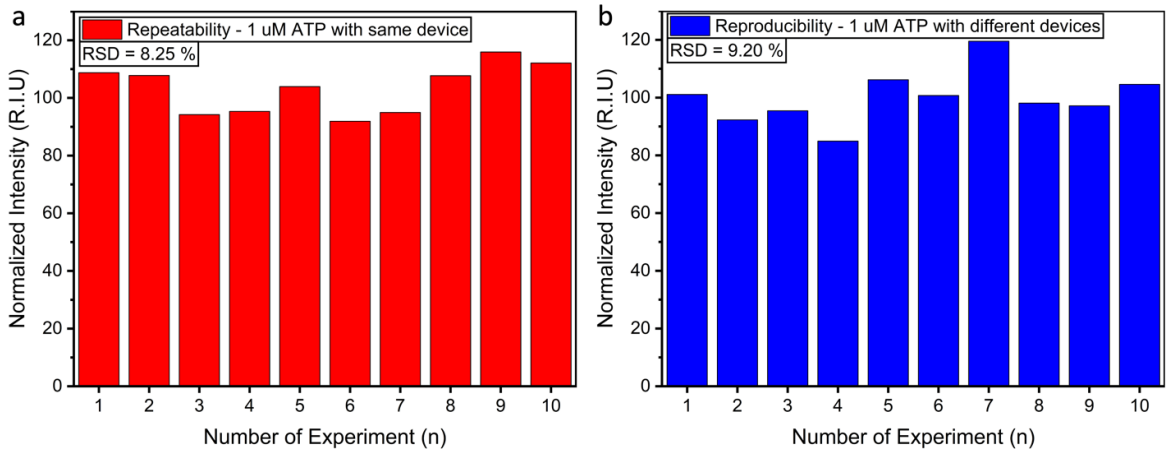

Fig. 4. Repeatability and reproducibility of the CMOS device; a) Repeatability (reusability) of the biosensor demonstrating 10 measurements (n=10) of 1 mM ATP in UltraSnap buffer using the same device b) Reproducibility of the biosensor demonstrating 10 measurements (n=10) of 1 mM ATP in UltraSnap buffer using 10 different devices.

on the measurement of CL intensities for 1 µM of ATP. The CL signal was successfully recorded using the same device with a fresh sample solution in each of 10 consecutive uses. The resulting RSD was calculated to be 8.25%, indicating a relative consistency in results over the 10 usages. However, given the device's cost-effectiveness (with the CMOS chip priced at $5 and the approximate cost of the PDMS device at $1), it can also be considered as a disposable device, making its reusability a less significant concern.

3.4.5 CMOS vs Luminometer comparison analysis

To assess the performance of the CMOS device in comparison to the commercial luminometer, a widely employed method for ATP detection in food safety applications, spiked ATP solutions of varying concentrations were measured using both devices. The recovered ATP concentrations, determined using the calibration equations from Fig. 3c and Fig. 3d, are presented in Fig. 5a. The results demonstrate a close alignment between the ATP concentrations measured by the CMOS and the luminometer with the actual concentrations spiked into the solution. Specifically, the coefficient of determination (R^2) for the y = x line is 0.95 for the luminometer and 0.98 for CMOS. Fig. 5b illustrates the recovered ATP concentrations measured by the Luminometer plotted against the recovered ATP concentrations measured by CMOS. This comparison reveals a trend close to the y=x line, indicating a closely related performance of both the luminometer and CMOS for ATP detection, as evidenced by Pearson's correlation coefficient of 0.98589.

The Bland-Altman plot as a method for assessing agreement between two measurement techniques is depicted in Fig. 5c. This plot illustrates the difference between the ATP concentrations recovered by the Luminometer and CMOS plotted against the mean values of these measurements. The proximity of the mean difference between measurements (blue line, 8.32) to zero indicates that both measurements are reporting relatively similar results and a consistent level of agreement. The scattered data does not exhibit a specific trend, implying the absence of systematic bias. The analysis demonstrates a limit of agreement ranging from -117 to +133 nM, which is sufficiently narrow, suggesting that the two methods for ATP detection can be deemed interchangeable.

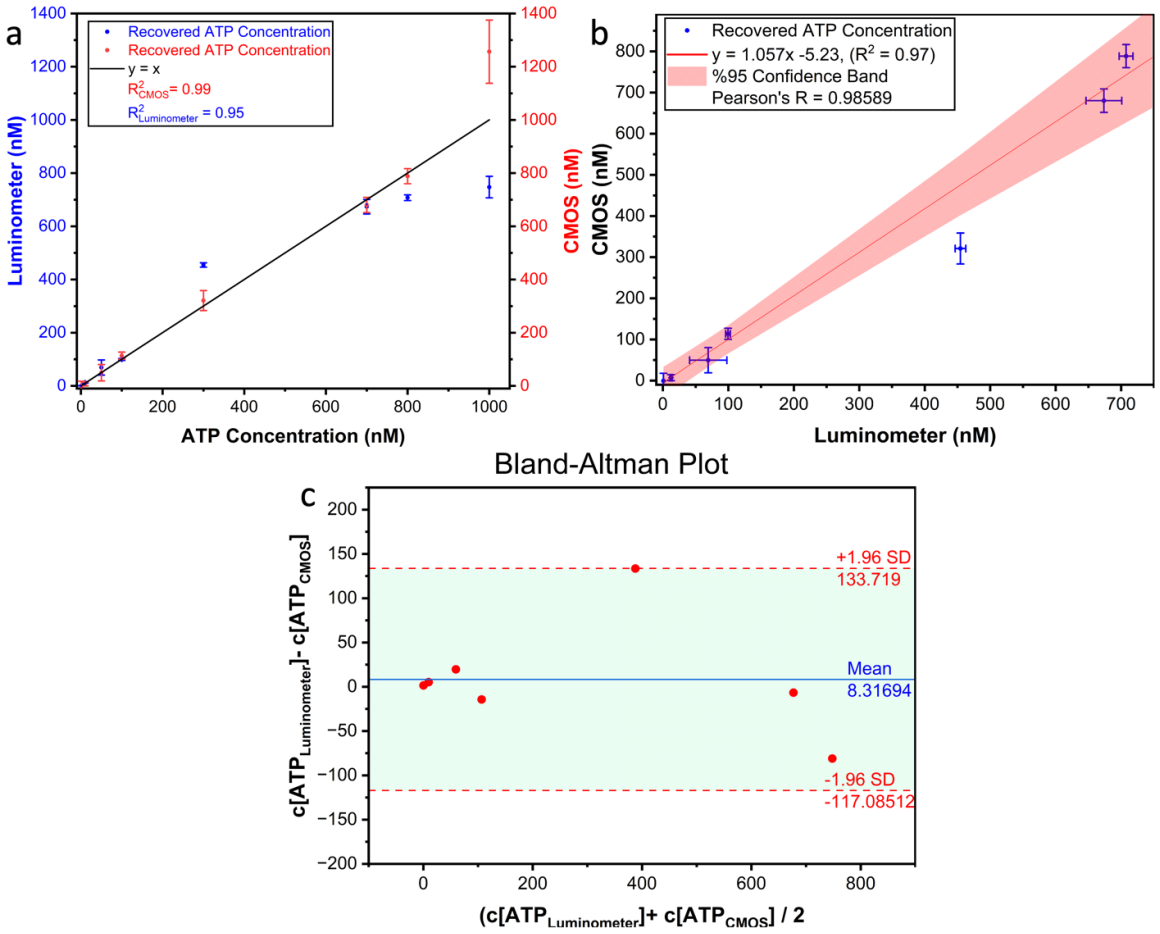

Fig. 5. Comparison between the performance of Hygiena EnSURE Luminometer and CMOS for detection of ATP. a) Performance analysis of Hygiena EnSURE Luminometer and CMOS for spiked ATP samples b) Correlation analysis of Hygiena EnSURE Luminometer and CMOS performance for detection of spiked ATP samples. c) Bland-Altman plot demonstrating the level of agreement between EnSURE Luminometer and CMOS for ATP detection and presenting potential biased trend.

Notably, in Fig. 5c, a stronger agreement is observed for concentrations below 200 nM. It is important to acknowledge the difference in sample volumes between the two methods, with 10 µL in the CMOS device and 400 µL in the Hygiena EnSURE Luminometer. This difference in sample volumes should be considered a limitation of the Bland-Altman plot, potentially impacting the overall level of agreement between the two methods.

3.4.6 Real sample analysis - detection of surface contamination

In Fig. 6a-c we present real sample analysis of microbial contamination of various surfaces. Elevator buttons, cell phones, fast food tables, microwave buttons, and wallets were swabbed and

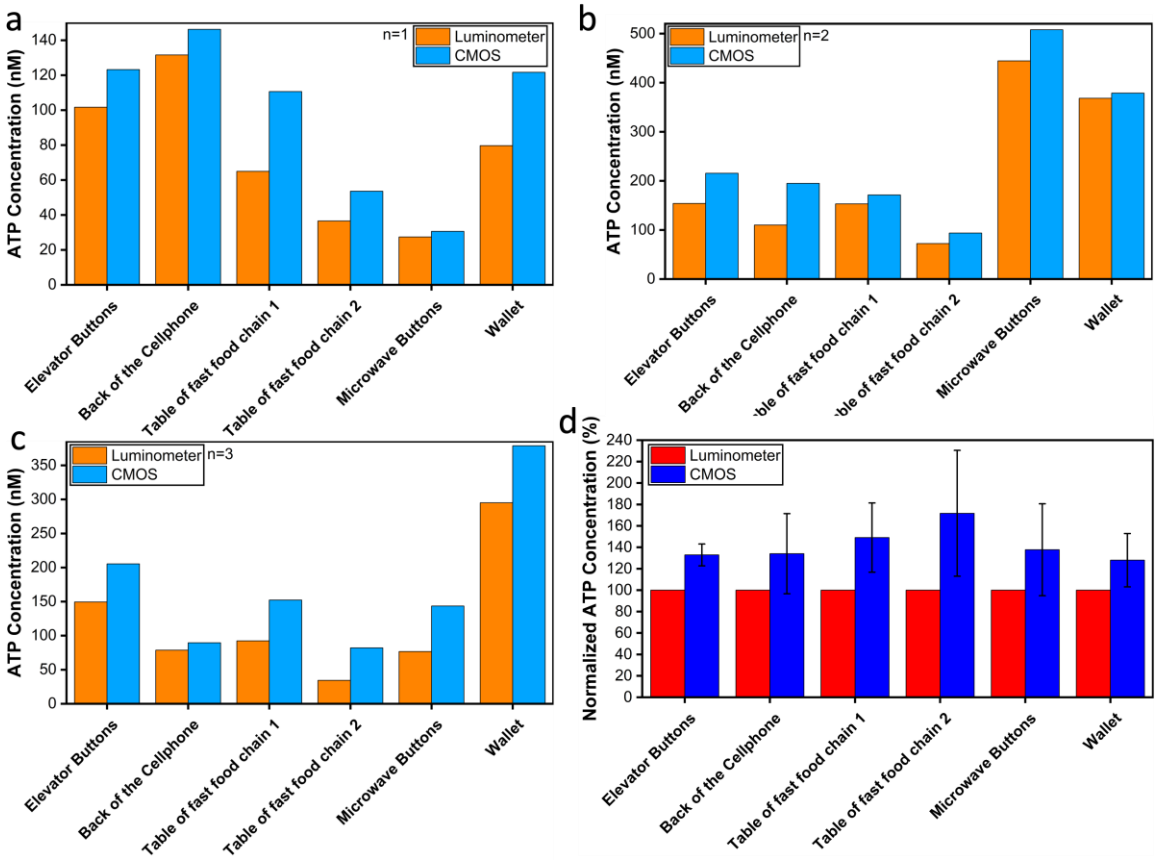

Fig. 6. Real sample analysis. Measuring different surfaces for ATP and potential contamination using CMOS. Surfaces were chosen based on their relationship with food safety. Hygiena UltraSnap swabs were employed for sampling. The same surface area was sampled three times (a), (b), and (c) to measure ATP using both the Luminometer and CMOS. The recovered ATP concentration is determined based on the calibration graphs illustrated in Fig. 3c and 3d for the Luminometer and CMOS, respectively. (d) shows the comparison between the recovered concentrations with the Luminometer and CMOS, normalized for the Luminometer values.

measured with both Luminometer and CMOS sensor. Both devices reported similar trends for microbial contamination. Among the various surfaces measured, the highest level of contamination are the back of the personal cellphone and elevator buttons (with ATP concentrations range from 100 to 200 nM), and wallet and microwave buttons (with ATP concentration range between 50 and 500 nM). Furthermore, the dining table at a fast-food chain restaurant was found to have a range of ATP between 50 and 150 nM. Both devices indicate a similar trend in ATP concentrations that are recovered. In Fig. 6d we present a statistical comparison of the measurements (recovered ATP concentrations) recorded with the two devices. The data is normalized for the Luminometer values. The recovered ATP concentrations with the CMOS sensor are consistently higher (on average 40% higher) than those by the Luminometer. This could be due to the different sample preparation methods. In the case of the CMOS device, the whole sample is placed directly onto the CMOS sensor via the PDMS well. On the other hand, for the Luminometer, the reagents are mixed in the UltraSnap tube and will be adsorbed on the swab and may adhere to the walls of the tube. These residuals of the sample may not reach the detection region at the bottom of the tube. This would lead to lower readings and recovered concentrations.

3.5 Conclusions

In this article, we introduce a novel device based on a pixelated CMOS image sensor for ATP detection. The CMOS device presented here exhibits reliable performance for ATP detection, demonstrating good linearity up to 1 μM and a limit of detection (LOD) of 225 fmol. Additionally, we compare the performance of this device with a commercial luminometer commonly used to evaluate food safety. While maintaining the same level of performance, including similar linearity and LOD, the CMOS device is significantly more cost-effective. The cost of a CMOS image sensor is approximately $5-20, whereas a commercial luminometer can cost between $3000 and $10000.

To demonstrate the functionality of the device, we prepared polydimethylsiloxane (PDMS) sample wells that hold the liquid sample and protect the electrical circuits of the image sensor. Commercial ATP detection kits including the Invitrogen ATP determination kit and Hygiena UltraSnap were used to characterize the analytical performance of the detector. The results were validated using a portable luminometer. The new detection strategy enables high-sensitivity detection of ATP (fmol of ATP) that is comparable to the LOD of existing luminometers. These results were consistent across a variety of CMOS image sensors, showing

high reproducibility of the measurements. It requires low amounts of samples and reagents that are beneficial in terms of sample accessibility and cost-effectiveness. The platform has been used to assess the amount of ATP after environmental swabbing of a variety of surfaces including tables in fast-food chain restaurants, kitchen counter, and personal cell phones. The results of the surface swabbing experiments showed the detection of low ATP levels and were validated using a commercial luminometer. In addition, the platform can be adapted to particular analytical needs such as the detection of specific microbial species by immunofunctiolization of the CMOS-imaging surface or enhancement of the CL by turning the CMOS-imaging sensor into a plasmonic substrate.

Overall, the CMOS device presented in this article proves to be a portable, user-friendly platform for ATP detection at the point of need. It exhibits good reproducibility, with an RSD of 9.20% and can be reused with an RSD of 8.25%, and it shows good agreement with a commercial luminometer. Moreover, we used this device to measure ATP concentrations from various surfaces relevant to food safety, highlighting its potential for use outside laboratory setting. Overall, the CMOS device demonstrates its potential for application in the food safety industry, where a distinct standard can be established to assess the cleanliness of surfaces.

While ATP-based bioluminescence assays offer rapid detection of microbial contamination, these technologies fail to discriminate the type or species of the contaminant. The distinction between extracellular ATP, dead cells, food residues, and other organic materials, and intracellular ATP also remains challenging. Further developments will need to address these key requirements.

In addition, current commercially available luminometers and bioluminescence kits are expensive compared to traditional culture-based techniques. Ultimately, the low stability of bioluminescence reagents and low light emission require continuous improvement of bioluminescence methods to enhance the sensitivity and accuracy of the measurements.

3.6 Authors contributions

All authors designed the experiments, interpretated the results, and wrote the manuscript. RA and MI performed the experiments and analyzed the data. SWH supervised the project.

3.7 Conflicts of interest

RA and SWH are co-founders of a McGill spinoff company, Phoela Health Inc.

3.8 Acknowledgments

This work was financially supported by the Natural Sciences and Engineering Research Council of Canada (NSERC), Discovery Grant RGPIN-2018-05675 (to S.W.-H.); Louis-Ho Scholarship in Technological Innovation from Faculty of Engineering, McGill University. RA acknowledges funding from the McGill Engineering Doctoral Award (MEDA) and Fonds de recherche du Quebec - Nature et technologies (FRQNT) for doctoral studies.

3.9 References

[1] W. H. Organization, WHO estimates of the global burden of foodborne diseases: foodborne disease burden epidemiology reference group 2007-2015. World Health Organization, 2015.

[2] J. M. Lorenzo, P. E. Munekata, R. Dominguez, M. Pateiro, J. A. Saraiva, and D. Franco, "Main Groups of Microorganisms of Relevance for Food Safety and Stability: General Aspects and Overall Description," (in eng), Innovative Technologies for Food Preservation, pp. 53-107, 2018.

[3] M. K. Thomas, R. Murray, L. Flockhart, K. Pintar, A. Fazil, A. Nesbitt, B. Marshall, J. Tataryn, and F. Pollari, "Estimates of foodborne illness-related hospitalizations and deaths in Canada for 30 specified pathogens and unspecified agents," (in eng), Foodborne Pathog Dis, vol. 12, no. 10, pp. 820-7, Oct 2015, doi: 10.1089/fpd.2015.1966.

[4] S. L. Jones, S. C. Ricke, D. Keith Roper, and K. E. Gibson, "Swabbing the surface: critical factors in environmental monitoring and a path towards standardization and improvement," (in eng), Crit Rev Food Sci Nutr, vol. 60, no. 2, pp. 225-243, 2020, doi: 10.1080/10408398.2018.1521369.

[5] C. Griffith, Surface Sampling and the Detection of Contamination. Handbook of Hygiene Control in the Food Industry. 2016:673-96. doi: 10.1016/B978-0-08-100155-4.00044-3. Epub 2016 Jul 15.

[6] J. Kadariya, T. C. Smith, and D. Thapaliya, "Staphylococcus aureus and staphylococcal food-borne disease: an ongoing challenge in public health," (in eng), Biomed Res Int, vol. 2014, p. 827965, 2014, doi: 10.1155/2014/827965.

[7] V. Jasson, L. Jacxsens, P. Luning, A. Rajkovic, and M. Uyttendaele, "Alternative microbial methods: An overview and selection criteria," Food microbiology, vol. 27, no. 6, pp. 710-730, 2010.

[8] N. Martínez, M. C. Martín, A. Herrero, M. Fernández, M. A. Alvarez, and V. Ladero, "qPCR as a powerful tool for microbial food spoilage quantification: Significance for food quality," Trends in Food Science & Technology, vol. 22, no. 7, pp. 367-376, 2011/07/01/ 2011, doi: https://doi.org/10.1016/j.tifs.2011.04.004.

[9] S. Liu, J. Zhao, Y. Guo, X. Ma, C. Sun, M. Cai, Y. Chi, and K. Xu, "Application of ATP-based bioluminescence technology in bacterial detection: a review," Analyst, 10.1039/D3AN00576C vol. 148, no. 15, pp. 3452-3459, 2023, doi: 10.1039/D3AN00576C.

[10] K. Narsaiah, S. N. Jha, R. Bhardwaj, R. Sharma, and R. Kumar, "Optical biosensors for food quality and safety assurance-a review," (in eng), J Food Sci Technol, vol. 49, no. 4, pp. 383-406, Aug 2012, doi: 10.1007/s13197-011-0437-6.

[11] P. E. Stanley, "A review of bioluminescent ATP techniques in rapid microbiology," (in eng), J Biolumin Chemilumin, vol. 4, no. 1, pp. 375-80, Jul 1989, doi: 10.1002/bio.1170040151.

[12] Y. Ando, K. Niwa, N. Yamada, T. Enomoto, T. Irie, H. Kubota, Y. Ohmiya, and H. Akiyama, "Firefly bioluminescence quantum yield and colour change by pH-sensitive green emission," Nature Photonics, vol. 2, no. 1, pp. 44-47, 2008/01/01 2008, doi: 10.1038/nphoton.2007.251.

[13] R. Mempin, H. Tran, C. Chen, H. Gong, K. Kim Ho, and S. Lu, "Release of extracellular ATP by bacteria during growth," BMC microbiology, vol. 13, pp. 1-13, 2013.

[14] J. A. Poulis, M. de Pijper, D. A. A. Mossel, and P. P. A. Dekkers, "Assessment of cleaning and disinfection in the food industry with the rapid ATP-bioluminescence technique combined with the tissue fluid contamination test and a conventional microbiological method," International Journal of Food Microbiology, vol. 20, no. 2, pp. 109-116, 1993/11/01/ 1993, doi: https://doi.org/10.1016/0168-1605(93)90098-2.

[15] K. Venkateswaran, N. Hattori, M. T. La Duc, and R. Kern, "ATP as a biomarker of viable microorganisms in clean-room facilities," Journal of Microbiological Methods, vol. 52, no. 3, pp. 367-377, 2003/03/01/ 2003, doi: https://doi.org/10.1016/S0167-7012(02)00192-6.

[16] B. Bottari, M. Santarelli, and E. Neviani, "Determination of microbial load for different beverages and foodstuff by assessment of intracellular ATP," Trends in Food Science & Technology, vol. 44, no. 1, pp. 36-48, 2015/07/01/ 2015, doi: https://doi.org/10.1016/j.tifs.2015.02.012.

[17] W. D. McElroy and A. Green, "Function of adenosine triphosphate in the activation of luciferin," Archives of Biochemistry and Biophysics, vol. 64, no. 2, pp. 257-271, 1956/10/01/ 1956, doi: https://doi.org/10.1016/0003-9861(56)90268-5.

[18] K. A. Whitehead, L. A. Smith, and J. Verran, "The detection of food soils and cells on stainless steel using industrial methods: UV illumination and ATP bioluminescence," International journal of food microbiology, vol. 127, no. 1-2, pp. 121-128, 2008.

[19] V. G. Frundzhyan, I. M. Parkhomenko, L. Y. Brovko, and N. N. Ugarova, "Improved bioluminescent assay of somatic cell counts in raw milk," Journal of dairy research, vol. 75, no. 3, pp. 279-283, 2008.

[20] T. Takahashi, Y. Nakakita, J. Watari, and K. Shinotsuka, "A new rapid technique for detection of microorganisms using bioluminescence and fluorescence microscope method," Journal of bioscience and bioengineering, vol. 89, no. 5, pp. 509-513, 2000.

[21] D. E. Turner, E. K. Daugherity, C. Altier, and K. J. Maurer, "Efficacy and limitations of an ATP-based monitoring system," (in eng), J Am Assoc Lab Anim Sci, vol. 49, no. 2, pp. 190-5, Mar 2010.

[22] T. Sakakibara, S. Murakami, N. Hattori, M.-o. Nakajima, and K. Imai, "Enzymatic treatment to eliminate the extracellular ATP for improving the detectability of bacterial intracellular ATP," Analytical biochemistry, vol. 250, no. 2, pp. 157-161, 1997.

[23] K. S. Gracias and J. L. McKillip, "A review of conventional detection and enumeration methods for pathogenic bacteria in food," Canadian journal of microbiology, vol. 50, no. 11, pp. 883-890, 2004.

[24] Y. Jeong, Y. M. Kook, K. Lee, and W. G. Koh, "Metal enhanced fluorescence (MEF) for biosensors: General approaches and a review of recent developments," (in eng), Biosens Bioelectron, vol. 111, pp. 102-116, Jul 15 2018, doi: 10.1016/j.bios.2018.04.007.

[25] E. P. Morozova, T. E. Smoliarova, K. A. Lukyanenko, M. A. Kirillova, M. N. Volochaev, A. S. Kichkailo, R. Ranjan, and V. A. Kratasyuk, "Metal-enhanced bioluminescence by detergent stabilized Ag and Au nanoparticles," (in eng), Talanta, vol. 254, p. 124157, Mar 1 2023, doi: 10.1016/j.talanta.2022.124157.

[26] E. Karimi, M. Nikkhah, and S. Hosseinkhani, "Label-Free and Bioluminescence-Based Nano-Biosensor for ATP Detection," Biosensors, vol. 12, no. 11, p. 918, 2022. [Online]. Available: https://www.mdpi.com/2079-6374/12/11/918.

[27] S. U. Kim, E. J. Jo, Y. Noh, H. Mun, Y. D. Ahn, and M. G. Kim, "Adenosine Triphosphate Bioluminescence-Based Bacteria Detection Using Targeted Photothermal Lysis by Gold

Nanorods," (in eng), Anal Chem, vol. 90, no. 17, pp. 10171-10178, Sep 4 2018, doi: 10.1021/acs.analchem.8b00254.

[28] A. Nascetti, M. Mirasoli, E. Marchegiani, M. Zangheri, F. Costantini, A. Porchetta, L. Iannascoli, N. Lovecchio, D. Caputo, G. de Cesare, S. Pirrotta, and A. Roda, "Integrated chemiluminescence-based lab-on-chip for detection of life markers in extraterrestrial environments," Biosensors and Bioelectronics, vol. 123, pp. 195-203, 2019/01/01/ 2019, doi: https://doi.org/10.1016/j.bios.2018.08.056.

[29] E. Llaudet, S. Hatz, M. Droniou, and N. Dale, "Microelectrode Biosensor for Real-Time Measurement of ATP in Biological Tissue," Anal Chem, vol. 77, no. 10, pp. 3267-3273, 2005/05/01 2005, doi: 10.1021/ac048106q.

[30] A. Hellmann, A. Schundner, M. Frick, and C. Kranz, "Electrochemical detection of ATP release in-vitro and in-vivo," Current Opinion in Electrochemistry, vol. 39, p. 101282, 2023/06/01/ 2023, doi: https://doi.org/10.1016/j.coelec.2023.101282.

[31] M. Mirasoli, A. Nascetti, D. Caputo, M. Zangheri, R. Scipinotti, L. Cevenini, G. de Cesare, and A. Roda, "Multiwell cartridge with integrated array of amorphous silicon photosensors for chemiluminescence detection: development, characterization and comparison with cooled-CCD luminograph," (in eng), Anal Bioanal Chem, vol. 406, no. 23, pp. 5645-56, Sep 2014, doi: 10.1007/s00216-014-7971-9.

[32] M. M. Calabretta, R. Álvarez-Diduk, E. Michelini, A. Roda, and A. Merkoçi, "Nano-lantern on paper for smartphone-based ATP detection," (in eng), Biosens Bioelectron, vol. 150, p. 111902, Feb 15 2020, doi: 10.1016/j.bios.2019.111902.

[33] Z. Hu, D. Zhang, H. Lin, H. Ni, H. Li, Y. Guan, Q. Jin, Y. Wu, and Z. Guo, "Low-cost portable bioluminescence detector based on silicon photomultiplier for on-site colony detection," Analytica Chimica Acta, vol. 1185, p. 339080, 2021/11/15/ 2021, doi: https://doi.org/10.1016/j.aca.2021.339080.

[34] X. Hu, R. Abbasi, and S. Wachsmann-Hogiu, "Microfluidics on lensless, semiconductor optical image sensors: challenges and opportunities for democratization of biosensing at the micro-and nano-scale," Nanophotonics, vol. 12, no. 21, pp. 3977-4008, 2023, doi: doi:10.1515/nanoph-2023-0301.

[35] R. Abbasi, J. Liu, S. Suarasan, and S. Wachsmann-Hogiu, "SE-ECL on CMOS: a miniaturized electrochemiluminescence biosensor," Lab on a Chip, 10.1039/D1LC00905B vol. 22, no. 5, pp. 994-1005, 2022, doi: 10.1039/D1LC00905B.

[36] M. M. Calabretta, R. Álvarez-Diduk, E. Michelini, A. Roda, and A. Merkoçi, "Nano-lantern on paper for smartphone-based ATP detection," Biosensors and Bioelectronics, vol. 150, p. 111902, 2020/02/15/ 2020, doi: https://doi.org/10.1016/j.bios.2019.111902.
[37] M. Imanbekova, A. S. Perumal, S. Kheireddine, D. V. Nicolau, and S. Wachsmann-Hogiu, "Lensless, reflection-based dark-field microscopy (RDFM) on a CMOS chip," Biomed. Opt. Express, vol. 11, no. 9, pp. 4942-4959, 2020/09/01 2020, doi: 10.1364/BOE.394615.
[38] M. Imanbekova, A. M. Saridag, M. Kahraman, J. Liu, H. Caglayan, and S. Wachsmann-Hogiu, "Complementary Metal-Oxide-Semiconductor-Based Sensing Platform for Trapping, Imaging, and Chemical Characterization of Biological Samples," ACS Applied Optical Materials, vol. 1, no. 1, pp. 329-339, 2023/01/27 2023, doi: 10.1021/acsaom.2c00066.

Transition to Chapter IV

In the previous chapter, the fabrication, characterization, and application of the chemiluminescence device integrated with a CMOS image sensor were demonstrated. In this configuration, the optical lens and IR filter of the CMOS were removed, exposing the surface of the CMOS imaging sensor and microlens array. The bioluminescence reaction of luciferin and ATP in the presence of the enzyme luciferase occurs on the surface of the CMOS imaging sensor, which collects almost half of the signals from the CL reaction. The ability of this biosensor to detect surface contamination through the concentration of ATP, collected using commercial Ultrasnap swabs, was evaluated. The performance of this device was compared with that of a commercial luminometer, the common method for assessing surface cleanliness in the industry. While the CMOS-based biosensor demonstrated similar performance to the luminometer, it is significantly cheaper and can be a viable option for use in all food-related industries, including kitchens, restaurants, and warehouses.

Electrochemiluminescence (ECL) and chemiluminescence (CL) are both luminescent techniques used in biosensing applications, yet they differ significantly in their mechanisms and advantages. While chemiluminescence involves the emission of light through a chemical reaction, ECL combines electrochemical and luminescent processes, generating light in response to an electrical stimulus applied to the electrode. One of the primary advantages of ECL over CL is the precise control over the reaction afforded by the applied electric potential. This control enables the modulation of luminescent intensity and timing, leading to improved sensitivity and specificity in detection. Additionally, ECL systems can be designed to minimize background interference by controlling the emission phases temporally and spatially, thus enhancing signal-to-noise ratios. Moreover, ECL allows for the possibility of multiplexing through potential-dependent emission, enabling the simultaneous detection of multiple analytes. This level of control and flexibility makes ECL a highly versatile and powerful tool in the development of integrated biosensor platforms, offering significant improvements in performance and applicability over traditional chemiluminescence methods.

In this chapter, an ECL platform integrated with a CMOS image sensor is introduced for the point-of-care detection of uric acid, a biomarker for gout disease. This biosensor utilizes a single-electrode electrochemical system configuration, where the electric potential gradient along the indium tin oxide (ITO) single electrode drives the ECL reaction. As a result, ECL signals are emitted, and the emission is detected by the CMOS image sensor. To precisely

control the small sample volume (2 μL), a microfluidic device containing two parallel channels is employed, with one channel serving as a control and the other for testing. Different concentrations of hydrogen peroxide and uric acid were measured using this platform, yielding a linear range of 25-300 μM. As the ECL reaction occurs close to the surface of the sensor and photodiodes, nearly half of the emitted signal is detected, resulting in improved sensitivity compared to cellphone and microscope-based detection methods. This device demonstrated good reproducibility and reusability across different experiments. Furthermore, uric acid measurements from saliva and urine samples confirmed the potential of this device for point-of-care applications.

This chapter is based on my first-author article. The contributions of each author are as follows:

RA and SWH conceived the idea. RA and SS designed the experiments. RA performed the experiments with assistance from JL and SS. RA analyzed the data and wrote the manuscript with input from all co-authors. SWH supervised the project. All authors reviewed and approved the manuscript in its current form.

Chapter IV. SE-ECL on CMOS: a miniaturized electrochemiluminescence biosensor

Reza Abbasi [a], Juanjuan Liu [a] , Sorina Suarasan [b] and Sebastian Wachsmann-Hogiu *[a]

a) Department of Bioengineering, McGill University, Montreal, QC, Canada.

b) Nanobiophotonics and Laser Microspectroscopy Center, Interdisciplinary Research Institute in Bio-Nano-Sciences, Babes-Bolyai University, T. Laurean 42, Cluj-Napoca 400271, Romania.

* sebastian.wachsmannhogiu@mcgill.ca.

4.1 Abstract

Biosensors exhibit high potential for the detection of analytes of interest at the point-of-need. Over the past two decades, combination of novel biosensing systems – such as electrochemiluminescence (ECL) biosensors – and advances in microfluidic techniques have allowed the development of lab-on-a-chip devices with enhanced overall performance and simplified sample-handling. However, recording data with conventional platforms requires advanced and complicated instruments, such as sensitive photodetectors coupled to microscopes, to capture the photons from the chemiluminescent reaction. In this work, we integrated microfluidic and luminol/hydrogen peroxide ECL systems on a complementary metal-oxide-semiconductor (CMOS) chip for sample handling and data collection on the same platform. This was achieved by the adaptation of a single electrode as electrochemical transducer and a CMOS chip as built-in detector. We demonstrated the application of this platform for the detection of uric acid (UA), a biomarker of gout disease. A linear detection range was observed from 25 to 300 µM, with a detection limit (LOD) as low as 26.09 µM. The device showed high reusability and reproducibility within the linear detection range, while maintaining high selectivity for UA detection. The analytical performance has also been evaluated in simulated saliva and urine samples, demonstrating the potential utility in medical diagnosis at the point-of-need. Compared to other ECL imaging platforms, this device showed an eightfold increase in photon collection efficiency. Overall, this approach has promising potential as an inexpensive, portable, and efficient ECL platform for measuring analytes at the point-of-need.

4.2 Introduction

Point-of-need testing has tremendous value in diagnostics (medical and non-medical) in resource-poor areas. The ideal point-of-need device is a portable 'sample-in-answer-out' system, which requires simplicity in operation [1, 2]. However, most diagnostic technologies require quantitative, diagnostic-level performance, and necessitate specialized instrumentation, limiting their use in point-of-need applications [3]. To this end, certain biosensors can be adapted to be used at the point-of-need.

In order to adapt biosensors to resource-poor locations, device miniaturization for portability, cost-effectiveness, and easy sample processing need to be considered while maintaining efficacy [4, 5]. Often, at the point-of-need only a limited amount of sample is available, leading the sample handling issues that need to be addressed. Microfluidic technologies can address these challenges by integrating microchannels, chambers, pumps, and other components to manipulate the small volume of sample through pressure or capillary force [6]. These platforms also show advantages such as minimized consumption of reagents and the potential for automation and integration of many analytical procedures into a single device [7]. Therefore, lab-on-a-chip platforms make the collection of biological fluids less invasive and their analysis feasible at the point-of-need. Current improvements in lab-on-a-chip devices include miniaturization of key fluidic components for enhanced compactness, easier sample handling, high performance, and reduced cost [8]. However, for the most part, lab-on-a-chip platforms require complex external instruments to read the signal [9]. Consequently, incorporating detectors into the lab-on-a-chip biosensing platforms is needed to address this issue.

The process of light emission from the chemiluminescence (CL) reaction is a complex multi-step reaction in aqueous conditions. Briefly, the reaction of a CL agent, such as luminol, paired with an oxidant, like hydrogen peroxide (H_2O_2), generates an intermediate that exhibits CL emission. During this oxidation reaction, the luminol (3-aminophthalhydrazide or 5-amino-2,3-dihydro- 1,4-phthalazinedione) is oxidized into the dicarboxylate ion and loses molecular nitrogen while gaining oxygen atoms, producing 3-aminophthalate. The resulted 3-aminophthalate is in an excited state because the electrons in the oxygen atoms are elevated to higher orbitals. The electrons quickly return to a lower energy level, releasing a fraction of the excess energy as photons. The whole reaction occurs in the presence of a catalyst, for example, iron (present in hemoglobin) or gold nanoparticles (AuNPs). Although the reaction can occur even without a catalyst, the emitted signal will be quite weak to visualize [10, 11].

On the other hand, instead of a catalyst, an electric potential difference can be utilized to oxidize luminol and produce the excited state. The resulting electrogenerated chemiluminescence from the oxidation of luminol can be used to design biosensors exhibiting high sensitivity and a wide linear range of operation [12].

Electrochemiluminescence (ECL) is a rapidly growing bioanalytical technology with numerous advantages, such as potential for high temporal and spatial resolution, high signal-to-noise ratio, broad dynamic range, and rapid measurement [13]. ECL is an electric field-driven electrochemical process that involves high-energy electron transfer reactions in molecules at electrode surfaces to generate excited states for light emission [14, 15]. Typically, low electric potential differences are needed to drive the ECL reaction in most systems [16-19], making it a good candidate for miniaturization and integration with microfluidic devices and optical readers.

Most ECL devices consist of an electrolytic cell with three electrodes (a working electrode, a counter electrode, and a reference electrode) immersed in an electrolyte and connected to a power supply. An electrogenerated chemical reaction on the working electrode occurs after applying electrical potential on the electrolytic cell. Recording and analyzing the ECL emission requires specialized photodetectors. Signal collection is generally achieved using single-point photodetectors (such as photomultiplier tubes or avalanche photodiodes) due to their high gain, sensitivity, and linearity [20-24]. However, these types of detectors cannot be used in portable devices due to their size, high voltage supply, and power consumption, and cannot be easily integrated into multiplexed detection designs [25]. Other commonly used optical detectors in ECL systems are linear or 2D pixelated detectors, such as charge-coupled devices (CCD) [20, 25-27], that are coupled with a microscope and objective lens [28]. More recently, smartphone-based detectors can be employed in ECL systems. However, the capability of these detectors is limited by the low numerical aperture of the optical system leading to poor optical collection efficiency [16]. On the other hand, CMOS sensors are small, have low power consumption, and can image large fields of view. Thus, they are suitable for the development of portable and miniaturized ECL systems that can be advantageous for point-of-need applications [20].

In addition to improving the detection system, miniaturization of the ECL configuration needs to be achieved. One particular implementation of ECL that we identified to be more amenable to miniaturization is based on a single electrode electrochemiluminescence (SE-ECL) configuration demonstrated by Gao et al. in 2018 [29]. In their work, the electrode system

consists of one single electrode that induces a gradient of potential along the surface. By applying an external voltage to the single electrode, a potential difference between the two ends of the microelectrochemical cell initiates the ECL emission. The electric potential difference in this system is directly proportional to the applied external voltage and the length of the electrochemical cell. This group successfully demonstrated the application of their device in the detection of different analytes, including hydrogen peroxide (H_2O_2) and uric acid (UA). Compared to traditional three-electrode systems, SE-ECL-based devices show advantages in portability, cost efficiency, simplicity of operation, and potential for multiplexing [22, 29].

In addition to the single electrode system, other approaches to fabricate miniaturized ECL devices include screen printing [20-23] and photolithography [24, 25]. However, these types of devices require multiple steps for fabrication and time-consuming processes [16]. As a result, further optimization is needed for the miniaturization and integration of these ECL systems. Integrating ECL sensing mechanisms, including signal detection, into a single mini-device is a development that may play a significant role in applications that require point-of-need testing.

In this work, we integrate microfluidic and luminol-based ECL on a CMOS chip to build a miniaturized SE-ECL enzymatic sensor. In our platform, we took advantage of the (i) single electrode design to initiate the ECL reaction, (ii) microfluidic techniques for sample handling, and (iii) an inexpensive and energy-efficient CMOS sensor for capturing the signal from luminol/H_2O_2 reaction. We hypothesize and demonstrate that photon collection is significantly improved compared to other ECL systems due to the close proximity of ECL reactions to the detector, leading to the detection of almost half of the photons emitted from the luminescence reaction. We further evaluate the performance of our system by detecting UA in artificial body fluids, including urine and saliva. UA is an end-product of metabolic breakdown of purine nucleotides and has long been used as a biomarker for assessing physiological health [30]. Gout, hyperuricemia, Lesch-Nyhan syndrome, cardiovascular disease, kidney illness, and other disorders are all linked to abnormal UA levels [31]. Electrochemical techniques to analyze UA in physiological samples by measuring the generated H_2O_2 from enzymatic reactions using uricase have been the focus of extensive research [32-36], but they generally show poor sensitivity due to low photon counts. By combining a microfluidic platform on a CMOS chip, we are able to demonstrate sensitive detection of UA via SE-ECL.

4.3 Experimental section

4.3.1 Materials

Luminol was purchased from Ward's science (Ontario, Canada). Sodium bicarbonate was purchased from Bioshop Canada Inc.. Sodium hydroxide and hydrogen peroxide of 30% were from Thermo Fisher Scientific. Uric acid and triton X-100 were acquired from Bio Basic Inc.. Uricase from Candida species (activity of 4 units/mg powder at 25 °C), glucose (anhydrous dextrose,) and creatinine were purchased from Sigma-Aldrich. PDMS (Polydimethylsiloxane) (SYLGARD™ 184 Silicone Elastomer Kit) was purchased from DOW Corning Corporation. SU-8 2075 photoresist was purchased from MicroChem (Kayaku Advanced Materials, Inc., USA). Conductive silver epoxy was purchased from MG Chemicals (Ontario, Canada). Ascorbic acid was acquired from Anachemia Inc. (VWR International Co). Artificial Saliva, ASTM E2721-16, was purchased from Pickering Laboratories Inc. (USA). Surine™ (negative urine control) was acquired from Cerilliant, Sigma. Indium Tin Oxide (ITO)-coated Poly Ethylene Terephthalate (PET) was obtained from Sheldahl Inc. (USA). Milli Q water was used to prepare solutions.

4.3.2 Methods

4.3.2.1 Sample preparation.

The electrolyte used for ECL measurements was a mixture of 0.1 M sodium bicarbonate and 1 mM luminol. Specifically, to prepare the electrolyte, 0.1 M sodium bicarbonate was prepared, and the pH was adjusted accordingly by adding 1 M NaOH. It was then mixed with 10% v/v 10 mM luminol that was prepared in NaOH (0.1 M) to obtain a final concentration of 1 mM for luminol. Further, the analytes (H_2O_2 or UA) were added to this electrolyte for detection. The pH used for measurements was 10.7 unless otherwise.

For H_2O_2 detection, 10 mM H_2O_2 was prepared by diluting the concentrated H_2O_2 solution (9.8 M) in water and then mixed with the prepared electrolyte containing carbonate buffer and luminol. To create the calibration curve for H_2O_2 detection, different concentrations of H_2O_2 were prepared in the electrolyte.

Similarly, for UA detection, 1 mM UA was prepared in the electrolyte containing carbonate buffer and luminol for further dilutions. Further, different concentrations of UA from 25 μM to 1000 μM (25, 50, 100, 200, 300, 500, 800, and 1000 μM) were prepared by diluting the stock

solution of 1 mM UA in the same electrolyte with carbonate buffer and luminol. The uricase solution of 1 mg/ml was prepared using NaOH (0.001 M, pH 11) and kept at -20 °C for further use. To evaluate the selectivity for UA detection, interfering molecules, i.e., ascorbic acid (5 μM), creatinine (10 μM), and glucose (50 μM) were added to the prepared UA solution for ECL measurement. 1% v/v of triton X-100 was added to the final solutions before each experiment to improve mixing of components.

4.3.2.2 Preparation of the solutions for simulated samples.

To prepare the solutions for simulated sample analysis, artificial body fluids (saliva or Surine™) were mixed with the electrolyte containing carbonate buffer (0.1 M) and luminol (1 mM) at two different ratios (1:9 and 1:1). Further, 50 μM or 300 μM of UA was prepared in the mixture of the electrolyte and artificial body fluids using 1mM and 6mM stock solutions of UA, respectively, and the ECL intensities were captured. By using the calibration equation of UA detection, the concentration of UA corresponding to the obtained intensity (average of 3 experiments) was calculated, and the recovery rate was reported by comparing the measured concentration with the known (added) concentration.

4.3.2.3 Fabrication of the miniaturized SE-ECL device.

Fig. 1 A describes the fabrication steps of the miniaturized ECL device. To build such a platform, a backside-illuminated 5-megapixel imaging CMOS sensor camera module (OV5647, OmniVision technologies) was used and controlled by a Raspberry Pi 4 computer. The original lens and IR filter were removed to minimize the distance between the sample and the sensor surface and to maximize the photon collection efficiency. The microfluidic device was built by soft lithography. Briefly, the SU-8 photoresist on silicon wafer was exposed to 365-nm UV light using a mask aligner (the OAI Model 200) to create the positive master mold. Then PDMS prepared in a 10:1 (monomer: crosslinker) ratio was used to replicate the pattern. This device was then sealed with the ITO-coated PET using oxygen plasma treatment (Diener Electronic, PICO) at 60 W for 2 minutes, followed by 30 minutes of incubation at 70 °C for irreversible bonding. The microfluidic unit was then aligned and mounted onto the active area of CMOS sensor such that the channels are sealed, the liquid is uniformly distributed in the space between the ITO layer and the PDMS enclosure, and a controlled electric field can be applied along the channels.

The ITO-coated PET film comprises of two distinct layers: a PET film with a thickness of 127 mm and an ITO coating with a thickness ranging from 10 to 300 nm. In order to choose the optimal thickness of ITO film for ECL experiments, two material factors have been considered: the sheet resistance and optical transparency of the ITO. The difference in the sheet resistance leads to a different current intensity that affects the gradient of the electrical potential on the ITO electrode. The different ITO coating thickness, on the other hand, results in variable electrical resistance of the ITO-coated film. More specifically, a larger ITO coating thickness leads to lower resistance. The ECL becomes more robust as the ITO resistance increases, reaching its peak at 100 ohm/square [29]. On the other hand, since the ECL optical signal needs to pass through the ITO-coated PET, the transmittance is another critical factor in the overall performance of the device. According to the film manufacturer (Sheldahl, Inc.), ITO with 60 ohm/square resistance has the largest transmittance for light with a wavelength of 419 nm (CL light) and is almost 10 % higher than the ITO with 100 ohm/square resistance. Thus, all SE-ECL devices in this study were fabricated using ITO with 60 ohm/square.

The device was then connected to a digital power supply (Sky Toppower STP6005) using alligator clips and copper wires. Conductive silver epoxy was used to connect the copper wires to the surface of the ITO-coated PET (cold soldering). Eventually, the final PET-microfluidic system was placed on the CMOS sensor to create a miniaturized ECL on the CMOS. The field of view (FOV) of the device is 3.67 mm × 2.73 mm, which is the active area of the CMOS sensor, and the spatial resolution of the system is 1.4 μm, limited by the pixel size [37]. A 4-point probe (Lucaslabs, Signatone Pro4) and a profilometer (Bruker, DektakXT) were utilized to measure the sheet resistivity of ITO and the height of the microfluidic channel, respectively (Fig. 2 A and B).

4.3.2.4 ECL measurements.

For UA detection, a final concentration of 200 μg/ml of uricase was added to the sample solution and incubated for 10 minutes before applying voltage. For the ECL experiments, the sample was transferred to the channels through the inlets using a syringe and a 30 G needle. As illustrated in Fig. 1 C, the sample filled the channels as well as both inlets and outlets. The measurements were performed in complete darkroom. A voltage of 5 V was applied to the device and the ECL emission was observed and recorded using a raspberry pi 4 computer and then analyzed via Fiji ImageJ to extract grey values corresponding to the detected photons. The measured grey values of the control channel were subtracted from those recorded for the test

channel and the results were presented. The limit of detection (LOD) in Fig. 3 A and B was calculated according to LOD = 3SD/S, where SD is the standard deviation of the blank measurements when there is no analyte, and S is the slope of the linear equation obtained from the calibration plot. In order to study the reusability (repeatability, using the same device), and reproducibility (using different devices), and selectivity (in the presence of interfering molecules), 50 and 300 μM of UA were used for ECL measurements. For controlling the imaging parameters, a Python script was written, and the following conditions were applied: resolution = 2592 × 1944 pixels (full field of view), framerate = 1/6 s, shutter speed = 6 s exposure time, ISO = 800 (gain 8X). Thirty seconds of sleep time was applied before each experiment to give the camera an appropriate time to adjust the parameters. Also, to make a fair comparison between the ECL-on-CMOS platform and other platforms, including microscopes and smartphones, a Nikon eclipse Ti2 equipped with a Prime 95B 25 mm BSI CMOS camera (cooled to -25 °C), and Samsung Galaxy S21 ultra were employed. A 4X objective lens with a 30 mm working distance was chosen for the microscope to have the same field of view and capture the full length of both microfluidic channels. The imaging parameters (ISO, gain, exposure time) were chosen to be the same as the experiment with the CMOS detector. The pro imaging mode was used in the smartphone to adjust the imaging parameters to be similar to those of the other systems. The test channel in this experiment contained 300 μM H_2O_2 as the analyte. The distance between the ECL reaction and the detector was 30 mm for the microscope with a 4X objective, 300 μm for the CMOS system, and approximately 10 cm for the smartphone.

4.4 Results and discussion

4.4.1 Fabrication of the ECL-on-CMOS device.

The ECL biosensing platform was fabricated as shown in Fig**. 1** A, by using a backside-illuminated CMOS sensor and a microfluidic chip containing two channels sealed with ITO-coated PET. First, a microfluidic device composed of two channels with 3,500 × 650 μm dimensions was fabricated with PDMS and then sealed with an ITO-coated PET film. The sealed microfluidic channels are electrochemical cells whereas the conductive ITO-coated PET acts as a single electrode (Fig. **1** B). This was then attached directly to the CMOS sensor. To apply the electrical potential to the electrochemical cell, two copper wires connected the device to a power supply. These wires were in contact with the ITO on two ends of the microfluidic channels. The channels were filled with carbonate electrolyte containing luminol, H_2O_2, and

triton X-100. The CMOS sensor was connected to the Raspberry Pi 4 system to record ECL emission images (Fig. 1 D).

A SE-ECL configuration is adapted in this device. In SE-ECL systems, the resistance of the ITO electrode creates a gradient of potential along the channel. When a specific voltage is applied, the relative fraction of the potential difference inside the electrochemical cell and the applied voltage

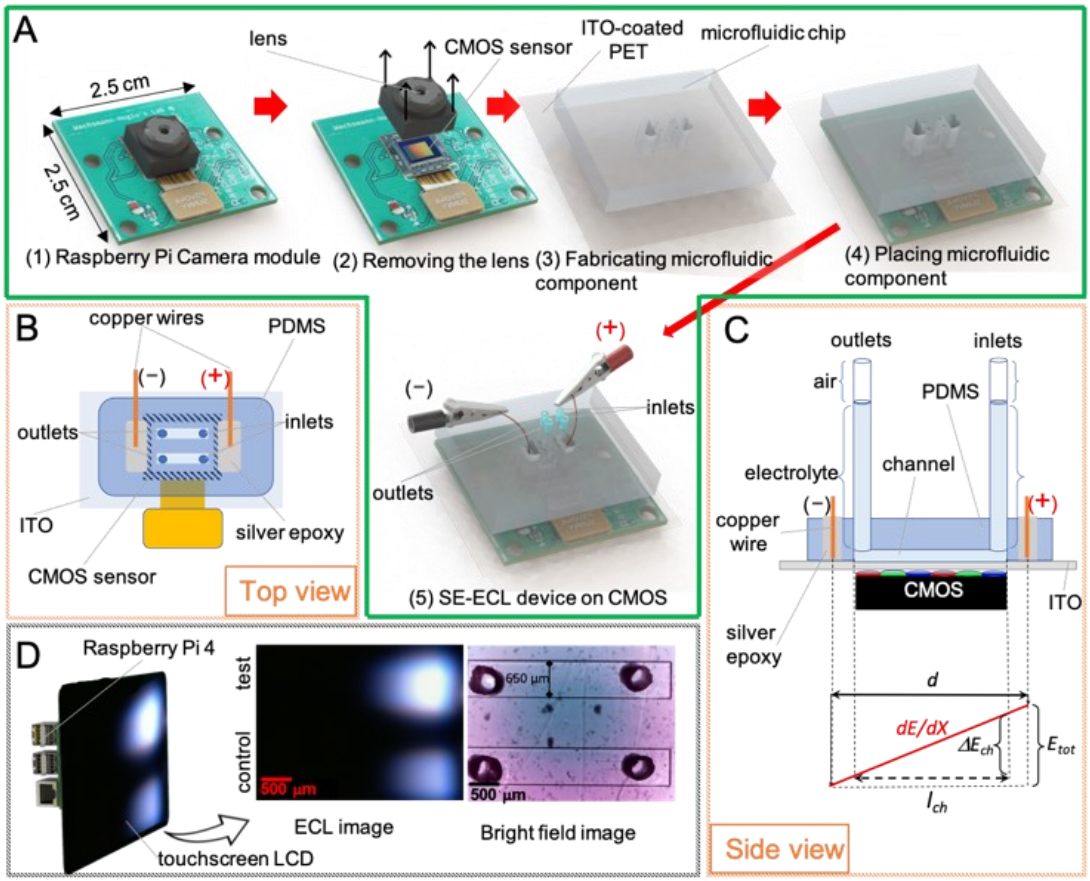

Fig. 1. Schematic of the SE-ECL on CMOS: A) process of manufacturing; (1) the Raspberry Pi camera model V1. (2) Removing the original lens from the CMOS sensor (3) Fabricating microfluidic component sealed with ITO-coated PET. (4) Placing the microfluidic device on top of CMOS sensor (5) Connecting the final device to the power supply, Raspberry Pi 4, and touchscreen LCD using copper wires and flat-flexible-cable (FFC). B) Top schematic view of the final SE-ECL on CMOS device. C) Side view (cross section) of the final device. D) The bright field image of the channels (right) and ECL image of the channels (middle) captured by the CMOS camera; the bright field image was taken using point source illumination and the ECL image was taken in a completely dark room.

corresponds to the relative length of the channel and the distance between wires, as given in equation 1 [26].

$$\Delta E_{ch} = E_{tot} \left(\frac{l_{ch}}{d}\right) (1)$$

where ΔE_{ch} is the potential difference inside the electrochemical cell, E_{tot} is the voltage applied by a power supply, l_{ch} is the length of the channel and d is the distance between wires, as illustrated in Fig**. 1** C. When ΔE_{ch} is large enough, the faradaic reaction co-occurs at both ends of the channels, with oxidation of luminol at higher electric potential and reduction of H_2O_2 at lower electric potential. Under these conditions, the luminol is oxidized at the higher electric potential of the channel and generates an excited electronic state, which then relaxes to the ground state by emitting light with wavelengths centered at around 419 nm (blue light) [27].

To investigate the background signal contribution to the recorded ECL intensity in the test channel, a control experiment was performed in the parallel control channel (Fig.1 D, ECL image, bottom channel) under the same conditions, but in the absence of analytes. The reported ECL intensities are obtained by subtracting the intensity recorded in the control channel from the one recorded in the test channel.

4.4.2 Characterization of the CMOS SE-ECL device.

The resistivity of the ITO-coated PET film plays an important role in the distribution of the potential gradient, which is an important characteristic of the SE-ECL configuration. Therefore, to study the stability of the ITO resistivity, different currents were applied onto the ITO-PET film and corresponding potentials were recorded by the 4-point probe. The sheet resistance was calculated using equation 2 when the distance used for voltage measurement is at least twice the thickness of the film.

$$R_s = k\frac{\Delta V}{I} \quad (2)$$

where R_s is the sheet resistance, k is the geometrical correction factor which is 4.532 for the aforementioned experimental setup [38, 39], ΔV is the measured voltage, and I is the applied current. As a result (Fig. 2 A), the sheet resistance of the ITO-coated PET is 59.04 ohm/square with a relative standard deviation (RSD) of 1.75%, which indicates good uniformity.

To further characterize the microfluidic component of the device, the depth of microfluidic channels was measured using a profilometer and the surface profile is presented in Fig. 2 B. The height of each channel was measured to be 143 µm. Considering other channel dimensions that were mentioned before (w= 650 µm, l= 3.5 mm), we calculated the volume of each channel to be 3.3 × 10^8 μm^3, corresponding to a volume of the solution (electrolyte) of 3.3 µl in each channel. During the experiment, the channels are filled with the reagents at maximum capacity, i.e., 3.3 ml of mixed luminol, H_2O_2, and Carbonate buffer. The 3.3 µl of electrolyte inside each channel contributes to the ECL emission. This amount of electrolyte corresponds to 3.3 nmol of luminol that emits light in the oxidation reaction.

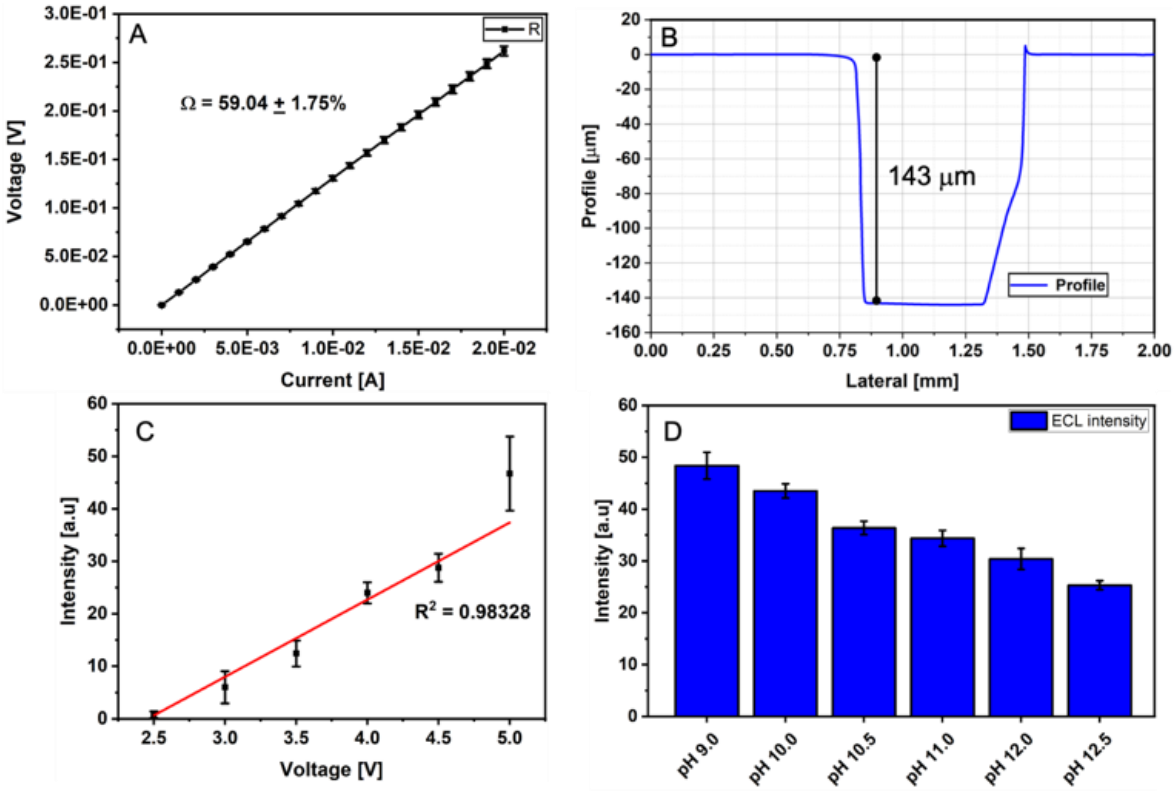

Fig. 2. System characterization: A) The sheet resistivity of the ITO coated PET using a 4-point probe. B) The profile of the microfluidic channel showing the height of one channel measured by a profilometer. C) Dependence of the SE-ECL intensity on the applied voltage. D) Image-based SE-ECL intensity in carbonate buffer with different pH values. The electrolyte used for measurements presented in panels C and D is 0.1 M carbonate buffer ($NaHCO_3$ and NaOH), concentration of Luminol is 1.0 mM, percentage of triton X-100 is 1% v/v, and the voltage is set to 5 V. Test channel contains 300 µM H_2O_2.

Next, to explore the effect of the applied voltage on SE-ECL performance, H_2O_2 was used to measure the ECL intensity at different voltages ranging from 2.5 to 5 V. As shown in Fig. 2 C, a linear relationship between the intensity and the voltage was obtained, as expected from equation 1. When E_{tot} is more than 2.5 V, the ΔE_{ch} is sufficient to drive the reaction, and thus the faradaic reaction occurs simultaneously at both ends of channels. Since this reaction is driven by electric potential difference, increasing the voltage results in increasing the emission until 5 V. The blue ECL emission of luminol was observed at the positive side of the channel starting at around 2.5 V. Increasing the value of E_{tot}, the emission region of the channel gradually expands toward the center, allowing the ECL reaction to occur over a greater surface area [40]. It is worth mentioning that above 5 V, the luminescence signal became saturated and the CMOS sensor was unable to process the actual data as it was above its full-well and maximum charge transfer capacity. Saturation of the CMOS detector limits the linear range and the performance of the device in the saturation range is not reliable. Thus, the result of ECL experiments above 5V have not been analyzed. Eventually, the device will operate at its optimum voltage of 5V, which is a safe voltage for the operator and produces the largest signal for the concentration range selected for this application. While it is technically possible to shift the concentration range to the lower limits of detection by increasing the voltage, higher voltages result in higher electrical currents and material temperature, which alter the enzyme activity and can damage the ITO-coated PET. In addition, at higher potentials, the oxidation of water takes over as the major process, and a significant amount of gas evolution is frequently observed due to the generation of molecular O_2 [26, 40].

Furthermore, to study the effect of electrolyte pH on SE-ECL performance, ECL intensities were recorded with H_2O_2 in electrolytes at different pH values. The results revealed that raising the pH decreases the intensity of the ECL (Fig. 2 D). While other previously published articles reported the optimum pH range for the ECL reaction of luminol to be between 10 and 11 [29, 41-43], we observed a higher emission intensity at pH 9. Some chemical substances, such as phenolic compounds and amino acids, have been studied in the literature to see how they affect luminol intensity at various pH levels. These chemicals inhibited luminol intensity at lower pH levels, but a substantial increase in luminol intensity was found at higher pH levels. Maximum CL intensity was reported between pH 8.0 and pH 9.5. In this pH range, both inhibitory and boosting signals were found. However, the lifetime of the emission is longer in a higher pH range (pH between 10-11) [44]. Therefore, in the following studies, we chose pH 10.7, which is a good compromise between the ECL intensity and lifetime.

4.4.3 Performance of the CMOS SE-ECL device.

To evaluate the performance of the SE-ECL system for the luminol-H_2O_2 reaction, the sensitivity, and the LOD of the CMOS SE-ECL device for H_2O_2 detection were measured. The ECL intensity corresponding to H_2O_2 at different concentrations was reported. At least three experiments were conducted for each concentration, and based on the average intensity of each concentration, the relationship between the H_2O_2 concentration and the ECL intensity, a calibration plot was presented (Fig. 3 A). A linear detection range from 25 to 300 μM was obtained with a coefficient of determination $R^2 = 0.986$, and LOD for H_2O_2 was calculated to be 17.75 μM.

Next, to explore the capability of our system to be employed in the detection and screening of an analyte that is a biomarker of several diseases, we chose to investigate UA. UA is a product resulting from purine metabolism in the human body [45]. Elevated UA levels in urine or serum can impair renal function and may be used as indicator of gout, cardiovascular and renal disease, hypertension, and other conditions. Low UA levels have been linked to molybdenum insufficiency, copper toxicity, and the progression of multiple sclerosis. As a result, the detection of UA in human physiological fluids is critical for diagnosing individuals with diseases linked with abnormal purine production and catabolism [46].

The oxidation of UA in the presence of the enzyme uricase that produces H_2O_2 is described in equation 3.

$$\underset{\text{(Uric acid)}}{C_5H_4N_4O_3} + 2H_2O + O_2 \xrightarrow{uricase} \underset{\text{(Allantoin)}}{C_4H_6N_4O_3} + H_2O_2 + CO_2 \quad (3)$$

H_2O_2 is the product of the enzymatic oxidation reaction of UA, and in this work, the luminol-H_2O_2 system was used to detect UA.

Following the same procedure detailed for H_2O_2 detection, the calibration plot of UA was obtained by recording ECL intensities of UA at different concentrations (Fig. 3 B). The results show a linear detection range for UA from 25 μM to 300 μM with a coefficient of determination $R^2 = 0.968$, and a LOD of 26.09 μM. While the linear range is comparable with values reported in the literature for ECL detection (Table 1), the LOD is however somewhat higher (worse),

mainly due to the lack of electronic gain in this system compared with other reports (for example those using PMTs have higher slope due to electron multiplication), sample handling, and the high standard deviation of the blank for the luminol concentration chosen in this experiment. However, the LOD reported here is still within (or lower) than the physiological range of UA in body fluids such as saliva or urine, which has been reported to be 70 – 320 μM in saliva and 1.49 – 4.46 mM in urine [47, 48]. Besides, to the best of our knowledge, there are no studies demonstrating ECL detection of uric acid in saliva.

To further explore the efficiency of the reaction (equation 3), the calibration plots (Fig 3 A) and (Fig. 3 B) for H_2O_2 and UA were compared to each other. Theoretically, this reaction should produce as much H_2O_2 as the stoichiometric ratio of H_2O_2 to UA (limiting reagent) indicates. Based on equation 3, the molar ratio between UA and H_2O_2 in the balanced equation is 1 to 1. As a result, in a constant volume, by oxidation of a certain concentration of UA in the reaction, the same concentration of H_2O_2 should be released. However, the amount of H_2O_2 actually produced by the reaction is usually less than the theoretical yield and is referred to as the actual yield.

Thus, the efficiency of the reaction in equation 3 is defined as:

Efficiency of the reaction (percent yield) = (actual yield / theoretical yield) × 100. As shown in Fig. 3 B, any given amount of UA added to the reaction solution correlates with an intensity value proportional to the actual amount of H_2O_2 produced, which itself can be calculated from Fig 3 A. On the other hand, based on the stoichiometric ratio of equation 3, the theoretical amount (mol) of produced H_2O_2 is equal to the amount of UA (mol) added to the solution.

Hence, the efficiency of every experiment (i.e., every intensity value) can be calculated by dividing the actual concentration of produced H_2O_2 by the concentration of uric acid added. In other words, the actual yield and theoretical yield can be calculated from Fig.3 B and Fig.3 A, respectively. By comparing the results from calibration curve of UA and H_2O_2 (Fig. 3 A and Fig. 3 B), the efficiency of the reaction (equation 3) for each given concentration was calculated and then the average of all efficiencies in the linear concentration range was obtained to be 57.1%. In addition to some experimental errors, there are often losses as a result of an incomplete reaction, and unwanted side reactions such as the conversion of the H_2O_2 to the

Table 1. ECL detection of UA using various methods in literature. Table is categorized based on the real sample reported in the literature

Detector	Luminophore/Coreactants	Method	Sample	Linear range	LOD	REF
PMT	$Ru(bpy)_3^{2+}$/ TPrA	ECL quenching in the presence of ascorbic acid	urine	1- 80 µM	1 µM	[31]
PMT	$Ru(bpy)_3^{2+}$	Disposable biosensor based on cathodic ECL of tris(2,2-bipyridine) ruthenium (II)	urine	10 - 1000 µM	3.1 µM	[49]
PMT	MWCNTs/ ZnBCBTP	ECL Enhanced by the Synergetic Effect of Porphyrin and Multi-walled Carbon Nanotubes	urine	0 - 300 µM	1.4 µM	[50]
PMT	$Ru(bpy)_3^{2+}$/TPrA	separation of uric acid by capillary electrophoresis and quenching the ECL signal	urine and serum	2.0 - 100 µM	0.02 µM	[51]
PMT	luminol / H2O2	The uricase has been embedded in polypyrrole (PPy) matrix on platinum electrode	sea food (porphyra and kelp)	75 pM - 8.3 µM	75 pM	[52]
PMT	BTPPO / H2O2	modified ITO film with Nickel (II) tetrasulfophthalo-cyanine (NiTSPc) and using 3 electrode system	serum	60 - 600 µM	8.0 µM	[53]
PMT	Au NRs and S2O8 2-	label free ECL biosensor based on Au NRs@TiO2 Nanocomposite	serum	40 nM - 28 µM	15 nM	[54]

PMT	luminol / H2O2	One-pot synthesis of popcorn-like Au@Polyluminol nanoflowers	serum	3.0 - 300 µM	1.00 µM	[55]
smartphone	luminol / H2O2	ECL detection of enzymatic oxidation using the single electrode electrochemical cell	—	5.0 - 50.0 µM	Not reported	[29]
CMOS	Luminol / H2O2	Miniaturized lab-on-a-chip ECL detection by catalytic reaction using uricase	urine and saliva	25 – 300 µM	26.09 µM	This work

Abbreviations: * TPrA: tri-n-propylamine BTPPO: bis-[3,4,6-trichloro-2-(pentyloxy-carbonyl)-phenyl] oxalate MWCNT: multiwalled carbon nanotubes ZnBCBTP: 5,15-bis(4-carboxylphenyl)-10,20-bis(2,4,6-trimethylphenyl)

water due to the instability of the H_2O_2 at low concentrations and at room temperature.

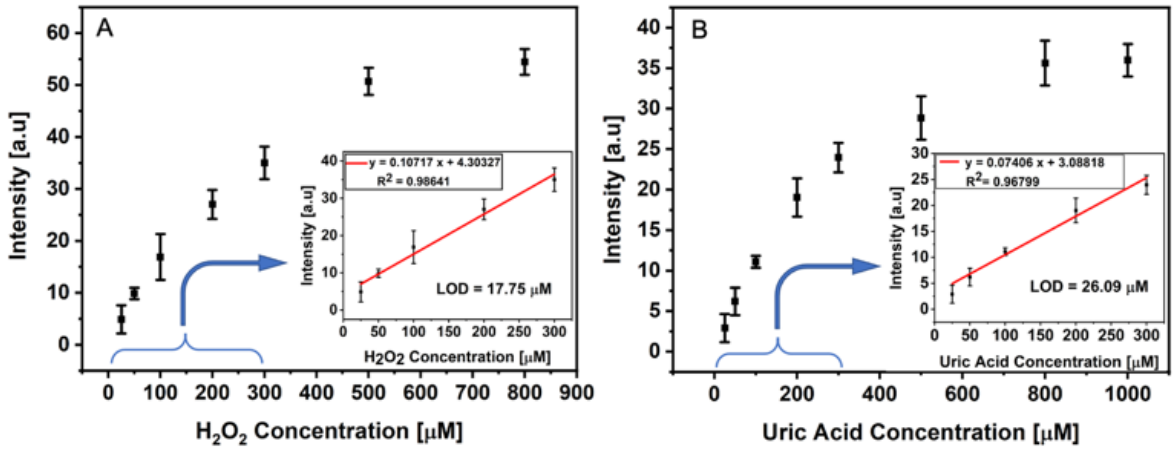

Fig. 3. Calibration graphs: A) ECL image-based intensity of the luminol/H_2O_2 system with different concentrations of H_2O_2. The inset shows the linear range and the calibration equation. B) ECL analysis of H_2O_2 produced during the oxidation of the uric acid catalyzed by uricase after 10 minutes incubation time. The inset shows the linear range and the calibration equation for uric acid. The electrolyte is 0.1 M carbonate buffer ($NaHCO_3$ and NaOH), pH is 10.7, concentration of luminol is 1.0 mM, concentration of uricase is 200 µg/ml, percentage of triton X-100 is 1% v/v, and the voltage is 5 V.

4.4.4 Reproducibility, reusability, and selectivity of the CMOS SE-ECL device.

The reproducibility of different devices and the reusability of one device in multiple experiments are important characteristics of a biosensor to validate its potential for practical applications. Hence, these parameters were studied, and the results are shown in Fig. 4 A and Fig. 4 B.

Specifically, to evaluate the reproducibility of the fabrication process, five different devices were examined to detect 50 μM and 300 μM of UA each, as the low and the high concentration within the reported linear range of this device, in the electrolyte solution. The ECL intensities are collected, and the RSD of the intensity for these five experiments was calculated to be 14.79% for 50 μM of UA and 7.52% for 300 μM of UA. These numbers indicate good reproducibility for the detection of UA at different concentrations in the linear detection range. The observed variation is due to several factors. On one hand, the resistivity of the ITO PET differs slightly between devices, as shown in Fig. 2A, with a tolerance of approximately 1.75%. In addition to the ITO resistivity, the distance between the two driving electrodes (d in Fig. 1 C) can also introduce some errors. Another source of error that can contribute to the variability of both reproducibility and reusability is the efficiency of the oxidation reaction of UA.

The manufactured SE-ECL device could technically be cleaned and reused. In order to test this practicality of this approach, the reusability (repeatability) of the same device for multiple experiments was then studied by measuring the SE-ECL intensities of 50 and 300 μM of UA. We were able to record the ECL signal using the same device with fresh electrolyte solution each time for 5 times. The RSD was calculated to be 7.00% and 2.06% for 50 and 300 μM of UA, respectively. After 5 experiments, the ECL intensity has gradually decreased, and after the 9th experiment, a dramatic fall in the ECL intensity was observed (results not shown). This is probably due to the damage of the ITO coating as a result of the passing current and induced heat, which consequently leads to decreased conductivity. However, since the device is inexpensive (the cost of the CMOS chip is 1$ and the approximate cost of the microfluidic device is 3$), it can be used as a disposable device, and its reusability might not be an issue of significant concern.

There are various chemicals in body fluids that might interfere with the ECL detection of UA. For example, glucose, ascorbic acid (AA), and creatinine, which are concurrently present in

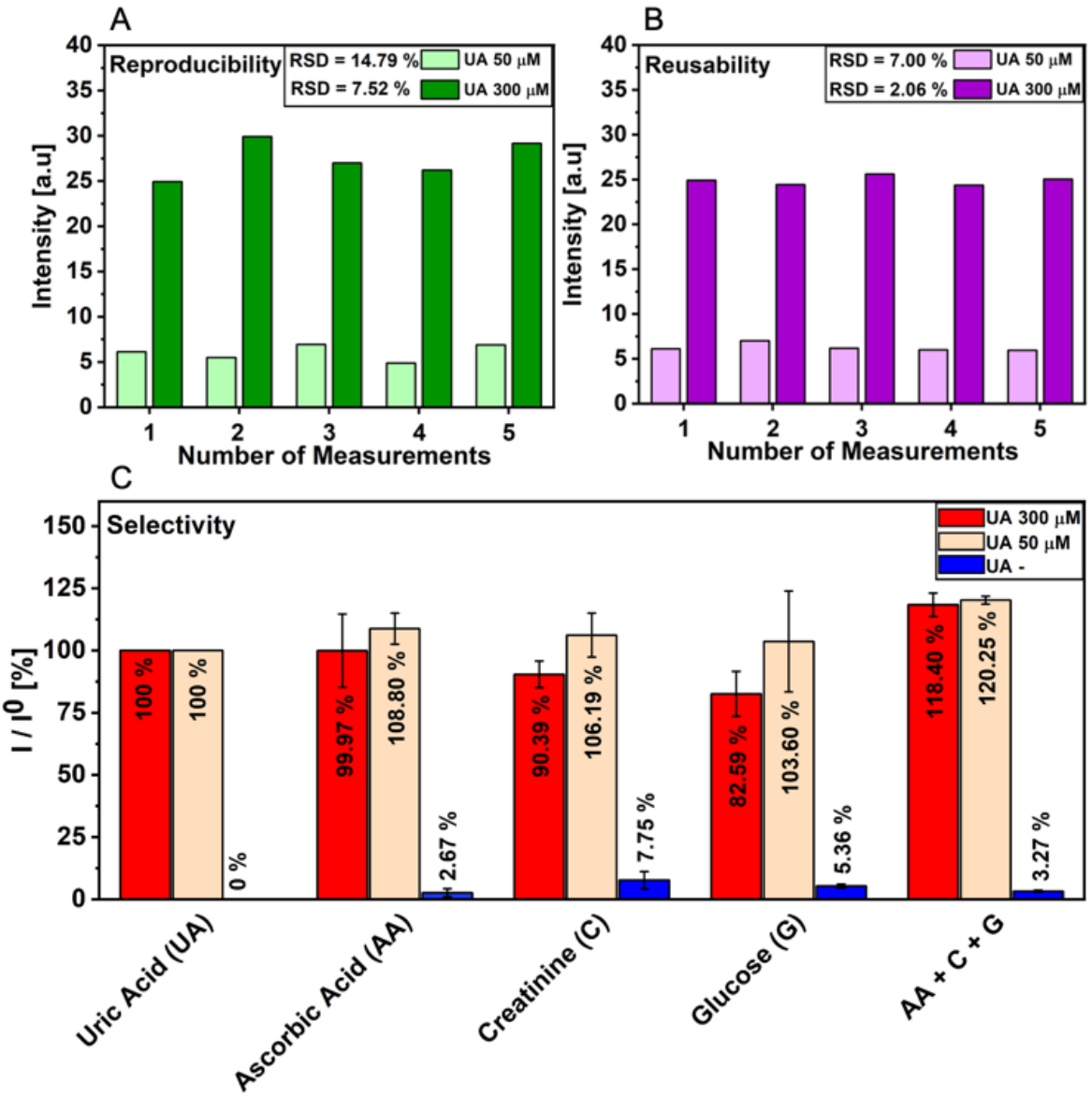

Fig. 4. Biosensing performance for detection of uric acid: A) Reproducibility of the SE-ECL on CMOS device using same (fresh) samples and different setups for detection of 50 and 300 µM of UA. B) Reusability (repeatability) of the SE-ECL on CMOS device using same (fresh) samples and same setup for detection of 50 and 300 µM UA. C) Selectivity of the SE-ECL on CMOS device for detecting UA over interference in the presence of 50 µM UA (orange), 300 µM of UA (red) and without uric acid (blue). On the y axis, $\boldsymbol{I}$ is the ECL intensity of UA measured in the presence of interference, and $\boldsymbol{I^0}$ is the ECL intensity with UA alone. The electrolyte is 0.1 M carbonate buffer ($NaHCO_3$ and NaOH), pH is 10.7, concentration of luminol is 1.0 mM, percentage of triton X-100 is 1% v/v, concentration of uricase is 200 µg.ml^{-1}, and the voltage is 5 V.

body fluids, may interfere with the detection of UA. Therefore, the selectivity of the fabricated device in the presence of glucose, AA, and creatinine was studied by detecting 50 and 300 µM

of UA in the electrolyte solution with and without interference. In this study, concentrations of these interfering molecules were chosen based on their typical physiological concentrations in human saliva [56-58].

We recorded ECL UA intensities in the electrolyte with (I on the y axis in Fig. 4 C) and without interfering molecules (I^0 on the y axis in Fig. 4 C). The relative intensities (I/I^0) for detecting 300 μM of UA in the presence of AA, creatinine, and glucose, were 99.97%, 90.39%, and 82.59%, respectively (red bars in Fig. 4 C). Also, the relative intensities for detecting 50 μM of UA in the presence of the interfering molecules were 108.80%, 106.19%, and 103.60%, respectively (orange bars in Fig. 4 C). When all interferences were introduced together with UA in the electrolyte, the relative intensities compared to UA alone were 118.40% for 300 μM of UA and 120.25% for 50 μM.

Furthermore, a negative control experiment that does not include UA reveals very low ECL intensities (blue bars in Fig. 4 C). In the presence of AA, creatinine, and glucose, the relative ECL intensities compared to the ECL intensity from solution with UA alone were measured to be 2.67%, 7.75%, and 5.36%, respectively. In presence of all three interferences (AA, creatinine, and glucose), the ECL intensity was 3.27% relative to the ECL intensity with UA alone. This result showed that our device is specific to detecting UA. This specificity comes from the uricase, which is an enzyme that catalyzes the oxidation reaction of UA.

4.4.5 Simulating real sample conditions.

We demonstrated so far that UA can be detected using the miniaturized SE-ECL configuration on a CMOS platform. Next, we studied the potential of the device to be used for the detection of UA in body fluids including saliva and urine. Normal physiological ranges of UA are 70 – 320 μM in saliva and 1.49 – 4.46 mM in urine. In order to measure the ECL intensity of UA in body fluids, these samples need to be mixed with the electrolyte. We chose the ratio of saliva: electrolyte to be 1: 1 as it is within the linear range of our device. We calculated the recovery rates of UA at final concentrations of 50 μM and 300 μM, which match the low and high ends of the normal concentrations in saliva. To account for higher concentrations of UA present normally in urine, we also diluted a high concentration of UA (similar to the condition in urine) in a mixture of electrolyte and artificial urine for a final concentration of 300 μM, such that the measurement can be performed within the linear range of our device. 50 and 300 μM of UA in the electrolyte containing artificial body fluids were detected by our device (n=3) and the ECL

intensities were obtained. Based on the calibration plot, the recovery rate was calculated and presented in Table 2.

Table 2. Simulated real sample analysis using body fluids and recovery rate.

Sample	Ratio to the electrolyte	UA added (μM)	UA found (μM)	RSD (%)	Recovery (%)
Saliva	1:1	50	44.88	3.64	89.76
Saliva	1:1	300	317.77	2.02	105.92
Urine	1:1	50	41.82	4.09	83.63
Urine	1:1	300	366.29	4.87	122.10
Urine	1:9	300	334.75	7.75	111.58

The recovery rates for 50 μM UA in saliva and urine are 89.76% and 83.63%, with RSDs of 3.64% and 4.09%, respectively. The recovery rates for 300 μM UA in saliva and urine are 105.92% and 122.10%, with RSDs of 2.02% and 4.87%, respectively.

Further, we studied the effect of dilution on the recovery rate, since the physiological concentration of UA in human urine is higher than the linear range of UA calibration plot in this study. After mixing the artificial urine with the electrolyte in 1:9 ratio, the recovery rates for 300 μM of UA is 111.58% with a RSD of 7.75%.

4.4.6 Comparison between CMOS SE-ECL and other signal reading platforms (microscope and smartphone).

The advantage of our system compared to other detection systems comes from the fact that the sample is located very close to the detector, leading to a large solid angle for photon collection, as illustrated in Fig. 5 C. This detection solid angle is larger than the solid angle offered by most microscope objectives, which are limited by the working distance and aperture of the objective lens (Fig. 5 D). In order to demonstrate that the CMOS-based ECL system has an advantage over lens-based systems, we compare the collection efficiency of our CMOS-based SE-ECL system with other light collection systems.

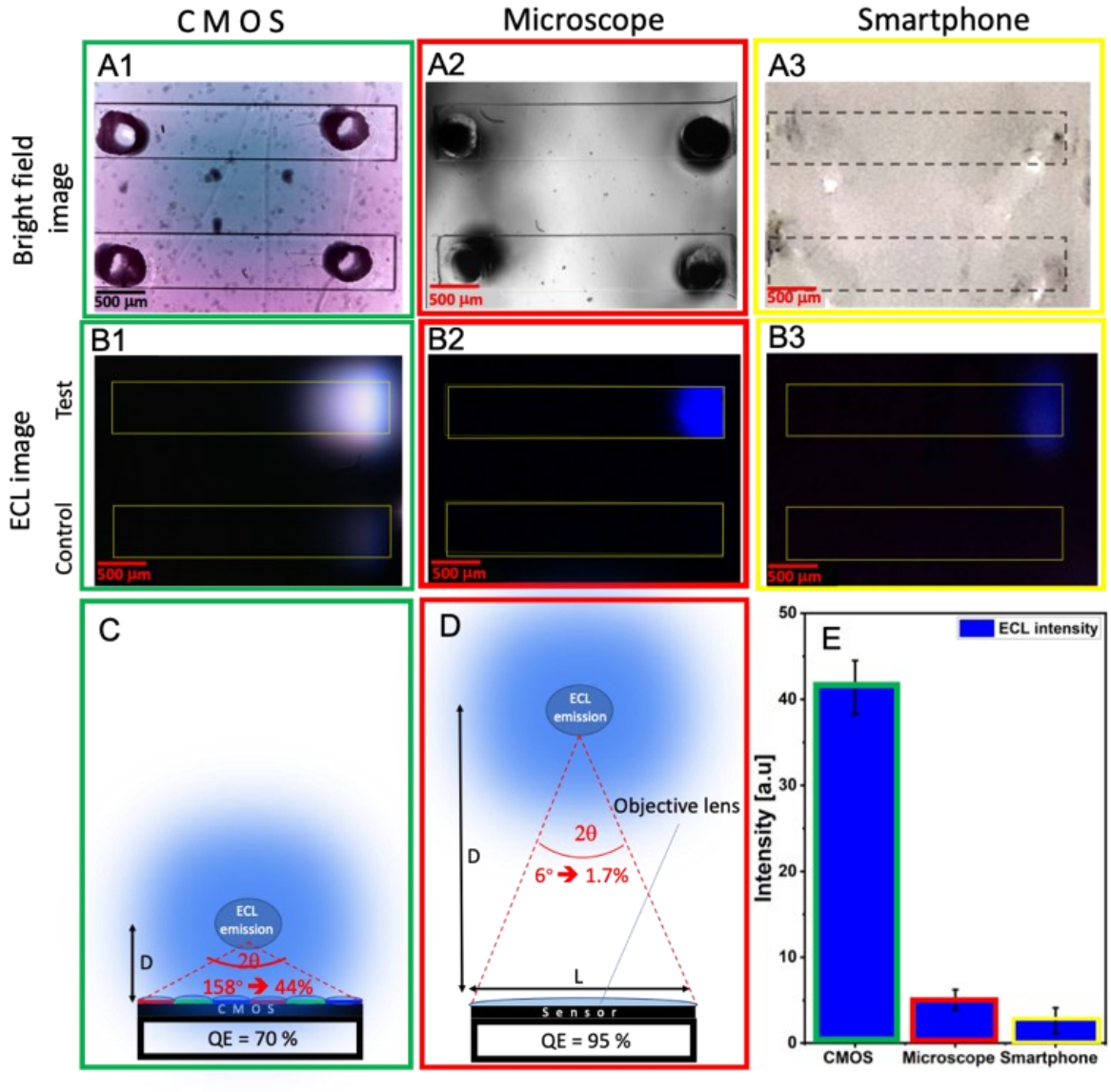

Fig. 5. Comparison between 3 different devices for capturing ECL photons: microscope, smartphone and CMOS. Panel A1, A2, and A3 show the bright field images of the channels captured by 1) CMOS sensor (OmniVision OV5647) 2) microscope (Nikon eclipse Ti2 mounted with Prime 95B 25 mm BSI

CMOS camera) with a 4X objective 3) smartphone (Samsung Galaxy S21 Ultra). Panels B1, B2 and B3, show the ECL images corresponding to the panel A1, A2, and A3 respectively, captured by each device. The upper channel is the test and the lower one is the control. ECL images in panels B1 and B2 were enhanced and the brightness was increased by 35% for better observation. C) Schematic of the CMOS setup, and D) schematic of the microscope setup showing the distance of the photo detector and the place of the ECL reaction in SE-CMOS setup (D = 300 μm) and microscope with a 4X objective (D = working distance 30 mm), respectively. SE-CMOS in a lensless platform can collect almost 44% of the photons while the microscope with a 4X objective lens can collect 1.7% of the whole slid angle of ECL reaction. E) Comparing the ECL image-based intensities of the three aforementioned devices. The electrolyte used in all experiments is 0.1M carbonate buffer ($NaHCO_3$ and NaOH), pH is 10.7, concentration of luminol is 1.0 mM, percentage of *t*riton X-100 is 1% v/v, and the voltage is 5 V. Test channel contains 300 μM H_2O_2.

We adapted the SE-ECL device to different systems, including a microscope and a smartphone, and compared the detected ECL intensities under the same experimental conditions (Fig. 5). To have a fair comparison, all the imaging parameters such as ISO (gain) and exposure time were set to be the same. Also, the magnification was chosen (4X for the microscope objective lens) such that the whole area of both channels could be visualized (Fig. 5 A1, Fig. 5 A2, and Fig. 5 A3). ECL images of the microfluidic device are captured using different detectors (Fig.5 B1, Fig.5 B2, and Fig.5 B3), and the results of ECL intensities are compared in Fig.5 E. Overall, the ECL image captured by the CMOS shows higher intensity than either the microscope or smartphone, indicating that the CMOS platform has an overall higher efficiency for collecting photons.

In this study, we assume that the ECL emission is characteristic to Lambertian emitters. Therefore, the collection efficiency (η) of each platform is the fraction of the cone of light subtended by the detector divided by the whole solid angle emitted from the ECL reaction.

The angle of the detected cone of light cone and the corresponding solid angle were calculated as:

$$2\theta = Arctan\left(\frac{D}{L}\right) \qquad (4)$$

$$\Omega = 2\pi\left(1 - \cos\theta\right) \quad (5)$$

where 2θ is the apex angle of the cone, *D* is the distance between the ITO electrode (where the ECL reaction happens) and the detector (or lens), *L* is the diameter of the sensor (or diameter

of the entrance pupil), and Ω is the solid angle subtended by the detector. Based on equation (5), when $\theta = \pi/2$, the spherical cap becomes a hemisphere having a solid angle of 2π steradians. As a result, the whole ECL emission has a solid angle of 4π steradians. Therefore, the collection efficiency of the detector was calculated as:

$$\eta(\%) = \left(\frac{\Omega}{4\pi}\right) \times 100 \quad (6)$$

where η is the collection efficiency. For the microscope, D is the working distance or the focal length of the 4X lens, which is 30 mm, and θ can be calculated using the equation:

$$NA = n\,sin(\theta) \quad (7)$$

where the numerical aperture (NA) of the 4X lens is 0.10, and accordingly, θ is almost 6 degrees.

Considering the whole solid angle as 360 degrees, the collection efficiency in the microscope is almost 1.7%. Using the same calculation for CMOS (this work) and measuring D = 300 μm and L = 3200 μm (the average length and width of the CMOS sensor), the collection efficiency is almost 40%. This calculation is not applicable for the smartphone as the focus was being changed automatically during the experiment. The main difference between these platforms is the distance between the location of the ECL reaction (from where the photons are emitted) and the detector, i.e., the distance between the ITO electrode and the detector. In our platform, the reaction happens closer to the photodetector, leading to significantly higher collection efficiencies compared with a microscope capable of imaging a similar field of view.

Another difference between these platforms is the quantum efficiency (QE) of the imaging sensor. The sensor of the microscope (Prime 95B 25 mm BSI CMOS) has a relatively large QE (close to 95%). The CMOS sensor employed in this work (OmniVision OV5647 BSI) has a relatively lower QE of 70% (according to the manufacturer website). Considering both quantum efficiency and collection efficiency (QE and η), the microscope detector converts ~1.6% of the ECL photons into electrons, while this number for the CMOS platform is ~28% or almost 17.5 times higher. However, this difference is based on the calculation at room temperature. In reality, the measured improvement in the recorded ECL intensities is only a factor of approximately 10 (shown in Fig 5 E), due to additional factors such as cooling to -25 °C of the sensor used in the microscope setup that reduces the dark current.

4.5 Conclusions

In this work, microfluidic and luminol-based ECL systems were integrated onto a CMOS sensor to build a miniaturized ECL enzymatic sensor that enables sample handling and data collection on the same platform. The miniaturization was made possible by the use of a SE-ECL system that reduces the complexity of a multi-electrode approach. The performance of this device was characterized as a function of applied voltage, pH of the solution, and concentration of H_2O_2. As expected, the SE-ECL emission intensity depends linearly on the applied voltage, which allows for predictable tuning of the biosensor parameters. Maximum SE-ECL intensity was recorded at a solution pH of approximately 9.5. Considering the measured lifetime of the emission (which is longer in a higher range of pH), we chose to further work with a pH of 10.7, which is a good compromise between the ECL intensity and lifetime, for improved performance.

First, the performance of the system towards luminol-H_2O_2 reaction was evaluated and a linear range between 25 μM to 300 μM, and a LOD for H_2O_2 detection of 17.75 μM were reported. Next, UA was detected, and a linear detection range was observed from 25 μM to 300 μM, with a LOD as low as 26.09 μM. The repeatability (reusability), reproducibility, and selectivity of the device towards the measurement of UA were also studied. The device showed high reusability and reproducibility with the relative standard deviation of the measured intensity of 7.00% and 14.79%, respectively, at 50 μM UA concentration, and 2.06% and 7.52%, respectively, at 300 μM of UA concentration. Moreover, the sensing performance of the SE-ECL CMOS biosensor was evaluated to demonstrate that detection of UA at physiological concentrations is reproducible, reusable, and selective in the presence of interferences such as glucose, creatinine, and ascorbic acid.

The device has several advantages over the traditional ECL platforms. It shows higher collection efficiency compared with microscopes or smartphones as detectors. By utilizing simple and inexpensive fabrication materials and methodologies, and an inexpensive imaging device (the cost of a CMOS sensor is approximately 1$, and the retail price is approximately $10) as a detector, we designed and fabricated an SE-ECL platform that is inexpensive, portable, and practical for point-of-need testing. In addition, because the ECL emission is spatially resolved and confined to the surface of the electrode near the positive side, the size, shape, and location of the ECL reaction can be easily identified and controlled. Since the CMOS sensor can detect even lower ECL emissions than demonstrated in this article, further

miniaturization and consequently multiplexing can be achieved, once challenges related to the design of the microfluidic inlets and stability of ITO in the presence of high electrical currents are addressed. We believe that this study will pave the way towards concurrent screening of multiple analytes in different types of biological assays.

4.6 Author Contributions

RA helped design the experiments, performed experiments, analyzed and interpreted data, wrote the first draft of the manuscript; JL helped with data collection and interpretation; SS helped with initial experiments and data interpretation; SWH conceived the idea, designed the experiments, helped interpret data, supervised and managed the project. All authors made significant contributions to writing the manuscript.

4.7 Conflicts of interest

There are no conflicts to declare.

4.8 Acknowledgements

This work was financially supported by DND-IDEAS (SWH), NSERC Discovery (SWH), and Faculty of Engineering at McGill University. RA acknowledge the McGill Engineering Doctoral Award (MEDA).

4.9 References

[1] J. Liu, R. Siavash Moakhar, A. Sudalaiyadum Perumal, H. N. Roman, S. Mahshid, and S. Wachsmann-Hogiu, "An AgNP-deposited commercial electrochemistry test strip as a platform for urea detection," *Scientific Reports,* vol. 10, no. 1, p. 9527, 2020/06/12 2020, doi: 10.1038/s41598-020-66422-x.

[2] J. Liu, M. Jalali, S. Mahshid, and S. Wachsmann-Hogiu, "Are plasmonic optical biosensors ready for use in point-of-need applications?," *Analyst,* 10.1039/C9AN02149C vol. 145, no. 2, pp. 364-384, 2020, doi: 10.1039/C9AN02149C.

[3] D. Liu, J. Wang, L. Wu, Y. Huang, Y. Zhang, M. Zhu, Y. Wang, Z. Zhu, and C. Yang, "Trends in miniaturized biosensors for point-of-care testing," *TrAC Trends in Analytical Chemistry,* vol. 122, p. 115701, 2020/01/01/ 2020, doi: https://doi.org/10.1016/j.trac.2019.115701.

[4] P. K. Drain, E. P. Hyle, F. Noubary, K. A. Freedberg, D. Wilson, W. R. Bishai, W. Rodriguez, and I. V. Bassett, "Diagnostic point-of-care tests in resource-limited settings," *The Lancet Infectious Diseases,* vol. 14, no. 3, pp. 239-249, 2014/03/01/ 2014, doi: https://doi.org/10.1016/S1473-3099(13)70250-0.

[5] D. Mabey, R. W. Peeling, A. Ustianowski, and M. D. Perkins, "Diagnostics for the developing world," *Nature Reviews Microbiology,* vol. 2, no. 3, pp. 231-240, 2004/03/01 2004, doi: 10.1038/nrmicro841.

[6] F. Bragheri, R. Martinez Vazquez, and R. Osellame, "Chapter 12.3 - Microfluidics," in *Three-Dimensional Microfabrication Using Two-photon Polymerization*, T. Baldacchini Ed. Oxford: William Andrew Publishing, 2016, pp. 310-334.

[7] A. St John and C. P. Price, "Existing and Emerging Technologies for Point-of-Care Testing," (in eng), *Clin Biochem Rev,* vol. 35, no. 3, pp. 155-167, 2014. [Online]. Available: https://pubmed.ncbi.nlm.nih.gov/25336761 https://www.ncbi.nlm.nih.gov/pmc/articles/PMC4204237/.

[8] F. S. Ligler, "Perspective on Optical Biosensors and Integrated Sensor Systems," *Analytical Chemistry,* vol. 81, no. 2, pp. 519-526, 2009/01/15 2009, doi: 10.1021/ac8016289.

[9] M. C. Estevez, M. Alvarez, and L. M. Lechuga, "Integrated optical devices for lab-on-a-chip biosensing applications," *Laser & Photonics Reviews,* vol. 6, no. 4, pp. 463-487, 2012, doi: https://doi.org/10.1002/lpor.201100025.

[10] R. Singh, A. Feltmeyer, O. Saiapina, J. Juzwik, B. Arenz, and A. Abbas, "Rapid and PCR-free DNA Detection by Nanoaggregation-Enhanced Chemiluminescence," *Scientific Reports,* vol. 7, no. 1, p. 14011, 2017/10/25 2017, doi: 10.1038/s41598-017-14580-w.

[11] B. Al Mughairy and H. A. J. Al-Lawati, "Recent analytical advancements in microfluidics using chemiluminescence detection systems for food analysis," *TrAC Trends in Analytical Chemistry,* vol. 124, p. 115802, 2020/03/01/ 2020, doi: https://doi.org/10.1016/j.trac.2019.115802.

[12] T. Jiao, Q. Huang, Y. Xiao, X. Shen, J. Zhou, and F. Gao, "Electrochemiluminescent Detection of Hydrogen Peroxide via Some Luminol Imide Derivatives with Different Substituent Groups," *Journal of Chemistry,* vol. 2013, p. 375372, 2013/11/12 2013, doi: 10.1155/2013/375372.

[13] S. Kirschbaum and A. Baeumner, "A review of electrochemiluminescence (ECL) in and for microfluidic analytical devices," *Analytical and bioanalytical chemistry,* vol. 407, 03/15 2015, doi: 10.1007/s00216-015-8557-x.

[14] A. J. Bard, *Electrogenerated chemiluminescence*. CRC Press, 2004.

[15] M. M. Richter, "Electrochemiluminescence (ECL)," *Chemical Reviews,* vol. 104, no. 6, pp. 3003-3036, 2004/06/01 2004, doi: 10.1021/cr020373d.

[16] M. Bhaiyya, P. K. Pattnaik, and S. Goel, "A brief review on miniaturized electrochemiluminescence devices: From fabrication to applications," *Current Opinion in Electrochemistry,* vol. 30, p. 100800, 2021/12/01/ 2021, doi: https://doi.org/10.1016/j.coelec.2021.100800.

[17] S. Wang, L. Ge, Y. Zhang, X. Song, N. Li, S. Ge, and J. Yu, "Battery-triggered microfluidic paper-based multiplex electrochemiluminescence immunodevice based on potential-resolution strategy," *Lab on a Chip,* 10.1039/C2LC40707H vol. 12, no. 21, pp. 4489-4498, 2012, doi: 10.1039/C2LC40707H.

[18] W. Li, M. Li, S. Ge, M. Yan, J. Huang, and J. Yu, "Battery-triggered ultrasensitive electrochemiluminescence detection on microfluidic paper-based immunodevice based on dual-signal amplification strategy," *Analytica Chimica Acta,* vol. 767, pp. 66-74, 2013/03/12/ 2013, doi: https://doi.org/10.1016/j.aca.2012.12.053.

[19] J. L. Delaney, E. H. Doeven, A. J. Harsant, and C. F. Hogan, "Use of a mobile phone for potentiostatic control with low cost paper-based microfluidic sensors," *Analytica Chimica Acta,* vol. 790, pp. 56-60, 2013/08/06/ 2013, doi: https://doi.org/10.1016/j.aca.2013.06.005.

[20] H. J. Kwon, E. C. Rivera, M. R. C. Neto, D. Marsh, J. J. Swerdlow, R. L. Summerscales, and P. P. Tadi Uppala, "Development of smartphone-based ECL sensor for dopamine detection: Practical approaches," *Results in Chemistry,* vol. 2, p. 100029, 2020/01/01/ 2020, doi: https://doi.org/10.1016/j.rechem.2020.100029.

[21] D. Wang, C. L. Liu, Y. Liang, Y. Su, Q. P. Shang, and C. S. Zhang, "A Simple and Sensitive Paper-Based Bipolar Electrochemiluminescence Biosensor for Detection of Oxidase-Substrate Biomarkers in Serum," (in English), *J. Electrochem. Soc.,* vol. 165, no. 9, pp. B361-B369, 2018, doi: 10.1149/2.0551809jes.

[22] M. Liu, D. Wang, C. Liu, R. Liu, H. Li, and C. Zhang, "Battery-triggered open wireless electrochemiluminescence in a microfluidic cloth-based bipolar device," *Sensors and Actuators B: Chemical,* vol. 246, pp. 327-335, 2017/07/01/ 2017, doi: https://doi.org/10.1016/j.snb.2017.02.076.

[23] H.-R. Zhang, Y.-Z. Wang, W. Zhao, J.-J. Xu, and H.-Y. Chen, "Visual Color-Switch Electrochemiluminescence Biosensing of Cancer Cell Based on Multichannel Bipolar Electrode Chip," *Analytical Chemistry,* vol. 88, no. 5, pp. 2884-2890, 2016/03/01 2016, doi: 10.1021/acs.analchem.5b04716.

[24] Z. Zhou, L. Xu, S. Wu, and B. Su, "A novel biosensor array with a wheel-like pattern for glucose, lactate and choline based on electrochemiluminescence imaging," *Analyst,* 10.1039/C4AN00687A vol. 139, no. 19, pp. 4934-4939, 2014, doi: 10.1039/C4AN00687A.

[25] K. L. Rahn, T. D. Rhoades, and R. K. Anand, "Alternating Current Voltammetry at a Bipolar Electrode with Smartphone Luminescence Imaging for Point-of-Need Sensing," *ChemElectroChem,* vol. 7, no. 5, pp. 1172-1181, 2020, doi: https://doi.org/10.1002/celc.202000079.

[26] E. Villani, N. Shida, and S. Inagi, "Electrogenerated chemiluminescence of luminol on wireless conducting polymer films," *Electrochimica Acta,* vol. 389, p. 138718, 2021/09/01/ 2021, doi: https://doi.org/10.1016/j.electacta.2021.138718.

[27] Y. Zhang, R. Zhang, X. Yang, H. Qi, and C. Zhang, "Recent advances in electrogenerated chemiluminescence biosensing methods for pharmaceuticals," *Journal of Pharmaceutical Analysis,* vol. 9, no. 1, pp. 9-19, 2019/02/01/ 2019, doi: https://doi.org/10.1016/j.jpha.2018.11.004.

[28] D. Hao, G. Weiliang, and S. Bin, "Electrochemiluminescence Single-Cell Analysis: Intensity and Imaging-Based Methods," *ChemPlusChem,* Article vol. 85, no. 4, pp. 725-733, 2020, doi: 10.1002/cplu.202000145.

[29] W. Gao, K. Muzyka, X. Ma, B. Lou, and G. Xu, "A single-electrode electrochemical system for multiplex electrochemiluminescence analysis based on a resistance induced potential difference," *Chemical Science,* 10.1039/C8SC00410B vol. 9, no. 16, pp. 3911-3916, 2018, doi: 10.1039/C8SC00410B.

[30] G. Dryhurst, *Electrochemistry of biological molecules*. Elsevier, 2012.

[31] Z. Chen and Y. Zu, "Selective detection of uric acid in the presence of ascorbic acid based on electrochemiluminescence quenching," *Journal of Electroanalytical Chemistry,* vol. 612, no. 1, pp. 151-155, 2008/01/01/ 2008, doi: https://doi.org/10.1016/j.jelechem.2007.09.018.

[32] J. S. N. Dutt, M. F. Cardosi, C. Livingstone, and J. Davis, "Diagnostic Implications of Uric Acid in Electroanalytical Measurements," *Electroanalysis,* vol. 17, no. 14, pp. 1233-1243, 2005, doi: https://doi.org/10.1002/elan.200403258.

[33] E. Popa, Y. Kubota, D. A. Tryk, and A. Fujishima, "Selective Voltammetric and Amperometric Detection of Uric Acid with Oxidized Diamond Film Electrodes," *Analytical Chemistry,* vol. 72, no. 7, pp. 1724-1727, 2000/04/01 2000, doi: 10.1021/ac990862m.

[34] R. Aguilar, M. M. Dávila, M. P. Elizalde, J. Mattusch, and R. Wennrich, "Capability of a carbon–polyvinylchloride composite electrode for the detection of dopamine, ascorbic acid and

uric acid," *Electrochimica Acta,* vol. 49, no. 6, pp. 851-859, 2004/03/01/ 2004, doi: https://doi.org/10.1016/j.electacta.2003.10.002.

[35] T. Nakaminami, S.-i. Ito, S. Kuwabata, and H. Yoneyama, "Uricase-Catalyzed Oxidation of Uric Acid Using an Artificial Electron Acceptor and Fabrication of Amperometric Uric Acid Sensors with Use of a Redox Ladder Polymer," *Analytical Chemistry,* vol. 71, no. 10, pp. 1928-1934, 1999/05/01 1999, doi: 10.1021/ac981168u.

[36] C. Retna Raj and T. Ohsaka, "Voltammetric detection of uric acid in the presence of ascorbic acid at a gold electrode modified with a self-assembled monolayer of heteroaromatic thiol," *Journal of Electroanalytical Chemistry,* vol. 540, pp. 69-77, 2003/01/02/ 2003, doi: https://doi.org/10.1016/S0022-0728(02)01285-8.

[37] M. Imanbekova, A. S. Perumal, S. Kheireddine, D. V. Nicolau, and S. Wachsmann-Hogiu, "Lensless, reflection-based dark-field microscopy (RDFM) on a CMOS chip," *Biomed. Opt. Express,* vol. 11, no. 9, pp. 4942-4959, 2020/09/01 2020, doi: 10.1364/BOE.394615.

[38] D. S. Perloff, F. E. Wahl, and J. Conragan, "Four-Point Sheet Resistance Measurements of Semiconductor Doping Uniformity," *J. Electrochem. Soc.,* vol. 124, no. 4, pp. 582-590, 1977/04/01 1977, doi: 10.1149/1.2133355.

[39] C. A. Bishop, "Chapter 5 - Process Diagnostics and Coating Characteristics," in *Vacuum Deposition Onto Webs, Films and Foils (Third Edition)*, C. A. Bishop Ed. Boston: William Andrew Publishing, 2015, pp. 85-128.

[40] E. Villani and S. Inagi, "Mapping the Distribution of Potential Gradient in Bipolar Electrochemical Systems through Luminol Electrochemiluminescence Imaging," *Analytical Chemistry,* vol. 93, no. 23, pp. 8152-8160, 2021/06/15 2021, doi: 10.1021/acs.analchem.0c05397.

[41] Y. Li, X. Ma, W. Wang, S. Yan, F. Liu, K. Chu, G. Xu, and Z. J. Smith, "Improving the limit of detection in portable luminescent assay readers through smart optical design," *Journal of Biophotonics,* vol. 13, no. 1, p. e201900241, 2020, doi: 10.1002/jbio.201900241.

[42] C. Plieth, "Peroxide-Induced Liberation of Iron from Heme Switches Catalysis during Luminol Reaction and Causes Loss of Light and Heterodyning of Luminescence Kinetics," *ACS Omega,* vol. 4, no. 2, pp. 3268-3279, 2019/02/28 2019, doi: 10.1021/acsomega.8b03564.

[43] X. Liu, W. Qi, W. Gao, Z. Liu, W. Zhang, Y. Gao, and G. Xu, "Remarkable increase in luminol electrochemiluminescence by sequential electroreduction and electrooxidation," *Chemical Communications,* 10.1039/C4CC06633B vol. 50, no. 93, pp. 14662-14665, 2014, doi: 10.1039/C4CC06633B.

[44] P. Khan, D. Idrees, M. A. Moxley, J. A. Corbett, F. Ahmad, G. von Figura, W. S. Sly, A. Waheed, and M. I. Hassan, "Luminol-Based Chemiluminescent Signals: Clinical and Non-clinical Application and Future Uses," *Applied Biochemistry and Biotechnology,* vol. 173, no. 2, pp. 333-355, 2014/05/01 2014, doi: 10.1007/s12010-014-0850-1.

[45] H. Wan, K. Zhang, Y. Wang, Y. Chen, W. Zhang, F. Xia, Y. Zhang, N. Wang, and Y. Lu, "The Associations Between Gonadal Hormones and Serum Uric Acid Levels in Men and Postmenopausal Women With Diabetes," (in English), *Frontiers in Endocrinology,* Original Research vol. 11, no. 55, 2020-February-20 2020, doi: 10.3389/fendo.2020.00055.

[46] X. Dong, "Study on detection methods for uric acid in biological samples," *International Journal of Pharmaceutical Sciences and Research,* vol. 8, no. 2, p. 925, 2017.

[47] J. L. Riis, C. I. Bryce, M. J. Matin, J. L. Stebbins, O. Kornienko, L. v. Huisstede, and D. A. Granger, "The validity, stability, and utility of measuring uric acid in saliva," *Biomarkers in Medicine,* vol. 12, no. 6, pp. 583-596, 2018, doi: 10.2217/bmm-2017-0336.

[48] J. Perelló, P. Sanchis, and F. Grases, "Determination of uric acid in urine, saliva and calcium oxalate renal calculi by high-performance liquid chromatography/mass spectrometry," *Journal of Chromatography B,* vol. 824, no. 1, pp. 175-180, 2005/09/25/ 2005, doi: https://doi.org/10.1016/j.jchromb.2005.07.024.

[49] J. Ballesta-Claver, R. Rodríguez-Gómez, and L. F. Capitán-Vallvey, "Disposable biosensor based on cathodic electrochemiluminescence of tris(2,2-bipyridine)ruthenium(II) for uric acid determination," (in eng), *Anal Chim Acta,* vol. 770, pp. 153-60, Apr 3 2013, doi: 10.1016/j.aca.2013.01.045.

[50] L. Zhang, C. Zhao, Y. Bai, Q. Wang, P. Ma, X. Ma, and P. Zhu, "Electrochemiluminescence Enhanced by the Synergetic Effect of Porphyrin and Multi-walled Carbon Nanotubes for Uric Acid Detection," *Electroanalysis,* vol. n/a, no. n/a, 2021, doi: https://doi.org/10.1002/elan.202100287.

[51] Y. Tao, X. Zhang, J. Wang, X. Wang, and N. Yang, "Simultaneous determination of cysteine, ascorbic acid and uric acid by capillary electrophoresis with electrochemiluminescence," *Journal of Electroanalytical Chemistry,* vol. 674, pp. 65-70, 2012/06/01/ 2012, doi: https://doi.org/10.1016/j.jelechem.2012.03.009.

[52] H. Chu, X. Wei, M. Wu, J. Yan, and Y. Tu, "An electrochemiluminescent biosensor based on polypyrrole immobilized uricase for ultrasensitive uric acid detection," *Sensors and Actuators B: Chemical,* vol. 163, no. 1, pp. 247-252, 2012/03/01/ 2012, doi: https://doi.org/10.1016/j.snb.2012.01.047.

[53] Z. Lin, Z. Chen, Y. Liu, J. Wang, and G. Chen, "An electrochemiluminescent biosensor for uric acid based on the electrochemiluminescence of bis-[3,4,6-trichloro-2-(pentyloxycarbonyl)-phenyl] oxalate on an ITO electrode modified by an electropolymerized nickel phthalocyanine film," *Analyst,* 10.1039/B716281B vol. 133, no. 6, pp. 797-801, 2008, doi: 10.1039/B716281B.

[54] M. Jiang and J.-S. Chen, "A lable-free ECL biosensor for the detection of uric acid based on Au NRs@ TiO2 Nanocomposite," *Int J Electrochem Sci,* pp. 2333-2344, 2019.

[55] F. Lou, A. Wang, J. Jin, Q. Li, and S. Zhang, "One-pot synthesis of popcorn-like Au@Polyluminol nanoflowers for sensitive solid-state electrochemiluminescent sensor," *Electrochimica Acta,* vol. 278, pp. 255-262, 2018/07/10/ 2018, doi: https://doi.org/10.1016/j.electacta.2018.04.194.

[56] E. Mäkilä and P. Kirveskari, "A study of ascorbic acid in human saliva," *Archives of Oral Biology,* vol. 14, no. 11, pp. 1285-1292, 1969/11/01/ 1969, doi: https://doi.org/10.1016/0003-9969(69)90201-5.

[57] R. Venkatapathy, V. Govindarajan, N. Oza, S. Parameswaran, B. Pennagaram Dhanasekaran, and K. V. Prashad, "Salivary Creatinine Estimation as an Alternative to Serum Creatinine in Chronic Kidney Disease Patients," *International Journal of Nephrology,* vol. 2014, p. 742724, 2014/04/10 2014, doi: 10.1155/2014/742724.

[58] S. Gupta, M. T. Nayak, J. D. Sunitha, G. Dawar, N. Sinha, and N. S. Rallan, "Correlation of salivary glucose level with blood glucose level in diabetes mellitus," (in eng), *J Oral Maxillofac Pathol,* vol. 21, no. 3, pp. 334-339, Sep-Dec 2017, doi: 10.4103/jomfp.JOMFP_222_15.

Transition to Chapter V

The preceding chapter detailed the development of a miniaturized ECL enzymatic sensor integrated into a CMOS chip. This platform combined microfluidics with a luminol-based ECL system, enabling on-chip sample handling and data acquisition. The sensor's compact design was achieved through the implementation of a single-electrode ECL (SE-ECL) configuration, simplifying the system compared to multi-electrode approaches. The sensor's performance was thoroughly evaluated under varying conditions of voltage, pH, and hydrogen peroxide concentration. Demonstrating its analytical capabilities, the sensor accurately and selectively detected uric acid at physiologically relevant levels, even in the presence of potential interferents. This CMOS-based SE-ECL platform offers several advantages over traditional ECL systems, including enhanced light collection efficiency, low cost, portability, and spatial control over the ECL reaction. Future optimizations, such as addressing microfluidic inlet design and ITO electrode stability, could enable further miniaturization and multiplexing capabilities, expanding the sensor's potential applications.

To this end, in this chapter, we introduce the optimized, miniaturized, and multicolor SE-ECL capable of detecting 4 different analytes. To simplify the detection process and enable simultaneous analysis of multiple analytes, the optimized SE-ECL approach was implemented. By carefully controlling the applied voltage, distinct ECL emissions were generated, allowing for the differentiation of various analytes. The influence of electrode dimensions on light emission intensity was investigated, with longer and wider electrodes demonstrating enhanced signal output. Moreover, the application of alternating current (AC) voltage was explored, resulting in significantly increased light intensity compared to direct current. A proof-of-concept demonstration showcased the potential of this method for multiplexed detection by simultaneously distinguishing four distinct colors on a CMOS image sensor, within a compact device format.

This chapter is based on my first-author article. The contributions of the authors are as follows:

RA and SWH conceived the idea. RA designed and performed the experiments, analyzed the data, and wrote the main body of the manuscript. SWH supervised the project. RA and SWH reviewed and approved the manuscript in its current form.

Chapter V. Optimization and miniaturization of SE-ECL for potential-resolved multi-color, multi-analyte detection

Reza Abbasi[1], Sebastian Wachsmann-Hogiu[1*]

[1]Department of Bioengineering, McGill University, Montreal, Canada

*Corresponding author

5.1 Abstract

Electrochemiluminescence (ECL) is a bioanalytical technique with numerous advantages, including the potential for high temporal and spatial resolution, a high signal-to-noise ratio, a broad dynamic range, and rapid measurement capabilities. To reduce the complexity of a multi-electrode approach, we use a single-electrode electrochemiluminescence (SE-ECL) configuration to achieve the simultaneous emission and detection of multiple colors for applications that require multiplexed detection of several analytes. This method exploits intrinsic differences in the electric potential applied along single electrodes built into electrochemical cells, enabling the achievement of distinct colors through selective excitation of ECL luminophores. We present results on the optimization of SE-ECL intensity for different channel lengths and widths, with sum intensities being 5 times larger for 6 cm vs 2 cm channels and linearly increasing with the width of the channels. Furthermore, we demonstrated for the first time that applying Alternating Current (AC) voltage within the single electrode setup for driving the ECL reactions has a dramatic effect on the emitted light intensity, with square waveforms resulting in higher intensities vs sine waveforms. Additionally, multiplexed multicolor SE-ECL on a 6.5 mm × 3.6 mm CMOS semiconductor image sensor was demonstrated for the first time, with the ability to simultaneously distinguish four different colors, leading to the ability of measuring multiple analytes.

Keywords: Electrochemiluminescence, Single-Electrode, Multiplexed Detection, CMOS Image Sensor

5.2 Introduction

The emission of light upon a chemiluminescence (CL) reaction is a complex series of steps that take place in an aqueous environment. In simple terms, when a CL substance like luminol reacts with an oxidizing agent such as hydrogen peroxide (H_2O_2), an intermediate product is formed, which emits light. This entire process is often facilitated by a catalyst, like iron found in hemoglobin, or gold nanoparticles. While the reaction can also happen without a catalyst, it has a significantly lower reaction rate, which reduces the emitted light and leads to a lower signal [1, 2]. Alternatively, instead of a catalyst, luminol can be oxidized through an electric potential difference to create the excited state. This electric field-induced oxidation and its resulting CL have shown promise to both extend the sensitivity of biosensors and broaden their operational range [3, 4].

Electrochemiluminescence (ECL) is a quickly growing technique in bioanalysis that comes with several benefits. These include the potential for precise temporal and spatial resolution, a strong signal and low noise, a wide operational range, and quick measurements [5]. ECL operates on the principle of using an electric field to drive electrochemical processes, involving high-energy electron transfer within molecules on electrode surfaces, which leads to the creation of excited states that emit light [6, 7]. ECL biosensing relies on identifying changes in ECL emissions as indicators of interactions between distinct recognition components and their respective target analytes [8]. The detection principles classify ECL biosensor strategies into three primary groups: enzyme-catalyzed biosensing, nucleic acid biosensing, and antigen-antibody immunoassays [9, 10].

In most systems, low electric potential differences are required to initiate the ECL reaction [11-14]. Most ECL setups contain an electrolytic cell containing three electrodes (working, counter, and reference) submerged in an electrolyte and connected to a power supply. Applying electric potential to the electrolytic cell triggers an electrochemical reaction on the working electrode [4]. The working electrode primarily consists of platinum, gold, carbon, and Indium Tin Oxide (ITO), all of which can be modified with biorecognition elements to serve in biosensing applications [8]. Appealing characteristics of ITO include notable electrical conductivity (10^{-5} Ωcm), significant visible light transparency (85%), favorable physical and chemical stability and robust bonding with diverse substrates. Recently, significant interest has been directed

towards ECL biosensors employing ITO electrodes as fundamental components, primarily owing to their exceptional optical transparency. [8, 15]

In a conventional electrochemical arrangement featuring three electrodes, the working electrode is linked directly to a power source, enabling the imposition of a potential difference between it and the counter electrode. This leads to polarization of the working electrode relative to the solution, prompting electrochemical processes (oxidation or reduction) to take place at the interface between the electrode and the solution. As another configuration of ECL, in Bipolar electrochemistry (BPE), the situation contrasts significantly as it involves concurrent oxidation and reduction reactions occurring on the opposite poles of a single electrode. Furthermore, this electrode isn't physically connected to the power supply via direct electrical contact [16]. One straightforward approach for conducting a BPE-ECL experiment, Open BPE configuration, involves placing a conductive item within an electrolyte solution, positioned between two stimulating electrodes linked to an external power source. By applying a bias voltage, a consistent potential gradient is created within the electrolyte, resulting in distinct potential values assigned to each location within the solution. This polarization drives the reactions on the BPE and it depends on the size fitting to the following relation:

$$\Delta V = E \times L \qquad (1)$$

Here, ΔV represents the maximum polarization voltage (V), E signifies the electric field (V/m), and L denotes the object's characteristic dimension in alignment with the electric field (m). This relation implies that for smaller objects, a greater electric field is necessary [16]. When a sufficiently substantial ΔV_{max} is attained, the object serves as a bipolar electrode, facilitating the coupling of both reduction and oxidation reactions. Following the same concept of BPE-ECL, Gao et al. demonstrated a single-electrode electrochemiluminescence (SE-ECL) configuration in 2018 [17]. Unlike BPE-ECL, in which the potential gradient is created within the electrolyte, a single electrode is the basis of the SE-ECL system, where the potential gradient occurs along its surface.

In SE-ECL systems, the ITO electrode's resistance introduces a potential gradient throughout the channel. When a specific voltage is applied, the proportionate division of potential difference within the electrochemical cell and the applied voltage corresponds to the relative dimensions of the channel and wire separation, expressed by equation 2 [4].

$$\Delta E_{ch} = E_{tot} \left(\frac{l_{ch}}{d}\right) \quad (2)$$

In this equation, ΔE_{ch} represents the potential difference within the electrochemical cell, E_{tot} is the voltage supplied by a power source, l_{ch} denotes the channel length, and d stands for the wire spacing. When the value of ΔE_{ch} is sufficiently significant, faradaic reactions occur concurrently at both channel ends. Luminol oxidation occurs at the higher electric potential, while H_2O_2 reduction takes place at the lower electric potential. In these circumstances, luminol is oxidized within the higher electric potential segment of the channel, resulting in the creation of an excited electronic state. Subsequently, this state transitions to the ground state by emitting light with a wavelength centered around 419 nm, corresponding to blue light [18, 19].

Recent years witnessed a growing interest in ECL sensing, which was in turn amplified by innovations in single-electrode systems. Since the pioneering work of SE-ECL, where simultaneous multiplex detection of H_2O_2, glucose, and uric acid, was presented [17], the focus shifted towards improving the applicability of these systems. One such effort included merging SE-ECL with wireless energy transmission, which allowed for real-time analysis through the rectification of electrical currents [20]. Soon after enzymeless detection was made possible by the integration of laser-induced graphene (LIG) into SE platforms, expanding ECL detection across multiple analytes [21]. By crafting SEs on polyimide substrates using precise CO_2 laser settings, graphene was synthesized, enabling quantification of H_2O_2, D-glucose, xanthine, and dopamine [21]. The same principle was later used for the detection of vitamin B12 with SE-ECL systems with electrodes made through laser-induced graphene patterns [22]. The simplicity of single-electrode electrochemiluminescence allows it to be easily integrated with novel manufacturing methods like 3D printing, resulting in a new class of portable and adaptable sensing platforms [23]. 3D-printed single-electrode ECL (3DP-SE-ECL) devices were made using commercially available conductive filaments like graphene and carbon, and validated as a lactate detection platform [23]. Another promising fabrication approach is based on paper-based electrochemical systems. As a portable and cost-effective method, this allowed for single-detecting electrodes to be fabricated using controlled ablation of reduced graphene oxide on paper substrates [24]. This paper-based approach was further developed through integration with wax lamination, and reduced graphene oxide and used for the fabrication of adaptable and disposable P-SE-ECL devices [25]. SE systems have also shown promising use in high-throughput ECL immunoassays [26]. Combining a single carbon ink screen-printed

electrode with a plastic cover, provided an electrically-responsive surface for immobilizing antibodies with superior bioaffinity. Upon introduction of the samples, the biomarker-antibody interaction on the electrode reduces electron transfer and lowers ECL intensity within the luminol–H_2O_2 system [27]. In a similar approach, another fabrication method of SE-ECL, introduced multiple microelectrochemical cells within a single electrode by attaching a perforated plastic board onto an ITO electrode. This design enabled parallel electrochemical reactions through non-contact regulation, with comprehensive investigations into parameters influencing polypyrrole film growth and gradient characteristics assessed via thickness measurements, surface morphology analysis, and contact angle determinations [28]. An equivalent device was also fabricated by affixing a plastic sticker featuring 24 apertures onto a carbon nanotube (CNT)/graphene film electrode that had been modified with $Ru(phen)_3^{2+}$. This device demonstrated its utility for ECL detection of dopamine [29].

Recently, significant attention has been dedicated towards combining microfluidic devices with semiconductor imaging sensors [30]. As an example, previously, we combined microfluidic components with luminol–H_2O_2 ECL systems within a complementary metal-oxide-semiconductor (CMOS) chip to enable both sample manipulation and data acquisition on an integrated platform. This was accomplished by repurposing a single electrode as an electrochemical transducer and incorporating a CMOS chip as an integrated detector. We demonstrated the utility of this approach in detecting uric acid from saliva and urine [4]. In this article, we further demonstrate the potential of the single electrode setup for multicolor ECL multiplexing. This novel approach harnessed variations in applied electric potential in single electrode configuration to enable potential-resolved multicolor ECL.

To further enhance the signal intensity and ability to multiplex for the detection of multiple analytes, we introduce here for the first time the use of Alternating Current (AC) voltage to drive the ECL reaction within the single electrode configuration. Additionally, we combined microfluidic technology and multi-color ECL on a CMOS chip to create a compact multicolor SE-ECL sensor. Our approach leverages a single electrode design to induce ECL reactions for various colors, employs microfluidic techniques for effective sample handling, and utilizes a cost-effective and energy-efficient CMOS sensor to capture signals generated during ECL reactions.

5.3 Experimental section

5.3.1 Materials

Luminol was bought from Ward's Science in Ontario, Canada, while sodium bicarbonate was acquired from Bioshop Canada Inc.. Sodium hydroxide, hydrogen peroxide of 30% and Tetra-n-butylammonium hexafluorophosphate ($TBAPF_6$) 98% were from Thermo Fisher Scientific. 2-(Dibutylamino) Ethanol 99%, Tris (2,2'-Bipyridil) Dichlororuthenium ($[Ru(bpy)_3]^{2+}$), Tris[2-phenylpyridinato-C2,N] iridium ($Ir(ppy)_3$), Tripropylamine (TPrA) 98%, and Acetonitrile HPLC were purchased from Sigma Aldrich. Uric Acid, triton X-100 and glucose oxidase (notatin, GOx, activity of 100 units/mg powder at 25 °C) were acquired from Bio Basic Inc.. Uricase from Candida species (activity of 4 units/mg powder at 25 °C) and Glucose (anhydrous dextrose,) were purchased from Sigma-Aldrich. PDMS (Polydimethylsiloxane) (SYLGARD™ 184 Silicone Elastomer Kit) was purchased from DOW Corning Corporation. (USA). SU-8 2050 photoresist was purchased from MicroChem (Kayaku Advanced Materials, Inc., USA). Conductive silver epoxy was purchased from MG Chemicals (Ontario, Canada). Milli Q water was used to prepare solutions.

Raspberry Pi 4 2GB Model B-128 GB was purchased from CanaKit. Raspberry Pi Camera Module 3 was obtained from PiShop (Ontario, Canada). Indium Tin Oxide (ITO)-coated Poly Ethylene Terephthalate (PET) sheet was obtained from Sigma Aldrich. Medical grade, pressure-sensitive double-sided tape (ARcare®-90445Q) was obtained from Adhesive Research Inc. (USA). Silicon wafer was obtained from University Wafers Inc.

5.3.2 Methods

5.3.2.1 Sample preparation.

The electrolyte utilized in ECL measurements, resulting in a blue color, comprised a mixture of 0.1 M sodium bicarbonate and 1 mM luminol. To prepare the electrolyte, a 0.1 M sodium bicarbonate solution was created, and the pH was adjusted to 10.7 accordingly by adding 1 M NaOH. This solution was then combined with 10% v/v of a 10 mM luminol solution, previously prepared in NaOH (0.1 M), resulting in a final luminol concentration of 1 mM. For H_2O_2 detection, a 10 mM H_2O_2 solution was generated by diluting a concentrated H_2O_2 solution (9.8 M) with water. Subsequently, 0.5 mM (H_2O_2) was introduced into the prepared electrolyte

containing carbonate buffer and luminol for detection. An Acetonitrile solution containing 0.1 M $TBAPF_6$ was prepared and utilized for Red, Green, and Yellow-Orange electrochemiluminescence (ECL) measurements. Specifically, for Red ECL measurements, a solution of 0.125 mM $[Ru(bpy)_3]^{2+}$ and 50 mM TPrA in Acetonitrile was prepared. In the case of Green ECL measurements, 1.5 mM $Ir(ppy)_3$ and 50 mM TPrA were prepared in the Acetonitrile solution. For Yellow-Orange ECL measurements, concentrated solutions of Ru and $Ir(ppy)_3$ in Acetonitrile were combined to maintain final concentrations of 0.125 mM and 1.5 mM, respectively.

5.3.2.2 Fabrication of the SE-ECL device.

To build this platform, a backside-illuminated 12-megapixel imaging CMOS sensor camera module (IMX708, SONY) was used for imaging and controlled by a Raspberry Pi 4 computer. For the lens-based system, the focal plane was set to 10 cm which was the minimum manual focus distance. In this system, microfluidic channels were built using a DLP 3D printer (ELEGOO Mars 3Pro) and were sealed using ITO-coated PET. The ITO-coated PET is composed of two separate layers: a PET layer with a thickness of 127 μm and an ITO coating with a thickness of 23 nm. The varying thickness of the ITO coating results in different electrical resistances for the ITO-coated film. To be precise, a thicker ITO coating corresponds to a lower resistance. The ECL becomes more resilient with increasing ITO resistance, reaching its maximum at 100 ohms per square [17]. The device was then connected to the arbitrary waveform generator (SDG7052A-SIGLENT) using alligator clips and copper wires. The connection to the surface of the ITO-coated PET was established through the application of conductive silver epoxy (cold soldering method).

5.3.2.3 Fabrication of lensless SE-ECL on CMOS device.

To establish this platform, an initial step involved the fabrication of a microfluidic device with four channels measuring 2500×500 μm. For this purpose, we use a silicon wafer that offers a smooth and flat surface, which is essential for creating precise and well-defined microstructures. This silicon wafer serves as a template for creating multiple copies of the microstructures. In our device fabrication, we used a silicon wafer as a substrate to fabricate a master mold out of SU-8 photoresist. The microfluidic device was finally constructed using PDMS replicated from the master mold and subsequently sealed with an ITO-coated PET film.

The attachment of the PDMS microfluidic device to the ITO-coated PET was achieved by cutting pressure-sensitive double-faced tape to match the dimensions of the microfluidic channels using a cutting plotter (GRAPHTEC CE7000). The patterned tape and microfluidic channel were then precisely aligned and affixed to the ITO-coated PET using a mask aligner (OAI Model 200). As shown in Figure 1, the microfluidic chip was directly positioned onto the CMOS sensor, creating a lensless imaging/sensing platform. To regulate the electrical potential of the electrochemical cell, the device was linked to a waveform generator (SIGLENT SDG7052A) via two copper wires. These wires established contact with the ITO at both ends of the microfluidic channels.

5.3.2.4 ECL measurements.

After applying the test solution to the channels, the measurements were conducted in a completely dark environment. The device was subjected to either an AC voltage of 24 Vpp or a DC voltage of 12V. The resulting ECL emission was observed and recorded using the CMOS sensor connected to a Raspberry Pi 4 computer. Subsequently, the recorded data were analyzed using Fiji ImageJ to extract grayscale values corresponding to the detected photons from the whole channel. For controlling the imaging parameters, a Python script was written, and the following conditions were applied: resolution = 4608×2592 pixels (full field of view), frame rate = 1/8 s, shutter speed = 8s exposure time, ISO = 800 (gain 8X). A ten-second period of sleep time was implemented before each experiment to allow the camera sufficient time to adjust its parameters.

5.4 Results and Discussion

5.4.1 Improvement and characterization of SE-ECL light emission in AC electric fields

The SE-ECL device for this purpose was constructed as illustrated in Fig. 1, employing a backside-illuminated CMOS sensor and a 3D-printed chip comprising five channels sealed with ITO-coated PET using pressure-sensitive double-faced tape. Initially, a 3D-printed device with dimensions of 50×3 mm was created using a DLP 3D printer, forming five channels, and subsequently sealed with an ITO-coated PET film. The top-open channels functioned as electrochemical cells, while the conductive ITO-coated PET served as a single electrode (Fig. 1). To supply electrical potential to the electrochemical cell, the device was linked to a

waveform generator via two copper wires. These wires made contact with the ITO on both ends of each channel. Different electrolytes, contributing to distinct colors, were filled into the channels. The blue-colored channel contained a 0.1 M carbonate buffer ($NaHCO_3$ and NaOH) with luminol (1mM), H_2O_2 (0.5 mM), and Triton X-100 (1% v/v). The red channel contained 0.125 mM $[Ru(bpy)_3]^{2+}$ and 50 mM TPrA in Acetonitrile (0.1 M $TBAPF_6$). The green-colored channel had 1.5 mM $Ir(ppy)_3$ and 50 mM TPrA, and the yellow-orange-colored channel was filled with a mixture of red and green electrolytes. The CMOS sensor recorded the ECL emission and bright-field images. Positioned at a working distance of 10 cm for optimal proximity and field of view, the CMOS sensor was connected to the Raspberry Pi 4 system for data collection (Fig. 1).

The applied potential is a critical factor in all ECL devices. As demonstrated in prior research [4], a linear relationship between intensity and voltage, as anticipated by Equation 2, has been established. When E_{tot} reaches a sufficiently high level (5V in the present study), ΔE_{ch} becomes adequate to drive the reaction, leading to the occurrence of the faradaic reaction simultaneously at both ends of the channels. Since this reaction is propelled by the electric potential difference, an increase in voltage corresponds to an augmentation in emission. The blue ECL emission of luminol was observed at the positive side of the channel. By elevating the value of E_{tot}, the emission region of the channel gradually extends toward the center, enabling the ECL reaction to transpire over a larger surface area [31].

Here, for the first time, Alternating Current (AC) voltage has been employed in a single electrode configuration, and the impact of sinusoidal and square AC voltage on ECL emission has been examined. Due to the AC voltage, the positive side of the channel undergoes continuous changes.

Since the excitation of luminol and ECL emission occurs at the positive side of the electrochemical system, increasing the recording time (sensor exposure time) led to the observation of ECL emission from both sides (Fig. 2a). Because of having ECL emission on both sides, the mean intensity of each channel excited by AC voltage is higher than the same channel excited by DC voltage. However, this difference is not twofold since in sinusoidal AC voltage, especially at low frequencies, there is always a brief period during which the signal is off. Furthermore, to minimize the signal-off time, AC voltage with a square waveform was employed. In this scenario, the potential difference is almost always at its maximum on one

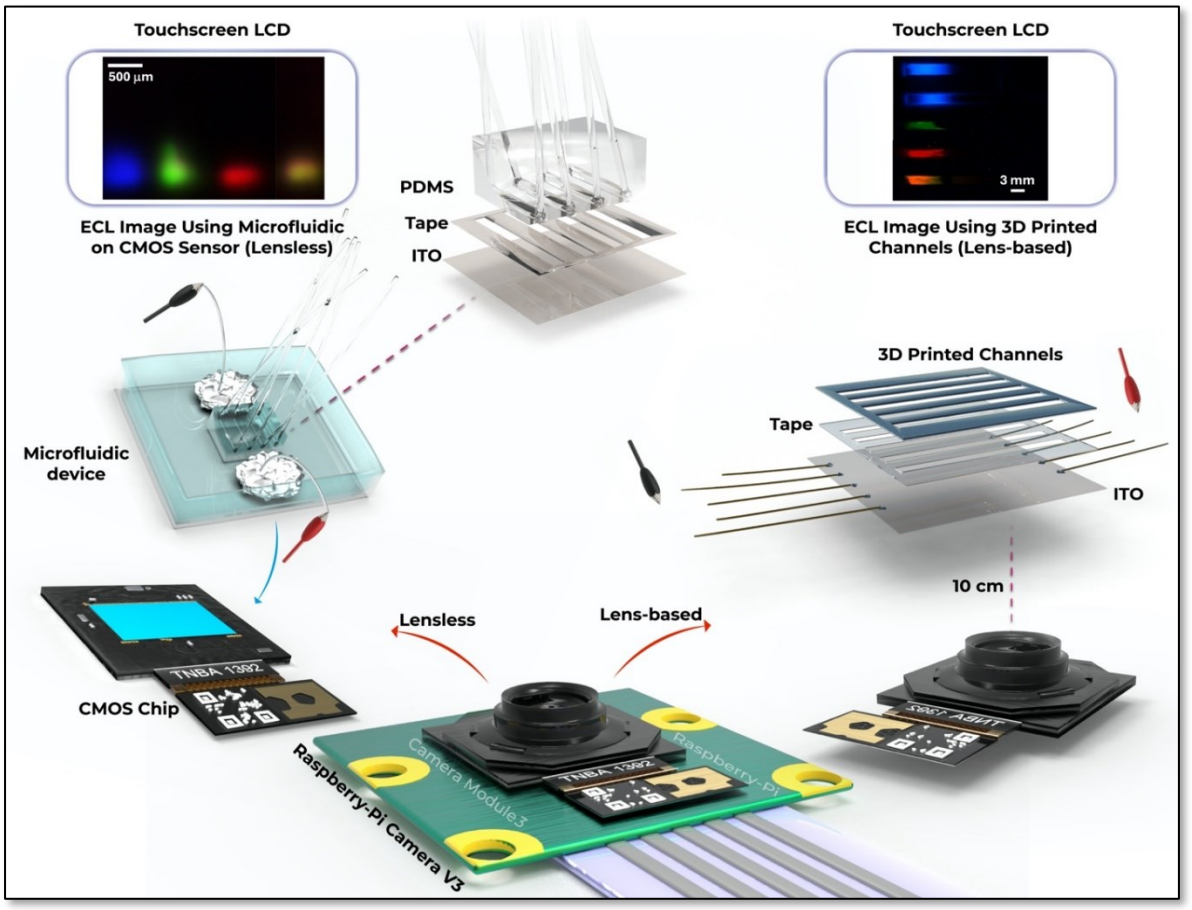

Fig. 1. Schematic of Multicolor SE-ECL. For the lens-based platform, a backside-illuminated 12-megapixel imaging CMOS sensor camera module controlled by a Raspberry Pi 4 computer was used with a lens corresponding to a working distance of 10 cm. Microfluidic channels were built using a DLP 3D printer and were sealed using ITO-coated PET. An arbitrary waveform generator is used for the applied electric fields. For the lensless platform, first, a microfluidic device with four channels was fabricated using PDMS replicated from a master mold made of SU-8 and subsequently sealed with an ITO-coated PET film. The resulting SE-ECL images are shown on the touch screen LCD that was connected to a Raspberry-Pi 4 computer.

side of the channel, resulting in almost twice the ECL signal compared to the same device using DC voltage (Fig. 2b).

Since it was observed that AC voltage increased the mean ECL intensity of each channel, the frequency of AC voltage was further investigated. For this purpose, two different lengths of channels (10 mm and 20 mm) were utilized, and various frequencies ranging from 0.2 Hz to 100 Hz of AC voltage were applied to the Luminol-H_2O_2 system. It was noted that in the longer

channel (20 mm), the mean intensity remained constant until a frequency of 25 Hz (Fig. 3a). However, at higher frequencies, particularly after 25 Hz, the mean ECL intensity started to decrease.

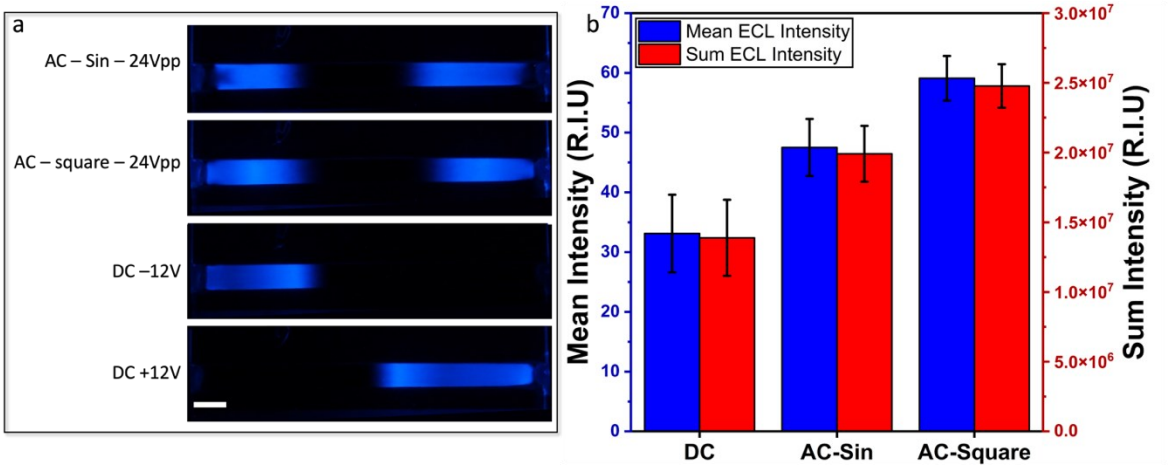

Fig. 2. Dependence of the ECL intensity on the applied potential form. a) ECL images of SE-ECL setups excited by different potential type captured by the lens-based CMOS sensor. The scale bar is 3 mm. b) Quantitative analysis of ECL images on panel a. The electrolyte used for measurements is 0.1 M carbonate buffer ($NaHCO_3$ and NaOH), the concentration of Luminol is 1.0 mM concentration of H_2O_2 is 0.5 mM, the percentage of triton X-100 is 1% v/v, and the voltage is set to 24 V_{pp}. for AC with 3Hz frequency 12V for DC.

A similar observation of decreasing mean intensity at higher frequencies (higher than 50 Hz) was made for the shorter channel (Fig 3c). This observation can be explained by the diffusion rate of luminol molecules in the electrolyte. The diffusion rate relates to the speed or rate at which particles or molecules spread, moving from an area of higher concentration to an area of lower concentration. It is measured by how rapidly diffusion occurs. The rate of diffusion (ROD) can be calculated using the following formula:

$$ROD = \frac{D \times A \times \Delta C}{\Delta x} \qquad (3)$$

In this equation, D represents the diffusion coefficient, which varies based on the characteristics of the substance and the medium it is diffusing through, A is the surface area through which diffusion occurs, ΔC indicates the concentration disparity between the two regions, and Δx represents the distance over which diffusion occurs.

For the longer channel (20 mm), the rate of diffusion is not as fast as the changing positive side of the electrochemical cell in the high-frequency range. In the shorter channel (10 mm), since the distance over which diffusion takes place (Δx) is shorter, the decrease in mean intensity was observed at higher frequencies.

The mean ECL intensity of each pulse for both channels are illustrated in Fig. 3b and Fig. 3d. In both cases, the mean intensity decreases with increasing frequency, as the higher number of pulses are detected within one single long exposure photograph.

As seen in Equation 2, the channel length (l_{ch}) is important in determining the potential applied to the electrochemical cell, a significant characteristic of the SE-ECL configuration, and influences the intensity of ECL emission. Therefore, to investigate the dependency of SE-ECL intensity on channel length, varying channel lengths ranging from 20 mm to 60 mm with the same channel width (3 mm) were employed. The corresponding ECL emissions from the luminol-H_2O_2 system were recorded by the CMOS sensor, as illustrated in Fig. 4a. An intensity profile of the ECL is shown in Fig. 4b, where the maximum intensity is relatively constant for all channel lengths and the length of the emission increases for longer channels. Fig. 4c and Fig. 4d depict the mean intensity and sum intensity of each channel length. The sum intensity, representing the total intensity of all pixels, increased with the elongation of the channel length. This can be attributed to the fact that in a longer channel, more luminol molecules are excited from broader range of the channel leading to increased light emission. However, the mean intensity decreased with the increase in channel length, due to the larger proportion of unilluminated pixels.

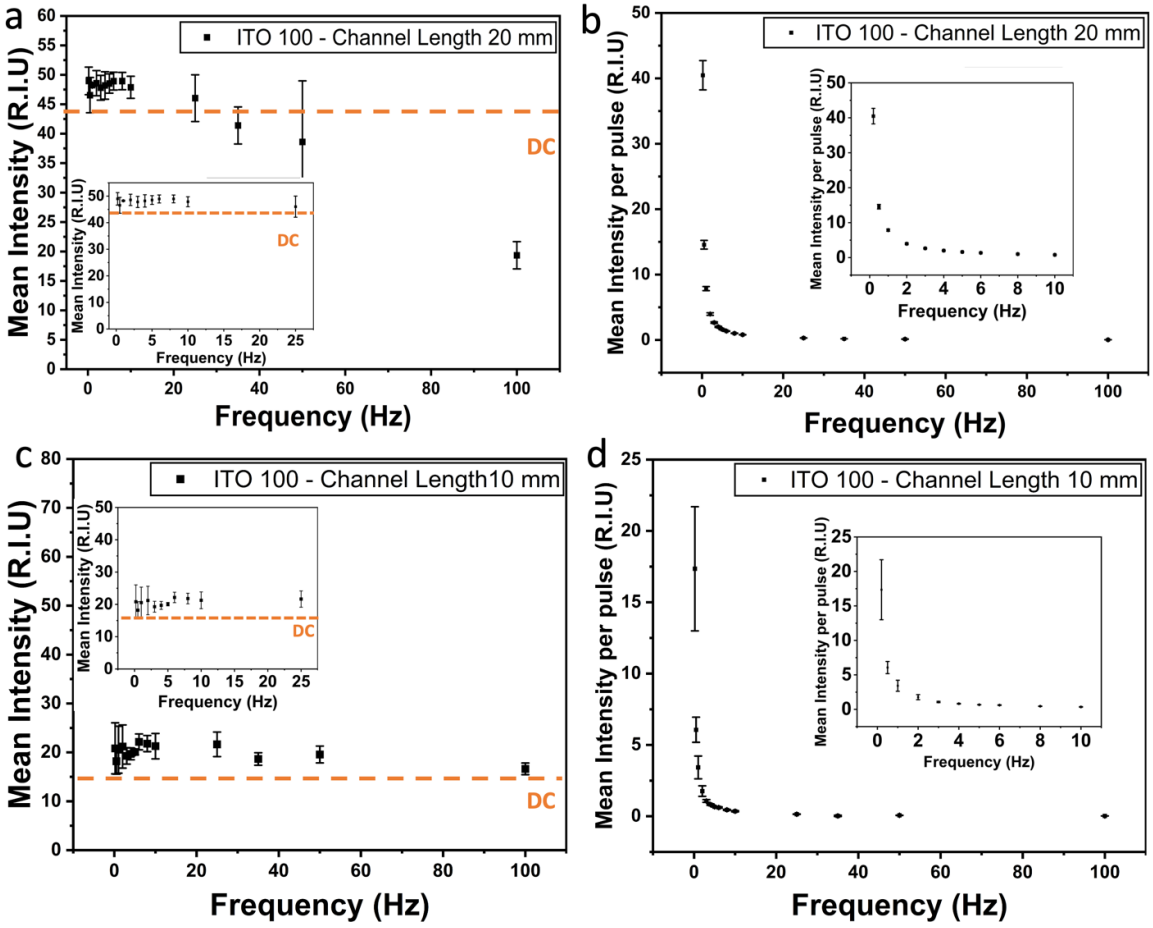

Fig. 3. Dependence of the ECL intensity on the frequency of the applied electric field. a) Mean intensity for channel length 20 mm, inset shows the frequency range 0-25 Hz. b) Mean intensity per each pulse for channel length 20 mm, inset shows the frequency range 0-10 Hz. c) Mean intensity for channel length 10 mm, inset shows the frequency range 0-25 Hz. d) Mean intensity per each pulse for channel length 10 mm, inset shows the frequency range 0-10 Hz. The electrolyte used for measurements is 0.1 M carbonate buffer ($NaHCO_3$ and NaOH), concentration of Luminol is 1.0 mM concentration of H_2O_2 is 0.5 mM, percentage of triton X-100 is 1% v/v, and the voltage is set to 24 V_{pp}. The orange dotted line is indicating the ECL Intensity for 12V DC.

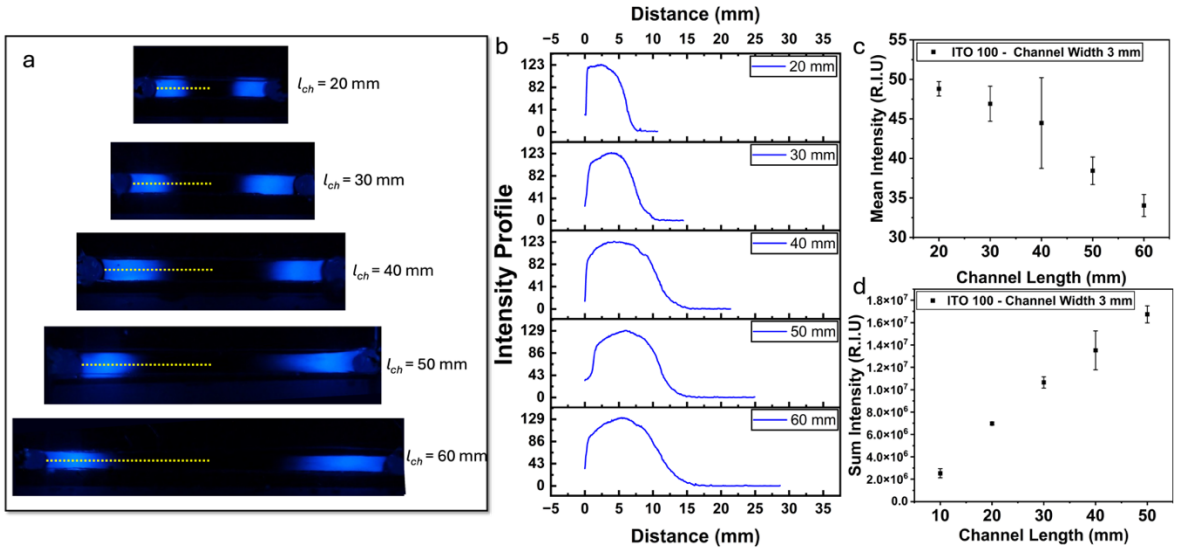

Fig. 4. Dependence of the SE-ECL intensity on channel length. a) ECL images of SE-ECL setups with different channel lengths captured by CMOS. b) ECL intensity profile in each channel with different lengths. c) Mean intensity for channel length. d) Sum intensity for each channel length. Channel width is 3 mm. The electrolyte used for measurements is 0.1 M carbonate buffer ($NaHCO_3$ and NaOH), the concentration of Luminol is 1.0 mM concentration of H_2O_2 is 0.5 mM, the percentage of triton X-100 is 1% v/v, and the voltage is set to 24 V_{pp} and frequency is 3 Hz.

To further characterize the dimensions of the device, the width of the channel was investigated, and the corresponding ECL emission was recorded by the lens-based CMOS sensor (Fig. 5a). Channels of varying widths, ranging from 1 mm to 30 mm, all with the same length (15 mm), were employed, and the sum intensity was plotted in Fig. 5b. It was observed that both mean and sum intensity increased with the widening of the channel. This phenomenon can be attributed to the fact that increasing the channel width results in an augmented volume of the electrolyte and a greater number of luminol molecules, while the black region, representing the part with a low potential difference that is insufficient for the excitation of luminol, remains constant.

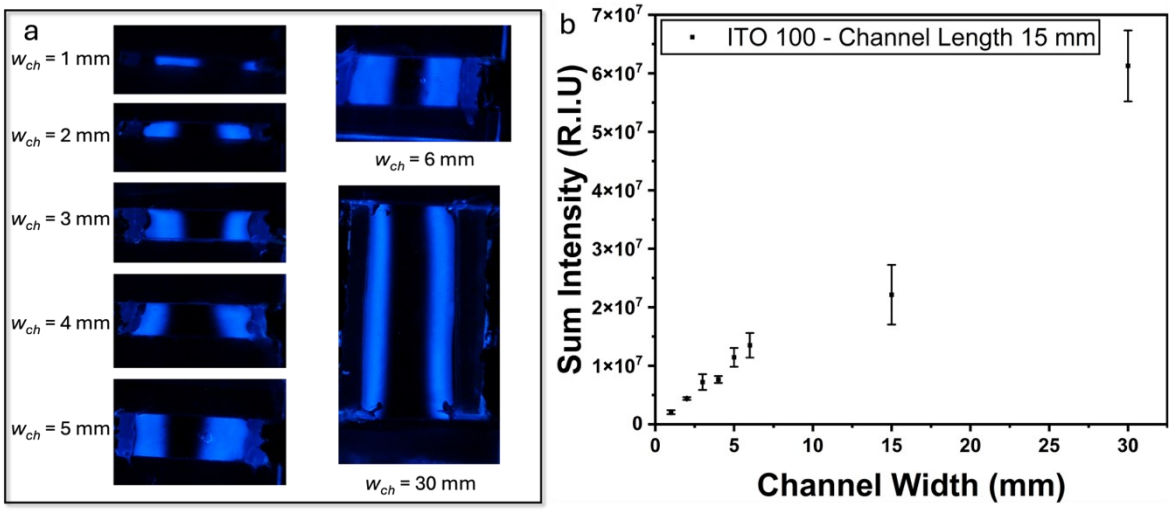

Fig. 5. Dependence of the SE-ECL intensity on channel width. a) ECL images of SE-ECL setups with different channel widths captured by CMOS. b) Sum intensity for channel width. The channel length is 15 mm. The electrolyte used for measurements is 0.1 M carbonate buffer ($NaHCO_3$ and NaOH), the concentration of Luminol is 1.0 mM concentration of H_2O_2 is 0.5 mM, the percentage of triton X-100 is 1% v/v, and the voltage is set to 24 V_{pp} and frequency is 3 Hz.

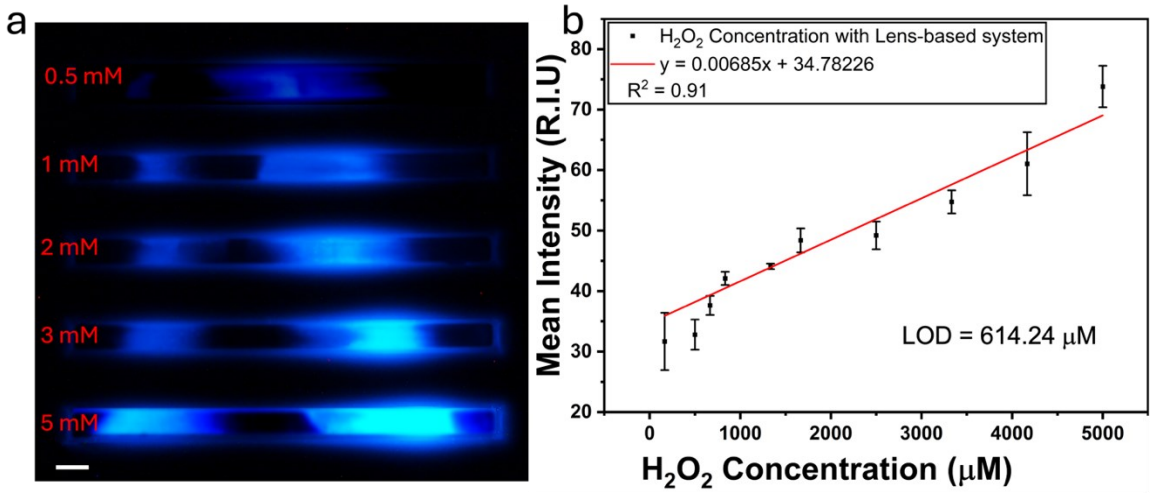

Fig. 6. Limit of Detection of SE-ECL for a lens-based system, using H_2O_2 as analyte. a) Representative image the electrochemiluminescence measured simultaneously for H_2O_2 at five different concentrations in five different microfluidic channels with a lens-based system. Scale bar is 3 mm. b) Mean SE-ECL intensities for different concentrations of H_2O_2 measured in different microfluidic channels and the corresponding LOD. The electrolyte is 0.1 M carbonate buffer ($NaHCO_3$ and NaOH), the concentration of Luminol is 5 mM, and the percentage of triton X-100 is 1% v/v. The voltage is set to square wave AC of 24 Vpp, with a 3 Hz frequency.

To demonstrate the ability of detecting simultaneously different concentrations, we used a lens-based system to record SE-ECL intensities for different concentrations of H_2O_2 in different channels. This data is shown in Fig. 6a and was obtained with applied electric fields of square wave AC, 24 Vpp, and 3 Hz frequency. Measurements were performed 3 times for each concentration and the data (mean intensity values) are shown in Fig. 6b. By using the formula $LOD=3SD_{blank}/slope$ we calculated a 614.24 mM LOD for H_2O_2, which is approximately 35 times larger than the LOD previously reported with lens-free system (Fig. 3A in [4]). This is due to the differences in the photon collection angle, where higher collection angle (almost 160^0 solid angle in the lens-free system compared with approximately 2.3^0 for the lens-based system) leads to a significant improvement in the LOD for the lens-free system.

5.4.2 Multiplexing via multicolor SE-ECL

The variation in colors is more noticeable to the human eye than differences in single-color intensity, thereby enhancing visual recognition. Additionally, this diversity in colors facilitates easier image analysis and, consequently, simplifies multiplexing. Luminophore materials, such as Ru(II) and Ir(III) compounds, have been widely utilized due to the ability of their metals to be in a low oxidation state (electron-rich) and their ligands to possess low-lying empty orbitals. As a result, charge transfer occurs. [32, 33]. Moreover, the ECL emission quantum efficiency of [Ir (ppy)$_3$] is fainter than that of $[Ru(bpy)_3]^{2+}$ in certain conditions. Consequently, there is a sufficient separation between the green ECL emission peak of [Ir(ppy)$_3$] (λ_{max}=518 nm) and the red emission of $[Ru(bpy)_3]^{2+}$ (λ_{max}=620 nm) to distinguish their signals in experiments. [34] The lower excitation potentials required for [Ir(ppy)$_3$] compared to $[Ru\ (bpy)_3]^{2+}$ result in the green ECL of the [Ir(ppy)$_3$] and $[Ru(bpy)_3]^{2+}$ mixture occurring at a lower potential. This means that ECL emission coming from [Ir(ppy)$_3$] is dominant at low potentials [35]. Simultaneous emission from both luminophores, [Ir(ppy)$_3$] and $[Ru(bpy)_3]^{2+}$, displaying annihilation ECL can be observed at an appropriate potential [36]. The mixture of [Ir(ppy)$_3$] and $[Ru(bpy)_3]^{2+}$ produces a yellow ECL image due to the overlap in their excitation spectra. In this case, there is insufficient free energy to form the [Ir(ppy)$_3$]* emitter. [34]

Applying an elevated electrical potential to the mixture of [Ir(ppy)$_3$] and $[Ru(bpy)_3]^{2+}$ amplifies the quenching of [Ir(ppy)$_3$]* caused by the radical cation state of $TPrA^{+}$* [37, 38]. Until the level of $TPrA^{+}$* attains a crucial concentration, leading to ECL quenching, the close proximity of the redox potentials of TPrA and [Ir(ppy)$_3$] allows the dominance of the [Ir(ppy)$_3$]* reaction

for a short time. This means that the rate of suppression reaction depends on the concentration of the co-reactant [37]. It has been mentioned in the literature that the switch-off effect is evident for [Ir(ppy)$_3$], but only with a relatively high co-reactant concentration [34]. Hence, at a high potential range in the mixed [Ir(ppy)$_3$] and [Ru(bpy)$_3$]$^{2+}$, only the red ECL is visible. Notably, the limitation of the red ECL region at high potential suggests potential polarization inducing local pH decrease, which inhibits the oxidation reaction, generating fewer co-reactant radicals and leading to ECL extinction [34, 39]. This phenomenon holds promise for applications in multiplexed sensing and screening of ECL luminophores, as [Ir(ppy)$_3$] exhibits ECL annihilation behavior in the high potential regime, enabling the design of potential-resolved ECL systems [34, 35].

Whether utilizing a three-electrode system, BPE, or SE, the potential difference serves as the driving force for ECL reactions [4, 40]. Unlike BPE-ECL, in which the potential gradient is created within the electrolyte, in SE-ECL systems, the ITO electrode's resistance introduces a potential gradient throughout the channel. When the value of E_{tot} and consequently ΔE_{ch} is sufficiently significant, faradaic reactions occur concurrently at both channel ends.

In order to demonstrate the ability to distinguish different colors at different voltages, we used a mixture of green and red electrolytes (Ir(ppy)$_3$ and [Ru(bpy)$_3$]$^{2+}$) in the same microfluidic channel and applied different potentials from 5 to 12 V. Fig. 7a shows the ECL color transitioning from green to yellow, and then to orange and red with increasing potential. When subjected to lower potentials (5 V), the green ECL emission can be distinguished due to the excitation of Ir(ppy)$_3$ in this potential range. Both luminophores are excited at a potential range from 5.5 V to 7.5 V, resulting in a multicolor appearance. At 8 V, the red ECL of [Ru(bpy)$_3$]$^{2+}$ becomes predominant.

To demonstrate the ability to resolve spatially two different luminophores, we measured simultaneously [Ru(bpy)$_3$]$^{2+}$ and Ir(ppy)$_3$ at the same applied potential (12 V) in one microfluidic channel. The results are shown in Fig. 7b where the two ECL luminophores have distinct oxidation potentials, leading to spatial separation of their emissions. In the higher potential range (closer to the positive electrode), red ECL emission of [Ru(bpy)$_3$]$^{2+}$ can be distinguished. Moving from the positive electrode towards the negative electrode (approaching lower potential difference) green ECL of Ir(ppy)$_3$ becomes predominant.

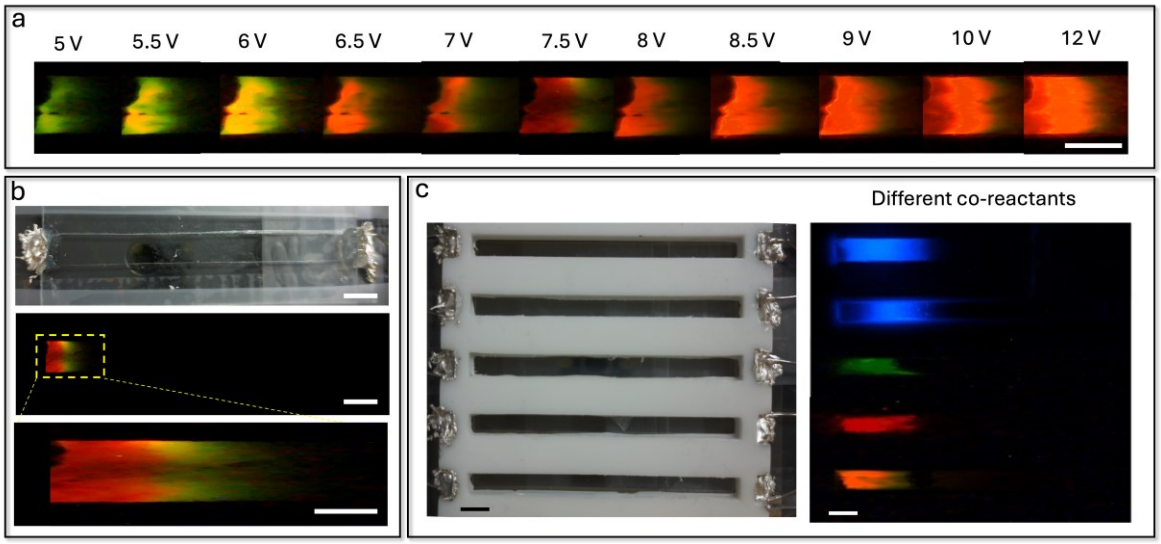

Fig. 7. Multicolor multiplexed SE-ECL with lens-based system. a) Potential-resolved multicolor ECL using different SE-devices and by applying different potentials. b) Simultaneous, spatially resolved multicolor ECL in one channel with single electrode configuration, where the positive electrode is on the left side of the channel. Red, yellow, and green can be distinguished. c) Photograph of 3D printed microfluidic channels (left) and corresponding multicolor multiplexing (right) of ECL in separate channels with different co-reactants (each color corresponds to a different co-reactant) with single electrode configuration in one SE-ECL device. The electrolyte used for all ECL measurements shown in this figure: Blue - 0.1 M carbonate buffer ($NaHCO_3$ and NaOH), the concentration of Luminol is 1.0 mM concentration of H_2O_2 is 0.5 mM, the percentage of triton X-100 is 1% v/v; Red - 0.125 mM $[Ru(bpy)_3]^{2+}$ and 50 mM TPrA in Acetonitrile (0.1 M $TBAPF_6$); Green - 1.5 mM $Ir(ppy)_3$ and 50 mM TPrA; Yellow-Orange - 0.125 mM $[Ru(bpy)_3]^{2+}$, 1.5 mM $Ir(ppy)_3$ and 50 mM TPrA in Acetonitrile (0.1 M $TBAPF_6$). The voltage in panels b and c is set to 12 V DC. The scale bar in all panels is 3 mm.

In many applications, the ability to separate more than two different luminophores is important. This can be done by using multiple separate channels, each containing one or a mixture of electrolytes. In Fig. 7c we demonstrate an approach for channel-based multicolor ECL, where by applying the same potential difference to all channels (12 V), each filled with distinct luminophores (Luminol, $Ir(ppy)_3$, and $[Ru(bpy)_3]^{2+}$), we can observe emission from each luminophore at their specific color (blue, green, and red, respectively). When both red and green luminophores are present, the ECL emission results in an orange color.

These approaches can be further extended towards more complex multicolor ECL by employing a mixture of several ECL luminophores with spectral, spatial, and potential-resolved

ECL in a SE configuration. This multicolor SE-ECL exhibits potential for multiplexing applications in the biosensing of different analytes.

5.4.3 Integration of multicolor SE-ECL onto a CMOS image sensor

To construct this platform, a microfluidic device, featuring four channels with dimensions of 2500 μm × 500 μm, was created as described in the Materials and Methods section. The bright field transmission images in Fig. 8a and Fig. 8c help visualize this platform that includes four microfluidic channels. The spatial resolution of the device is determined by the CMOS pixel size, which is 1.4 μm, and the field of view (FOV) is defined as the size of the photosensitive area of the CMOS sensor, which measures 6.5 mm × 3.6 mm. To control the electrical potential of the electrochemical cell, the device was connected to the waveform generator (SIGLENT SDG7052A) using two copper wires. These wires made contact with the ITO on both ends of the microfluidic channels.

To demonstrate the ability to detect multiple colors onto the CMOS image sensor, different electrolytes, each contributing to distinct colors, were filled into the channels. The blue-colored channel (channel 1) contained a carbonate electrolyte with luminol (1mM), H_2O_2 (0.5 mM), and Triton X-100 (1% v/v). The red channel (channel 2) contained 0.125 mM $[Ru(bpy)_3]^{2+}$ 50 mM TPrA in Acetonitrile (0.1 M $TBAPF_6$). The green-colored channel (channel 3) had 1.5 mM Ir(ppy)3 and 50 mM TPrA, and the orange-colored channel (channel 4) was filled with a mixture of red and green electrolytes (Fig. 8b).

The usability of this platform for the detection of different analytes is demonstrated next. For this purpose, we show in Fig. 8d simultaneous measurements of three different analytes: Uric Acid (blue), Glucose (blue), and TPrA (red). Uric Acid and Glucose were selected as two examples of analytes that can be detected due to the production of H_2O_2 through catalytic reactions in the presence of their enzymes. We have previously demonstrated the capability of our platform to detect Uric Acid within the physiological range in both saliva and urine [4]. Uric Acid is a byproduct resulting from the metabolic breakdown of purine nucleotides and has traditionally served as a biomarker for evaluating overall physiological health [4]. Conditions such as gout, renal illness, hyperuricemia, Lesch–Nyhan syndrome, cardiovascular disease, and various other disorders have been associated with irregular levels of Uric Acid [4].

Glucose, on the other hand, plays a crucial role in the human body, and a deficiency in this biomolecule can lead to significant disorders. To facilitate proper metabolic processes, every cell in the human metabolism system necessitates energy. Glucose serves as the primary source of energy for muscles, the brain, various tissues, and other essential body components [25]. Elevated blood sugar levels can contribute to heart, nerve, and eye disorders [41]. Conversely, low glucose levels can result in severe issues, including headaches, weakness, anxiety, and nervousness [21].

Finally, TPrA is commonly employed as a co-reactant of $[Ru(bpy)_3]^{2+}$ in ECL systems. However, it is a substance known for its high toxicity and carcinogenic properties, posing a threat to both human health and the environment [42]. Consequently, assessing the concentration of TPrA is crucial to ensuring human health and environmental protection. Additionally, TPrA serves as a co-reactant in the ruthenium ECL system used for DNA and protein assays [43, 44]. As demonstrated in Fig. 8e and Fig. 8f, the device exhibits a linear detection range for Uric Acid between 25 and 300 μM (data from Ref. [4]) and for Glucose between 20 and 300 μM, with a strong correlation coefficient ($R^2 = 0.968$ and $R^2 = 0.967$, respectively). The limit of detection (LOD) was determined to be 26.09 μM for Uric Acid and 16.21 μM for Glucose. While the linear range is comparable to existing literature on ECL detection [4, 45], the LOD is slightly higher. This can be attributed to several factors: lower electronic gain in our system compared to others (e.g., photomultiplier tubes with electron multiplication), sample handling limitations, and the large standard deviation of the blank for the chosen luminol concentration. Nevertheless, the reported LOD remains within (or even lower than) the physiological range of both analytes in biological fluids. For comparison, the physiological concentration range of Uric Acid is 70 – 320 μM in saliva and 1.49 – 4.46 mM in urine [46, 47] and the salivary glucose level is 40-300 mM [48]. We have previously assessed the device's performance in terms of repeatability (reusability) and reproducibility for uric acid detection [4]. By measuring the analyte with the same device five times and by measuring the same analyte with five different devices, we demonstrated satisfactory reusability and reproducibility, respectively [4]. The relative standard deviation (RSD) for repeatability was 2.06% and 7.00% for 300 μM and 50 μM Uric Acid concentrations, respectively. The RSD for reproducibility was 7.52% and 14.79% for 300 μM and 50 μM Uric Acid concentrations, respectively. This indicates consistent performance across multiple measurements. [4]

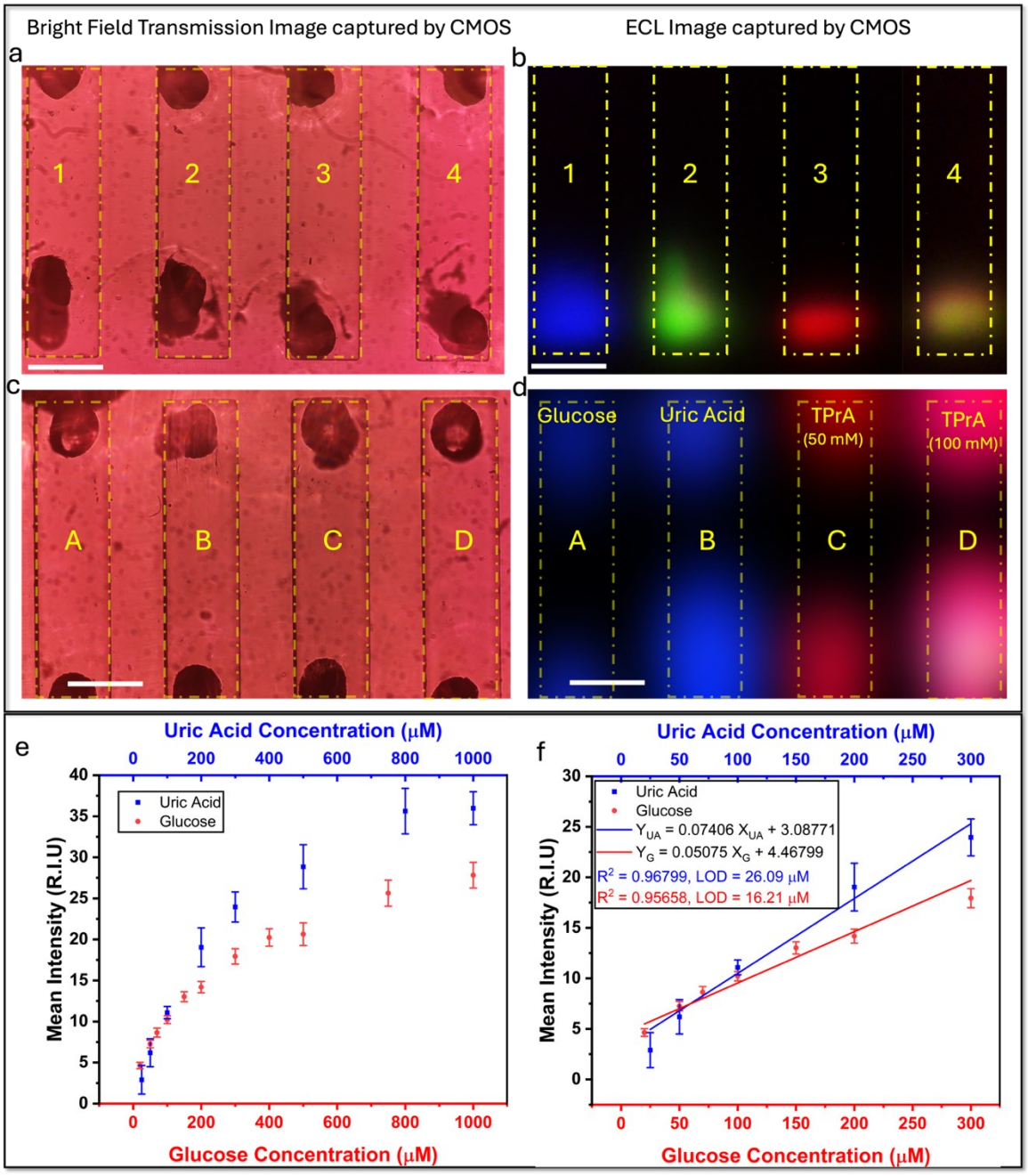

Fig. 8. Multicolor multiplexed SE-ECL directly on the CMOS image sensor. a) and c) Bright-field transmission image captured by a lensless CMOS image sensor showing four microfluidic channels, each with dimensions of 2500 μm × 500 μm. Black circles in this image are shadows of inlet and outlet tubes. These two microfluidic devices in a) and c) have been used for ECL measurement in panel b) and d), respectively. b) ECL image of the multicolor SE-ECL captured by lensless CMOS sensor. Each channel is filled with a different electrolyte. The electrolytes used for ECL measurements are: in channel 1: 0.1 M carbonate buffer ($NaHCO_3$ and NaOH), Luminol at 1.0 mM, H_2O_2 at 0.5 mM, percentage of

triton X-100 at 1% v/v; in channel 2: 1.5 mM $Ir(ppy)_3$ and 50 mM TPrA; in channel 3: 0.125 mM $[Ru(bpy)_3]^{2+}$ and 50 mM TPrA in Acetonitrile (0.1 M $TBAPF_6$); in channel 4: 0.125 mM $[Ru(bpy)_3]^{2+}$, 1.5 mM $Ir(ppy)_3$, and 50 mM TPrA in Acetonitrile (0.1 M $TBAPF_6$). The voltage is set to 12 V DC. The brightness of the ECL image in panel b has been enhanced for visualization purposes. d) ECL image of the multicolor multiplexed SE-ECL captured by the lensless CMOS sensor demonstrating the detection of three different analytes: Glucose (300 mM), Uric Acid (300 mM), and TPrA (50 mM and 100 mM). The electrolyte in channels A and B contains 0.1 M carbonate buffer ($NaHCO_3$ and NaOH), Luminol at 1.0 mM, and Triton X-100 at 1% v/v. In channels C and D, 50 mM, and 100 mM TPrA in Acetonitrile (0.1 M $TBAPF_6$) were mixed with 0.125 mM $[Ru(bpy)_3]^{2+}$, respectively. The voltage is set to square wave AC of 24 Vpp, with a 3 Hz frequency. The scale bar in panels a)-d) is 500 mm. e) Calibration graphs for Uric Acid (data from reference [4]) and Glucose showing the analysis of H_2O_2-Luminol ECL signals generated during the oxidation of Uric Acid catalyzed by 200 mg/ml uricase and oxidation of Glucose catalyzed by 1 mg/ml glucose oxidase, respectively. Incubation time is 10 minutes. f) linear range and calibration equations for Uric Acid and Glucose for data shown in e).

5.5 Conclusions

In this article we demonstrate improvements to SE-ECL configurations for higher sensitivity and specificity in the detection of analytes and for compact integration of the sample with a CMOS image sensor. These advancements take advantage of intrinsic differences in the electric potential applied along single electrodes built into electrochemical cells, enabling the achievement of distinct colors through selective excitation of ECL luminophores. First, we demonstrated that improvements to ECL emission can be achieved via optimization of the channel length and width. Next, we demonstrated for the first time that AC-driven SE-ECL emission leads to an increased emitted light intensity vs DC voltage, with square waveforms resulting in higher intensities compared with sine waveforms. Additionally, multiplexed multicolor SE-ECL of Ru (II) and Ir (III) luminophores was demonstrated for the first time, with the ability to simultaneously distinguish four different colors or three different analytes. The analytes can be separated by channel alone, by potential along the same channel, and by potential and color within one channel. By combining a multi-channel microfluidic chip with SE-ECL, the system was further miniaturized and implemented onto a 6.5 × 3.6 mm CMOS semiconductor image sensor. The strategy involves a single electrode design to initiate ECL reactions with different colors, incorporates microfluidic methods for efficient sample manipulation, and utilizes an economical and energy-efficient CMOS sensor for capturing the

light emitted during ECL reactions. Overall, these improvements will undoubtedly lead to the development of more accurate and miniaturized biosensors to be used in point of care/need biomedical, food safety, or environment monitoring applications.

5.6 Author Information

Corresponding Author: Sebastian Wachsmann-Hogiu (sebastian.wachsmannhogiu@mcgill.ca)

5.7 Declaration of Interest

The authors are co-founders of a 2023 McGill spinoff company, Phoela Health Inc.

5.8 Author Contributions

SHW and RA conceived the idea, RA performed the experiments, data analysis, and prepared the first draft of the manuscript, SWH and RA interpreted the data and finalized the manuscript, SWH provided the funding and supervision for the project.

5.9 Research Funding

This work was financially supported by the National Sciences and Engineering Research Council of Canada (NSERC), Discovery Grant RGPIN-2018-05675 and Louis-Ho Scholarship in Technological Innovation from Faculty of Engineering, McGill University. RA acknowledges funding from the McGill Engineering Doctoral Award (MEDA) and Fonds de recherche du Quebec - Nature et technologies (FRQNT) for doctoral studies.

5.10 References

[1] R. Singh, A. Feltmeyer, O. Saiapina, J. Juzwik, B. Arenz, and A. Abbas, "Rapid and PCR-free DNA Detection by Nanoaggregation-Enhanced Chemiluminescence," *Scientific Reports,* vol. 7, no. 1, p. 14011, 2017/10/25 2017, doi: 10.1038/s41598-017-14580-w.

[2] B. Al Mughairy and H. A. J. Al-Lawati, "Recent analytical advancements in microfluidics using chemiluminescence detection systems for food analysis," *TrAC Trends in Analytical Chemistry,* vol. 124, p. 115802, 2020/03/01/ 2020, doi: https://doi.org/10.1016/j.trac.2019.115802.

[3] T. Jiao, Q. Huang, Y. Xiao, X. Shen, J. Zhou, and F. Gao, "Electrochemiluminescent Detection of Hydrogen Peroxide via Some Luminol Imide Derivatives with Different Substituent Groups," *Journal of Chemistry,* vol. 2013, p. 375372, 2013/11/12 2013, doi: 10.1155/2013/375372.

[4] R. Abbasi, J. Liu, S. Suarasan, and S. Wachsmann-Hogiu, "SE-ECL on CMOS: a miniaturized electrochemiluminescence biosensor," *Lab on a Chip,* 10.1039/D1LC00905B vol. 22, no. 5, pp. 994-1005, 2022, doi: 10.1039/D1LC00905B.

[5] S. Kirschbaum and A. Baeumner, "A review of electrochemiluminescence (ECL) in and for microfluidic analytical devices," *Analytical and bioanalytical chemistry,* vol. 407, 03/15 2015, doi: 10.1007/s00216-015-8557-x.

[6] A. J. Bard, *Electrogenerated chemiluminescence*. CRC Press, 2004.

[7] M. M. Richter, "Electrochemiluminescence (ECL)," *Chemical Reviews,* vol. 104, no. 6, pp. 3003-3036, 2004/06/01 2004, doi: 10.1021/cr020373d.

[8] Y. Wei, H. Qi, and C. Zhang, "Recent advances and challenges in developing electrochemiluminescence biosensors for health analysis," *Chemical Communications,* 10.1039/D2CC06930J vol. 59, no. 24, pp. 3507-3522, 2023, doi: 10.1039/D2CC06930J.

[9] Y. Huang, Y. Yao, Y. Wang, L. Chen, Y. Zeng, L. Li, and L. Guo, "Strategies for Enhancing the Sensitivity of Electrochemiluminescence Biosensors," *Biosensors,* vol. 12, no. 9, p. 750, 2022. [Online]. Available: https://www.mdpi.com/2079-6374/12/9/750.

[10] A. Barhoum, Z. Altintas, K. S. S. Devi, and R. J. Forster, "Electrochemiluminescence biosensors for detection of cancer biomarkers in biofluids: Principles, opportunities, and challenges," *Nano Today,* vol. 50, p. 101874, 2023/06/01/ 2023, doi: https://doi.org/10.1016/j.nantod.2023.101874.

[11] M. Bhaiyya, P. K. Pattnaik, and S. Goel, "A brief review on miniaturized electrochemiluminescence devices: From fabrication to applications," *Current Opinion in Electrochemistry,* vol. 30, p. 100800, 2021/12/01/ 2021, doi: https://doi.org/10.1016/j.coelec.2021.100800.

[12] S. Wang, L. Ge, Y. Zhang, X. Song, N. Li, S. Ge, and J. Yu, "Battery-triggered microfluidic paper-based multiplex electrochemiluminescence immunodevice based on potential-resolution strategy," *Lab on a Chip,* 10.1039/C2LC40707H vol. 12, no. 21, pp. 4489-4498, 2012, doi: 10.1039/C2LC40707H.

[13] W. Li, M. Li, S. Ge, M. Yan, J. Huang, and J. Yu, "Battery-triggered ultrasensitive electrochemiluminescence detection on microfluidic paper-based immunodevice based on dual-signal amplification strategy," *Analytica Chimica Acta,* vol. 767, pp. 66-74, 2013/03/12/ 2013, doi: https://doi.org/10.1016/j.aca.2012.12.053.

[14] J. L. Delaney, E. H. Doeven, A. J. Harsant, and C. F. Hogan, "Use of a mobile phone for potentiostatic control with low cost paper-based microfluidic sensors," *Analytica Chimica Acta,* vol. 790, pp. 56-60, 2013/08/06/ 2013, doi: https://doi.org/10.1016/j.aca.2013.06.005.

[15] X. Mi, H. Li, R. Tan, and Y. Tu, "Dual-Modular Aptasensor for Detection of Cardiac Troponin I Based on Mesoporous Silica Films by Electrochemiluminescence/Electrochemical Impedance Spectroscopy," *Analytical Chemistry,* vol. 92, no. 21, pp. 14640-14647, 2020/11/03 2020, doi: 10.1021/acs.analchem.0c03130.

[16] L. Bouffier, S. Arbault, A. Kuhn, and N. Sojic, "Generation of electrochemiluminescence at bipolar electrodes: concepts and applications," *Analytical and Bioanalytical Chemistry,* vol. 408, no. 25, pp. 7003-7011, 2016/10/01 2016, doi: 10.1007/s00216-016-9606-9.

[17] W. Gao, K. Muzyka, X. Ma, B. Lou, and G. Xu, "A single-electrode electrochemical system for multiplex electrochemiluminescence analysis based on a resistance induced potential difference," *Chemical Science,* 10.1039/C8SC00410B vol. 9, no. 16, pp. 3911-3916, 2018, doi: 10.1039/C8SC00410B.

[18] Y. Zhang, R. Zhang, X. Yang, H. Qi, and C. Zhang, "Recent advances in electrogenerated chemiluminescence biosensing methods for pharmaceuticals," *Journal of Pharmaceutical Analysis,* vol. 9, no. 1, pp. 9-19, 2019/02/01/ 2019, doi: https://doi.org/10.1016/j.jpha.2018.11.004.

[19] E. Villani, N. Shida, and S. Inagi, "Electrogenerated chemiluminescence of luminol on wireless conducting polymer films," *Electrochimica Acta,* vol. 389, p. 138718, 2021/09/01/ 2021, doi: https://doi.org/10.1016/j.electacta.2021.138718.

[20] X. Ma, L. Qi, W. Gao, F. Yuan, Y. Xia, B. Lou, and G. Xu, "A portable wireless single-electrode system for electrochemiluminescent analysis," *Electrochimica Acta,* vol. 308, pp. 20-24, 2019/06/10/ 2019, doi: https://doi.org/10.1016/j.electacta.2019.04.015.

[21] M. L. Bhaiyya, P. K. Pattnaik, and S. Goel, "Miniaturized Electrochemiluminescence Platform With Laser-Induced Graphene-Based Single Electrode for Interference-Free Sensing of Dopamine, Xanthine, and Glucose," *IEEE Transactions on Instrumentation and Measurement,* vol. 70, pp. 1-8, 2021, doi: 10.1109/TIM.2021.3071215.

[22] M. Bhaiyya, P. K. Pattnaik, and S. Goel, "Electrochemiluminescence sensing of vitamin B12 using laser-induced graphene based bipolar and single electrodes in a 3D-printed portable system," *Microfluidics and Nanofluidics,* vol. 25, no. 5, p. 41, 2021/04/07 2021, doi: 10.1007/s10404-021-02442-x.

[23] M. Bhaiyya, P. Rewatkar, P. K. Pattnaik, and S. Goel, "Novel 3D printed single electrode-based portable and miniaturized electrochemiluminescence platform to detect lactate from human serum," *Journal of Micromechanics and Microengineering,* vol. 33, no. 2, p. 024001, 2022/12/29 2023, doi: 10.1088/1361-6439/acac3e.

[24] E. Vidal, C. E. Domini, D. C. Whitehead, and C. D. Garcia, "From glow-sticks to sensors: single-electrode electrochemical detection for paper-based devices," *Sensors & Diagnostics,* 10.1039/D2SD00041E vol. 1, no. 3, pp. 496-503, 2022, doi: 10.1039/D2SD00041E.

[25] M. L. Bhaiyya, S. Gangrade, P. K. Pattnaik, and S. Goel, "Laser Ablated Reduced Graphene Oxide on Paper to Realize Single Electrode Electrochemiluminescence Standalone Miniplatform Integrated With a Smartphone," *IEEE Transactions on Instrumentation and Measurement,* vol. 71, pp. 1-8, 2022, doi: 10.1109/TIM.2022.3179008.

[26] A. Firoozbakhtian, M. Hosseini, Y. Guan, and G. Xu, "Boosting Electrochemiluminescence Immunoassay Sensitivity via Co–Pt Nanoparticles within a Ti3C2 MXene-Modified Single Electrode Electrochemical System on Raspberry Pi," *Analytical Chemistry,* vol. 95, no. 40, pp. 15110-15117, 2023/10/10 2023, doi: 10.1021/acs.analchem.3c03285.

[27] F. Du, Z. Dong, Y. Guan, A. M. Zeid, D. Ma, J. Feng, D. Yang, and G. Xu, "Single-Electrode Electrochemical System for the Visual and High-Throughput Electrochemiluminescence Immunoassay," *Analytical Chemistry,* vol. 94, no. 4, pp. 2189-2194, 2022/02/01 2022, doi: 10.1021/acs.analchem.1c04709.

[28] Y. Shi, E. Villani, Y. Chen, Y. Zhou, Z. Chen, A. Hussain, G. Xu, and S. Inagi, "High-Throughput Electrosynthesis of Gradient Polypyrrole Film Using a Single-Electrode Electrochemical System," *Analytical Chemistry,* vol. 95, no. 2, pp. 1532-1540, 2023/01/17 2023, doi: 10.1021/acs.analchem.2c04570.

[29] F. Du, Z. Dong, F. Liu, S. Anjum, M. Hosseini, and G. Xu, "Single-electrode electrochemical system based on tris(1,10-phenanthroline)ruthenium modified carbon nanotube/graphene film electrode for visual electrochemiluminescence analysis,"

Electrochimica Acta, vol. 420, p. 140431, 2022/07/10/ 2022, doi: https://doi.org/10.1016/j.electacta.2022.140431.

[30] X. Hu, R. Abbasi, and S. Wachsmann-Hogiu, "Microfluidics on lensless, semiconductor optical image sensors: challenges and opportunities for democratization of biosensing at the micro-and nano-scale," *Nanophotonics,* vol. 12, no. 21, pp. 3977-4008, 2023, doi: doi:10.1515/nanoph-2023-0301.

[31] E. Villani and S. Inagi, "Mapping the Distribution of Potential Gradient in Bipolar Electrochemical Systems through Luminol Electrochemiluminescence Imaging," *Analytical Chemistry,* vol. 93, no. 23, pp. 8152-8160, 2021/06/15 2021, doi: 10.1021/acs.analchem.0c05397.

[32] A. Juris, V. Balzani, F. Barigelletti, S. Campagna, P. Belser, and A. von Zelewsky, "Ru(II) polypyridine complexes: photophysics, photochemistry, eletrochemistry, and chemiluminescence," *Coordination Chemistry Reviews,* vol. 84, pp. 85-277, 1988/03/01/ 1988, doi: https://doi.org/10.1016/0010-8545(88)80032-8.

[33] D. Lazowick, T. J. Meyer, M. Pressman, and D. Peterson, "Orbital Herniation Associated With Noninvasive Positive Pressure Ventilation," *Chest,* vol. 113, no. 3, pp. 841-843, 1998/03/01/ 1998, doi: https://doi.org/10.1378/chest.113.3.841.

[34] Y. Luo, F. Lv, M. Wang, L. Lu, Y. Liu, and X. Xiong, "A multicolor electrochemiluminescence device based on closed bipolar electrode for rapid visual screening of Salmonella typhimurium," *Sensors and Actuators B: Chemical,* vol. 349, p. 130761, 2021/12/15/ 2021, doi: https://doi.org/10.1016/j.snb.2021.130761.

[35] W. Guo, H. Ding, C. Gu, Y. Liu, X. Jiang, B. Su, and Y. Shao, "Potential-Resolved Multicolor Electrochemiluminescence for Multiplex Immunoassay in a Single Sample," *Journal of the American Chemical Society,* vol. 140, no. 46, pp. 15904-15915, 2018/11/21 2018, doi: 10.1021/jacs.8b09422.

[36] E. Kerr, E. H. Doeven, G. J. Barbante, C. F. Hogan, D. J. Hayne, P. S. Donnelly, and P. S. Francis, "New perspectives on the annihilation electrogenerated chemiluminescence of mixed metal complexes in solution," *Chemical Science,* 10.1039/C6SC01570K vol. 7, no. 8, pp. 5271-5279, 2016, doi: 10.1039/C6SC01570K.

[37] E. H. Doeven, E. M. Zammit, G. J. Barbante, P. S. Francis, N. W. Barnett, and C. F. Hogan, "A potential-controlled switch on/off mechanism for selective excitation in mixed

electrochemiluminescent systems," *Chemical Science,* 10.1039/C2SC21707D vol. 4, no. 3, pp. 977-982, 2013, doi: 10.1039/C2SC21707D.

[38] G. J. Barbante, N. Kebede, C. M. Hindson, E. H. Doeven, E. M. Zammit, G. R. Hanson, C. F. Hogan, and P. S. Francis, "Control of Excitation and Quenching in Multi-colour Electrogenerated Chemiluminescence Systems through Choice of Co-reactant," *Chemistry – A European Journal,* vol. 20, no. 43, pp. 14026-14031, 2014, doi: https://doi.org/10.1002/chem.201403767.

[39] H. Li, L. Bouffier, S. Arbault, A. Kuhn, C. F. Hogan, and N. Sojic, "Spatially-resolved multicolor bipolar electrochemiluminescence," *Electrochemistry Communications,* vol. 77, pp. 10-13, 2017/04/01/ 2017, doi: https://doi.org/10.1016/j.elecom.2017.02.006.

[40] R. M. Crooks, "Principles of Bipolar Electrochemistry," *ChemElectroChem,* vol. 3, no. 3, pp. 357-359, 2016, doi: https://doi.org/10.1002/celc.201500549.

[41] M. Bhaiyya, P. Rewatkar, M. Salve, P. K. Pattnaik, and S. Goel, "Miniaturized Electrochemiluminescence Platform With Laser-Induced Graphene Electrodes for Multiple Biosensing," *IEEE Transactions on NanoBioscience,* vol. 20, no. 1, pp. 79-85, 2021, doi: 10.1109/TNB.2020.3036642.

[42] M. Liu, R. Liu, D. Wang, C. Liu, and C. Zhang, "A low-cost, ultraflexible cloth-based microfluidic device for wireless electrochemiluminescence application," *Lab on a Chip,* 10.1039/C6LC00289G vol. 16, no. 15, pp. 2860-2870, 2016, doi: 10.1039/C6LC00289G.

[43] Y. Xu, B. Lou, Z. Lv, Z. Zhou, L. Zhang, and E. Wang, "Paper-based solid-state electrochemiluminescence sensor using poly(sodium 4-styrenesulfonate) functionalized graphene/nafion composite film," *Analytica Chimica Acta,* vol. 763, pp. 20-27, 2013/02/06/ 2013, doi: https://doi.org/10.1016/j.aca.2012.12.009.

[44] D.-Y. Liu, Y.-Y. Xin, X.-W. He, and X.-B. Yin, "The electrochemiluminescence of ruthenium complex/tripropylamine systems at DNA-modified gold electrodes," *Biosensors and Bioelectronics,* vol. 26, no. 5, pp. 2703-2706, 2011/01/15/ 2011, doi: https://doi.org/10.1016/j.bios.2010.08.074.

[45] L. Zhang, C. Zhao, Y. Bai, Q. Wang, P. Ma, X. Ma, and P. Zhu, "Electrochemiluminescence Enhanced by the Synergetic Effect of Porphyrin and Multi-walled Carbon Nanotubes for Uric Acid Detection," *Electroanalysis,* vol. 34, no. 2, pp. 302-309, 2022, doi: https://doi.org/10.1002/elan.202100287.

[46] J. L. Riis, C. I. Bryce, M. J. Matin, J. L. Stebbins, O. Kornienko, L. v. Huisstede, and D. A. Granger, "The validity, stability, and utility of measuring uric acid in saliva," *Biomarkers in Medicine,* vol. 12, no. 6, pp. 583-596, 2018, doi: 10.2217/bmm-2017-0336.

[47] J. Perelló, P. Sanchis, and F. Grases, "Determination of uric acid in urine, saliva and calcium oxalate renal calculi by high-performance liquid chromatography/mass spectrometry," *Journal of Chromatography B,* vol. 824, no. 1, pp. 175-180, 2005/09/25/ 2005, doi: https://doi.org/10.1016/j.jchromb.2005.07.024.

[48] S. Gupta, M. T. Nayak, J. Sunitha, G. Dawar, N. Sinha, and N. S. Rallan, "Correlation of salivary glucose level with blood glucose level in diabetes mellitus," *Journal of Oral and Maxillofacial Pathology,* vol. 21, no. 3, pp. 334-339, 2017, doi: 10.4103/jomfp.JOMFP_222_15.

Chapter VI. Discussion

The goal of this thesis was to develop an integrated optical, microfluidic, and chemiluminescence system utilizing a complementary metal-oxide-semiconductor (CMOS) chip. The comprehensive literature review in Chapter Two demonstrated that for the development of a fully integrated optical biosensor suitable for point-of-care applications, the CMOS sensor emerged as the optimal choice for a detector. CMOS sensors offer several advantages as pixelated detectors compared to traditional optical detectors such as photomultiplier tubes (PMTs) and avalanche photodiodes (APDs). Unlike PMTs and APDs, which are typically bulky, expensive, and require high voltage for operation, CMOS sensors are compact, cost-effective, and operate at low voltage, making them ideal for portable and scalable biosensing devices. Moreover, when compared to charge-coupled devices (CCDs), CMOS sensors exhibit superior attributes, particularly in terms of power consumption and integration capability. While CCDs are known for their high-quality imaging and sensitivity, they are less energy-efficient and more challenging to integrate with other electronic components. CMOS sensors, on the other hand, are highly energy-efficient, offer faster readout speeds, and can be seamlessly integrated with on-chip signal processing circuitry, thus enhancing the overall functionality and performance of the biosensor. These advantages underscore the suitability of CMOS sensors in developing advanced, point-of-care optical biosensors.

Another option for an optical detector in biosensors, including chemiluminescence (CL) biosensors, is the use of a smartphone camera [74]. Smartphone cameras offer several advantages, such as high accessibility, portability, and cost-effectiveness. They provide a convenient platform for point-of-care diagnostics due to their ubiquity and the integration of advanced imaging capabilities in modern smartphones. Additionally, smartphone cameras are equipped with high-resolution sensors and powerful image processing software, making them capable of detecting subtle optical signals. However, despite these benefits, there are notable disadvantages associated with their use as biosensor detectors. One significant drawback is the variability in camera specifications across different smartphone models. Variations in sensor quality, lens configuration, and image processing algorithms can lead to inconsistent data acquisition and analysis. This inconsistency necessitates the development of calibration protocols, post-processing algorithms, or open-source applications to standardize and adjust

the imaging parameters, ensuring accurate and reliable results. Such additional steps can complicate the biosensing process and limit the straightforward applicability of smartphone cameras in a standardized biosensor platform. Consequently, I evaluated adopting other detectors such as CMOS image sensor for our integrated optical biosensor platform, given the challenges associated with ensuring uniform performance across various devices.

It is also important to note that smartphone cameras operate as lens-based platforms. The reliance on lenses in smartphone cameras presents both benefits and limitations for their use in biosensing applications. On one hand, lenses can enhance image resolution and focus, enabling detailed visualization of the target analytes. However, the inherent complexity and variability of lens systems pose significant challenges. Lenses introduce optical aberrations and require precise alignment, which can complicate the design and operation of biosensors. Moreover, the diversity in lens specifications across different smartphone models worsens the need for extensive calibration and adjustment to achieve consistent and accurate measurements.

Conversely, lensless imaging platforms offer a promising alternative for biosensing applications. By eliminating the need for lenses, lensless systems reduce optical complexity and potential aberrations, resulting in a more straightforward and robust design. Lensless imaging typically involves the use of diffraction and computational algorithms to reconstruct images, which can simplify the optical setup and enhance the system's compactness and portability [75]. Additionally, lensless systems can achieve high-resolution imaging without the need for bulky lens assemblies, making them ideal for integration into miniature and cost-effective biosensors. The absence of lenses also reduces the dependence on mechanical adjustments and alignment, thereby improving the ease of use and reliability of the biosensing platform. These advantages highlight the potential of lensless imaging systems to overcome the limitations associated with lens-based platforms, offering a more efficient and scalable solution for point-of-care diagnostics and other biomedical applications.

Lensless contact imaging is a technique where the sample is placed in close proximity to the sensor. This method can be implemented through either geometric shadow-based or luminescence-based modalities. Shadow-based imaging significantly reduces diffraction artifacts due to the extremely small sample-sensor distance. This simplification bypasses the need for intricate image reconstruction algorithms, making it a more straightforward approach compared to diffraction shadow imaging [76]. Luminescence-based contact imaging,

encompassing CL, ECL, and bioluminescence (BL) techniques, offers enhanced optical contrast relative to shadow-based methods. Furthermore, it enables quantitative analysis of sample constituents.

Luminescence-based lensless contact imaging harnesses the light emitted from samples through CL, ECL, or BL to produce images with superior optical contrast and quantitative analyte detection capabilities. The close proximity between the sample and sensor optimizes photon collection [76]. In CL-based lensless contact imaging, light generated from chemical reactions is captured by the sensor. This technique employs labels such as luminol or enzymes to quantify various biomolecules, making it valuable for food safety, diagnostics, and health monitoring. BL-based imaging utilizes genetically engineered cells emitting light upon analyte interaction. The direct correlation between bioluminescence intensity and cell viability renders this method suitable for toxicity assessment. ECL-based imaging leverages light emission from electrochemical reactions. In addition to the parameters of CL, ECL reactions are more controlled due to the use of electric potential, making them potentially advantageous for lensless contact imaging.

For selecting an appropriate CMOS sensor, I considered several critical factors to optimize the performance of the biosensor platform. One of the primary considerations was achieving a large field of view (FOV). A larger FOV is advantageous as it allows for an expanded detection region, enabling the simultaneous analysis of multiple targets and increasing the throughput of the biosensing system. Additionally, I prioritized sensors with smaller pixel sizes to enhance the resolution of the captured images. Higher resolution is crucial for accurately detecting and quantifying low-abundance biomolecules, as it provides finer detail and clarity in the images. Another important factor in my selection process was the adoption of backside-illuminated (BSI) technology. BSI sensors are more sensitive to light because their design minimizes the obstruction of light by the metal wiring layers, allowing more photons to reach the photodiodes. This increased light sensitivity is particularly beneficial in low-light conditions typical of many biosensing applications, ensuring higher signal-to-noise ratios and improving the overall accuracy and reliability of the measurements. By considering these factors—large field of view, smaller pixel size, and backside-illuminated technology—I aimed to enhance the detection capabilities and performance of the CMOS-based biosensor.

In selecting chemiluminescence as the optical modality for this project, I considered its distinct advantages over other optical methods such as spectrometry and fluorescence. Chemiluminescence, which involves the emission of light as a result of a chemical reaction, offers several key benefits that make it particularly suitable for sensitive and specific biosensing applications. Unlike spectrometry, which often requires complex instrumentation and can suffer from interference due to the absorption and scattering of light by the sample matrix, chemiluminescence generates light intrinsically, thereby eliminating the need for an external light source and reducing background noise significantly. This intrinsic generation of light not only simplifies the detection system but also enhances the signal-to-noise ratio, leading to more accurate and reliable measurements. Furthermore, compared to fluorescence, chemiluminescence avoids issues related to photobleaching and phototoxicity, as there is no requirement for light excitation, which can degrade fluorescent markers and damage biological samples over time. The absence of excitation light also eliminates the need for filter sets and dichroic mirrors, reducing optical complexity and improving ease of integration with microfluidic systems. Additionally, chemiluminescence assays typically exhibit high sensitivity, often detecting analytes at very low concentrations, making them ideal for applications requiring precise quantification of biomolecules. These advantages underscore the rationale behind choosing chemiluminescence as the optical detection method in this project, as it provides a robust, sensitive, and straightforward approach for developing an integrated biosensing system.

The ATP assay plays a critical role in food safety by providing a rapid and reliable method for detecting microbial contamination and verifying sanitation processes. ATP, or adenosine triphosphate, is a universal energy molecule found in all living cells, and its presence on surfaces and equipment can indicate the existence of biological contamination. This makes ATP assays an essential tool for ensuring hygiene in food processing environments, ultimately safeguarding public health. The developed bioluminescence biosensor for ATP detection presents a promising alternative to commercial luminometers, which are currently considered the gold standard for on-site testing and typically cost several thousand dollars. By integrating optical, and bioluminescent technologies, the biosensor offers comparable sensitivity and specificity in detecting ATP. Moreover, the compact and portable design of the biosensor facilitates its use in various settings, providing a cost-effective and efficient solution for continuous and real-time monitoring of food surface contamination. This ensures compliance

with stringent health regulations and standards, making it an accessible and practical tool for a wide range of food safety applications.

In addition to the aforementioned advantages of CL, shifting to ECL provided an additional parameter that can be precisely controlled: the electric potential. The ability to modulate the electric potential introduces a new dimension of control over the CL process, allowing for precise tuning of the luminescent response. This control is particularly beneficial for multiplexing applications, as different luminophores can be selectively activated at specific potentials, enabling the simultaneous detection of multiple analytes within a single assay. Furthermore, since the location of ECL emission is proximate to the working electrode, the spatial control of the emission is feasible. This spatial control allows for the targeted illumination of specific regions within the microfluidic device, enhancing the resolution and specificity of the detection process. By leveraging the electric potential and spatial control, the developed ECL biosensor can achieve high sensitivity and specificity, making it a versatile and powerful tool for a wide range of biosensing applications. This advancement not only improves the performance of the biosensor but also broadens its potential applications in complex analytical scenarios, thereby contributing to the field of biosensor technology.

By shifting to ECL, the need for controlling and manipulating small sample volumes increased, necessitating the design and integration of a microfluidic chip into the system. The microfluidics field emerged in the 1980s as a response to challenges associated with handling minuscule liquid volumes. Its applications expanded rapidly, encompassing biomedical diagnostics, environmental monitoring, and food safety. Given the limitations in sample availability common in biomedical research, microfluidics gained significant traction. Over time, a shift from traditional materials like glass and silicon to polymers facilitated the integration of microfluidics with biological processes, giving rise to bio-microfluidics [76]. These systems excelled in manipulating biological samples on a small scale while simulating in vivo conditions.

The subsequent development of lab-on-a-chip technology enabled microfluidic devices to perform complete sample-to-result analyses. These point-of-care devices offered cost-effective, disposable alternatives to centralized diagnostic laboratories. By integrating microfluidics with image sensors, compact biosensing systems capable of capturing both sample shadows and analyte-specific optical signals were created. This integration enhanced

throughput and sensitivity, enabling applications from cell counting to analyte quantification across various fields. Nevertheless, realizing the full potential of these systems has been hindered by challenges related to material selection, fabrication methods, and detection techniques.

Microfluidic device miniaturization has gained substantial interest due to its potential for reduced reagent consumption, enhanced sensitivity, and increased throughput. However, integrating these miniaturized systems with lensless platforms remains a formidable challenge.

Microfluidic devices necessitate the manipulation of liquids within sub-100 micrometer dimensions. This requires enclosed channels to direct fluid flow. Initial microchips often employed techniques adapted from the semiconductor industry, utilizing glass and silicon substrates. Subsequently, the emergence of soft lithography facilitated a shift towards silicone-based materials, particularly polydimethylsiloxane (PDMS), due to its favorable optical, mechanical, and biocompatible properties. Soft lithography replicates patterns from a hard mold onto a soft polymer, enabling the creation of microchannels. Although photolithography was the predominant mold fabrication method, the associated costs and technical expertise spurred the exploration of alternative approaches. For geometries resembling existing materials, direct molding became a practical option [76].

Despite their advantages, these techniques were limited to two-dimensional structures with uniform heights. To address this, researchers sought to adapt 3D printing for microfluidics fabrication [76]. While early 3D printers lacked the necessary spatial resolution, recent advancements have enabled the creation of sub-100 micrometer channels, facilitating the production of complex microfluidic systems. However, chemical interactions between 3D-printed materials and PDMS can impede the curing process, necessitating post-treatment steps.

To further enhance microfluidic complexity, the field has explored beyond traditional stereolithography. Two-photon polymerization offers exceptional spatial resolution by utilizing non-linear light absorption to create minute solid structures within a liquid resin. This technique enables the fabrication of intricate three-dimensional microfluidic components. Additionally, nanolithography has emerged as a powerful tool for creating nanometer-scale patterns, providing precise control over picoliter liquid volumes.

As mentioned before, maintaining close proximity between the sample and image sensor is crucial for both shadow-based and luminescence-based lensless contact imaging. For shadow-based imaging, minimizing the distance between the sample and sensor enhances image contrast by reducing diffraction artifacts, resulting in shadows that more accurately represent the sample's physical features. In luminescence-based imaging, this proximity is essential to maximize photon capture efficiency, as the emitted light disperses rapidly. By positioning the sample close to the sensor, a greater number of photons can be collected before significant light divergence occurs. Furthermore, in multi-channel microfluidic devices, minimizing this distance aids in accurately identifying the luminescence source. To achieve optimal sample-sensor alignment, the microfluidic device is designed to conform to the image sensor's topography, ensuring direct contact between the fluidic channel and the sensor's active area. However, integrating microfluidic components with the image sensor presents challenges due to the significant size disparity between microelectronic elements and microfluidic ports. To overcome this, the entire microfluidic device can be accommodated within the sensor's active area, or the fluidic channels can be extended beyond the sensor by embedding it in a planarizing material like epoxy.

Post-fabrication, PDMS microchannels are typically sealed using materials such as glass, silicon, or other polymers to create an impermeable barrier. This process often involves forming irreversible chemical bonds between the PDMS and the sealing material. Traditionally, this bonding has relied on the creation of hydroxyl groups through oxygen plasma or chemical oxidation, which facilitates adhesion between silicone-based surfaces. However, this method is primarily suitable for flat surfaces and silicone-based materials, limiting its applicability in more complex scenarios.

Integrating microfluidic devices with lensless imaging platforms presents unique challenges due to the uneven surface of image sensors. To address this, a polymer coating can be applied to the chip to create a flat surface, enabling conventional bonding techniques. This coating can also potentially match the refractive index of the surface of the sensor. However, the high viscosity of common PDMS formulations necessitates dilution with solvents, which can introduce risks to other device components. Furthermore, the additional polymer layer between the lens and chip can introduce optical aberrations.

The incorporation of liquid sample loading mechanisms into peripheral equipment poses an additional challenge for integrating lensless platforms into biomicrofluidic systems. In the field of micro total analysis systems (microTAS), which aim to miniaturize and automate the entire analytical process, this challenge is particularly pertinent. In this project, I manually prepared solutions and pipetted them into the microfluidic channels. While this approach allowed for precise control over the experimental conditions, it is labor-intensive and susceptible to variability. To further improve the system, the integration of automated mixing, incubation, and sample handling directly on the microfluidic chip could be implemented. This would involve the development of on-chip mechanisms for fluid manipulation, such as integrated pumps and mixers, enabling the entire process to be performed within the microfluidic device. Such advancements would enhance the reproducibility and efficiency of the biosensing system, aligning it more closely with the principles of microTAS. By automating these steps, the system could achieve higher throughput and consistency, paving the way for more sophisticated and reliable biomicrofluidic applications.

To further improve the ECL device, I expanded its capabilities to include multiplexing, thereby enhancing its throughput and enabling the simultaneous detection of multiple analytes. Several options exist to achieve high throughput multiplexing in ECL devices. One approach involves the use of arrays of electrodes, where each electrode can be individually addressed and functionalized with different capture probes, allowing parallel detection of multiple targets. Another strategy employs different luminophore tags, each emitting light at distinct wavelengths, facilitating the discrimination of various analytes based on their emission spectra. In my project, I implemented multicolor multiplexing by tuning the ECL color through the adjustment of the applied electric potential. By precisely controlling the electric potential, it was possible to elicit different luminescent responses from various luminophores, enabling the simultaneous detection and differentiation of multiple targets within a single assay. This method leverages the unique electrochemical properties of luminophores and their potential-dependent emission characteristics, providing a robust and efficient approach to multiplexing in ECL devices. Through this enhancement, the ECL device achieved higher sensitivity and specificity, broadening its applicability in complex biosensing scenarios.

In all ECL data analyses conducted, I primarily focused on the correlation between light intensity and variations in concentration and voltage. The results consistently demonstrated a

positive correlation, with increased concentration and voltage leading to higher light intensity. However, an area that warrants further investigation is the correlation between the emission area (or distance) and these parameters. Increasing the concentration of hydrogen peroxide results in a greater amount of luminol being excited and emitting light from the same region, leading to an increase in the intensity while the region of emission remains relatively constant. In contrast, raising the voltage causes a larger area of the electrochemical cell to exceed the threshold electric potential required for luminol excitation, thereby expanding the emission area as well. This phenomenon aligns with the concept of "ECL based on distance readout," where the spatial distribution of ECL emission provides valuable analytical information [77]. Studying the emission distance or area could offer additional insights into ECL behavior, particularly in single-electrode configuration ECL devices. By exploring these spatial dimensions, it is possible to enhance the understanding and optimization of ECL systems, potentially leading to improved sensitivity and specificity in biosensing applications.

Another area that can be further improved in this platform is the data handling and user interface. In this project, I connected the biosensor platform to a Raspberry Pi computer, which in turn was connected to a touchscreen LCD for data display and interaction. While this setup provided a robust and accessible means of interfacing with the biosensor, it is possible to streamline the system further by incorporating a Bluetooth module. By doing so, data from the biosensor could be wirelessly transferred to a smartphone, eliminating the need for the Raspberry Pi and LCD. An application could be developed for the smartphone to perform the necessary data analysis and present the results in a user-friendly manner. This approach would not only simplify the hardware requirements and reduce costs but also enhance the portability and convenience of the biosensor platform. Users would benefit from the seamless integration with mobile technology, allowing for more intuitive and flexible interaction with the biosensor, thereby broadening its applicability and accessibility in various settings.

In this chapter, various aspects of the integrated optical, microfluidic, and electrochemiluminescence system developed in this project have been analyzed and evaluated. The choice of a CMOS sensor was justified based on its large field of view, high resolution due to smaller pixel size, and enhanced sensitivity from backside-illuminated technology. Chemiluminescence was selected as the optical modality for its superior signal-to-noise ratio and absence of photobleaching, outperforming other methods such as spectrometry and

fluorescence. The potential for further improvements was identified, including the shift to ECL for added control through electric potential, and the exploration of spatial control of ECL emission for enhanced biosensor functionality. The current manual sample preparation process was recognized as an area for future automation, aligning with the principles of micro total analysis systems (microTAS) for improved efficiency and reproducibility. Additionally, the integration of a Bluetooth module for data transfer to smartphones was proposed to streamline the user interface and enhance portability. The innovative approach of studying emission area and distance in ECL, inspired by the "ECL based on distance readout" concept, was highlighted as a promising avenue for advancing ECL technology. A critical next step involves navigating regulatory pathways such as FDA approval and ISO certification. These processes will require robust clinical validation and documentation to demonstrate compliance with industry standards. Overall, these discussions underscore the potential of the developed biosensor platform to significantly contribute to the fields of biosensing and point-of-care diagnostics, with several pathways for future enhancement and optimization.

Conclusions and outlook

This PhD thesis has focused on the development and optimization of an integrated optical, microfluidic, and chemiluminescence (CL) biosensor platform utilizing a complementary metal-oxide-semiconductor (CMOS) chip. The project studied (Aim 1) and successfully demonstrated(Aim 2 and Aim 3) the potential of combining CL and ECL with microfluidics and CMOS technology to create a portable, sensitive, and cost-effective diagnostic tool for point-of-care (POC) applications. The use of CMOS sensors, with their large field of view, high resolution, and enhanced sensitivity, proved to be a crucial factor in achieving the desired performance. The integration of CL and electrochemiluminescence (ECL) modalities into the platform allowed for the detection and quantification of various analytes with high sensitivity and specificity, making the system suitable for diverse applications, including medical diagnostics, environmental monitoring, and food safety.

This work also highlighted the advantages of ECL over other optical methods, such as fluorescence, particularly in terms of background noise reduction, signal-to-noise ratio, and the ability to control the luminescent response through electric potential. The successful implementation of multicolor multiplexing and the exploration of spatial control of ECL emission further enhanced the platform's functionality, enabling the simultaneous detection of multiple analytes (Aim 3). Additionally, the incorporation of microfluidic devices enabled precise sample handling and improved the system's overall efficiency.

Adenosine triphosphate (ATP) detection plays a vital role in ensuring food safety by serving as a reliable indicator of microbial contamination and overall cleanliness in food processing environments. ATP, a molecule present in all living cells, including bacteria, yeasts, and molds, is used as a universal marker for detecting the presence of organic matter and microbial load on surfaces and in food products. The rapid and accurate detection of ATP is crucial for preventing foodborne illnesses and maintaining high hygiene standards in the food industry. Traditional methods, such as culture-based techniques, involve growing microorganisms on selective media, which, although highly specific, can be time-consuming and may delay the decision-making process. In contrast, the use of a luminometer for on-site ATP testing offers a faster and more practical approach, allowing for real-time monitoring and immediate corrective actions. This method is based on the bioluminescence reaction between ATP and luciferase

enzyme, which produces light proportional to the amount of ATP present. As a result, luminometers provide a rapid and quantitative measure of contamination, making them an invaluable tool for ensuring food safety in real-time and minimizing the risk of foodborne outbreaks.

The development of the ATP detection biosensor (presented in chapter III) based on Complementary Metal-Oxide-Semiconductor (CMOS) technology presents a transformative advancement for food safety, offering a cost-effective and user-friendly alternative to traditional luminometers. CMOS-based biosensors leverage the integration of bioluminescence detection directly onto a microchip, enabling the miniaturization and mass production of highly sensitive ATP detection devices at a fraction of the cost of conventional luminometers. This significant reduction in cost makes these biosensors more accessible to a broader range of food industry stakeholders, particularly small and medium-sized enterprises that may have previously been unable to afford frequent and comprehensive hygiene monitoring. Additionally, the user-friendly nature of CMOS-based ATP biosensors simplifies the testing process, requiring minimal technical expertise and reducing the potential for operator error. By facilitating more widespread and regular monitoring of ATP levels, these biosensors enhance the ability to promptly identify and address microbial contamination, ultimately contributing to safer food production and reducing the incidence of foodborne illnesses.

Uric acid is a crucial biomarker for the diagnosis of gout, a form of inflammatory arthritis characterized by the accumulation of monosodium urate crystals in joints, leading to severe pain, swelling, and redness. Gout often manifests as sudden and intense episodes of joint pain, commonly affecting the big toe, but it can also involve other joints such as the knees, ankles, and wrists. Elevated levels of uric acid in the blood, known as hyperuricemia, are strongly associated with the development of gout, as they lead to the formation of these painful crystals. Gout is a prevalent condition in North America, with an increasing incidence due to factors such as obesity, dietary habits, and an aging population. In Canada, gout affects approximately 3.2% of the population, with higher prevalence observed in men and older adults. The disease not only impacts the quality of life due to recurrent painful flare-ups but also poses a significant burden on healthcare systems due to its chronic nature and the need for ongoing management.

Additionally, detecting uric acid at the point of care or point of need is critical for effectively managing gout, particularly during urate-lowering therapy (ULT) (presented in chapter IV).

ULT aims to reduce and maintain uric acid levels below a specific threshold to prevent the formation of urate crystals and subsequent gout flare-ups. Regular monitoring of uric acid levels is essential to ensure that the therapy is working effectively and to adjust the dosage as needed. Point-of-care testing offers the advantage of providing immediate results, allowing for timely interventions and more personalized management of the disease. For patients, this means they can avoid the delays and inconvenience associated with traditional laboratory testing, enabling more frequent and accessible monitoring. This is especially important during the early stages of ULT, where achieving and maintaining target uric acid levels is crucial to prevent further joint damage and improve overall outcomes. Moreover, point-of-care detection can empower patients by giving them the tools to actively participate in managing their condition, potentially reducing the frequency and severity of gout attacks and improving their quality of life.

Finaly, the detection of multiple analytes (presented in chapter V), such as uric acid and glucose, at the point of care represents a significant advancement in health monitoring, offering a comprehensive approach to managing chronic diseases and metabolic disorders. By integrating the detection of these critical biomarkers into a single device, healthcare providers and patients can obtain real-time insights into various physiological conditions, enabling more precise and timely interventions. For instance, simultaneous monitoring of uric acid and glucose levels can be particularly beneficial for individuals managing gout and diabetes, where tight control of these biomarkers is essential to prevent complications. Moreover, the versatility of the device's configuration allows for the detection of additional analytes, such as cholesterol, lactate, and creatinine, further broadening its application across different health conditions. This multi-analyte detection capability not only enhances the efficiency of point-of-care testing but also reduces the need for multiple devices, lowering costs and simplifying the user experience. Such advancements contribute to more personalized and proactive healthcare, improving patient outcomes by enabling continuous monitoring and more informed decision-making.

However, several challenges remain, particularly in terms of automating the sample preparation process and improving data handling and user interface design. The manual preparation and handling of samples, while effective, were labor-intensive and subject to variability. Future work should focus on automating these processes to increase throughput and reproducibility.

The integration of wireless data transfer and smartphone-based analysis was also identified as a potential improvement, which could simplify the hardware requirements and enhance the portability of the platform.

Building on the findings of this research, future work should focus on several key areas to further enhance the capabilities and applicability of the developed biosensor platform. One priority is the automation of sample preparation, mixing, and handling directly on the microfluidic chip. This could be achieved by developing on-chip mechanisms such as integrated pumps and mixers, which would align the system more closely with the principles of micro total analysis systems (microTAS) and improve its reproducibility and efficiency.

Another area for future exploration is the enhancement of multiplexing capabilities through the continued refinement of ECL techniques. By further optimizing the control of electric potential and the use of different luminophores, the platform could be expanded to detect a broader range of analytes simultaneously. This would be particularly valuable in medical diagnostics, where the simultaneous detection of multiple biomarkers is crucial for accurate and timely disease diagnosis.

The integration of wireless data transfer via Bluetooth modules and the development of smartphone applications for data analysis and visualization should also be pursued. This would not only reduce the system's complexity and cost but also enhance its portability and user-friendliness, making it more accessible for POC applications in diverse settings.

Finally, future research should explore the potential of combining ECL with other emerging technologies, such as machine learning algorithms, to improve data analysis and interpretation. By leveraging machine learning, the platform could achieve more sophisticated and accurate diagnostic capabilities, paving the way for more advanced and accessible biosensing solutions in the future.

Reference list

(non-manuscript sections)

[1] R. Abbasi, X. Hu, A. Zhang, I. Dummer, and S. Wachsmann-Hogiu, "Optical Image Sensors for Smart Analytical Chemiluminescence Biosensors," *Bioengineering,* 11, 912. https://doi.org/10.3390/bioengineering11090912.

[2] R. Abbasi, M. Imanbekova, and S. Wachsmann-Hogiu, "On-chip bioluminescence biosensor for the detection of microbial surface contamination," *Biosensors and Bioelectronics,* vol. 254, p. 116200, 2024/06/15/ 2024, doi: https://doi.org/10.1016/j.bios.2024.116200.

[3] R. Abbasi, J. Liu, S. Suarasan, and S. Wachsmann-Hogiu, "SE-ECL on CMOS: a miniaturized electrochemiluminescence biosensor," *Lab on a Chip,* 10.1039/D1LC00905B vol. 22, no. 5, pp. 994-1005, 2022, doi: 10.1039/D1LC00905B.

[4] R. Abbasi and S. Wachsmann-Hogiu, "Optimization and miniaturization of SE-ECL for potential-resolved, multi-color, multi-analyte detection," *Biosensors and Bioelectronics,* vol. 257, p. 116322, 2024/08/01/ 2024, doi: https://doi.org/10.1016/j.bios.2024.116322.

[5] B. Purohit, P. R. Vernekar, N. P. Shetti, and P. Chandra, "Biosensor nanoengineering: Design, operation, and implementation for biomolecular analysis," *Sensors International,* vol. 1, p. 100040, 2020/01/01/ 2020, doi: https://doi.org/10.1016/j.sintl.2020.100040.

[6] Y.-C. Chen, Y.-L. Jian, K.-H. Chiu, and H.-K. Yak, "Simultaneous Speciation of Iron(II) and Iron(III) by Ion Chromatography with Chemiluminescence Detection," *Analytical Sciences,* vol. 28, no. 8, pp. 795-799, 2012, doi: 10.2116/analsci.28.795.

[7] Y. Hu, G. Li, and Z. Zhang, "A flow injection chemiluminescence method for the determination of lincomycin in serum using a diperiodato-cuprate (III)–luminol system," *Luminescence,* vol. 26, no. 5, pp. 313-318, 2011, doi: 10.1002/bio.1230.

[8] C. Zhang, H. Qi, and M. Zhang, "Homogeneous electrogenerated chemiluminescence immunoassay for the determination of digoxin employing Ru(bpy)2(dcbpy)NHS and carrier protein," *Luminescence,* vol. 22, no. 1, pp. 53-59, 2007, doi: 10.1002/bio.926.

[9] W. Neupert, R. Oelkers, K. Brune, and G. Geisslinger, "A new reliable chemiluminescence immunoassay (CLIA) for prostaglandin E2 using enhanced luminol as substrate," *Prostaglandins,* vol. 52, no. 5, pp. 385-401, 1996/11/01/ 1996, doi: https://doi.org/10.1016/S0090-6980(96)00103-7.

[10] A. J. Bard, *Electrogenerated chemiluminescence*. CRC Press, 2004.

[11] M. M. Richter, "Electrochemiluminescence (ECL)," *Chemical Reviews,* vol. 104, no. 6, pp. 3003-3036, 2004/06/01 2004, doi: 10.1021/cr020373d.

[12] S. Kirschbaum and A. Baeumner, "A review of electrochemiluminescence (ECL) in and for microfluidic analytical devices," *Analytical and bioanalytical chemistry,* vol. 407, 03/15 2015, doi: 10.1007/s00216-015-8557-x.

[13] W. Gao, K. Muzyka, X. Ma, B. Lou, and G. Xu, "A single-electrode electrochemical system for multiplex electrochemiluminescence analysis based on a resistance induced potential difference," *Chemical Science,* 10.1039/C8SC00410B vol. 9, no. 16, pp. 3911-3916, 2018, doi: 10.1039/C8SC00410B.

[14] R. Singh, A. Feltmeyer, O. Saiapina, J. Juzwik, B. Arenz, and A. Abbas, "Rapid and PCR-free DNA Detection by Nanoaggregation-Enhanced Chemiluminescence," *Scientific Reports,* vol. 7, no. 1, p. 14011, 2017/10/25 2017, doi: 10.1038/s41598-017-14580-w.

[15] B. Al Mughairy and H. A. J. Al-Lawati, "Recent analytical advancements in microfluidics using chemiluminescence detection systems for food analysis," *TrAC Trends in Analytical Chemistry,* vol. 124, p. 115802, 2020/03/01/ 2020, doi: https://doi.org/10.1016/j.trac.2019.115802.

[16] S. K. Vashist, "Point-of-care diagnostics: Recent advances and trends," ed: Multidisciplinary Digital Publishing Institute, 2017.

[17] W. Lv, H. Ye, Z. Yuan, X. Liu, X. Chen, and W. Yang, "Recent advances in electrochemiluminescence-based simultaneous detection of multiple targets," *TrAC Trends in Analytical Chemistry,* vol. 123, p. 115767, 2020/02/01/ 2020, doi: https://doi.org/10.1016/j.trac.2019.115767.

[18] M.-S. Wu, Z. Liu, H.-W. Shi, H.-Y. Chen, and J.-J. Xu, "Visual Electrochemiluminescence Detection of Cancer Biomarkers on a Closed Bipolar Electrode Array Chip," *Analytical Chemistry,* vol. 87, no. 1, pp. 530-537, 2015/01/06 2015, doi: 10.1021/ac502989f.

[19] Y.-Z. Wang, C.-H. Xu, W. Zhao, Q.-Y. Guan, H.-Y. Chen, and J.-J. Xu, "Bipolar Electrode Based Multicolor Electrochemiluminescence Biosensor," *Analytical Chemistry,* vol. 89, no. 15, pp. 8050-8056, 2017/08/01 2017, doi: 10.1021/acs.analchem.7b01494.

[20] B. Babamiri, R. Hallaj, and A. Salimi, "Ultrasensitive electrochemiluminescence immunoassay for simultaneous determination of CA125 and CA15-3 tumor markers based on PAMAM-sulfanilic acid-Ru(bpy)32+ and PAMAM-CdTe@CdS nanocomposite," *Biosensors*

and Bioelectronics, vol. 99, pp. 353-360, 2018/01/15/ 2018, doi: https://doi.org/10.1016/j.bios.2017.07.062.

[21] B. S. Munge, T. Stracensky, K. Gamez, D. DiBiase, and J. F. Rusling, "Multiplex Immunosensor Arrays for Electrochemical Detection of Cancer Biomarker Proteins," *Electroanalysis,* vol. 28, no. 11, pp. 2644-2658, 2016, doi: https://doi.org/10.1002/elan.201600183.

[22] P. S. Pakchin, S. A. Nakhjavani, R. Saber, H. Ghanbari, and Y. Omidi, "Recent advances in simultaneous electrochemical multi-analyte sensing platforms," *TrAC Trends in Analytical Chemistry,* vol. 92, pp. 32-41, 2017/07/01/ 2017, doi: https://doi.org/10.1016/j.trac.2017.04.010.

[23] H. Chen, C. Chen, S. Bai, Y. Gao, G. Metcalfe, W. Cheng, and Y. Zhu, "Multiplexed detection of cancer biomarkers using a microfluidic platform integrating single bead trapping and acoustic mixing techniques," *Nanoscale,* 10.1039/C8NR06367B vol. 10, no. 43, pp. 20196-20206, 2018, doi: 10.1039/C8NR06367B.

[24] J. Tian, L. Zhou, Y. Zhao, Y. Wang, Y. Peng, and S. Zhao, "Multiplexed detection of tumor markers with multicolor quantum dots based on fluorescence polarization immunoassay," *Talanta,* vol. 92, pp. 72-77, 2012/04/15/ 2012, doi: https://doi.org/10.1016/j.talanta.2012.01.051.

[25] J. Chang, X. Wang, J. Wang, H. Li, and F. Li, "Nucleic Acid-Functionalized Metal–Organic Framework-Based Homogeneous Electrochemical Biosensor for Simultaneous Detection of Multiple Tumor Biomarkers," *Analytical Chemistry,* vol. 91, no. 5, pp. 3604-3610, 2019/03/05 2019, doi: 10.1021/acs.analchem.8b05599.

[26] C. Li, Z. Fu, Z. Li, Z. Wang, and W. Wei, "Cross-talk-free multiplexed immunoassay using a disposable electrochemiluminescent immunosensor array coupled with a non-array detector," *Biosensors and Bioelectronics,* vol. 27, no. 1, pp. 141-147, 2011/09/15/ 2011, doi: https://doi.org/10.1016/j.bios.2011.06.031.

[27] L. Wang, W. Wei, J. Han, and Z. Fu, "Individually addressable electrode array for multianalyte electrochemiluminescent immunoassay based on a sequential triggering strategy," *Analyst,* 10.1039/C2AN15965A vol. 137, no. 3, pp. 735-740, 2012, doi: 10.1039/C2AN15965A.

[28] F. Deiss, C. N. LaFratta, M. Symer, T. M. Blicharz, N. Sojic, and D. R. Walt, "Multiplexed Sandwich Immunoassays Using Electrochemiluminescence Imaging Resolved at the Single

Bead Level," *Journal of the American Chemical Society,* vol. 131, no. 17, pp. 6088-6089, 2009/05/06 2009, doi: 10.1021/ja901876z.

[29] M.-S. Wu, H.-W. Shi, L.-J. He, J.-J. Xu, and H.-Y. Chen, "Microchip Device with 64-Site Electrode Array for Multiplexed Immunoassay of Cell Surface Antigens Based on Electrochemiluminescence Resonance Energy Transfer," *Analytical Chemistry,* vol. 84, no. 9, pp. 4207-4213, 2012/05/01 2012, doi: 10.1021/ac300551e.

[30] Y. Zhang, W. Liu, S. Ge, M. Yan, S. Wang, J. Yu, N. Li, and X. Song, "Multiplexed sandwich immunoassays using flow-injection electrochemiluminescence with designed substrate spatial-resolved technique for detection of tumor markers," *Biosensors and Bioelectronics,* vol. 41, pp. 684-690, 2013/03/15/ 2013, doi: https://doi.org/10.1016/j.bios.2012.09.044.

[31] K. Kadimisetty, S. Malla, K. S. Bhalerao, I. M. Mosa, S. Bhakta, N. H. Lee, and J. F. Rusling, "Automated 3D-Printed Microfluidic Array for Rapid Nanomaterial-Enhanced Detection of Multiple Proteins," *Analytical Chemistry,* vol. 90, no. 12, pp. 7569-7577, 2018/06/19 2018, doi: 10.1021/acs.analchem.8b01198.

[32] X. Sun, B. Li, C. Tian, F. Yu, N. Zhou, Y. Zhan, and L. Chen, "Rotational paper-based electrochemiluminescence immunodevices for sensitive and multiplexed detection of cancer biomarkers," *Analytica Chimica Acta,* vol. 1007, pp. 33-39, 2018/05/12/ 2018, doi: https://doi.org/10.1016/j.aca.2017.12.005.

[33] X. Zhang, Q. Zhai, H. Xing, J. Li, and E. Wang, "Bipolar Electrodes with 100% Current Efficiency for Sensors," *ACS Sensors,* vol. 2, no. 3, pp. 320-326, 2017/03/24 2017, doi: 10.1021/acssensors.7b00031.

[34] C. Liu, D. Wang, and C. Zhang, "A novel paperfluidic closed bipolar electrode-electrochemiluminescence sensing platform: Potential for multiplex detection at crossing-channel closed bipolar electrodes," *Sensors and Actuators B: Chemical,* vol. 270, pp. 341-352, 2018/10/01/ 2018, doi: https://doi.org/10.1016/j.snb.2018.04.180.

[35] X. Zhang, C. Chen, J. Li, L. Zhang, and E. Wang, "New Insight into a Microfluidic-Based Bipolar System for an Electrochemiluminescence Sensing Platform," *Analytical Chemistry,* vol. 85, no. 11, pp. 5335-5339, 2013/06/04 2013, doi: 10.1021/ac400805f.

[36] X. Zhang, J. Li, X. Jia, D. Li, and E. Wang, "Full-Featured Electrochemiluminescence Sensing Platform Based on the Multichannel Closed Bipolar System," *Analytical Chemistry,* vol. 86, no. 11, pp. 5595-5599, 2014/06/03 2014, doi: 10.1021/ac501246k.

[37] Q. Zhai, X. Zhang, Y. Han, J. Zhai, J. Li, and E. Wang, "A Nanoscale Multichannel Closed Bipolar Electrode Array for Electrochemiluminescence Sensing Platform," *Analytical Chemistry,* vol. 88, no. 1, pp. 945-951, 2016/01/05 2016, doi: 10.1021/acs.analchem.5b03685.

[38] X. Ma, L. Qi, W. Gao, F. Yuan, Y. Xia, B. Lou, and G. Xu, "A portable wireless single-electrode system for electrochemiluminescent analysis," *Electrochimica Acta,* vol. 308, pp. 20-24, 2019/06/10/ 2019, doi: https://doi.org/10.1016/j.electacta.2019.04.015.

[39] L. Qi, Y. Xia, W. Qi, W. Gao, F. Wu, and G. Xu, "Increasing Electrochemiluminescence Intensity of a Wireless Electrode Array Chip by Thousands of Times Using a Diode for Sensitive Visual Detection by a Digital Camera," *Analytical Chemistry,* vol. 88, no. 2, pp. 1123-1127, 2016/01/19 2016, doi: 10.1021/acs.analchem.5b04304.

[40] X. Feng, N. Gan, H. Zhang, Q. Yan, T. Li, Y. Cao, F. Hu, H. Yu, and Q. Jiang, "A novel “dual-potential” electrochemiluminescence aptasensor array using CdS quantum dots and luminol-gold nanoparticles as labels for simultaneous detection of malachite green and chloramphenicol," *Biosensors and Bioelectronics,* vol. 74, pp. 587-593, 2015/12/15/ 2015, doi: https://doi.org/10.1016/j.bios.2015.06.048.

[41] B. Zhou, M. Zhu, Y. Hao, and P. Yang, "Potential-Resolved Electrochemiluminescence for Simultaneous Determination of Triple Latent Tuberculosis Infection Markers," *ACS Applied Materials & Interfaces,* vol. 9, no. 36, pp. 30536-30542, 2017/09/13 2017, doi: 10.1021/acsami.7b10343.

[42] X. Liu, H. Jiang, Y. Fang, W. Zhao, N. Wang, and G. Zang, "Quantum Dots Based Potential-Resolution Dual-Targets Electrochemiluminescent Immunosensor for Subtype of Tumor Marker and Its Serological Evaluation," *Analytical Chemistry,* vol. 87, no. 18, pp. 9163-9169, 2015/09/15 2015, doi: 10.1021/acs.analchem.5b02660.

[43] B. Babamiri, R. Hallaj, A. Salimi, and K. Akhtari, "Potential-resolved electrochemiluminescence immunoassay for simultaneous determination of CEA and AFP tumor markers using dendritic nanoclusters and Fe3O4@SiO2 nanoparticles," *Microchimica Acta,* vol. 184, no. 9, pp. 3613-3623, 2017/09/01 2017, doi: 10.1007/s00604-017-2386-x.

[44] B. Zhou, M. Zhu, Y. Qiu, and P. Yang, "Novel Electrochemiluminescence-Sensing Platform for the Precise Analysis of Multiple Latent Tuberculosis Infection Markers," *ACS Applied Materials & Interfaces,* vol. 9, no. 22, pp. 18493-18500, 2017/06/07 2017, doi: 10.1021/acsami.7b03211.

[45] F. Han, H. Jiang, D. Fang, and D. Jiang, "Potential-Resolved Electrochemiluminescence for Determination of Two Antigens at the Cell Surface," *Analytical Chemistry,* vol. 86, no. 14, pp. 6896-6902, 2014/07/15 2014, doi: 10.1021/ac501571a.

[46] B. Zhou, Y. Qiu, Q. Wen, M. Zhu, and P. Yang, "Dual Electrochemiluminescence Signal System for In Situ and Simultaneous Evaluation of Multiple Cell-Surface Receptors," *ACS Applied Materials & Interfaces,* vol. 9, no. 3, pp. 2074-2082, 2017/01/25 2017, doi: 10.1021/acsami.6b12411.

[47] H. Gao, Q. Dang, S. Xia, Y. Zhao, H. Qi, Q. Gao, and C. Zhang, "Highly selective electrogenerated chemiluminescence biosensor for simultaneous detection of matrix metalloproteinase-2 and matrix metalloproteinase-7 in cell secretions," *Sensors and Actuators B: Chemical,* vol. 253, pp. 69-76, 2017/12/01/ 2017, doi: https://doi.org/10.1016/j.snb.2017.05.142.

[48] S. Wang, L. Ge, Y. Zhang, X. Song, N. Li, S. Ge, and J. Yu, "Battery-triggered microfluidic paper-based multiplex electrochemiluminescence immunodevice based on potential-resolution strategy," *Lab on a Chip,* 10.1039/C2LC40707H vol. 12, no. 21, pp. 4489-4498, 2012, doi: 10.1039/C2LC40707H.

[49] Y. He, J. Li, and Y. Liu, "Reusable and Dual-Potential Responses Electrogenerated Chemiluminescence Biosensor for Synchronously Cytosensing and Dynamic Cell Surface N-Glycan Evaluation," *Analytical Chemistry,* vol. 87, no. 19, pp. 9777-9785, 2015/10/06 2015, doi: 10.1021/acs.analchem.5b02048.

[50] H. Yang, F. Lu, Y. Sun, Z. Yuan, and C. Lu, "Fluorescent Gold Nanocluster-Based Sensor Array for Nitrophenol Isomer Discrimination via an Integration of Host–Guest Interaction and Inner Filter Effect," *Analytical Chemistry,* vol. 90, no. 21, pp. 12846-12853, 2018/11/06 2018, doi: 10.1021/acs.analchem.8b03394.

[51] Z. Yuan, Y.-C. Chen, H.-W. Li, and H.-T. Chang, "Fluorescent silver nanoclusters stabilized by DNA scaffolds," *Chemical Communications,* 10.1039/C4CC02981J vol. 50, no. 69, pp. 9800-9815, 2014, doi: 10.1039/C4CC02981J.

[52] G. Zou, X. Tan, X. Long, Y. He, and W. Miao, "Spectrum-Resolved Dual-Color Electrochemiluminescence Immunoassay for Simultaneous Detection of Two Targets with Nanocrystals as Tags," *Analytical Chemistry,* vol. 89, no. 23, pp. 13024-13029, 2017/12/05 2017, doi: 10.1021/acs.analchem.7b04188.

[53] J. Zhou, L. Nie, B. Zhang, and G. Zou, "Spectrum-Resolved Triplex-Color Electrochemiluminescence Multiplexing Immunoassay with Highly-Passivated Nanocrystals as Tags," *Analytical Chemistry,* vol. 90, no. 21, pp. 12361-12365, 2018/11/06 2018, doi: 10.1021/acs.analchem.8b04424.

[54] F. Zhang, Y. He, K. Fu, L. Fu, B. Zhang, H. Wang, and G. Zou, "Dual-wavebands-resolved electrochemiluminescence multiplexing immunoassay with dichroic mirror assistant photomultiplier-tubes as detectors," *Biosensors and Bioelectronics,* vol. 115, pp. 77-82, 2018/09/15/ 2018, doi: https://doi.org/10.1016/j.bios.2018.05.006.

[55] Y. Lv, Z. Zhou, Y. Shen, Q. Zhou, J. Ji, S. Liu, and Y. Zhang, "Coupled Fluorometer-Potentiostat System and Metal-Free Monochromatic Luminophores for High-Resolution Wavelength-Resolved Electrochemiluminescent Multiplex Bioassay," *ACS Sensors,* vol. 3, no. 7, pp. 1362-1367, 2018/07/27 2018, doi: 10.1021/acssensors.8b00292.

[56] C.-F. Kuo, L.-C. See, S.-F. Luo, Y.-S. Ko, Y.-S. Lin, J.-S. Hwang, C.-M. Lin, H.-W. Chen, and K.-H. Yu, "Gout: an independent risk factor for all-cause and cardiovascular mortality," *Rheumatology,* vol. 49, no. 1, pp. 141-146, 2009, doi: 10.1093/rheumatology/kep364.

[57] K.-H. Yu, D.-Y. Chen, J.-H. Chen, S.-Y. Chen, S.-M. Chen, T.-T. Cheng, S.-C. Hsieh, T.-Y. Hsieh, P.-F. Hsu, C.-F. Kuo, M.-C. Kuo, H.-C. Lam, I.-T. Lee, T.-H. Liang, H.-Y. Lin, S.-C. Lin, W.-P. Tsai, G. J. Tsay, J. C.-C. Wei, C.-H. Yang, and W.-C. Tsai, "Management of gout and hyperuricemia: Multidisciplinary consensus in Taiwan," *International Journal of Rheumatic Diseases,* vol. 21, no. 4, pp. 772-787, 2018, doi: https://doi.org/10.1111/1756-185X.13266.

[58] P. Mathieu, P. Pibarot, É. Larose, P. Poirier, A. Marette, and J.-P. Després, "Visceral obesity and the heart," *The International Journal of Biochemistry & Cell Biology,* vol. 40, no. 5, pp. 821-836, 2008/01/01/ 2008, doi: https://doi.org/10.1016/j.biocel.2007.12.001.

[59] S. Takahashi, Y. Moriwaki, Z. Tsutsumi, J.-i. Yamakita, T. Yamamoto, and T. Hada, "Increased visceral fat accumulation further aggravates the risks of insulin resistance in gout," *Metabolism - Clinical and Experimental,* vol. 50, no. 4, pp. 393-398, 2001, doi: 10.1053/meta.2001.21688.

[60] N. J. Pagidipati, C. N. Hess, R. M. Clare, A. Akerblom, P. Tricoci, D. Wojdyla, R. T. Keenan, S. James, C. Held, K. W. Mahaffey, A. B. Klein, L. Wallentin, and M. T. Roe, "An examination of the relationship between serum uric acid level, a clinical history of gout, and cardiovascular outcomes among patients with acute coronary syndrome," *American Heart Journal,* vol. 187, pp. 53-61, 2017/05/01/ 2017, doi: https://doi.org/10.1016/j.ahj.2017.02.023.

[61] D. Dhawan and S. Sharma, "Abdominal Obesity, Adipokines and Non-communicable Diseases," *The Journal of Steroid Biochemistry and Molecular Biology,* vol. 203, p. 105737, 2020/10/01/ 2020, doi: https://doi.org/10.1016/j.jsbmb.2020.105737.

[62] K. L. Rock, H. Kataoka, and J.-J. Lai, "Uric acid as a danger signal in gout and its comorbidities," *Nature Reviews Rheumatology,* vol. 9, no. 1, pp. 13-23, 2013/01/01 2013, doi: 10.1038/nrrheum.2012.143.

[63] A. Petersmann, M. Nauck, D. Müller-Wieland, W. Kerner, U. A. Müller, R. Landgraf, G. Freckmann, and L. Heinemann, "Definition, classification and diagnosis of diabetes mellitus," *Experimental and clinical endocrinology & diabetes,* vol. 126, no. 07, pp. 406-410, 2018.

[64] M. J. Klag, D. E. Ford, L. A. Mead, J. He, P. K. Whelton, K.-Y. Liang, and D. M. Levine, "Serum Cholesterol in Young Men and Subsequent Cardiovascular Disease," *New England Journal of Medicine,* vol. 328, no. 5, pp. 313-318, 1993, doi: 10.1056/nejm199302043280504.

[65] H. K. Saini, A. S. Arneja, and N. S. Dhalla, "Role of cholesterol in cardiovascular dysfunction," (in eng), *Can J Cardiol,* vol. 20, no. 3, pp. 333-46, Mar 1 2004.

[66] M. Dehlin, L. Jacobsson, and E. Roddy, "Global epidemiology of gout: prevalence, incidence, treatment patterns and risk factors," *Nature Reviews Rheumatology,* vol. 16, no. 7, pp. 380-390, 2020/07/01 2020, doi: 10.1038/s41584-020-0441-1.

[67] A. Chait and L. J. den Hartigh, "Adipose Tissue Distribution, Inflammation and Its Metabolic Consequences, Including Diabetes and Cardiovascular Disease," (in eng), *Front Cardiovasc Med,* vol. 7, pp. 22-22, 2020, doi: 10.3389/fcvm.2020.00022.

[68] V. Bhole, J. W. J. Choi, S. Woo Kim, M. de Vera, and H. Choi, "Serum Uric Acid Levels and the Risk of Type 2 Diabetes: A Prospective Study," *The American Journal of Medicine,* vol. 123, no. 10, pp. 957-961, 2010/10/01/ 2010, doi: https://doi.org/10.1016/j.amjmed.2010.03.027.

[69] Y. Huang, J. Tan, L. Cui, Z. Zhou, S. Zhou, Z. Zhang, R. Zheng, Y. Xue, M. Zhang, S. Li, N. Zhu, J. Liang, G. Li, L. Zhong, and Y. Zhao, "Graphene and Au NPs co-mediated enzymatic silver deposition for the ultrasensitive electrochemical detection of cholesterol," (in eng), *Biosens Bioelectron,* vol. 102, pp. 560-567, Apr 15 2018, doi: 10.1016/j.bios.2017.11.037.

[70] H. Zhong, R. Yuan, Y. Chai, W. Li, X. Zhong, and Y. Zhang, "In situ chemo-synthesized multi-wall carbon nanotube-conductive polyaniline nanocomposites: characterization and application for a glucose amperometric biosensor," (in eng), *Talanta,* vol. 85, no. 1, pp. 104-11, Jul 15 2011, doi: 10.1016/j.talanta.2011.03.040.

[71] R. Devi and C. S. Pundir, "Construction and application of an amperometric uric acid biosensor based on covalent immobilization of uricase on iron oxide nanoparticles/chitosan-g-polyaniline composite film electrodeposited on Pt electrode," *Sensors and Actuators B: Chemical,* vol. 193, pp. 608-615, 2014/03/31/ 2014, doi: https://doi.org/10.1016/j.snb.2013.12.010.

[72] Z. Chen and Y. Zu, "Selective detection of uric acid in the presence of ascorbic acid based on electrochemiluminescence quenching," *Journal of Electroanalytical Chemistry,* vol. 612, no. 1, pp. 151-155, 2008/01/01/ 2008, doi: https://doi.org/10.1016/j.jelechem.2007.09.018.

[73] J. Ballesta-Claver, I. F. Díaz Ortega, M. C. Valencia-Mirón, and L. F. Capitán-Vallvey, "Disposable luminol copolymer-based biosensor for uric acid in urine," (in eng), *Anal Chim Acta,* vol. 702, no. 2, pp. 254-61, Sep 30 2011, doi: 10.1016/j.aca.2011.06.054.

[74] G. Liu, Y. Wu, Y. Wang, W. Ye, M. Wu, and Q. Liu, "Smartphone-Based Portable Sensing Systems for Point-of-Care Detections," in *Portable and Wearable Sensing Systems*, 2024, pp. 89-110.

[75] S. Moon, H. O. Keles, Y. G. Kim, D. Kuritzkes, and U. Demirci, "Lensless imaging for point-of-care testing," in *2009 Annual International Conference of the IEEE Engineering in Medicine and Biology Society*, 3-6 Sept. 2009 2009, pp. 6376-6379, doi: 10.1109/IEMBS.2009.5333765.

[76] X. Hu, R. Abbasi, and S. Wachsmann-Hogiu, "Microfluidics on lensless, semiconductor optical image sensors: challenges and opportunities for democratization of biosensing at the micro-and nano-scale," *Nanophotonics,* vol. 12, no. 21, pp. 3977-4008, 2023, doi: doi:10.1515/nanoph-2023-0301.

[77] N. Hao, Y. Zou, Y. Qiu, L. Zhao, J. Wei, J. Qian, and K. Wang, "Visual Electrochemiluminescence Biosensor Chip Based on Distance Readout for Deoxynivalenol Detection," *Analytical Chemistry,* vol. 95, no. 5, pp. 2942-2948, 2023/02/07 2023, doi: 10.1021/acs.analchem.2c04698.